W13

DEOXIDATION STUDIES: THE INTERACTION OF VITREOUS SILICA WITH MOLTEN ALUMINIUM AND SYSTEMS OF ALUMINIUM, MANGANESE, IRON AND SILICON.

A Thesis submitted to the Council For National Academic Awards for the Degree of

DOCTOR OF PHILOSOPHY

by

IGOR DE ABREU E LIMA, Hut.Ing.,MSc.

DEPARTMENT OF METALLURGY
SHEFFIELD CITY POLYTECHNIC

December, 1979

This Thesis is based on an investigation carried out during the period January 1974 to March 1977 at Sheffield City Polytechnic. During this period, regular meetings were held to discuss the progress of the work and the following conference was attended:

"Chemical Interactions of Materials with Environments at High Temperatures", Imperial College, London, 2-3 July, 1975.

In addition, the following modules, from the Post-Graduate Course, were attended:

Computing and Numerical Methods
Process Metallurgy
Metals and Competitive Materials
Arc Furnace Steelmaking
Oxygen Steelmaking
Continuous Casting

The results obtained in this investigation and the theories developed are, to the best of my knowledge, original except where reference has been made to other investigators. No part of this Thesis has been submitted for a Degree at any other University or College.

December 1979

ACKNOWLEDGMENTS

The author is indebted to the Brasilian Research Council (CNPq), University of Rio de Janeiro (COPPE-UFRJ) for providing the financial assistance during the period of this investigation. He wishes to express his gratitude to Dr.G.Briggs for his incentives and guidance given so freely during the course of this investigation and to Dr. W.J.M. Salter of Alloy & Stainless Steelworks Group,BSC for his help and suggestions.

Thanks are also due to Dr.A.W.D.Hills, Dr.R.Acheson, Dr.F.B.Pickering, Mr.J.P.Storch and Mr.R.H.Parker for their help and suggestions.

The valuable assistance of the technical staff of the Department of Metallurgy, particularly of Mr.D.Latimer, Mr.J.Bradshaw and Dr.D.B.Lewis and also of Mr.D.McKay of the Deparment of Production and Mechanical Engineering and also of the secretarial staff of the Department of Metallurgy in the preparation of this Thesis is gratefully acknowledged.

SYNOPSIS

The interaction of aluminium with silica and silicates is thermodynamically inevitable and leads to reaction effects in many systems. The resultant reactions can continue over a wide temperature range including both liquid and solid state systems such as molten aluminium handling units and the heat treatment of aluminium deoxidised steel.

The development of the reaction product layer under controlled conditions has allowed the reaction rate constants for the reaction between liquid aluminium and vitreous silica to be calculated as a function of temperature. These determinations show that the aluminium reduction of the silica is almost entirely controlled and maintained by the transport of the metallic species through the porous matrix of a solid oxide reaction product.

At temperatures between 760°C and 860°C the reaction product layer is porous as a result of volume changes of phases formed during reaction and the reaction rate increases with temperature. At intermediate temperatures the reaction progress is interrupted and the reaction rate indeterminate probably as a consequence of the formation of a compact matrix resulting from volume changes associated with polymorphic changes of the alumina formed. There is also some speculation in relation to a spinel phase formed between silica and alumina in the reaction front at intermediate temperatures.

At temperatures above 1110°C the rate of reaction becomes a function of the sintering of the alumina in the product layer with the formation of a fissured matrix and temperature, where the process is additionally controlled by the composition of saturated liquidus of the metallic system involved.

It is clear that the morphologies of the reaction product layer dictate the variation in the rates of reaction observed over the different temperature ranges.

It is proposed that alloying the liquid aluminium with silicon up to an equivalent of 15 atomic percent does not affect the progress of the reaction at all. Equilibrium saturation of liquid aluminium with iron or manganese effectively reduces the solubility of silicon at specific temperatures thereby reducing rates of counter-diffusing of silicon and aluminium and hence the rate of reaction.

Contents Page

Contents Page

CHAPTER 3

Contents Page

CONTENTS

Contents Page

CHAPTER 1

I. INTRODUCTION

Aluminium is used in the refining of liquid steel, basically, because it is a strong deoxidizing agent. This function it performs consistently and at low cost. There is considerable evidence that aluminium in molten steels can cause reactions to take place between pre-existing non-metallic inclusions and dissolved aluminium, providing that the formed new phase is more stable than the pre-existing inclusions. Particular characteristics assumed by this phase such as the change of density and mass per unity volume allow it to emerge from the liquid bath, as a result of which the metal becomes more pure.

The present work was undertaken to determine the consistency of the reaction between vitreous silica and liquid aluminium pure or alloyed with different concentrations of either silicon, manganese or iron and, in turn, to investigate this reaction in relation to the real situation in which the silica rich complex $FeO-2FeO.SiO_2-SiO_2$ system is attacked by aluminium.

Many experimental techniques have been developed to measure continuously the thickening of a porous product layer developed under controlled conditions, the measurements being interpreted using the "shrinking core" model*. These results are then used in the prediction of the rate of reaction, according to an experimental strategy**.

---

* Levenspiel,O., Ref.cit. in the References List, n.72.

** Hills, A.W.D., Ref.cit. in the References List, n.86.

An investigation of the liquid aluminium-vitreous silica reaction was considered appropriate as a continuation of a project which investigated the mechanism of secondary reactions between pre-existing silicate inclusions and deoxidizing aluminium***. This provided an excellent starting point for this work. In addition, since the microstructural changes occurring during reaction between silica and aluminium are very significant for the fabrication of fibre-reinforced composites, where effects such as diffusion-penetration and sub-sequent selective coarsening often lead to degradation of the produced material, several works related to this field also provided fundamentals for the initial experimental programme.

The investigations were conducted using small laboratory high temperature reactors. The behaviour of small laboratory reactors is difficult to interpret in terms of reaction kinetics, since it is determined not only by the reaction kinetics itself but also by the characteristics of the reactor. Therefore, a study on isolated vitreous silica rod immersed in liquid metal was envisaged for this work.

Any heterogeneous reaction will involve a number of different steps, especially if one reactant and one product are solids. The fluid reactants must be brought to the reaction region by transport processes such as diffusion and convection and the fluid products removed. The actual reaction in the reaction region will involve a chemical reaction step and often some solid-state diffusion process as well. Each of these steps will have an intrinsic rate and the rate at which it would occur were the other steps so fast as to provide no limit to the overall reaction rate. In fact, the overall reaction will occur at the rate of the step or steps with the lowest intrinsic rate or rates. Although these conditions describe the possible limiting cases, many important reactions have been evaluated in this way.

There existed in the literature some arguments as to the nature of the rate controlling steps for the reaction between liquid aluminium and vitreous silica and this investigation was appropriate to provide a test of the validity of the different mechanisms proposed by various workers.

***Wauby,P.E., Refs.cit. in References List nos.52 and 54.

2. LITERATURE SURVEY.

2.1 Introduction - the reaction between a liquid metal and a compound may be represented by the general expression[1]:

$$zMt + Me_xX_y \longrightarrow Mt_zX_y\,_{(Me_xX_y)} + xMe_{Mt} \qquad 2.1.$$

where X is a non metal and Me and Mt are metals, Me having a lower affinity for X than Mt.

The corresponding reaction between liquid aluminium and silica is:

$$4Al_{(l)} + 3SiO_{2(s)} \longrightarrow 2(\varphi)\ Al_2O_3 + 3(Si)^n_{Al} \qquad 2.2.$$

where $(\varphi)\ Al_2O_3$ is any of the polymorphs of alumina, which may occur as a result of the reaction and n signifies the variable concentration of silicon dissolved in the aluminium as a reaction product.

The above reaction between aluminium and silica may be considered in terms of the step-reactions as follows:[2,3]

$$3SiO_{2(s)} = 3(Si)^n_{Al} + 3O_{2(g)} \qquad 2.3.$$

and/or

$$3SiO_{2(s)} = 3Si_{(s)} + 3O_{2(g)} \qquad 2.3'.$$

$$4Al_{(l)} + 3O_{2(g)} = 2(\varphi)\ Al_2O_3 \qquad 2.4.$$

Equation 2.2. is the result of the summation of equations 2.3. and 2.4. These main-step reactions represent a somewhat simplified picture of the overall process. It is likely that the reduction of silica by aluminium may proceed by a series of intermediate steps. These will be considered later.

The reactant silica involved in the reaction may be in the uncombined or combined state, i.e. it could be amorphous silica or even crystalline quartz, both largely composed of free silica, or it could be any material containing substantial quantities of combined

silica such as ceramics or non-metallic inclusions etc. Whilst the reaction with both forms of silica is of interest, the present work is primarily concerned with vitreous silica. Whenever opportunities arise, however, the reaction with other types of silica will be examined.

The reaction may be further complicated if the aluminium contains other elements, e.g. silicon or transition metals such as manganese or iron. The effect of some of these elements on the reactions is also considered later.

The equilibrium of reaction 2.2. depends primarily upon the relative affinities of liquid aluminium and silicon for oxygen. Values of the free energy-change (ΔG^{o}_{T}) for the main-step reactions 2.3. and 2.4. may be obtained from the data in the literature[4]

Equation	$\Delta G^{o}_{800^{o}C}$/kJ mol^{-1}/
2.3.	+ 1407
2.4.	- 3092

Summation of these two values yields a free energy-change of -1685 kJ. mol^{-1} for the overall reaction 2.2. at a temperature of 800°C; this value of ΔG^{o} is large and negative and, therefore, one would expect that reaction 2.2. would be thermodynamically favourable. It is therefore expected that the extent of reaction between silica and molten aluminium will be controlled by kinetic factors. For a given surface area of silica, the depth of reaction is likely to depend upon the temperature, the time of contact of the silica with the molten aluminium and, as the reaction progresses, the liquid metal composition. The crystalline nature of the alumina formed and the accumulation of silicon in the molten aluminium are also likely to be important factors influencing the extent of reaction. Before consideration is given to the effect of these variables on the interaction mechanism between aluminium and silica, certain physical and chemical aspects of the structure of the reaction products will be examined.

2.2. Phase relationship in the system involving the reaction products - silicon is formed, as a product of the reaction, as either elemental silicon, according to equation 2.3'. or goes into solution in the liquid aluminium according to equation 2.3.

Silicon forms a single eutectic with aluminium at ~11.3 mass % Si at 577°C as shown in Fig. 2.1. There is limited solubility of silicon in aluminium at the eutectic temperature, but on cooling to room temperature the solubility of silicon decreases to virtually zero. The maximum solubility of silicon in aluminium at the eutectic temperature is 1.59 mass %. On cooling below this temperature, precipitation of pure silicon will occur within the grains of the primary aluminium rich phase. The covalent diamond-type structure of the silicon lattice cannot accept even small amounts of aluminium[6], and therefore, the solid silicon rich phase is essentially pure silicon.

The presence of a product layer of pure silicon on the surface of a partially reacted silica particle might act as a barrier to the penetration of aluminium from the melt and, hence, might prevent further reaction to form alumina. Devereux[7] has investigated the effect on the structure of reaction formed alumina-silicon cermets of silicon dissolution into aluminium-silicon melts. He expected that unless Ostwald ripening was occurring, the silicon produced by the reaction would not dissolve in the silicon saturated melt and, thus, would prevent the penetration of aluminium into the product layer. However, aluminium was detected in the product structure, suggesting that dissolution of silicon did occur. Although the author admitted that possibly saturation in the melt had not been complete, this would appear to be reasonable from his results.

Cisse et al.[8] carrying out work on the simultaneous refinement of primary and eutectic silicon in hypereutectic aluminium-silicon alloys, confirmed an earlier observation[9] that direct additions of finely dispersed alumina aided the nucleation of the silicon phase, but not the aluminium rich phase.

As mentioned previously, the overall reaction between molten aluminium and silica may proceed via a series of intermediate reactions. The contribution of these intermediate reactions to the overall mechanism will be considered in more detail later. It is possible, however, that some of these reactions may give rise to elemental silicon precipitation and this aspect will be examined briefly here.

Gershinsky et al.[10] has investigated the stoichiometry of the

reactions taking place between thin films of aluminium and silica. Their results indicated that below the melting point of aluminium, in addition to the main reaction expressed by equation 2.2., intermediate reactions such as

$$4Al + SiO_2 = 2Al_2O + Si \qquad 2.5.$$

$$2Al + SiO_2 = 2AlO + Si \qquad 2.6.$$

might be involved.

Thin film studies of the reduction of silica by aluminium at temperatures varying from 700 to 850°C and under high vacuum were carried out by Prabriputaloong et al.[4]. The only non-gaseous reaction product was silicon, observed only when the reaction was conducted at a pressure low enough to inhibit the oxidation of silicon, presumably into silicon monoxide. During the reaction alumina was also produced. Extrapolating from results obtained at higher temperatures by Brewer and Searcy[11], the authors roughly estimated the equilibrium vapour pressure of alumina at 800°C. The resultant value was found to be $\sim 1.3 \times 10^{-3} N.m^{-2}$. A column of molten aluminium 5Å high is heavy enough to exert a pressure of this magnitude. The interfacial reaction, therefore, cannot directly produce Al_2O in the gas phase, since none of the films used were <5Å thick. However, since aluminium can dissolve some oxygen[12], the reaction can proceed as follows: the silica at the interface is decomposed into its elements, which dissolve in the aluminium; the oxygen-gas then diffuses to the surface and it is released as Al_2O. This is likely to be a reliable explanation for the occurrence of reaction 2.5.

When enough residual oxygen-gas is present, the silicon concentration at the surface can be substantially zero, since the silicon is oxidized as soon as it reaches the surface. Thus, according to Prabriputaloong et al.[4], the silicon concentration at the surface will be independent of the film thickness and it will diffuse to the surface, being the rate of diffusion film thickness - independent, since it will be determined by the rate of the aluminium-silica reaction. Supporting evidence for this theory was the fact that for very thin films, when free silicon first appeared, aluminium seemed to be present only to a very limited extent, whereas for thicker films,

aluminium appeared to be abundant when silicon was first detected. This has been presented as consistent for the theory, since for the thin film a greater proportion of aluminium was supposed to be used up in the formation of Al_2O than for the thick film. The reverse is valid as far as silicon is concerned for the formation of silicon monoxide from residual oxygen gas.

Alumina and silicon have been observed to react according to reaction[13]:

$$Al_2O_3 + 2Si \rightarrow Al_2O + 2SiO \qquad 2.7.$$

According to some investigators, [14-16] this reaction is most unlikely to occur, because of the doubtful stability of solid silicon monoxide at high temperatures. Schafer and Speidel[14] reported that amorphous silicon monoxide is unstable at temperatures within the range of 1000 to 1150°C. Brewer et al.[15] found no evidence for the formation of solid silicon monoxide using high temperature X-ray diffraction analysis of mixtures of silicon and silica below 900°C. Their results indicated that solid silicon monoxide is thermodynamically unstable and decomposes into its components below 900°C.

Silicon and silica mixtures were examined by differential thermal analysis (d.t.a.) up to the melting point of silicon by Brewer and Greene[16] and again, no evidence was found for the formation of stable solid silicon monoxide. They postulated that partial reduction of silica to SiO_{2-x} may sometimes occur, which would give rise to a higher melting point [15]. It has also been pointed out that silicon monoxide prepared in a metastable amorphous or poorly crystallised form by condensation of silicon monoxide gas upon a cold surface, begins to decompose into silicon and silica within the temperature range of 400 to 700°C[17].

Contradictory evidence has been presented by Kochnev and Geld[18], who claimed to have prepared amorphous silicon monoxide by heating an intimate mixture of silica and silicon to 1250 to 1350°C.

The silicon-oxygen phase diagram has not been fully determined, but there appears to be grounds for assuming that a region of stability for the silicon monoxide exists above 900°C [19]. The oxidation of silicon in the temperature range 950 to 1350°C results in the formation

of a surface layer of amorphous oxidation product. In the initial stages of growth of the oxide, i.e. when the partial pressure of the oxygen in the gas phase and, therefore, at the silicon-oxygen interface, corresponds to the conditions favourable for the existence of the higher oxide, a crystalline silica phase may be formed. After formation of a continuous layer of oxide on the silicon surface, the supply of oxygen to the silicon-oxide interface is determined by oxygen diffusion through the surface layer. The oxygen concentration at the silicon-oxide interface gives rise to condition favourable for the formation of silicon monoxide. These deductions first presented by Sosman[19] have comprehensively been supported by the work of Smirnova et al.[20]. By using an electron-diffraction analysis at two different temperature ranges, i.e. 700 to 1000°C and 900 to 1250°C, the authors have investigated the thermal oxidation characteristics of silicon and found that silicon monoxide can be formed at the silicon-silica interface. Oxidation below 900°C takes place by the reaction

$$Si + O_2 \longrightarrow SiO_2 \qquad 2.8.$$

resulting in the formation of polycrystalline silica. Amorphous silica was formed in the temperature range of 950 to 1250°C, because the reaction proceeds via the formation of silicon monoxide. At temperature ~1000°C silicon reacts with silica according to the equation

$$SiO_2 + Si \rightleftharpoons 2SiO \qquad 2.9.$$

According to the authors[19,20], it is unlikely that the properties of the silicon-silica interface are governed by the presence of a transitional microlayer consisting of an amorphous mixture of silicon and silica formed by decomposition of silicon monoxide.

The sessile drop technique has been used by Marumo and Pask[21] to study the reactions and wetting behaviour in the aluminium-fused silica system. They noted that when the aluminium drop was not initially saturated with silicon, the following reaction occurred at the aluminium-silica interface:

$$Al + SiO_2 \longrightarrow (1-x)AlO + \frac{x}{2} Al_2O_3 + (Si)^n_{Al} \qquad 2.10.$$

The reduced silicon was free to go into solution in the molten aluminium. When the aluminium-drop was saturated with silicon, the redox reaction resulted in silicon being precipitated at the aluminium-silica interface:

$$Al + SiO \longrightarrow AlO + Si \qquad 2.11.$$

It is signficant that there have been very few studies of the sub-oxides of aluminium or silicon in the presence of each other. Although aluminium monoxide is thermodynamically unstable as a single phase, it is possible that it is stabilized by forming a solid solution with silicon monoxide, since its free energy would be reduced by the formation of such a solution[21]. Taking this into consideration, Marumo and Pask have postulated the stable existence of both sub-oxides in a spinel structure with alumina.

Some attempts have been made to study the sub-oxides of aluminium. At temperatures above the range 900 to 1000°C and at low pressures, there exists on an aluminium-surface an oxygen deficient layer of unknown thickness, which contains aluminium-monoxide in a spinel-type structure[22]. On cooling in vacuum, this structure persists. On exposure to oxygen or moisture, however, the cation distribution remains the same, but the valency of Al^{2+} increases to Al^{3+} resulting in a gamma (γ) - alumina (spinel-type structure).

By heating aluminium-alumina mixtures in an inert atmosphere of argon (or helium), Yanagida et al.[23] showed that for samples containing at least up to 50 mass %, the molten metal remained mixed with the oxide powder until the temperature came very close to the melting point of the oxide. The authors concluded that crystalline aluminium sub-oxides type aluminium monoxide had not formed under these conditions.

It has been postulated, however, that Al_2O sub-oxide may be formed according to the equation[24]

$$4Al_{(l)} + Al_2O_{3(s)} = 3Al_2O_{(g)} \qquad 2.12.$$

A mass spectrographic analysis by Porter et al.[25] of the vapour in

thermodynamic equilibrium with aluminium-alumina mixtures showed that the predominant species in the vapour were aluminium and Al_2O. Thermodynamic properties presented by the authors for this aluminium sub-oxide were in good agreement with those obtained by Brewer and Searcy[11], i.e. that Al_2O is involved when alumina is heated with aluminium or another reducing metal. The work carried out by Champion et al.[24] on the wetting and spreading of a molten drop of aluminium on aluminium oxide, over the temperature range 800 to 1500°C, has shown that the rate at which reaction 2.12. proceeds would be governed by the rate at which Al_2O is removed from the aluminium-alumina interface. The formation of Al_2O by reaction 2.12. is, therefore, only favourable at the periphery of the drop and results in the formation of a reaction ring. A number of important phenomena associated with the reaction have been summarised by the authors[24] as follows:

(a) the probable low solubility of Al_2O in the molten aluminium:

(b) the pressure on the aluminium-alumina interface due to the weight of aluminium. This pressure is likely to exceed the vapour pressure of Al_2O except near the periphery. The vapour pressure of Al_2O over a liquid aluminium and solid alumina mixture at 1350°C has been given as 30.1×10^{-8} $N.m^{-2}$ at a depth of approximately 1 mm below the molten aluminium surface[11];

(c) an observed decrease in the volume of the drop due to the evaporation of both Al_2O and aluminium.

It is significant to note that the relationships presented so far have been studied under diverse experimental conditions, but no attempt at a comparative thermodynamic study has been made.

2.3. <u>Transformations in alumina</u> - as mentioned before, it is possible that the structure of the alumina produced by reaction 2.2. is both time and temperature dependent. An examination of the polymorphism of the thermal transformations exhibited by alumina is, therefore, an essential requirement of this literature survey.

2.3.1. Polymorphs of alumina

2.3.1.1. Nomenclature - a number of metastable aluminium oxides, known as transition aluminas, are known to occur as a result of the dehydration of the several different forms of aluminium hydroxide. These transition aluminas may form as intermediate steps in the oxidation of aluminium to stable corundum.

The sequence of formation of these transition aluminas, based on x-ray and electron diffraction analysis, has been evaluated by numerous investigators[26-29]. As pointed out by Bye and Gauvin[30], the transition aluminas, however, usually exhibit poor crystallinity, yielding x-ray diffraction patterns with much line broadening and often leading to difficulties in correlation. Under certain conditions, duplex structures may also form[31]. This has led to inconsistencies in the nomenclature adopted for the identification of the various polymorphs. The prefixes adopted for the polymorphs of alumina in the work presented here, will follow the British system of classification[26,27]. These are: α (corundum), γ, δ, θ, $\kappa+\theta$ and $\chi+\gamma$. The American system involves the allocation of prefixes in a somewhat different manner[28,29]. A correlation can be found in discussions given by Rooksby[26] and Newsome et al.[28]. Whenever works with different terms appear, the equivalences listed in Table 2.1[28] will be used, in order to translate to the British nomenclature adopted in this work.

2.3.1.2. Structures - Lippens[32] has classified the polymorphic oxides of aluminium into two categories: 'low temperature' forms - not exceeding 600°C: $\chi+\gamma$, γ, δ; and 'high temperature' forms - virtually anhydrous: $\delta+\theta$, θ, $\kappa+\theta$ and α.

Of all forms listed in Table 2.1. only alpha-alumina has an established crystal structure based on a hexagonal close-packing of oxygen atoms with aluminium ions in 2/3 of the octahedral sites[33]. Gamma-alumina is a cubic, spinel-type of oxide. In actual fact it is considered as a defective spinel i.e. with not enough cations to fill all available sites in the structure[26]. X-ray evidence led Saalfeld[34] to conclude that γ-alumina had a tetragonally deformed spinel lattice with a = 7,96, c = 7.8 Å. However, many extra lines in the x-ray powder pattern, could not be interpreted in this way. A satisfactory

indexing of the x-ray powder pattern of γ-alumina, based on the assumption of a supercell of spinel consisting of three spinel blocks, has been achieved by Lippens et al.[35]. These authors also suggested that the monoclinic lattice of theta-alumina has a deformed spinel oxygen-lattice with aluminium atoms divided between the available octahedral and tetrahedral sites with preference for the latter. Thus, according to Lippens et al., θ-alumina might be regarded as an intermediate between the spinel lattice with predominantly octahedral positions and the hexagonal oxygen-arrangement of alpha-alumina, i.e. with aluminium ions in octahedral positions. Of all the available octahedral interstices in α-alumina, 2/3 are occupied by aluminium ions and 1/3 are vacant.

2.3.2. Mechanisms - it has been postulated that the crystal structure exerts considerable influence on the transformation of aluminas.[33,36,37]

A basic principle involved in the formation of the transition aluminas was first pointed out by Ervin[37] in 1952. The x-ray powder diffraction patterns of these aluminas have in common one strong line at 1.39 Å, which corresponds to the oxygen ion radius and is indexed as the $\{440\}$ line for the spinel unit cell. Planes giving rise to this reflection have the unique property of passing through the centres of all the anions and the possible cation positions for anions in cubic close packing. By deduction, therefore, all of these structures have oxygen ions in nearly cubic close packing and aluminium ions in the interstices. The $\{400\}$ line of the spinel pattern at about 1.99 Å comes from planes through all the anion positions and the octahedral cation positions. Its intensity is affected only by the relative distribution of cations between these two types of positions. On this basis, the varying degree of aluminium ion order within an unchanging oxygen ion network is responsible for the multiplicity of transition aluminas.

In the transformation gamma → theta-alumina Ervin's principle operates in terms of the continuity of the cubic close-packed oxygen system. This is a simple transformation without chemical change and is readily interpreted in terms of a reorganisation of the aluminium-cations. The final stage of the transformation to α-alumina involves changing from cubic to hexagonal packing. Little or no orientation relationship exists between the θ-alumina and the α-alumina, and the

transformation is probably one which proceeds by formation and growth of randomly, or nearly, orientated nuclei.[38]

According to Christian[39], most polymorphs are considered to be heterogeneously nucleated and the general characteristics of these reactions may be summarised as follows:

A. They are time and temperature-dependent.

B. They are thermodynamically irreversible: if phase ϕ_1 is converted into a new structure ϕ_2, the crystals of phase ϕ_1 formed on reversion of phase ϕ_2 will be crystallographically unrelated to those that were initially present.

C. Nucleation can be assisted by mechanical energy, but to a lesser degree than for diffusionless transformation.

D. The component of the reaction products may or may not be related in any way to the original phase.

Some works on heterogeneous nucleation mechanisms for alumina transformations have been reported by several investigators.

In the transformation of γ-alumina to α-alumina at 1100°C, it has been shown[40] that particles of γ-alumina feed corundum wafers, indicating a long range transfer of material. Brindley[38] has pointed out that the final stages of the transformation of metastable alumina into α-alumina, probably, involves the formation and growth of randomly orientated nuclei. Also Stirland et al.[41], looking at the final transformation of metastable aluminas to α-alumina, from a morphology standpoint, has suggested that material transport might possibly be by sintering and atomic re-arrangement. Iler[42] proposed the formation of an amorphous transitory phase, when θ-alumina transformed to α-alumina. The diminishing θ-crystals were connected to the growing α-crystals by the transitory phase through which both aluminium and oxide-ions diffused during the transformation.

The phase transformation of θ-alumina to the stable α-phase occurs by a nucleation and growth process, although little is known

about the initial nucleation step. According to Badkar and Bailey[31], electron diffraction patterns of very small α-nuclei, in the size range of the polycrystalline θ-matrix, will not be strong enough to be recognized in the background of spotty diffraction rings obtained from the adjacent polycrystalline area. Thus, a newly formed α-grain will not be detectable until it grows to a sufficiently large size to give a distinct diffraction pattern. The authors suggested that nucleation of the α-phase can occur in the θ-matrix on a scale that is coarse compared to the fine θ-crystallite grain size. They estimated that, on average, one α-grain forms per 10^5 θ-grains.

During the growth of the new α-alumina, a considerable redistribution of the fine porosity existing within the transition alumina matrix occurs. This porosity takes the form of large elongated interconnected pores trapped within the nucleating α-grains. These pores grow rapidly to a size approximately one hundred times that of the metastable θ-grains[31].

In the transformation of kappa + theta to alpha-alumina, the pore structure becomes progressively coarser with increasing temperatures above 1250°C. Sometimes this leads to secondary crystallization which produces an outgrowth of platelets, many of which display hexagonal facets[43]. This is particularly typical of transformation at higher temperatures and in the presence of a trace of a mineralizer such as fluoride. The mechanism of pore development has not been established with certainty, but Scott and Horseman[43] suggested that it may well take place by surface diffusion with regression of thinner pore walls and further growth of their thicker neighbours.

It has also been observed[31] that during growth of α-grains considerable redistribution of the fine interconnected porosity within the θ-matrix occurs. This matrix took the form of large, elongated and interconnected pores, which were left within the growing α-grains. It has also been pointed out by the authors that the α/θ interface migrates in the form of finger-like branches. The size of the fingers is relatively large ($\sim$500 to 100 Å wide) compared to the crystallite size of the θ-matrix (250 to 350 Å diameter). These observations suggest that the fine pores of the θ-matrix pin the α-phase interface and for growth of the α-phase to occur these pores must be removed.

2.3.3. Effect of impurities - so far it has been shown that the transformation of the transition aluminas to the stable α-phase apparently involves only a restructuring of the alumina lattice. It has been shown, however, that under certain circumstances, there may be retardation for the formation of the stable phase[31,32,44,45]. Simpkin[45] has studied the effect of iron and chromium ions on the thermal transformations and electro-kinetic properties of aluminium oxides. He suggested that the observed reduction in the rate of formation of α-alumina in the presence of Cr^{6+} may be due to the retarding effect of this ion on the synchro-shear process arising from its resistance to change from the previously favoured tetrahedral coordination.

Gauvin[44] also suggested that V^{4+} in the θ-lattice could possibly inhibit synchro-shear and, hence, retard the conversion of cubic-type close-packing of the oxide ions to hexagonal close-packing. In the case of $\kappa+\theta$-alumina transformation to α-alumina, the hexagonal close-packing of the oxide ions has already been attained. In this case, the observed retardation effect of the dissolved V^{4+} - ions could be in inhibiting the Al^{3+} - ions from attaining the octahedral position required for corundum.

2.3.4. Alumina polymorphs involved in the reaction between silica and aluminium - several polymorphs of alumina have been identified in studies on this interacting system. These aluminas will be briefly introduced in the following lines, though their effect on the mechanism of reaction considered will be examined later.

X-ray diffraction analysis carried out by Standage and Gani[46] have identified three distinct forms of aluminium oxide, namely gamma and theta and traces of alpha-alumina. The main forms γ and θ were assumed as being formed independently in different stages of reaction, though in both cases, some conversion to α-alumina could be observed. The same polymorphs have been detected by other investigators: Prabriputaloong and Piggott[47], who investigated the reaction between aluminium and vitreous silica at temperatures below the melting point of aluminium, found the product layer formed to be consisted of silicon and predominantly of θ-alumina with traces of α-alumina.

Electron diffraction and microprobe analysis carried out by Chou and Eldridge[48] revealed what was thought to be delta-alumina as a reaction

product, when aluminium-silica-silicon mixtures were annealed for long periods of time at 500°C.

Differential-Thermal-Analysis (d.t.a.) was carried out at temperatures ranging from 630° to 770°C by Galante et al.[49], in order to study the reaction of aluminium and aluminium-silicon alloys with vitreous silicates. X-ray diffraction analysis of the d.t.a.-residues showed that silicon, aluminium and α-alumina were the essential products of the reaction.

In tests carried out for long periods of time ranging from hours to days at temperatures varying from 850° to 1000°C, Devereux[7] detected α-alumina as the sole oxide phase of the reaction between molten aluminium and vitreous silica.

Drops of molten aluminium at temperatures varying from 660 to 1200°C were placed by Marumo and Pask[21] on vitreous silica. The resulting reaction product was constituted of different layers composed of θ and α-alumina precipitates as the polymorphs present among other reaction products.

Thermal degradation of silica fibre reinforced aluminium at temperatures in the range 500 to 600°C have been studied by Squires and Rayson[50]. X-ray analysis of reaction products in this work has shown that θ-alumina was the predominant polymorph and that its formation controls the degradation itself.

Many of the authors referred to so far and others[4,61,62] have presented different polymorphs of alumina as resulting products of reaction between silica and aluminium. There are contradictory opinions about predomimant polymorphic phase during reaction and at temperatures. There is as well no common opinion about the mechanism of alumina transformation during reaction, presumably important for the understanding of the nature of products involved.

2.4. Mechanisms of the reaction between molten aluminium and silica or silicates - Pickering[51] has shown that the addition of aluminium to rimming and balanced steel ingots in order to control the extent of carbon monoxide evolution has a drastic effect on the type of non-metallic inclusions present in the solid ingot. The inclusions present in the liquid iron during the rimming period were identified as

typical iron, manganese-silicates, some of which became entrapped in the solidified rim of the ingot. Depending on the amount of aluminium added, galaxite ($MnO.Al_2O_3$), hercynite ($FeO.Al_2O_3$) or alumina particles could be precipitated. The author showed that any excess aluminium had the effect of reducing the less stable oxide phases in the siliceous inclusions already present in the melt and that this continued until the inclusion became entrapped in the solidifying metal. According to Pickering, the spinel phases were first produced by the reaction of aluminium with the less stable iron and manganese oxides. By increasing the availability of the aluminium in the original matrix, further reaction may proceed with full conversion of the inclusion to a purely alumin ous form.

In later work on refining liquid iron, Waudby et al.[52] have shown that the addition of strong deoxidants could cause reactions to occur between the primary forms of inclusions and the deoxidant additions. The interaction between aluminium and silicate inclusions formed in rimming steels has been observed by Waudby[54]. In analysing the mechanism of this reaction, the author confirmed the results obtained by Pickering[51], in that aluminium first replaced the small amount of iron in the silicate inclusions. The reaction was very rapid and resulted in the formation of a rim of alumina around the inclusion. In some casts, however, the quantity of reacting aluminium appeared to be greater than that solely from the replacement of the small amount of iron initially present in the silicate. In this case, further replacement by aluminium had probably taken place inside the rim, i.e.

molten silicate $\longrightarrow$ solid alumina

This would have been associated with a decrease in the volume of the inclusion as a result of the closer-atomic packing in the crystalline alumina compared with that in the liquid silicate. This interpretation of the reaction has been schematically presented as follows:

Fe+Al sol.in liq.iron	$2Al^{3+} + 3O^{2-}$ Al_2O_3	$Si^{4+} + 2O^{2-}$ SiO_2
Melt	Reaction rim	Liq. silicate

In regions rich in aluminium, it has also been observed that further reaction with the silicate can take place during subsequent

heat treatment of the solid steel, resulting in considerable changes in the inclusion. It was found that the majority of the deoxidation products after solidification consisted of rims or envelopes of alumina with or without central cores of silica and containing large amounts of entrapped metal. By heat treating at 1200°C, the authors observed that the reaction between aluminium and silica recommenced, although at a very much slower rate. Hence, it has been postulated that the replacement of silicon by aluminium to form alumina occurs by a diffusion-controlled mechanism as diagrammatically shown below:

$$Al + Si^{4+} \quad Si + Al^{3+} \quad \| \quad Si^{4+} \| Si^{4+} + 2O^{2-} \quad SiO_2$$

$$\| \quad Al^{3+} \| 2Al^{3+} + 3O^{2-} \quad Al_2O_3$$

Waudby[54] proposed that, in simple ionic terms, silicon ions diffused through the alumina rim to the surrounding iron-matrix and were replaced by aluminium ions. This was possible, since Al^{3+} and Si^{4+} ions are much smaller than the O^{2-} ions in the alumina lattice. Consequently, the central silica core gradually became smaller with thickening of the surrounding alumina layer. At the same time, more and more metal was deposited between the alumina and the silica as a result of the replacement of iron by aluminium.

Stephenson, Gladman and Pickering[53] have studied the effect of manganese and aluminium in molten steel on the erosion of an alumino-silicate brick, containing 42% Al_2O_3. The contribution of the aluminium to the erosion process was to react with the silica in the manner as described earlier by equation 2.2. However, according to the authors, if sufficient reaction with aluminium takes place, and in conditions where the aluminium-silica reaction predominates, an alumina-rich layer would be expected to be formed on the surface of the brick, perhaps acting as a barrier to further attack.

Snow and Shea[55] did show that aluminium dissolved in liquid iron will react with siliceous refractory in a similar manner according to the reaction 2.2.

All commercial alumina-silica refractories containing up to 99% alumina, when exposed to molten aluminium by Brondyke[56] suffered

penetration by the interaction between aluminium and silica. This author has found no definite relationship between penetration and the silicon content of the refractory, but did find a relationship between the silicon released by the penetration reaction and the silica content of the refractory. Penetration was associated with wetting of the refractory and, then, with chemical reaction itself, the rate of reaction being governed by the rate of diffusion of aluminium through the aluminium oxide to the unreacted silica. Brondyke's interpretation of the kinetics of the reaction has been rejected by some investigators.

Standage and Gani[46] studied the effect of up to 2.5 mass% additions of bismuth and antimony to the melt on the reaction produced by immersing fused silica rods in molten aluminium in the temperature range 600° to 800°C. They assumed the reaction to be divided into three distinct steps: an induction period with no measurable penetration followed by the production of γ-alumina and then θ-alumina respectively. In the presence of liquid aluminium or dilute liquid aluminium alloys containing both bismuth and antimony, appreciable time was found to elapse before commencement of the reduction of the silica. It was shown that small alloying additions, particularly of bismuth, considerably changed the incubation period - and the activation energy for the reduction process.

There is good correlation between the incubation periods estimated by Squires and Rayson[50] from graphical data for experiments with pure aluminium and aluminium - 0.38 mass % Bi alloys obtained by Standage and Gani[46]. This is compared in Figure 2.2.

Devereux[7] observed that the products of the reaction between aluminium and silica initially take the form of spherical surface segments of an isotropic material. According to the author, these points were too few in number to form a continuous layer and could be considered as defects in an otherwise protective surface layer This would be consistent if transport of aluminium through the formed cermet to the receding silica/cermet interface were the slow step and if the aluminium could only pass from the liquid bulk metal to the cermet structure only at a small number of points on the cermet surface. Growth of alumina could then take place from these points in a preferential direction normal to the silica/cermet interface. Under certain conditions, an isotropic reaction product was found covering the entire surface. In this case, the small number of entry points for aluminium on the cermet surface was no longer dominant and the

existence of a rapid growth direction for alumina ceased to be significant. So that, Devereux suggested that the reaction mechanism became chemically controlled. This author also observed that reactions with high silicon alloys were characteristically slow, while those with pure aluminium were relatively fast. It has thus been suggested that a different step in the reaction mechanism was controlling in each case. This statement, however, was unsupported by further evidence.

In the reaction between liquid aluminium and solid silica, it has been pointed out[21], that since the aluminium becomes enriched in silicon during reaction, the change of surface tension in the system liquid-gas and its viscosity should be taken into account.

At 800°C the surface tension of aluminium is $860.10^{-3} N.m^{-1}$ and at 900°C this decreases to $850.10^{-3} N.m^{-1}$. Extrapolating to 1450°C, this value decreases further to $810.10^{-3} N.m^{-1}$ and might then be comparable with the surface tension of silicon, which at its melting point, 1450°C, is equal to $730.10^{-3} N.m^{-1}$.[57] The component which has a lower surface tension will be present to a higher concentration in the surface compared to the bulk ideal mixture in a binary alloy[59]. Marumo and Pask[21] deduced that the dissolution of silicon lowers the surface tension of the liquid aluminium. However, as the viscosity for pure aluminium is 1 $MN.s.m^{-2}$ and that for aluminium - 28.0 mass % Si alloy is 0.8 $MN.s.m^{-2}$ at 800°C,[60] consequently, the viscosity of aluminium itself and its change with silicon solution is so small that its effect on wetting could be considered to be negligible. Thus, it has been postulated that any decrease of contact angle should be considered to be mainly due to the contribution of the free energy of the reaction ($-\Delta G_{sol-liq}$) and subsequently also to the decrease in the surface tension of the liquid metal.

Fused silica has a surface tension in the solid-gas system in the range of 260×10^{-3} to 350×10^{-3} $N.m^{-1}$ [58], which is somewhat smaller than the values for metals and, therefore, it would be expected, if there were no reaction, the contact angle should be obtuse. Marumo and Pask observed, however, that the contact angle decreased and so, it was reasonable to assume that the free energy of the reaction contributed to the reduction of the surface tension in the

solid-liquid system. The difference in wetting behaviour at two different temperatures, as indicated in Fig. 2.3., was attributed by the authors to the faster rate of reaction at the higher temperature and also to the nature of the reaction taking place.

Despite the experimental evidence, there has been as yet no agreement as to the mechanism of the reaction between molten aluminium and solid silica, nor has a generalized correlation for the reaction rate been suggested. Many workers appear to assume that the complexity of the system makes the formulation of such a correlation impossible.

As previously mentioned, Brondyke[56] has suggested that the rate of reaction between molten aluminium and silica refractories could well be controlled by the diffusion of the liquid metal through the resultant alumina to the reactant silica. A similar standpoint has been assumed by other workers[52]. These authors, however, did not determine the rate of reaction, they did not study in detail the structure of the reaction products and nor was the effect on the reaction of composition changes in the aluminium considered.

Marumo and Pask have used a sessile drop technique to study the reaction between molten aluminium and fused silica at temperatures in the range 800°C to 1000°C and at a pressure of $4.0 \times 10^{-3} N.m^{-2}$. They concluded that the wetting of fused silica by the liquid metal was dependent upon the formation of a reaction zone, which consisted of three distinct product layers. It was postulated that the reaction proceeded by ionic interdiffusion of Si^{2+}, Al^{+} and Al^{3+} at the reaction temperatures. The layer adjacent to the metal drop was found to be primarily aluminium monoxide stabilised by a solid solution with silicon monoxide. A spinel constituted of aluminium monoxide and alumina stabilised with silicon monoxide was found adjacent to the fused silica. On cooling, these dissociated into aluminium, silicon and θ-alumina and/or α-alumina.

According to Marumo and Pask, if Al^{3+}, Al^{o} and Si^{o} were actually the species existing at the experimental temperatures, it would be necessary for the redox reaction to occur at the SiO_2 interface in order to form a replacing Al_2O_3 — matrix through which Al^{o} and Si^{o} interdiffuse. There would not, then, have been any logical explanation for the existence of the three distinct reaction layers with the concentration profiles indicated in Fig. 2.4. Any possible reaction mechanism based on penetration of molten aluminium into the reaction zone, thus, has to be discarded.

At the rece-ding SiO_2 interface the oxidation-reduction reaction was suggested to be:

$$SiO_2 + 2AlO \rightarrow Al_2O_3 + SiO \qquad 2.13.$$

in which $Si^{4+} \xrightarrow{red.} Si^{2+}$ and $Al^{2+} \xrightarrow{oxi.} Al^{3+}$ and resulted in the formation of the layer adjacent to the SiO_2. The reaction was, thus, controlled by mass-transport of Al^{2+} and Si^{2+} in the product layer. This interdiffusion controls the growth of the layer adjacent to the silica interface, which becomes appreciable at $900^{o}C$ and increases with temperature.

The kinetics of the degradation process, in which silica rods were attached by molten aluminium has also been studied by some other workers[4,46,48,50,61,62].

The linear rate of thickening of the alumina layer, previously observed[46] has been confirmed by Prabriputaloong and Piggott[62] and by Squires and Rayson[50]. It would appear, according to these authors, that formation of theta-alumina controls the rate of degradation. If the reaction rate had been controlled by mass-transport of aluminium and/or silicon through the alumina layer, it is unlikely that the linear rate of reaction would have been observed, since the concentration gradients would decrease as the reaction layer thickness increased.

The main steps of this reaction have been outlined by Squires and Rayson[50] as follows. At the alumina-silica interface, surplus aluminium, in solution in the alumina, reacts with silica forming more alumina, but of lower aluminium content, and silicon. The silicon produced must dissolve in the product layer and diffuses outwards, before eventually precipitating in the bulk liquid aluminium -

possibly, after transferring from solid solution in alumina to solid solution in metallic aluminium. The authors suggest that any of the following processes may be kinetically the slowest step and, hence, would control the overall rate of reaction:

i. solution of aluminium in alumina, exceeding stoichio-metric requirements;

ii. $Al(\text{in } Al_2O_3) + SiO_2 \rightarrow \text{more } Al_2O_3 + Si$;

iii. $Si(\text{in } Al_2O_3) \rightarrow Si(\text{in Al - solid solution with } Al_2O_3)$;

iv. $Si(\text{in Al-solid solution}) \rightarrow$ precipitated Si;

v. once a layer of silicon has completely encased the alumina, aluminium must diffuse through the silicon in order to maintain the reaction.

The existence of an induction period and the linear advance of the reaction front with time led Squires and Rayson and others[46] to the overall conclusion that some form of interface control must be involved in the process of reduction of silica by aluminium.

2.5. Kinetic models - the reaction between liquid aluminium and solid silica (and/or silicates), as previously mentioned, is a heterogeneous reaction, which is complicated by the formation of a solid phase firmly bound to the solid reactant and which has a decisive effect on the course of the reaction.

In order to accomplish a better understanding of the reaction kinetics, the basic principles governing the rate of each of the plausible mechanisms will be considered. The reaction kinetics predicted by these models will later be compared with the actual experimental results obtained in this work.

It has been shown earlier, in the introduction of this literature review, that the extent of the reaction between molten aluminium and silica is controlled by kinetic factors. In other words, when the pressure, temperature or composition is changed, a new equilibrium condition is established. The attainment of this new equilibrium condition depends on the kinetics of the process. In many

systems, equilibrium is never reached, but the rate at which it is approached, is just as important as knowledge of the equilibrium state.

For heterogeneous reactions, in broad terms, the product nucleus and the parent matrix or, alternatively, the product crystal and the parent melt, are separated by a reaction interface and two steps must occur for the reaction to proceed:

(a) material transport to the interface;

(b) chemical reaction at the phase boundary.

In some cases, depending on the nature of the reaction involved, a third requirement is the transport of reaction products away from the interface.

Any of these steps may limit the overall rate of reaction, since the overall rate will be determined by the slowest step.

2.5.1. Diffusion models

2.5.1.1. Parabolic rate law - if the rate is dependent on the thickness of the product layer, then, the parabolic law becomes applicable for heterogeneous reactions[63,64]. It may be assumed that, if local equilibrium occurs at the phase boundaries, i.e. if at phase boundaries all thermodynamic variables are fixed, and the local defect concentrations are also fixed for all time of reaction, then, an average concentration gradient of defects is formed in the product layer, which is inversely proportional to the layer thickness Δr. This results in a flux of ions[65]. The rate determining ionic flux is, therefore, given by $J \propto 1/\Delta r$. Since J is proportional to the instantaneous growth rate $d\Delta r/dt$ of the layer, it follows that $d\Delta r/dt \propto 1/\Delta r$. This expression may be integrated to give the parabolic growth law in the form below - see derivation in appendix A-2-1,

$$\Delta r^2 = 2K_D t \qquad 2.14.$$

where K_D is the parabolic rate constant.

In order to express Δr in terms of the fractional conversion R_x, which is a more useful quantity, in terms of observed experimental data, the following equation has been derived[66] -

see appendix A-2-2,

$$2K_D t/r_o^2 = \left[1 - (1-R_x)^{1/3}\right]^2 \qquad 2.15.$$

This is known as the Jander's equation derived for spheres only and relates the fraction of reaction completed to time. This equation predicts that the progress of the reaction is inversely proportional to the square of the particle radius and that a plot $\left[1 - 1 - R_x)^{1/3}\right]^2$ versus time should give a straight line, indicating a direct correlation with mass transport control across the product layer.

It has often been found that Jander's equation does not adequately represent reaction data, indicating that more complicated situations actually exist. Various improvements to this model have been suggested by several workers. These have been reviewed by Hulbert[67,68].

It has been found that the parabolic rate law describes the oxidation of metals, where in most cases the formation of a compact spinel-type product layer is involved[64,65]. It does not apply, however, to the oxidation of the alkali or alkaline earth metals[69]: it has been shown that magnesium and calcium oxides do not interfere with the passage of more oxygen towards the inner unoxidized core. Themelis[70] has also shown that the parabolic law is not applicable in the case of iron oxide reduction, since the removal of oxygen atoms leaves the iron lattice with a lower specific gravity than the original oxide.

2.5.2. Chemically-controlled reactions - when diffusion of a species through the product layer is so rapid that the reactants cannot combine fast enough at the reaction interface to establish equilibrium, the reaction becomes phase-boundary controlled and, therefore, the movement of the reaction interface is at a constant velocity. Implicated in this model is the fact that the thickness of the product layer has no effect on the velocity of the reaction and, hence, diffusion of the reactants through the product layer plays no part in controlling the overall reaction rate.

Equations relating the fractional conversion to time have been derived for simple geometrical systems[70-73], assuming:

i. the reaction rate is proportional to the surface area of the unreacted material;

ii. nucleation occurs instantaneously over the entire surface, so that the surface of the particle is uniformly covered by a layer of the product phase.

For a sphere of density ρ_o reacting from the surface inwards, the relationship between R_x and t is given by the expression[73]: see appendix A-2-3.

$$k_c t/r_o \rho_o = 1-(1-R_x)^{1/3} \qquad 2.16.$$

Experimental confirmation of this equation was first presented by Stalhane and Malberg[74], who reported that the reaction zone for reduction of iron oxides advances linearly with time. Spencer and Topley[75] have also derived an identical expression to equation 2.16. in order to quantify the thermal decomposition of Ag_2CO_3. Inspection of equation 2.16. shows that a plot of $(1-R_x)^{1/3}$ versus time should yield a straight line.

It has been observed that, in some cases, linearity may not be followed for 100% of the conversion process, and that deviations from linearity may be noted towards the end of the process[77]. Such deviations are most probably due to associated physical phenomena, which can either accelerate or retard the reaction. For instance, cracking or spalling may occur, thereby increasing the area of unreacted phase exposed to the reactant species and, thus, accelerating the process[76]. On the contrary, recrystallization of the product layer could result in a decrease of the number of available passages through which the reactant may advance to the unreacted material.

The mechanism which leads to a phase-boundary controlled reaction assumes that the nucleation step occurs instantaneously so that the surface of a reacting particle becomes uniformly covered by a layer of the product phase. However, nucleation of the product phase may not necessarily be followed by rapid surface growth, and another approach to the mechanism of reaction is to consider the nucleation of product at active sites, and the rate at which these nucleated particles grow.

2.5.3. Nuclei growth models - Langmuir[78] was one of the first to postulate that phenomenological aspects following a heterogeneous reaction are limited by the concepts of formation and growth of the product phase. In other words, the rate of nuclei formation and their subsequent growth and impingement may control the rate of growth of the product phase - at least in the early stages of the conversion process. This conversion process in a heterogeneous system is represented by the curve shown in Fig. 2.5.[79]. The overall process may be sub-divided into four individual periods: initial (I), induction (II), acceleratory (III) and deceleratory (IV). During the initial period (I) the reaction involves only a few atomic layers near the surface of the reactant. The extent of reaction during the induction period (II) is very limited, but after some critical time t_o the reaction rate increases rapidly during the acceleratory period (III). The maximum rate of conversion is achieved at the point of inflexion R_i, t_i which constitutes the start of the deceleratory period (IV). For $t > t_i$ the reaction rate decreases steadily, eventually falling to zero as the reaction approaches completion.

According to Jacobs[79], when nuclei are formed only on the surface, isotropic or anisotropic growth and overlap lead to the formation of a continuous interface between the internal unreacted material and the product layer outside. If the interface propagates inward at a constant rate, as it will if every molecule of reactant in the interface has the same probability of reacting, then, according to Jacobs, it follows that:

$$1 - (1-R_x)^{1/n} = k_N t \qquad 2.17.$$

with $n = 3$, when nucleus growth occurs as an essentially three-dimensional process. The author suggested that this equation provided an excellent fit to the deceleratory period and should be applied when direct observation identifies the presence of a coherent interface advancing at a constant rate.

It appears that this kind of phenomena can be observed only if the induction period, during which reaction spreads out from a number of nuclei, is long enough to be recorded on a conversion rate against time plot. This must be the main reason why almost all

reactions classified in terms of a nuclei growth model have been for experiments carried out at relatively low temperatures. At higher temperatures, the growing nuclei spread out faster with a coherent interface being attained in a very short time and, then, advancing at a constant rate towards the centre of the unreacted material. This rate of reaction should be controlled by the specific reaction rate constant and also by the area of the interface at which nucleation takes place. Consequently, nuclei growth-controlled reactions should obey a rate equation very similar in form to that described before for a linearly-advancing reaction interface.

Hulbert and Popovitch[68] have assumed that nuclei growth is equivalent to a first-order-reaction, since their results could be plotted according to a first-order rate equation such as:

$$\ln(1-R_x) = (k_N t)^m \qquad 2.18.$$

where m is a parameter which is a function of the reaction mechanism, the nucleation rate and the geometry of the nuclei. This equation may be transformed to give:

$$\ln\left[\ln\left(\frac{1}{1-R_x}\right)\right] = m.\ln t + \ln k_N \qquad 2.19.$$

A plot of $\ln\left[\ln\left(\frac{1}{1-R_x}\right)\right]$ versus ln t should yield a straight line with gradient m and an intercept of $\ln k_N$.

Themelis[70] has shown that an experimental relationship of the same form as equation 2.18. also applies for control by unsteady-state diffusion. This researcher has expressed considerable doubt about the assumption that nuclei growth may be considered to be a first-order reaction. He suggested that, while such a mechanism could be justified for homogeneous reaction, where all parts of the reaction system are subjected to similar chemical attack, it cannot apply rigorously to a heterogeneous reaction, when different depths of the same particle may be converted to different extents.

2.6. Activation energy - the concept of activation energy provides one of the most important means of interpretation of chemical kinetics and applies equally to homogeneous or heterogeneous reactions.

The temperature of the rate of a chemical reaction, as reflected by the value of the reaction rate constant, has been found to be well represented by the Arrhenius equation:

$$k = k_o \; e^{-E/RT} \qquad 2.20.$$

where k_o is a proportionality factor characteristic of the system (the frequency factor) and E is the activation energy for the process. From this law a plot of ln k versus 1/T gives a straight line with a gradient which is related to the activation energy for the reaction. Reactions with high values of E are, therefore, very temperature-sensitive, while reactions with low activation energy are relatively temperature-insensitive.

The value of the activation energy obtained from plots of rate against reciprocal temperature is not necessarily the one corresponding to the specific rate of the chemical reaction, but rather to the rate of whatever process is controlling the overall rate, e.g. whether it is diffusion or phase-boundary control. In many cases the appropriate value of the activation energy for the rate controlling process may not be known or may be the subject of much controversy. The situation may be further complicated, when the phenomenon is complex and involves both chemical and physical effects[77].

Based upon the assumption that experimental data could be analysed from a chemical reaction controlling mechanism point of view, some few researchers have established the values of the activation energy of the interaction between aluminium and silica[4,46,47,50,62]. Below the melting point of aluminium and as low as 400°C, with the formation mainly of θ-alumina and silicon, the value of the activation energy was found equal to 13.8 $\pm$ 12.5 kJ . mol^{-1}. This value, according to Prabriputaloong and Piggott[62] decreases abruptly at the melting point of the aluminium. The same authors[4] examined an Arrhenius plot of experimental results of studies on thin films of the reduction of silica by aluminium at 700°C, (thus at temperature very near the melting point of aluminium - 660°C, and where E = 71.1 $\pm$ 16.7 kJ . mol^{-1}) and confirmed their questionable statement.

In a different series of experiments silica was immersed into molten pure aluminium at 700 to 820°C under vacuum and in air at atmospheric pressure, Prabriputaloong and Piggott[62] established the respective activation energy values: in the absence of interference by air formed oxide film on the surface of the molten metal, the E value was 175.6 ± 29.9 KJ . mol^{-1}. With air present the activation energy was 158.84 ± 29.9 kJ . mol^{-1}.

These values of the activation energy were not very different from Standage and Gani's[46] value, 265.4 ± 6.3 kJ . mol^{-1} for reaction between pure liquid aluminium and silica with predominant formation of θ-alumina as the reaction product. When γ-alumina was observed to be the predominant reaction product phase, the value of the activation energy was estimated to be 183.3 ± 6.3 kJ . mol^{-1}.

Squires and Rayson[50] working with thermal degradation of silica fibre-reinforced aluminium estimated an activation energy value of 280.1 kJ . mol^{-1}.

Despite the variety of purposes of the kinetic studies on the reaction between aluminium and silica, there is, amongst investigators, an evident consensus of opinion on activation energy values: excluding temperatures very close to the melting point of aluminium, down to ~400°C and up to ~850°C these values varied from ~130 to approx. 280 kJ . mol^{-1}. In order to indicate this consensus in activation energy values, a number of Arrhenius plots reported were recalculated to the same units of reaction rate constant and assembled in Fig. 2.6. From the consistency of the slopes of the lines it may be concluded that the extent of reaction between silica and aluminium over a range of temperatures was governed by kinetic factors and that it was characterised by a single controlling mechanism. It was one of the tasks of the present work to clarify this situation.

2.7. Pertinent phase equilibria in multicomponent systems involving aluminium

As mentioned earlier, the mechanism and hence the kinetics of the reaction between molten aluminium and solid silica may be affected if the aluminium contains other elements, e.g. silicon or transition metals such as manganese or iron. The influence of silicon

on the progress of the reaction has already been considered throughout this literature review. No attempts have been made, however, to establish the effect which iron or manganese have on the kinetics of the reaction, although phase equilibria for certain systems involving aluminium, manganese, iron and silicon have already been largely established.

2.7.1. The aluminium-manganese binary system

An extensive bibliographic review on this system has been presented by Mondolfo[80]. The aluminium end of the aluminium-manganese equilibrium diagram is presented in Fig. 2.7. The most probable values of the solid solubility are 1.8 mass % Mn at 930K, 1.0 mass % Mn at 900K, 0.42 mass % Mn at 800K and 0.2 mass % Mn at 700K. By quenching from the liquid state, the solubility can increase up to 1.5 mass % Mn.

The eutectic between the intermetallic compound $MnAl_6$ and the aluminium-rich solid solution is at approximately 1.9 mass % Mn and occurs at 930K. On the manganese-rich side of the eutectic point, the liquidus rises steeply and the primary intermetallic phase is $MnAl_6$ up to a composition of 4.1 mass % Mn. $MnAl_6$ is formed by a peritetic reaction at 983K, from a phase whose formula is usually given as $MnAl_4$ (with 33.7 mass % Mn):

$$MnAl_4 + Liq. \longrightarrow MnAl_6 \qquad 2.21.$$

Above 4.1 mass % Mn and up to 13.0 mass % Mn the intermetallic compound $MnAl_4$ becomes the primary phase. Several other phases are formed at higher manganese contents. These, however, have been assumed as not pertinent to this work.

2.7.2. The aluminium-iron binary system

The experimental works which have been carried out in order to establish the equilibrium-phase diagram for the aluminium-iron system are comprehensively reviewed by Mondolfo[80]. The aluminium end of the binary equilibrium diagram is presented in Fig. 2.8.

There is a eutectic, $Al - FeAl_3$ at the aluminium end, at

928K, with a probable composition within the range 1.7 to 2.2 mass % Fe. The equilibrium solid solubility is of the order of 0.03 to 0.05 mass % Fe at the eutectic temperature, decreasing to minimum values at 700 K. By quenching from the liquid, supersaturated solutions can be produced containing up to 18.4 mass % Fe. The phase in quilibrium with aluminium is usually designated as $Fe\ Al_3$ (40.7 mass % Fe). This compound forms directly from the liquid at 1420 K.

Precipitation of $Fe\ Al_3$ from the solid solution is very slow for alloys containing the equilibrium amount ($\sim$0.04 mass % Fe) in solution. However, in alloys produced by quenching from the liquid, in which the amount of iron in solution is some two orders of magnitude higher, precipitation is much faster.

2.7.3. The aluminium-manganese-silicon ternary system

Besides the phases present in the binary system, i.e. Al, $MnAl_6$, $MnAl_4$ and Si, a large number of ternary phases are formed; among these the formula $Mn_3\ Si_2\ Al_{15}$ (26.3 mass % Mn, 8.9 mass % Si) fits best the range and the structure of both manganese and silicon in the ternary alloy. Fig. 2.9. shows the liquidus surfaces at the aluminium corner.

The solid solubility of manganese and silicon are somewhat reduced in the ternary alloys. Most of the phases in the system form by peritectic reaction as described, for example, by equation 2.21. Other reactions may be presented as:

$$Liq \longrightarrow Al + Mn\ Al_6 \qquad 2.22.$$

$$Liq \longrightarrow Al + Si \qquad 2.23.$$

Several other phases identified by many authors have been largely described elsewhere in the Mondolfo's bibliographic review[80].

2.7.4. The aluminium-iron-silicon ternary system[80]

The aluminium corner of the aluminium-iron-silicon ternary equilibrium diagram is shown in Fig. 2.10. There are two ternary phases that can be in equilibrium with aluminium: $Fe_2\ SiAl_8$ and $Fe\ SiAl_5$. However, completion of peritectic reactions is necessary for equilibrium

to be established:

$$\text{Liq} \longrightarrow \text{Al} + \text{Si} + \text{Fe Si Al}_5 \qquad 2.24.$$

$$\text{Liq} + \text{Fe Al}_3 \longrightarrow \text{Al} + \text{Fe}_2\text{ Si Al}_8 \qquad 2.25.$$

$$\text{Liq} + \text{Fe}_2\text{ Si Al}_8 \longrightarrow \text{Al} + \text{Fe Si Al}_5 \qquad 2.26.$$

More ternary phases form at higher iron and silicon contents. These have been comprehensively described by Mondolfo[80].

The phase Fe_2 Si Al_8 and others may be expected to appear in all the alloys in which they are primary, and that free silicon, generally as eutectic, may be present even in alloys with Fe : Si ratios of 4:1, because with fast cooling silicon solubility is reduced.

2.8. Implication for the present work - so far as this literature survey has identified the direct relevant background works on the reaction between liquid aluminium and solid silica (and/or silicates) in particular. Hitherto there has not been any agreement on the existence of phases derived from this reaction and the amount of information on their equilibrium is, for the most part, very meagre.

The complexity of the reaction system is likely to be aggravated by the constitution of the reaction products themselves, particularly of the alumina. The time and temperature-dependence of alumina transformations throughout the formation of its polymorphs during reaction has not been undertaken very often as an ultimate objective to predict the behaviour of the reacting system involved.

The evaluation of these interdependent factors should provide the basis needed in order to obtain the indentification of the mechanisms of interaction between molten aluminium and solid silica and data for the correlation of the reaction rate with concentration and temperature.

3. EXPERIMENTAL METHODS

3.1. Preliminary Work - before examining the reaction between silica and molten pure aluminium/aluminium alloys, a suitable reactor was designed and built. In addition, physical techniques for analysis and quantification of the mechanism of reaction of reacted specimens had to be developed. Consideration also had to be given to the preparation of aluminium alloys containing various amounts of iron, manganese and silicon. These various aspects of the work are described below.

3.1.1. The reactor - a photograph of the equipment used in the preliminary experiments is shown in Fig. 3.1. and a schematic diagram of the reactor and gas flow system is shown in Fig. 3.2.

The furnace tube was of impervious recrystallized alumina. It was 960 mm long by 58 mm ID gas tight and fitted with removable water cooled aluminium end pieces. For the preliminary studies of the interaction between silica and pure aluminium in the temperature range 750 to 1000°C the reactor was mounted vertically inside a 220 mm long by 67 mm ID recrystallized alumina tube. This outer tube was wound with Kanthal - A1 and acted as a resistance furnace operating up to a temperature of 1050°C. The spiral windings were embedded and properly supported in C - 60 refractory cement. The space between the two tubes was packed with Triton Kaowool, in order to minimise thermal convection. The furnace tube itself was insulated by surrounding it in a structure of refractory bricks held in place by a Sindanyo case.

The furnace windings were connected to a 7 kw power supply regulated by a Proportional Temperature Controller type SR-2 (CNS Instruments Ltd), with a platinum resistance thermometer as the temperature sensing device.

The furnace gave a hot zone of approximately 60 mm long inside the reactor, with a radial temperature variation of $\pm$ 5°C on the walls of the tube.

The machined aluminium cover on the bottom of the reactor

tube supported a centrally placed stainless steel rod with a cylindrical pedestal at the top. This was used to support the crucible in the hot zone - see Fig. 3.3. -. Alumina powder was packed into the annular space between the crucible and the cylindrical pedestal in order to avoid any chemical interaction between the two.

The crucible and support pedestal were totally enclosed in a stainless steel radiation shield in order to equalize the temperature distribution around them. A temperature exploration using a chromel-alumel thermocouple at different heights inside the crucible showed variations of less than $\pm$ 2°C. The radiation shield was welded to the end of a stainless steel rod, which acted as a support for it and which passed through the centre of the machined aluminium plate covering the top of the reactor tube. The silica rod to be immersed in the molten aluminium was inserted into the machined hollow end of the stainless steel rod, which supported the radiation shield and was held in position by means of a screw.

3.1.2. The gas purification system - in order to prevent oxidation of the metallic bath, high purity argon from storage cylinders was introduced into the reactor after first being passed through a purifying system - see Fig. 3.2. -. The oxidizing potential calculations for the experimentally used controlled atmosphere are presented in appendix A-3.1. The gas flow through the system was controlled with the aid of a rotameter (1100 rotam. max. 13 l/min) at a constant rate of 150 cm^3/min. The gas inlet and outlet for the reactor were respectively sited in the lower and upper plates sealing the ends of the tube. After leaving the reactor tube the argon-gas was bubbled through a bottle with distilled water before being exhausted to the atmosphere to give a visual indication of outflow from the system.

3.1.3. The preparation of materials for the preliminary studies - the important physical and chemical properties of the materials employed in the preliminary experiments are summarised in Table 3.1.

3.1.3.1. Aluminium - it was found that the oxide layer on the surface of the aluminium charge could produce a significant film of alumina on the surface of the melt. This might have coated the silica rod as it was being immersed in the melt and hence might have affected the course of the reaction. It was, therefore, necessary to remove as much

as possible of the alumina coating from the charge materials, before they were used in an experiment.

High purity aluminium was first melted in a magnesia crucible and cast into a cylindrical cast iron mould. The surface oxide film could then be machined off, resulting in a slug of an appropriate size and mass to be placed inside an alumina crucible, which was then heated in argon in the apparatus prior to the start of every experiment.

3.1.3.2. Silica - pure transparent vitreous silica rods of different diameters were used. These were cut into convenient lengths and annealed in air at 1280°C for eight hours to release any thermal stresses which might have been introduced during fabrication. No signs of devitrification (formation of cristobalite crystals) on the surface of the rod have been observed. After being slowly cooled to room temperature, they were washed in carbon tetrachloride and stored in clean cotton wool.

3.1.3.3. The crucibles used - a few recrystallized alumina crucibles were exposed to molten aluminium under an argon atmosphere and at about 800 - 950°C for periods of time varying from one to three hours. This was carried out in order to explore the resistance of alumina to attack by the melt. The only visible sign of attack appeared to be a slight groove located around the crucible at the position of the molten aluminium surface. This degree of attack was considered to be negligible, and thus, confirming that recrystallized alumina crucibles could effectively be used in subsequent experiments.

3.1.4. Procedure - for the preliminary studies, only the interaction between pure liquid aluminium and transparent vitreous silica rods, with diameters of 3.0, 5.0 and 10.0 mm was considered.

The procedure adopted essentially involved heating the reactor to a uniform temperature and immersing the preheated rod into the crucible of molten aluminium, whilst maintaining a steady flow of high purity argon through the reactor.

A series of experiments were carried out at temperatures

760, 815, 840, 860, 920 and 980°C. The immersion times varied from 0.5 to 120 minutes. Some of the experiments were repeated several times, using the same conditions, in order to check the reproducibility of the results obtained. An outline of the experimental programme is presented in Table 3.2.

In all the experiments the charge to the alumina crucible consisted of an ingot of 35 - 40 g of pure aluminium. The crucible and its contents were positioned centrally in the hot zone on the top of the pedestal and support rod. A Pt - Pt 13% Rh thermocouple which passed through the plate sealing the top end of the reactor tube was positioned just above the surface of the liquid aluminium in order to record the temperature until a steady value was attained. A second Pt - Pt 13% Rh thermocouple was then intermittently immersed into the molten metal in order to determine its temperature. Both thermocouples were calibrated against the same secondary standard and were contained within gas tight, recrystallized alumina sheaths. The temperature indicated by the second thermocouple, i.e. - the one immersed in the liquid metal, was taken as the experimental recorded value; it was, in general, found to be slightly lower than the temperature just above the melt. Typical values obtained are as follows:

$t_{ref} = 760^{o}C$; $t_s = 767^{o}C$ $t_{ref} = 860^{o}C$: $t_s = 869^{o}C$

$t_{ref} = 815^{o}C$; $t_s = 824^{o}C$ $t_{ref} = 920^{o}C$; $t_s = 926^{o}C$

$t_{ref} = 840^{o}C$; $t_s = 851^{o}C$ $t_{ref} = 980^{o}C$; $t_s = 988^{o}C$

where t_{ref} is the temperature in the liquid metal and t_s is the temperature above the liquid surface. The temperature above the aluminium surface was compared with the mean temperature of several values of several points within the melt. The central axis temperature indicated by the thermocouple immersed in the liquid metal, did not vary by more than $\pm$ 2°C.

In order to prevent any reaction between the silica rod and the lower gaseous aluminium oxides, Al_2O and/or AlO, which might have have been volatilized from the liquid surface, the rod and the radiation shield were suspended some distance above the hot zone until the temperature of the metal had stabilised at the desired value. By

observation through the window in the top of the reactor, the rod was then lowered to a position just above the liquid surface and left there for a period of about one minute in order to allow it to reach the temperature of the hot zone. At this moment, argon was blown onto the liquid metal surface by means of a lance which passed through the top of the reactor. The rod was then immersed into the liquid aluminium and a stopwatch was started. It has been assumed here that the difference in temperature above the liquid surface and in the bulk metal, as mentioned above, was sufficiently small not to affect the initial course of the reaction between the silica rod and the aluminium melt.

After the desired experimental time interval had elapsed, the rod was withdrawn from the melt and rapidly raised in the cooler part of the upper reactor tube. It was then removed from the reactor and allowed to cool to room temperature. After mounting in resin, the rod was sectioned into slices, and then remounted in resin prior to grinding and polishing.

Before removing the crucible from the reactor the liquid metal was thoroughly stirred. A sample of the metal was sucked into a small diameter silica tube and quenched into carbon tetrachloride. The resulting pin-sample was then subjected to chemical analysis. The analytical method is described in section 3.9.

3.2. Studies involving aluminium and aluminium alloys at elevated temperatures

3.2.1. Preparation of metallic starting materials

3.2.1.1. Aluminium-manganese and aluminium-iron alloys - in the case of polyphase alloys such as aluminium-manganese and aluminium-iron, it was feared that due to the variation in composition within a given alloy and particularly between alloys produced for individual experiments, a disparity of results might arise and these would be impossible to characterise. It was therefore decided that each series of experiments involving a particular aluminium-manganese or aluminium-iron alloy would be carried out with material from the same batch.

The composition of the basic metals employed in the preparation of the alloys is presented in Table 3.3. The average mass of

each melt was approximately 4.0 kg. The method used to produce the aluminium-manganese and aluminium-iron alloy with compositions varying from 5.0 to 15.0 atomic % Mn or from 5.0 to 15.0 atomic % Fe is described below.

In order to ensure homogeneity, a technique was adopted, which involved melting each alloy twice. For each alloy composition the aluminium and the desired amount of the alloying metal were first melted together under a protective atmosphere of argon in a pure magnesia crucible in an induction furnace. This was performed in order to ensure that all the manganese or iron melted. Before casting into a cast-iron mould, pin-samples were taken for analysis by sucking the molten metal into small diameter silica tubes, which were then rapidly quenched into cold carbon tetrachloride. After casting, the resultant ingot was broken up into pieces and again remelted in the induction furnace under argon in a Thermax G 10 crucible - see Table 3.3. In most cases only small corrections had to be made to the composition of the master-alloy. This remelting stage was carried out as rapidly as possible in order to minimise contamination of the melt from the crucible and also, in case of aluminium-manganese alloys, to minimise losses of manganese by volatilization.

At 150° C above the pouring temperature, i.e. 1050 - 1150°C, the alloy was transferred to a preheated magnesia crucible. Pin-samples for analysis were taken and quenched into carbon tetrachloride. The temperature was measured and the melt was then slowly poured into a tank of cold water, through which air was bubbled in order to ensure adequate circulation. As a result, small granules, 10.0 mm average diameter, were produced. In the case of aluminium-manganese alloys, a small amount of manganese, generally less than 2% of the amount charged, was lost due to volatilization.

Alloy losses in the case of aluminium-iron melts were even less than those with aluminium-manganese alloys.

The chemical analysis of the liquid metal pin-samples and randomly selected samples of the final alloy were almost identical. An acceptable degree of homogeneity was therefore achieved. The analyses of the alloys produced are presented in Table 3.3.

3.2.1.2. Aluminium-silicon alloys - the alloys were prepared by dissolving particles of silicon in molten aluminium in a magnesia crucible. Long holding times were required to dissolve the silicon particles. In this case a double melting practice was not necessary. The melt was poured into cold water, in the same manner as the previous alloys. Only small composition deviations from the required values were observed, as indicated in Table 3.3.

3.2.2. Modifications to the experimental apparatus - for studies of the reaction of molten aluminium and aluminium alloys with solid silica at temperatures somewhat higher than those used in the preliminary experiments, it was necessary to modify certain parts of the apparatus. A general view of the modified equipment is shown in Fig. 3.4.

Intermittent heating operation at temperatures ranging between 1100 to 1350°C limited the life of the Kanthal A-1 winding used in the original furnace. Due to oxidation the winding became brittle and could not withstand the stresses imposed on it due to heating and cooling. Therefore, a new furnace had to be constructed using "Crystalon hot rods" as the heating elements. These elements are silicon carbide rods with a high resistance to oxidation at elevated temperatures (~1650°C).

The insulating brick structure around the furnace consisted of "hot face" insulating bricks (HGI) and "Kipsulate" panels conventionally mounted in a Sindanyo case. This is shown schematically in Fig. 3.5a.

The heating elements were supplied with 7 - 9 kw power regulated by a "Dual Variac Controller" - (DVC), which is, in actual fact, a 2 x variable transformers connected in parallel and operating with a max. output of 62 amps. The DVC was controlled by a Eurotherm "on/off" switch control with high temperature protective palladium thermal-fuse placed in the furnace. The wiring diagram for the equipment is shown in Fig. 3.5b.

The materials from which the components within the reaction tube were made, also had to be changed - see Fig. 3.6. - . In the hot zone, graphite was used to support the crucible instead of stainless steel. Exploratory tests under a protective atmosphere of argon at ~1350°C with graphite crucibles containing liquid aluminium or aluminium alloy

with manganese or iron or silicon showed that they had good resistance to attack by the melt. Graphite crucibles were, therefore, used in all subsequent experiments.

Because the walls of the pedestal made of graphite were close to those of the alumina reactor tube, the radiation shield was not necessary. Instead a hollowed-out graphite plate was placed on the crucible partially closing the space above the crucible.

In order to facilitate some experiments under dynamic condition in which the silica rod was rotated, whilst immersed in the molten metal, a silica rod of longer length was fitted into an adapter passing through the top of the reactor and connected to a variable speed "Gallakamp" stirrer, as shown in Fig. 3.7.

3.2.3. Experimental programme and procedure

3.2.3.1. Static experiments - these were done by immersing initially silica rods of 3.0, 5.0 and 10.0 mm in diameter into pure molten aluminium and later by immersing silica rods of 10.0 mm in diameter only into molten aluminium alloys. These alloys as previously mentioned were made with 5.0, 10.0 and 15 atomic % of manganese, iron and silicon. Such alloys allowed a study to be made of the effect of the respective elements on the reaction process.

Four different temperatures were used: 1110, 1170, 1220 and 1265°C. The immersion time of the silica in the molten metal varied from 2.0 to 240 minutes.

3.2.3.2. Rotating experiments - a series of experiments were performed in which a silica rod of 10 mm diameter was rotated in molten pure aluminium and in aluminium alloyed with 5 atomic % Mn or 5 atomic % Fe. The rod was rotated in the liquid metal at 5, 15 and 35 revolutions per minute and at two different temperatures: 1170 and 1265°C.

An outline of both static and rotating experimental programmes carried out at elevated temperatures are shown in Table 3.4.

3.2.3.3. Procedure - for all the experimental runs, 50 - 60 g of

pure aluminium machined as previously described in the preliminary work, and of the desired alloy in granular form were placed in the graphite crucible and positioned in the hot zone of the reactor tube. The alloy was melted under an atmosphere of argon purified in the same manner as described before for the preliminary work - section 3.1, Fig. 3.2.

The temperature of the melt was measured by immersing a Pt - Pt 13% Rh thermocouple in an alumino-porcelain sheath. The thermocouple was also used to stir the liquid metal before immersion of the silica rod. When the melt reached the desired temperature, the prepared silica rod was positioned just above the liquid surface for approximately 30 sec., with argon being blown through a lance onto liquid surface. This minimises condensation of aluminium suboxides on the silica prior to immersion.

The same procedure was employed in the experiments in which the silica rod was rotated. The positioning of the rod at the central axis of the crucible was ensured by the presence of the graphite plate placed above the crucible.

The techniques adopted for the termination of an experiment and the sampling of the melt for chemical analysis were the same as those adopted in the preliminary experiments - Section 3.1.

3.3. Chemical analysis - the manganese and iron contents of the respective alloys with aluminium were analysed using an atomic absorption method, performed with a Unicam SP 90 Atomic Absorption Spectrometer as described in the Unicam Manual of instructions[81]. Standard operational conditions were adopted for the instrument.

Silicon was determined by the Gravimetric Regelsberger method. The metal was dissolved in sodium hydroxide solution and the solution, containing all the silicon as sodium silicate, was acidified with sulphuric acid, and fumed. The precipitated silica was filtred off, ignited and determined by loss of mass on fuming with hydrofluoric acid and sulphuric acid[82].

3.4. Specimen preparation for measurements and micro-structural analyses - as described earlier each specimen was withdrawn from the

melt and allowed to cool without touching any surface, thus avoiding any loss of integrity of the product layer as a result of differences in thermal contraction among the reaction products. The friability of the reaction layer required the specimens to be mounted in resin before cutting. Each specimen was sliced into three or four sections using a diamond cut off wheel. These were thoroughly cleaned in acetone and remounted in resin before grinding and polishing.

The mounted specimens were carefully ground on 240, 400 and 600 grit wet carborundum paper. For polishing, a retainer made by drilling three 32 mm diameter holes in a piece of 80 mm diameter by 22 mm thick perspex was placed over the polishing wheel. The specimens in the holes had sufficient clearance to turn, as a result of the movement of the automatic polishing arm. Polishing was performed on Hypocel Pellon - PSU type adhesive discs, initially impregnated with 45 μm diamond paste until the 600 grit scratches were removed, and then successively on discs impregnated with 25, 14, 6 μm diamond paste for periods of 2, 3 and 5 hours respectively. The specimens selected for microscopic examination and analyses were further polished for 1 - 2 hours on Microcloth with 1 and 0.25 μm diamond paste. Despite the precautions, it was practically impossible to achieve an entirely flat surface on the specimens, as a result of the surface relief effect produced at the outer edge. This, however, did not affect the measurements nor lead to any misinterpretations of the microstructures.

3.4.1. Reaction measurements - the thickness of the product layer and the radius of the unconverted silica surface were measured by placing the specimen on the rotary mechanical stage of a Zeiss Photomicroscope. The microscope was fitted with inter-changeable objective lenses of reasonably long focal length, but short depth of focus, and with x8-complan eyepieces with a wide field of view. In one of the eye pieces was a graticule marked with 0.1 mm divisions and calibrated for each magnification.

The selection of a truly representative section of a reacted specimen for examination, had to be carried out as carefully as possible, in view of the different planar configurations of the product layer. This is illustrated schematically in Fig. 3.8 a-d. From just below the liquid surface to approximately one fourth of the length of the immersed

rod, a deeper degree of penetration of the reaction front ("the neck") was observed. In addition, a deeper degree of penetration of the reaction front was observed over the lower one fifth of the immersed rod. As indicated in Fig. 3.8,a, the extremes of each specimen were cut off and rejected as being non-representative of the true extent of the reaction.

The section cut fron the length "l" could give any of the three product layer-unconverted rod configurations, shown in Figs. 3.8,b, c or d. In the case of 3.8,b, the product layer was non-uniform and the silica could be continuous from the interior to portions of its surface. In 3.8,c, the unreacted core was covered by a layer of uniform thickness. A uniform but irregular "solid-solid" interface, as shown in 3.8,d, was commonly developed when specimens were immersed for longer periods of time.

The thickness of the product layer $\Delta r = r_o - r_i$, where Δr is the thickness, r_o is the original radius of the rod and r_i is the radius of the unreacted core at any time, was estimated by calculating the average of 32 equi-distant measurements made randomly around the circumference of the rod. No matter what the microstructure was, the reacted distance was always measured from the periphery of the unreacted silica to the periphery of the rod.

In cases such as those depicted by Fig. 3.8,b, where the product layer in the very early stages of the reaction consisted of a small number of segments, the 32 measurements were made in regions covered only by the product layer. Again an average value was calculated.

3.5 X-ray diffraction studies - due to the number of phases (metallic and non-metallic) involved as the result of reaction of silica with aluminium and/or aluminium alloys with iron and manganese, and due to the relatively small quantity of sample material to be subjected to x-ray diffraction analysis, a systematic procedure of sampling had to be used. This consisted of crushing individual specimens in a tungsten carbide mortar and sieving, until a maximum particle size of 100 μm was achieved. The powder obtained was then divided into tho halves. X-ray diffraction analysis was carried out on one part and the obtained diffraction patterns were compared by superimposition to standard x-ray diffraction patterns for the metallic phases possibly involved in the reaction and previously ---- cont.

prepared as follows:

3.5.1. Aluminium - high purity aluminium ("Super-pure", British Al.Co.) with chemical analysis as indicated in Table 3.1. was used for this purpose. A slug was washed in 5 ml(40%) hydrofluoric acid + 95 ml distilled water, rewashed in distilled water and then immersed into alcohol for crushing. Small particles were further ground in an agate mortar till a particle size less than 75 μm was obtained. X-ray standard diffraction pattern was obtained by processing the aluminium powder as further described in section 3.5.6.

3.5.2. Silicon - observation under light microscope has shown pools of this element precipitated within the porous product matrix. This will be shown in Chapter 4. For x-ray purposes, thus, silicon was obtained by firing broken pieces of some pure aluminium-silica reactious specimens, all completely reacted in the range 1110 to 1265^{o}C, at temperature about 1000^{o}C for some hours and under argon atmosphere. Similar to depression of mercury in a capilliary tube, the silicon dispersed together with aluminium in the porous matrix was sweated-out (liquated) from it, and then collected, after cooling, for grinding. In order to reduce major traces of aluminium, the powder was then washed in etchant A - according to Table 3.5. X-ray standard diffraction pattern was obtained by processing the silicon powder as further described in section 3.5.6.

3.5.3. Aluminium-silicon alloys - standard x-ray pattern for these alloys has not been prepared, since it has been assumed that elemental (primary) and eutectic silicon would precipitate from any hyper-eutectic alloys as reaction products at temperatures and times used in the experiments.

3.5.4. Aluminium-manganese and aluminium-iron alloys - endeavour to obtain x-ray diffraction patterns for both manganese and iron alloyed with aluminium in the range 5.0 to 15.0 atomic%Mn,Fe, was not attempted. It was assumed that aluminium-manganese and aluminium-iron solid solutions which remain in the formed product layer would present somewhat different compositions from the original ones after reaction at temperatures and times.

3.5.5. Aluminas - the other part of obtained powder (Section 3.5.) was further ground in an agate mortar to produce powder of a particle size less than 75 μm. From this part, metallic constituents were removed by deep-etching using the reagents described in Table 3.5. In order to minimise contamination, the powder was thoroughly washed in absolute alcohol and then dried at 120°C. X-ray diffraction analysis was carried out and the resulting patterns were again compared by superimposing to those obtained for standards of alumina polymorphs supposedly involved in the reaction and previously prepared as follows: aluminium hydroxide/ $Al(OH)_3$/, Gibbsite, with particle size < 1 μm, supplied by M & B Chem. Lab. was fired in air. Recrystallised alumina crucibles were used to avoid co-lateral reaction. The temperatures and times programmed for this purpose were in first approximation those suggested in literature[41] and may be schematically represented as follows:

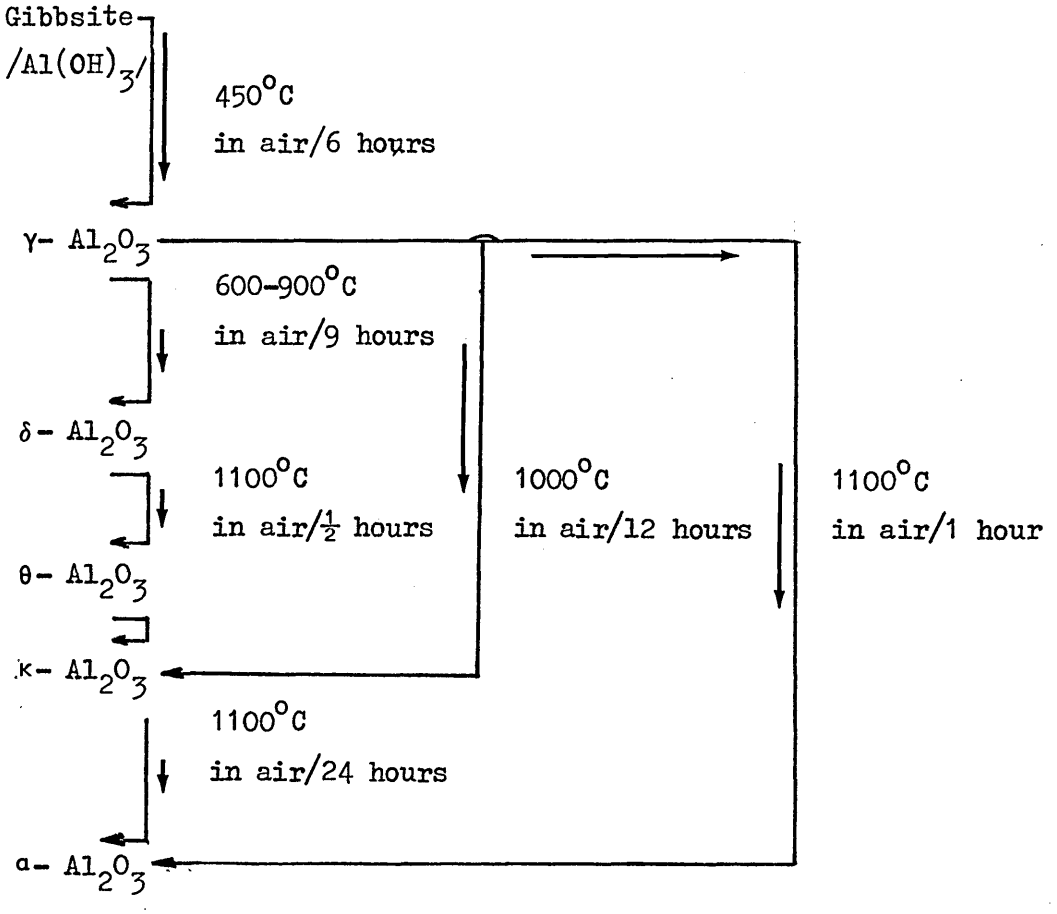

Slight modifications to this programme have been introduced and this will be presented and commented on in Chapter 4, together with results obtained.

3.5.6. X-ray techniques - For both standards and reaction specimens, the powders were packed into lithium-borate capilliary tube (0.3 or 0.5 mm diameter). The tube was placed in an 114.6 mm diameter Debye-Scherrer camera and exposed for 3 to 5 hours, using Cu-K_α-radiation

(Cu. K_{α_1} = 1.54051 Å; Cu. K_{α_2} = 1.54433 Å) which was filtered through a Ni-foil.

Standardisation of this method was facilitated by the controlled processing of the exposed films and, as a comparative technique was used, no other standardisation was necessary.

3.6. Scanning-electron microscopy - The general features of the microstructure of reacting specimens were also examined using a Phillips P EM-500 Scanning Electron Microscope (SEM). Theoretical principles and detailed procedures for using the SEM may be found elsewhere[84]. To improve their electrical conductivity the small broken pieces of reacted material were mounted with non-conductive glue (Plastic Padding) on a Silverdag paint. After this, the Silverdag was left to dry in vacuum. The specimen was then coated with gold to eliminate charging-up effects.

When an excessive amount of a previously liquid phase was present, which masked particular aspects of the internal features of the specimens, deep-etching had to be applied. The etchants used for this purpose have been summarized in Table 3.5.

Specimens at several stages in the process were qualitatively analysed using Element distribution x-ray maps and continuous line scanning patterns performed by Energy Dispersion Spectroscopy (EDS) located on several points on cross-sections of reacted specimens. Corresponding elemental analysis using Energy Dispersive Analysis of x-rays (EDAX) were also performed. Elemental distribution within examined areas has been identified by x-ray map[85]. For accurate analysis the surface of the specimens were polished on 0.25 μm diamond paste and then prepared as described above.

4. EXPERIMENTAL RESULTS

4.1. The kinetics of the reaction between vitreous silica and liquid aluminium

4.1.1. Introduction - in broad terms, the reaction between liquid aluminium and solid silica may be considered to involve two processes with the slower one effectively controlling the rate of the overall reaction. The two processes are:

a) The chemical reaction between aluminium and silica at the reaction front including the unreacted silica and the formed solid product layer.

b) The diffusion of aluminium (possibly of ions) through the formed solid product layer towards the unreacted core of silica.

Many of the equations relating the percentage of the total reacted silica $F(R_x)$, (experimental measurements have been made of the respective formed product layer, as mentioned in section 3.4.1.) to the time of reaction are of the form $F(R_x) = kt$, where k is the reaction rate constant, t is the time and $F(R_x)$ is the fraction reacted, which in first approximation depends upon the geometry of the solid reactant silica and on the mechanism of reaction. When the reaction rate is proportional to the surface area of the unreacted silica, and if it may be assumed that nucleation occurs instantaneously over the entire surface, so that there is a uniform covering of the silica by a solid product layer, then the relationship between percentage of the reacted silica and time may be expressed by the equation:

$$1 - (1 - R_x)^{0.5} = \frac{2kt}{\rho_{SiO_2} d_o} \qquad 4.1.1.1.$$

and where d_o and ρ_{SiO_2} are, respectively, the diameter and the density of the original reactant silica. For the reaction front progressing at a constant velocity, a plot of $\left[1 - (1 - R)^{0.5}\right]$ versus time should yield a straight line. Equation 4.1.1.1. may be rearranged as:

$$R_x = \left[(4kt/\rho_{SiO_2} \cdot d_o) - (4k^2t^2/\rho^2_{SiO_2} \cdot d_o^2)\right] \qquad 4.1.1.2.$$

if $(4kt/\rho_{SiO_2}.d_o) \gg (4k^2t^2/\rho_{SiO_2}.d_o^2)$, then $Rx \simeq 4kt/\rho_{SiO_2}.d_o$

the conversion of silica is linear with time. Expressing R_x in percentage, hence $[1 - (1 - R_x)^{0.5}]$ can also be expressed in percentage and the slope of the lines is expressed as the reciprocal time (sec^{-1}).

All the results reported here were calculated with $\Delta r = r_o - r_i$, as it has already been described elsewhere - see section 3.4.1. However, it should be pointed out, that if atomic mass quantities are considered, and assuming the densities of aluminium, transparent vitreous silica, alumina and silicon as 2300, 2200, 3800 and 2700 $kg.m^{-3}$ respectively, then according to the stoichiometric ratio of $\frac{2}{3}$ between product and reactant of reaction

$$4Al + 3SiO_2 = 2Al_2O_3 + 3Si \qquad 4.1.1.3.$$

the reactant and product volumes are:

$$4 \times 10^{-5}\ m^3 + 7.15 \times 10^{-5}\ m^3 = 11.15 \times 10^{-5}\ m^3$$
$$5.37 \times 10^{-5}\ m^3 + 3.65 \times 10^{-5}\ m^3 = 9.02 \times 10^{-5}\ m^3$$

This gives an overall volumetric contraction for a complete reaction 4.1.1.3 of 19,1%. However, whenever it was possible to measure the diameter of the mounted rod after reaction at any time, the shrinkage was always inferior to 2%. This will be discussed in Chapter 5.

It is worth mentioning that equations such as 4.1.1.1. only describe the overall kinetics of the solid-liquid reaction mechanism. They do not consider the effect of localised factors such as surface orientation, the presence of defects in the solid reactant, impurities in the liquid, and do not consider either the non-stoichiometry and general mineralogical changes in the structure of the product layer. Although such factors are unlikely to be of great importance in a diffusion controlled reaction, they may significantly affect the rate of reaction, if it is chemically controlled.

4.1.2 The liquid pure aluminium-silica reaction system - the experimental results obtained by immersing silica rods of different diameters in liquid pure aluminium for various lengths of time at different temperatures are presented in Table 4.1.2.1.; the results concern the measured values of the thickness of the product layer

formed, i.e. the difference between the original radius of the silica and the radius of the unreacted silica core after some immersion time t, and in terms of the function $[1-(1-R_X)^{0.5}]$. This function was plotted against time. These plots are presented in Figs. 4.1.2.1. -3, the diameters of silica rods as follows:

i. Temperature range 760 - 860°C: Figs. 4.1.2.1a, b, c, for respectively 3.0, 5.0 and 10.0 mm in diameter of the silica rods.

ii. Temperature range 920 - 860°C: Figs. 4.1.2.2a, b, for respectively 5.0 and 10.0 mm in diameters of the silica rods. These plots are presented together with the respective results obtained from the 860°C experiments for comparative purposes.

iii. Temperature range 1110 - 1265°C: Figs. 4.1.2.3a, b, c, for respectively 3.0, 5.0 and 10.0 mm in diameter of the silica rods.

The standard deviations related to each plot and described in the items i, ii, iii, above were calculated by means of a least-squares regression analysis, using the technique presented in Appendix A-4.1. These standard deviations are indicated in the respective legends of the plots as well as the straight line equations calculated for the plots. This manner of representing error will be invariably used for the other reacting systems involved in this work.

Inspection of the graphs presented shows that for all the various diameters of silica rods used in the ranges of temperature 760 - 860°C and 1110 - 1265°C, the data obeyed the linear relationship predicted by equation 4.1.1.1., with only slight deviations from this. The results obtained from experiments carried out at 920 and 980°C, with two different diameters of rods, i.e. 5.0 and 10.0 mm diameter are widely scattered. However, repeated experiments at these two temperatures, although not yielding reproducibility of results, consistently produced conversion rates which were lower than those obtained at temperature ranges immediately below this range.

The slopes of the linear plots shown in Figs. 4.1.2.1. and 4.1.2.3. were calculated and are presented in Table 4.1.2.2. These values were calculated by means of a least-squares linear regression analysis, using the technique described in Appendix A-4.1. For repeated experiments, an average value was taken. The slope of each line represents the rate of reaction. The results of linear regression analysis indicated a high degree of correlation with a straight line relationship.

The calculated values of the reaction rate constant k also presented in Table 4.1.2.2. are plotted as a function of temperature in Fig. 4.1.2.4. Examination of this graph shows that:

i. in the temperature range 760 - 860°C the lines follow a coherent relations-hip between reaction rate and temperature; the reaction rate exhibits a certain independence to the diameter of the silica rod. This may suggest a definitive control for reaction at this temperature range.

ii. above 860°C and below 1110°C the reaction is decelerated, with the rate reaching very low values. This suggests that in this temperature range either physical effects or a change in the reaction mechanism may be involved.

iii. in the temperature range 1110° - 1265°C the slope of the curves again increases and a better correlation is again obtained. The values of the reaction rate constant increase with temperature and the line exhibits a similar shape to that previously observed in the temperature range 760 - 860°C, even though reaction rates are slower at first.

The exponential shape of the curves in Fig. 4.1.2.4. for both lower and higher temperature intervals, i.e. within 760 to 860°C and within 1110 to 1265°C is indicative of a strong dependence of the reaction rates on temperature. In this case the reaction rate would be expected to follow an Arrhenius type relationship with temperature an given by:

$$k_c = k_o \cdot \exp(-E/RT) \qquad 4.1.2.1.$$

where k_c is the reaction rate constant $Kg.m^{-2}.sec^{-1}$

k_o is the proportionality factor for the reaction system (frequency factor)

E is the activation energy $KJ.mol^{-1}$

R is the ideal gas law constant $J.deg^{-1}.mol^{-1}$

T is the absolute temperature K

A comparison of the activation energies of the process using the data presented in Figs. 4.1.2.1. - 3. is shown in Fig. 4.1.2.5. Activation energy values were determined from the slope of the lines and are indicated in Table 4.1.2.2.

The consistency of the values seems to suggest that the reaction between liquid pure aluminium and vitreous silica involves the same rate controlling mechanism in both extreme temperature intervals. However, the positive "slope" of the lines drawn through the results obtained in the intermediate temperature interval, i.e. at 920°C and at 980°C suggests that physical effects of substantial importance are due to occur in this interval, thus, provoking a drastic deceleration in the progress of reaction.

The confirmation that there is a direct proportionality between the slopes measured from the curves presented in Figs. 4.1.2.1. and 4.1.2.3. and the reciprocal diameter of the silica rods, as it has been defined in equation 4.1.1.1. is represented in Fig. 4.1.2.6a, b, and relate to both extreme temperature intervals.

The relationship graphically represented so far, will be discussed in Chapter 5. in order to attempt a correlation of kinetic data.

4.1.3. The aluminium-silicon-silica reaction system - the measured values of the product layer thickness and the calculated percentage conversion of the rod at various times of immersion in liquid aluminium-silicon alloys are presented in Table 4.1.3. The function $[1 - (1-R_X)0.5]$, according to equation 4.1.1.1., was plotted

against time for each set of results for 5.0 to 15.0 atomic % Si at temperatures and these are respectively shown in Figs. 4.1.3 a, b, c.

The graphs show that the data obeyed the linearity predicted by equation 4.1.1.1. It can also be observed that for any of the specific concentrations of silicon in the bulk aluminium, the conversion values were very close to those obtained for pure liquid aluminium. This suggests the overall rate of reaction as being independent of the silicon concentrations in aluminium, at least up to 15 atomic % Si. Therefore, mass transfer of silicon in the molten metal phase may be eliminated as the controlling step under the experimental conditions employed in this work.

The relationship with temperature of the measured reaction rate constant for this reacting system will be introduced in the next section together with the ones for the aluminium-manganese and aluminium-iron reacting systems - see Tables 4.1.5 a, b, c.

4.1.4. The aluminium-manganese-silica and aluminium-iron-silica reaction systems - it was believed that the mechanism and hence the kinetics of the reaction between molten aluminium and silica might be affected by the presence of other elements other than silicon dissolved in the aluminium. For reasons indicated in Chapter 2, it was then decided that the effect of manganese and iron would be investigated.

In order to facilitate comparisons with the results obtained for the liquid pure aluminium-silica reaction system, experiments were carried out in the temperature range 1110 - 1265°C. Alloy compositions of 5.0, 10.0 and 15.0 atomic % of manganese or iron in aluminium were employed. Examination of the relevant equilibrium phase diagrams for these alloys in the temperature range of interest indicates that the alloy composition was above the liquidus and thus, no precipitation of intermetallic compounds would take place in the liquid metal during reaction. In all of these experiments 10.0 mm diameter silica rods were employed.

The results of the experiments carried out with aluminium alloys containing 5.0, 10.0 and 15.0 atomic % Mn and 5.0, 10.0 and 15.0 atomic % Fe at four different temperatures are presented in

Tables 4.1.4.1. and 4.1.4.2. respectively. For each set of experiments the function $\left[1 - (1-R_x)^{0.5}\right]$ has been plotted against time and at temperatures and the results are presented in Figs. 4.1.4.1. a, b, c and 4.1.4.2. a, b, c for aluminium-manganese and aluminium-iron alloys, respectively. Reproducibility of individual experiments was very good, especially in those carried out at higher temperatures. Deviations from linearity of some experiments may be explained by physical defects in the product layer or by compositional non-uniformity of the liquid aluminium alloy during reaction. The alloy containing higher concentrations of manganese and or iron at the lower temperature of the range considered, appeared to require a longer period of time before reaction commenced. This may be due to the need for some form of initial nuclei growth control before the coherent progress of reaction becomes predominant.

The reaction rate constant for each set of experiments carried out at a particular temperature and composition of aluminium alloy, i.e. of aluminium-silicon, aluminium-manganese and aluminium-iron alloy was calculated in the same manner as described in section 4.1.2. for the pure aluminium-silica reaction system. This is presented in Tables 4.1.5 a, b, c for silicon, manganese and iron as the alloying elements, respectively.

The values of the reaction rate constants are plotted as a function of temperature in Figs. 4.1.5 a, b, c for alloys of aluminium-silicon, aluminium-manganese and aluminium-iron, respectively, and they are compared with the values of the reaction rate constant of the pure aluminium-silica reaction system treated under identical thermal conditions as here.

It may be observed from these graphs that the reaction system aluminium-silicon alloys, and as mentioned earlier, the reaction rate constant is approximately the same as for the pure aluminium-silica reaction system, and furthermore, it is independent of the silicon concentrations in the bulk aluminium at least under the experimental conditions of this work. On the other hand, however, it may be also observed that the rate of reaction appears to be dependent upon the manganese and iron concentrations in the bulk aluminium at lower temperatures. With the increase of temperature, the values of the reaction rate constant for both the aluminium-manganese and the

aluminium-iron alloys increase again and show the tendency to approach the values for the pure aluminium-silica reaction system.

The shape of these curves for the temperature interval shows a strong dependence of the reaction rates upon temperature, so that it would be expected that the reaction rate follows the relationship with temperature expressed by equation 4.1.2.1. This function is plotted in Fig. 4.1.6. Activation energy values were established from the slopes of the lines and are indicated respectively for aluminium-silicon, manganese and iron alloys in Tables. 4.1.5 a, b, c.

4.1.5. Rotating experiments - all the results presented so far involved the use of a static silica rod immersed in liquid aluminium and/or in aluminium alloyed with silicon, manganese or iron. The possibility was considered that the silicon produced by the reaction might prevent the access of the reacting liquid phase through the solid reaction product towards the unreacted silica rod. Some experiments were, therefore, carried out, in which the silica rod 10 mm in diameter was rotated whilst immersed in liquid pure aluminium and in liquid aluminium containing 5.0 atomic % Mn or 5.0 atomic % Fe, and at two different temperatures, i.e. at 1110°C and at 1265°C. The measured values of the product layer thickness and the calculated percentage conversion of the rod at various times of immersion are presented in Table 4.1.6. and graphically shown in Figs. 4.1.7 a - f, respectively for pure aluminium and aluminium-manganese and aluminium-iron alloys in order to compare results, a reference plot of the respective static experiments is also introduced.

The obtained results indicate that rotation of the silica rod during immersion did not produce any considerable change in the observed rate of reaction. Values of the measured activation energies presented in Table 4.1.7, being very close to those for similar static experiments confirm the statement. The logarithmic rate constant versus the reciprocal absolute temperature has comparatively to similar static experiments been shown in Fig. 4.1.6.

The similarity to the reacting system, liquid pure aluminium-vitreous silica, and the consistency of the values of the activation energy suggest a single rate controlling mechanism for reaction between

liquid aluminium alloys with different but low concentrations of the alloying elements silicon, manganese and iron in the bulk aluminium, at temperatures between 1110 and 1165°C.

In general terms, it might be pointed out that the presence of alloying elements at least at a concentration not higher than 15 atomic % in the aluminium does not much affect the process. The extent of reaction over the temperature range is likely to be governed by kinetic factors. Small deviations from linearity of the progress of the reaction front towards the end of the process may most probably be associated with physical phenomena, which can either accelerate or decelerate the reaction. For instance, craking of the solid reaction product may occur, therefore, increasing the area of the unreduced silica rod and thus accelerating the process. On the other hand, some form of crystallization of the solid reaction product may result in a decrease of available passages through which the aluminium may advance to the unreacted surface of the silica rod. Microstructural evidence presented in section 4.3. illustrates the basis for these assumptions.

4.2. X-ray diffraction analysis.

4.2.1. Aluminium and silicon - there were no major problems in obtaining reliable standard x-ray diffraction patterns of these elements supposedly involved in the reaction as product phases. By superimposition of the x-ray patterns of reaction specimens and standard specimens, the diffraction lines of aluminium and silicon were characterised. The corresponding diffraction data of aluminium and silicon standards are given in Table 4.2.1., together with ASTM diffraction data for comparison.

4.2.2. Polymorphs of alumina - an extreme difficulty was experienced in estimation of the standard polymorphs of alumina prepared according to the heat treatment scheme presented in section 3.4. The x-ray diffraction patterns obtained had very much line broadening for some polymorphs, markedly between γ and δ-aluminas and also between ($\delta + \theta$), θ and ($\kappa + \theta$) -aluminas, giving rise to overlapping of many reflection lines. This was the major reason why the heat treatment programme was progressively altered. The best obtained results were as follows:

Heat treatments:	Obtained phases :
1. Gibbsite; 2.5 hours at 550°C	γ^*
2. Treatment 1. plus 6.0 hours at 800°C	$\gamma^* + \delta$
3. Treatment 2. plus 4.0 hours at 850°C	$\gamma^* + \theta$
4. Treatment 1. plus 2.5 hours at 1000°C	$\theta^* + (\kappa + \theta)$
5. Treatment 1. plus 4.0 hours at 1150°C	α^*

/* denotes apparently more intensive characteristic lines/

The corresponding x-ray diffraction data are presented in Table 4.2.2., together with respective ASTM data for comparison. Even under the altered firing programme indicated above, the broadening of characteristic lines among several aluminas could not be eliminated. This made the prospects for improving the accuracy and specifically identifying some polymorphs unsuccessful, particularly delta, delta + theta and theta + kappa aluminas which, in turn, would have been used as standards. The main difficulty lies in the large number of simultaneous phases exhibited during firing, when crystallization of some polymorphs, apparently, either accelerates or retards other consecutive transformations. It is likely, however, that these transformations follow characteristic sequences, which, in turn, are time and temperature dependent.

4.2.3. X-ray analysis of products of reaction between liquid pure aluminium and aluminium alloys and vitreous silica.

4.2.3.1. Lower temperature reaction products - the diffraction data of representative specimens at various temperatures and times are given in Table 4.2.3., together with aluminium and silicon (standards) data and alumina polymorphs (standards) data for comparison. The analysis has shown that apart from silicon and aluminium, both always present in all specimens, the product layer resulting from reaction at temperatures within 760 to 860°C consisted of a mixture of alumina polymorphs, markedly of θ and α-aluminas. It is possible, however, at these temperatures, other polymorphs such as gamma, delta, theta or a combination of these were involved as well, but due to considerable

overlapping of characteristic lines, these aluminas could not be clearly identified. In this regard, it should be added that line broadening was further aggravated due to the presence of residual aluminium (not totally eliminated by acid leaching, Table 3.5.) and/or silicon.

Despite the difficulty of identifying independent polymorphs of alumina, the d-spacings worked out show the tendency for the theta-alumina to transform into alpha-alumina with time of reaction. It is likely that other polymorphs, possibly involved but not identified, also will have been transformed to alpha via the theta-phase, during reaction. This will be discussed later.

4.2.3.2. Higher temperature reaction products - the x-ray diffraction analysis of specimens reacted at two specific temperatures, i.e. at 1110 and 1265^{o}C and corresponding times, as indicated in Table 4.2.3., has shown, apart from silicon and aluminium, theta and alpha-aluminas as the only phases present in the reaction product layer. This is evident from d-spacings worked out from characteristic lines and presented in Table 4.2.3. A duplex structure, consisting of both aluminas, thus is to be expected in the structure and this will be further demonstrated under view of both optical and electron micrographs. Similar results were obtained, when silica reacted with aluminium-manganese and aluminium-iron alloys with different compositions of manganese and iron at different times and temperatures. This is indicated in Tables 4.2.4.1 and 4.2.4.2. for both elements, respectively.

4.2.3.3. Intermediate temperature reaction products - aluminium, silicon and the alumina polymorphs theta, theta+kappa and alpha were identified as the products of the reaction carried out at 920 and 980^{o}C. The d-spacings worked out from corresponding lines are presented in Table 4.2.3. It is possible, however, that similar to the lower temperature reactions, other polymorphs were involved as not all lines were eliminated.

The characteristic x - ray diffraction analysis of reaction systems has not indicated any silicates present in the product layer whatsoever. Thermodynamic calculations to confirm this evidence will be

introduced later, in Chapter 5.

4.3. Microstructural examination of the reaction product layer

4.3.1. The pure aluminium - silica reaction system

4.3.1.1. Lower temperature reaction - the reaction products which developed when the silica rod reacted with liquid aluminium at temperatures betwwen 760 and 860° C were examined microscopically. The microstructures which developed in this temperature range did not differ significantly. A typical macrostructural change in the specimens with time at temperature is presented in Fig.4.3.1.1., where a sequence of continuous and symmetric growth of the product layer with increasing time at 860°C has been selected from the series of experiments with silica rods 5.0 mm in diameter. Spalling of the unreacted silica at first and then of the product layer did occur during cooling as a result of large difference in coefficients of thermal expansion between the silica and the product layer as a whole.

In view of the observed similarities among the reacting specimens, therefore, features of various specimens reacted at different temperatures and times are now described in order to identify:

a) The mechanism of the progressive coversion of silica into product phases.
b) The correlation of this mechanism with a kinetic model deduced to explain the reaction between vitreous silica and liquid aluminium.

(All specimens, here described, are identified in Tables 4.1.2.1. to 4.1.6.)

The beginning of the conversion of silica, when it first came into contact with liquid aluminium, in the low temperature range, is schematically idealized as follows:

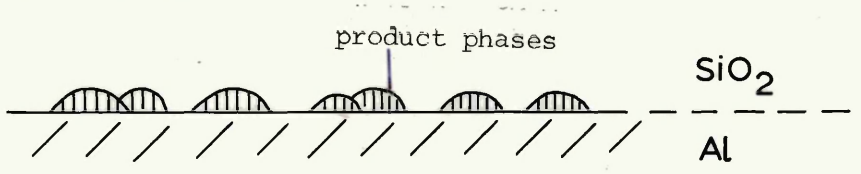

The reaction started in localized areas on the surface of the rod with the nucleation and growth of spherical segments, approximately of same size, Fig.4.3.1.2. It was observed in all specimens examined from the initial periods of reaction that some parts of the interface silica/aluminium did not react at first. With increasing temperature this effect became less evident. These observations suggest that the surface film of aluminium oxide on the melt is not normally drawn down into the liquid when the rod was immersed into it. However, the possibility that some portions of surface film have incidentally adhered to the rod at the moment of its immersion and, thus, acted as a barrier for reaction, cannot be excluded. Fig.4.3.1.3 shows that later removal of the melt surface film of aluminium oxide adhered to the rod allowed reaction to start immediately and to progress normally producing the feature shown in this micrograph.

As the reaction continues, the segments grow laterally, Fig.4.3.1.4, and impinge on each other to form a continuous reaction layer, Fig.4.3.1.5:

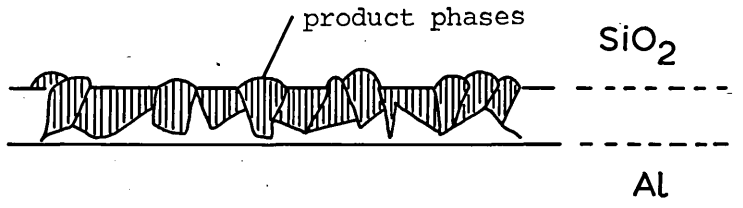

The segments grow also in the radial sense, i.e. normal to the receding silica surface, whilst new segments continue to form. This growth did not progress noticeably until a continuous layer had been formed on the periphery of the rod.

The process of formation of segments and their lateral growth is promoted by temperature, as previously mentioned. The growth of a continuous product layer is very fast at the higher temperatures in the range 760-860°C, occurring in only a few minutes, Fig.4.3.1.6. At this stage of reaction, the alumina formed is not the stable α-phase, but one of the metastable aluminas, probably Θ-alumina. With increasing time and, thus, with increasing thickness of the product layer and

also favoured by the presence of a liquid phase throughout this layer, polymorphic transformation of aluminas did occur. This will be introduced later in this section.

At intermediate stages of reaction, columnar cells of alumina are developed associated with the receding surface of silica, Fig.4.3.1.7. The texture of these columnar cells was beyond the resolution of the optical microscope. Therefore, they are shown in the scanning electron micrographs of different specimens presented in Figs.4.3.1.8, a-c. It is clear from this evidence that the columnar alumina growth is of a porous texture.

Some cracking occurred within the product layer during reaction, Fig.4.3.1.9. Large grains of recrystallizing product layer, shrinkage and porosity, independently or collectively, appear to be responsible for the crack itself. By cracking, at advanced stages of reaction, Fig.4.3.1.10, the interface of unreacted silica/product layer loses its original symmetry and thus aluminium must flow to the vicinity to the affected area for completion to be achieved.

Further examination of the interface region between the unreacted silica and the product layer (interaction front) indicates that:

1) It remains parallel to the receding silica surface and it is usually very regular in thickness, Fig.4.3.1.11. However, as noted in Fig.4.3.1.12,a, independently of temperature, some specimens presented an uneven interface between the interaction front and silica after the beginning of the reaction, when an aggregate two phase structure protrudes inside the silica and rapidly encases parts of it. The extensive precipitation of primary silicon in the bulk metal, Fig.4.3.1.12.c., indicates a large outward flow of this element through the product layer. It is seen that, as a consequence of the general thickening of the product layer with increasing time, these protrusions spread laterally, Fig.4.3.1.12,b. (compare to Fig.4.3.1.4).

2) It consists of material much finer than the neighbouring coarser matrix left behind, as the reaction progresses, Fig.4.3.1.11. When thermal cracking and/or recrystallization occur within the product layer, these defects act as nucleation centres for the formation of a structure similar to that of the actual interaction front, Fig.4.3.1.13.

3) It is rich in silicon as can be deduced from the light microstructural phase seen in the interface region in Fig.4.3.1.14. This is also shown by the elemental aluminium and silicon distribution X-ray maps and corresponding line scans that were carried out across the product layer and reaction region in a 30mm in diam. specimen reacted at 760°C for 25 minutes, Fig.4.3.1.15. These results clearly show the high concentration of silicon which falls rapidly moving outwards across the interface region and then falls very much more gradually across the bulk of the product layer. The concentration of aluminium falls in the corresponding but opposite way, gradually, moving across the product layer and then, rapidly across the interface region.

4) It is in intimate contact with the course matrix on one side and provided spalling did not occur on the silica side, the interaction front was bonded to it.

Typically, the fine, complex and, to a certain extent, unstable interaction front was transformed into the invariably coarse matrix left behind as the reaction progresses. Throughout this coarse matrix, and favoured by the columnar growth of alumina, liquid aluminium-silicon alloy was able to penetrate and always had access to the interaction region. Due to the sponge-like character of the alumina formed at the interaction front, the liquid is drawn-in, possibly, by capilliary effect also associated with volume changes. Fig.4.3.1.16. shows the porous nature of the alumina product layer. An attempt to observe eutectic alloy or silicon precipitated on cooling from the liquid within the pores was unsuccessful. The only response to etching was a decrease in the resolution of the microstructures, as Fig.4.3.1.17. shows.

In view of these evidences, the process of reaction for the lower temperature system is schematically idealized as follows:

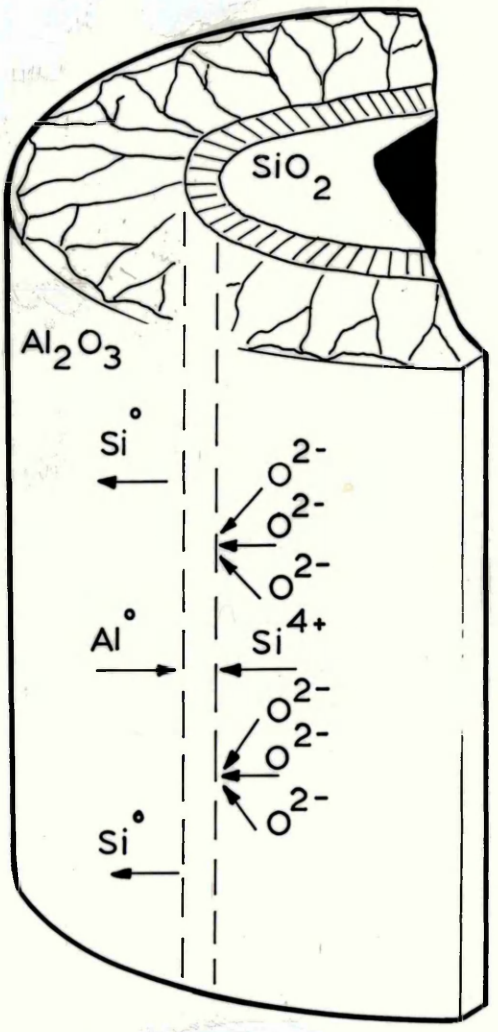

Observations indicated that the dimensions of the columnar alumina and, therefore, the spacing between these varied and that this variation may be temperature and time-dependent. Although this relationship was not established at the lower temperature interval it was confirmed by the microstructures resulting from reaction in the higher temperature range. The possible effect of this on the mechanism of reaction is discussed in Chapter 5.

The x-ray analysis data described in section 4.2.3.1.1 has indicated that Θ and α-aluminas exist in the product layer possibly together with more less stable phases as well. It has also been suggested (see section 4.2.3.1.1.) that these metastable aluminas recrystalize into more stable polymorphs in time . Fig.4.3.1.16. indicates that the product layer is porous, but consists of a single alumina phase.

It is possible, however, that the existence of different polymorphs contributes to the recrystallization of the alumina which was observed to occur during the more advanced stages of the reaction as shown clearly in Fig.4.3.1.18. Aluminium-silicon alloy was observed to segregate at the boundaries of these large grains, Fig.4.3.1.19. It was extremely difficult to examine these boundary regions. Fig.4.3.1.13. and 18. show the effect of etching and the appearance of these regions.

4.3.1.1.1.Heat treatment reactions - the reaction potential of the aluminium retained within the matrix was additionally investigated by heat treating a specimen 5.0mm in diam. previously reacted at 840^{o}C for 15 minutes. The specimen was placed in a platinum crucible and heated at 1220^{o}C for seven hours, under an atmosphere of argon. After cooling, the specimen was repolished with 1µm diamond paste, washed in acetone and examined microscopically. The result of this treatment is shown in Figs.4.3.1.20 a-c. This structure indicates that residual aluminium in the matrix from the interrupted reaction at 840^{o}C clearly reacted with the remaining silica to complete the conversion of this specimen.

The original product layer was partly dried-out of residual aluminium and has produced a silicon layer at the original interface prior to heat treatment. Therefore, it is considered that diffusion of silicon had not occurred beyond this interface. Comparable to the situation described in Fig.4.3.1.12, silicon supersaturates the remaining aluminium and it precipitates in any structure defects within the reaction specimen.

Fig.4.3.1.20,c shows, at higher magnification than Fig.4.3.1.20,a a portion of the outer limits of the "newly reacted system". The "old" interaction front recrystallized during the heat treatment and, due to its intimate contact with the coarser matrix behind it, produced a continuous layer of silicon. Similar precipitation of silicon within the original product layer, due to the depletion of aluminium, can also be observed and this is illustrated in Figs. 4.3.1.21-23.

The aluminium required for reaction is drawn to the unreacted silica along existing defects. Fig.4.3.1.21 shows a pre-existing crack now rich in silicon. Fig.4.3.1.22-23 shows discontinuous precipitation of silicon in the interior of large peripheral grains produced during the original reaction. Multiplication of precipitated silicon occurs by a branching mechanism with a corresponding depletion of aluminium in the matrix of the original reaction product layer. There was no evidence of reaction between aluminium and/or silicon and the alumina structure. Some transformation of alumina did occur during heat treatment, the result of it, possibly, assisting the squeezing out of molten aluminium, which on cooling solidifies on the alumina as spheres, Fig.4.3.1.24 and 25. This indicates a non-wetting relationship between the alumina and aluminium and/or silicon or both.

4.3.1.2. Higher temperature reaction

Fig.4.3.1.26. shows the core of a specimen 5.0 µm in diam. completely reacted in 45 min. at 1170°C. The product phases extend from the centre through a honeycombe type tunnel texture of recrystallised alumina like in an arterial system. Before this, the product layer developed in the same manner as previously presented in the lower temperature interval : nucleation and lateral impingement of spherical segments and radial thickening inwardly to the receding silica surface, Fig. 4.3.1.27-28.

The developed tunnel structure allows the liquid metal to penetrate readily and suggesting, thus, a constant potential of access for the continued progress of reaction. This situation is schematically idealized as follows:

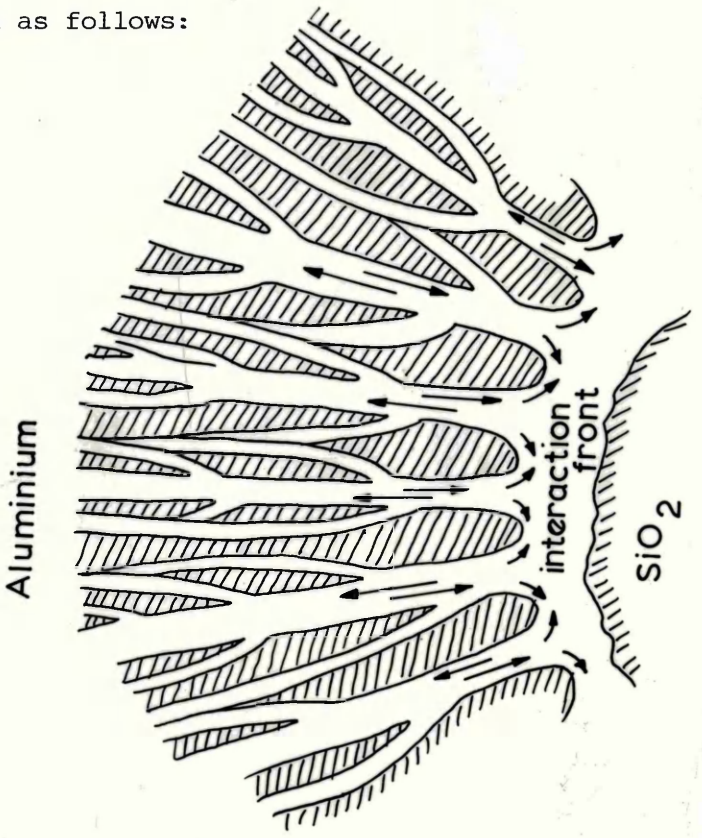

front

Many of the microscopic aspects of the interaction/present identified in the lower temperature reaction specimens were also evident in the higher temperature reaction. These are as follows:-

1) The interaction front moves parallel to the receding silica surface and it is usually regular in thickness. At the beginning of reaction it grows randomly but with thickening of the product layer it spreads laterally and the usual regularity is then achieved, Figs. 4.3.1.29., a-c.

2) It consists of material much finer than the coarse matrix left behind with progress of reaction.

3) It is composed of two layers Fig.4.3.1.30.; a darker layer close to the unreacted silica and a lighter layer on the side of the coarse matrix. This contrast is very sensitive to etching, Fig.4.3.1.29.,c. The thickness of the two layers can vary considerably, Fig.4.3.1 30.

4) Selective coarsening takes place during reaction in the interaction front, Figs.4.3.1.31.,a-b, with some islands of alumina being formed and where silicon precipitates in a network of aluminium. Both are in intimate contact with the coarsened phase and, thus, suggest that this phase is an effective nucleant for silicon precipitation from the aluminium-silicon liquid. Elemental aluminium and silicon distribution x-ray maps and corresponding line-scanning were performed through the interaction front of a specimen 3.0 mm in diam. reacted at 1220^{o}C for 15 minutes, Fig.4.3.1.32., and in which coarsening has taken place. Energy-dispersive micro-analysis of both elements is also indicated in this figure. Despite the large broadening in the aluminium line-scanning, the decrease of the overall concentration of this element across the interaction front can be seen to be very much less than occurs in the lower temperature product layer - see - Fig.4.3.1.15. The peaks of the silicon line scanning are attributed to the precipitation of this element during coarsening, as can be observed in the respective x-ray map.

5) The interaction front is in intimate contact with the coarse matrix on one side and, provided spalling of silica did not occur, the front was bonded to it, Figs.4.3.1.33, a_b.

As earlier indicated in Fig.4.3.1.31.,the coarse matrix results from recrystallization of the fine interaction front, previously formed. In this coarse matrix a dominant columnar texture of alumina developed with preferred reaction orientation, that is perpendicular to the interaction front, Figs.4.3.1.34-36.; the reaction species diffuse along these columns. Fig.4.3.1.37. shows a radial distribution

of silicon along the coarse matrix. This figure is related to Fig.4.3.1.38. which shows the distribution x-ray maps of silicon and aluminium in a 3.0mm in diam. specimen reacted at 1110°C for 15 mins. The peaks in the silicon line-scanning are a result of the inclination of the specimen ($\sim 45^{\circ}$) in regard to its radial position.

Referring to Figs.4.3.1.32. and 4.3.1.38. an idealized scheme for diffusion profile for counter-diffusion of silicon and aluminium across the interaction front at different temperatures and the corresponding phase relationships is arranged as follows:

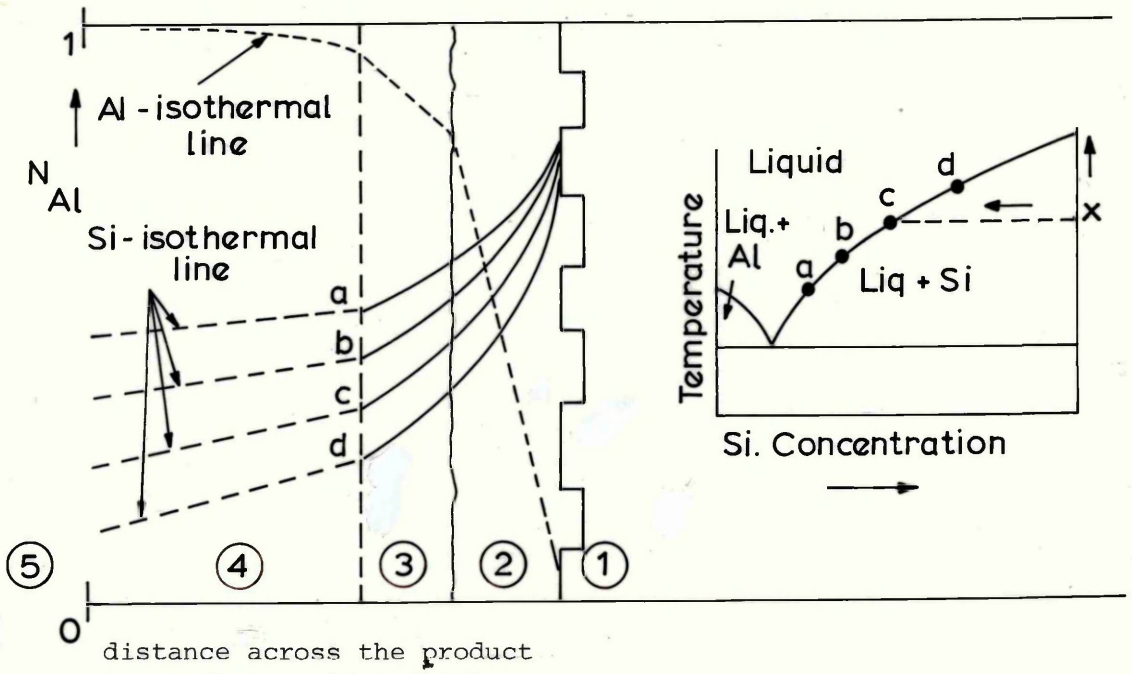

(1) silica
(2) reaction front
(3) diffusion zone
(4) coarsened matrix
(5) bulk liquid metal

a,b,c,d .... silicon equilibrium concentration with aluminium - silicon alloy at 1110, 1170, 1220 and 1265°C, respectively.

This scheme shows that diffusion of aluminium and/or silicon across the coarse matrix(4) is possible in the 100% liquid phase region for all concentrations up to the liquidus. When the concentrations of silicon exceed those of the liquidus then solid silicon coexists with the liquid aluminium-silicon phase of a specific composition. Aluminium is now confined to a part of the structure which will vary in proportion in relation to the concentrations of silicon present. This represents a marked decrease in the opportunity for aluminium diffusion in zone(3). When the concentrations of solid silicon are still high(2), the aluminium must diffuse through solid silicon to promote the reaction and, hence, the aluminium concentration will vary steeply across the interaction zone(2). Accordingly, the solid silicon must be transported in the opposite direction by diffusion in the liquid phase to maintain the equilibrium liquidus concentra-tion, for example, across section x → c of the isothermic, interface (3)/(4). At this interface silicon with concentration "c" is maintained in the liquid phase. The transport of silicon will be gradual in the liquid phase present in the coarse matrix from the liquidus composition of the aluminium-silicon alloy at the interface (3)/(4) (point c) to the aluminium richer composition of the aluminium-silicon alloy towards the peripheral regions of the rod. The morphologies of the product layer resulting from this mechanism of transport of the reaction species during reaction reflect this situation, but the proportion of aluminium-silicon products resulted during cooling has to be taken into account.

Fig.4.3.1.39. shows a cross-section of a specimen 5.0mm in diam. reacted at 1170°C for 30 min. Selective coarsening has taken place already within the fine interaction front. As the reaction proceeded, then islands became incorporated into the external coarse matrix, Fig.4.3.1.40. In this a pronounced columnar growth is observed. Nearest to the interaction front coarsening did occur in a very irregular manner or more appropriately described as pseudo-dendritic, Fig. 4.3.1.41. This indicates a continued removal of silicon from the external boundary of the interaction front by dissolving in the liquid aluminium and leading to the formation of pores. The liquid aluminium-silicon alloy then formed must have the

composition given by the liquidus line on the silicon rich side of the aluminium-silicon phase diagram - see latter scheme - and according to Fig.4.3.1.39 it varies progressively (decrease of silicon) across the radial section of the specimen. However, without changing the volume of the previously formed reaction products, some disturbances asscciated to physical effects such as agglomeration of the alumina cells, Fig.4.3.1.42 ,a-c, or to local thermodynamic non-equilibrium due to temperature gradients at interaction front*, causes effective alterations in the distribution of silicon in the metallic matrix and towards the peripheral regions of the rod. Additionally, small disturbances in the symmetry of the recrystallizing phases within the product layer occur and pools of liquid phase can form. Fig.4.3.1.43.a-c shows dendritic growth of aluminium close to the outer periphery of the product layer in such a pool.

Fig.4.3.1.44, which corresponds to Fig.4.3.1.39 (height b) shows, at higher magnification, circular colonies of alumina particles. The associated distribution of silicon and aluminium-silicon alloy to this is seen under better resolution in Fig.4.3.1.45, which corresponds to the specimen described in Fig.4.3.129,C before etching. Accordingly pools of silicon-rich aluminium-silicon alloy have been formed during reaction and thus on cooling precipitation of silicon has occurred within the cells of alumina. The electron micrographs presented in Fig.4.3.1.46,a show this and Fig.4.3.1.46,b shows an example of alumina cells grown in the colonies.

The decrease of silicon concentration in the aluminium-silicon alloy towards the periphery of the rod allows the liquid to reach eutectic composition which in turn, during cooling, solidifies in a more regular manner as presented in Fig.4.3.1.47 . At the periphery of the reaction layer the alloy concentrations reach the hypoeutectic regions of the binary aluminium-silicon system and the structure is mostly saturated with aluminium, Fig.4.3.1.48, where primary aluminium is in evidence.

---

*Heat loss is due to occur vertically along the transparent silica rod immersed into the aluminium. In some later experiments carried out with a full length of silicon rod along the reactor, an increase in temperature ($\sim 80^{\circ}C$) was observed on the top horizontal surface of the rod. Explanation for this lies on the physical principle of transmission of infra red radiation along the transparent rod.

Under the circumstance that the silicon concentration in the aluminium silicon alloy decreases as the reaction progresses, only small amounts of this element should escape into the bulk liquid metal. As a result of this, Fig. 4.3.1.49 aluminium dendritic regions is formed with silicon precipitated as silicon-aluminium eutectic in the interdendritic regions.

4.3.1.3 Reaction at intermediate temperatures - at temperatures 920°C and 980°C the reaction was discontinuous and its rate, as previously shown in section 4.1.2, drops drastically and reproducible results could not be obtained. Fig. 4.3.1.50, a shows an area of a specimen 5.0mm in diam. reacted at 920°C for 30 minutes. The interface of unreacted silica/product layer presented at higher magnification in Figs. 4.3.1.50, b-c is developed in an unusual way with continuous impingement of small spherical segments protruding inside the silica. Each segment appears to act as nuclei for a columnar structural growth.

Original traces of the interaction front can be recognised by the cracks running normal to the silica surface and by the segments surrounded by a different phase.

The interface of unreacted silica/product layer developed in a similar way in a specimen 10mm in diam. reacted at 920°C for 90 min., Fig. 4.3.1.51, and where the columnar type of the coarse matrix is retained in a elongated and orderly manner.

The microstructure presented in Fig. 4.3.1.52 shows a specimen 5.0mm in diam. reacted at 980°C for 90 min. Growth of large grains has taken place; aluminium-silicon alloy was observed to segregate at boundaries. Segregation of a similar alloy occurred in

further extension towards the unreacted silica which was unusually close to this surface, silicon was largely precipitated and for the rapid advance of the reaction front, silicon becomes dispersed behind it, in the coarse matrix. A view of the morphology of this area is presented in Fig.4.3.1.53.

The striking feature observed at this temperature, i.e. at 980°C, in some random specimens 5.0 and 10mm in diam. and reacted at different times was the formation of cubes (and/or cuboids) on the surface of the fine interaction front and to which they seem to be associated, Figs.4.3.1.54,a-c.

Since X-ray analysis did not indicate γ-alumina (which is cubic spinel type of aluminium oxide or defective spinel type - see section 2.3.1.2) present in specimens reacted at intermediate temperatures, an account for the cubic phase must be related to some other intermediate phase than pure alumina polymorph only. Any attempt to establish relationships between the geometrical shape of the particles (cubes or cuboids) and temperature, time and the radius of the reacting rod was unsuccessful.

4.3.2 The aluminium alloys-silica reaction systems

4.3.2.1 The aluminium/silicon-silica reaction system - the microstructures developed by immersing silica rods into liquid aluminium-silicon alloys with silicon concentrations varying from 5 to 15 atomic percent were similar to those of pure aluminium and were equivalent at both temperature and time. Fig.4.3.2.1,a-b shows a cross section of a specimen reacted for 15 min. at 1220°C. The silicon concentration was 10 atomic %. The similar double layer of fine phases are present close to the unreacted silica and the coarse matrix is developed in the usual columnar texture with the metallic phase dispersed within it. In this reaction system, and according to the binary phase aluminium-silicon equilibrium diagram, shown in Fig.2.1 and these temperatures and compositions of the liquid alloy of up to 15 atomic % of silicon, the liquid phase is capable of dissolving more and more silicon without affecting (inhibiting) the progress of

reaction whatsoever. This indicates that the reaction progresses independently of the initial concentrations of silicon in liquid aluminium at least up to 15 atomic % of silicon.

4.3.2.2 The aluminium/iron and the aluminium/manganese-silica reaction systems - Fig.4.3.2.2 shows an advanced stage of the reaction between silica and aluminium alloyed with 5 atomic % iron at 1170°C. The reaction progressed symmetrically with a pronounced columnar growth of the product layer radiating roughly perpendicular from the clearly defined interaction front. These columns show that the metallic phase transporting the reacting species is continuous up to the reaction front. This growth texture of the product layer was present in all specimens examined at the various times and temperatures in the range of temperatures studied and was related to any compositions of either iron or manganese added to the aluminium. Fig.4.3.2.3 shows a cross-section of a specimen reacted at 1265°C. The aluminium contained 15 atomic % manganese.

The interaction front shows similar characteristics to those previously described for the pure aluminium-silica reaction system : it forms parallel to the receding surface of silica and it is normally regular in overall thickness; it is fine, but can be composed of differences in the thickness of the contrasting zones present, Fig.4.3.2.4. There is evidence of some variations in the layer with selective coarsening occurring within it during reaction, Fig.4.3.2.5, a-b.

Elemental distribution X-ray maps and corresponding line-scanning were performed through the reaction front of some specimens of the aluminium-iron silica and aluminium-manganese-silica reaction systems with different initial compositions of the liquid alloy. These results are presented in Figs.4.3.2.6, a-d. Energy dispersive microanalysis of the elements involved is also indicated in these results.

On the basis of these obtained results a scheme of the counter-diffusion of silicon and aluminium in the presence of concentrations of iron (or manganese) at different temperatures and the corresponding phase relationships may be arranged as indicated

further.

Data for the trend in the variation of the liquidus is taken from the aluminium rich end of the aluminium-iron (and aluminium-manganese) binary systems, Figs.2.7-8. It is also taken from the silicon rich end of the silicon-iron and silicon-manganese systems[92], together with data from the aluminium-iron-silicon and aluminium-manganese-silicon, Figs.2.9-10 and ref.no.80.

The construction has been confined to the liquidus for the systems studied as this is the relationship involved in the reaction mechanism. Detailed comparison of the effect of the various concentrations will be described later in section 5.1.3.3.2 but the reaction system is schematically illustrated as follows:

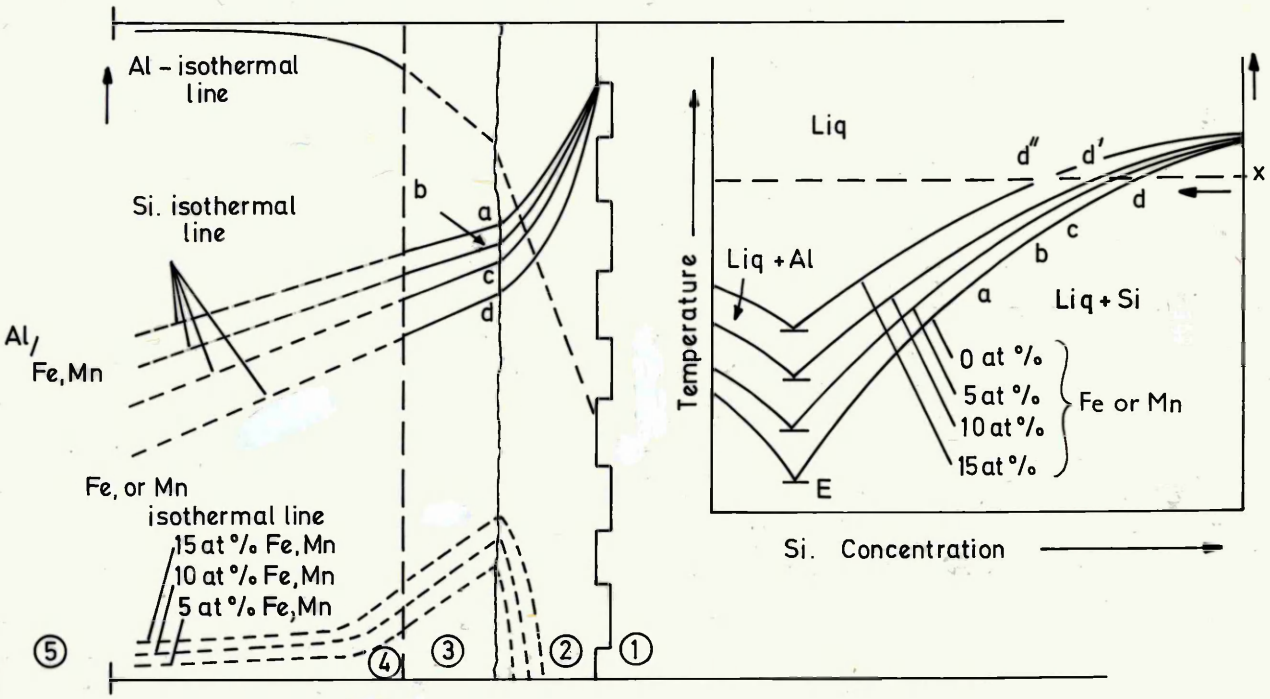

distance across the product layer, interaction front included.

(1) silica
(2) reaction front
(3) diffusion front
(4) coarsened matrix
(5) bulk liquid metal

a,b,c,d... silicon equilibrium concentration with aluminium-silicon alloy at temperatures.

d',d'' silicon equilibrium concentrations with aluminium-iron (or manganese) -silicon alloy at liquidus temperature.

The scheme for manganese present would be very similar on examination of the phase diagrams.

This scheme shows that counter-diffusion of aluminium and silicon across the coarse matrix (4) in a liquid phase is again possible. The comparison to the pure aluminium-silica reaction system, of the aluminium-iron (or manganese)-silicon liquid phase regions for all concentrations of silicon up to the liquidus is such that similarity must exist except in that the total concentration of aluminium and silicon is reduced by the presence of iron and/or manganese. At concentrations of silicon above those of the liquidus the liquid alloy and the solid silicon phases of a specific composition coexist and the aluminium and silicon concentrations will vary only as a consequence of the change in proportion of solid silicon plus liquid phase. Therefore, aluminium fast diffusion through zone (4) will decrease across zone (3) as the proportion of liquid phase changes. Across this zone the alloy components will also be partitioned by the diffusion of iron dissolved in the aluminium thus restricting the presence of solid silicon. Consequently, iron concentrates in the liquid phase and effectively has reduced the solubility of silicon in the matrix, thereby reducing rates of diffusion of silicon and aluminium.

At the interface (3)/(2), the local equilibrium of iron activity is achieved practically instantaneously and, hence, the aluminium concentration will vary steeply across the reaction zone (2), although in a rate inferior to that when aluminium was pure, since the mobility of silicon has also been lowered.

This proportion of aluminium-iron (or manganese)-silicon products resulted during cooling must also be taken into account for explaining the resulted microstructures developed in the coarse matrix. Fig.4.3.2.3 has shown the coarsened region recrystallised behind the interaction front as the reaction progressed. This indicates the continued removal of the product silicon from the interaction front towards the peripheral regions of the rod and, as earlier mentioned, with a gradual decrease in concentration.

The dissolution process is, however, slow and dependent on the iron (or manganese) content in the liquid alloy, for example, from point d' to point d" at temperature. In any case, silicon will ultimately form a ternary liquid phase alloy which composition lays in the near vicinity of the eutectic (ternary - point E). The typical result of this is the formation of deep eutectic valleys as indicated by the electron micrographs of various specimens shown in Figs.4.3.2.7, a-e .

5. DISCUSSION

5.1. Kinetic studies of the pure liquid aluminium - solid silica reaction system

5.1.1. Introduction

The mechanism for the reaction between silica and/or silicates and pure aluminium and its alloys has been investigated by many workers from diverse technological fields, e.g. steelmaking, aluminium processing, aluminium fibre reinforcement. Unfortunately, the complexity of the reaction mechanism, combined with the effect of differing experimental conditions, has led to conflicting conclusions regarding the nature of the rate controlling process. To date there has been no single quantitative interpretation which correlates the results of all investigators in all fields.

The purpose of this investigation was to develop an experimental technique by which interaction of pure silica with liquid aluminium and certain of its alloys, could be studied. From the results obtained, it was intended that a quantitative model would be developed which might be used to produce a unified interpretation of the results of other investigations into this reaction system.

The experimental investigation of high temperature reaction systems is inherently difficult and often the precise interpretation of quantitative data is limited by the accuracy of the measurements made. The apparatus and techniques devised for this particular investigation have already been described in Chapter 3 and, as emphasised in this section, every effort was made to reduce experimental errors to an absolute minimum. The errors arising in this work may be ascribed to the three parameters being quantitatively monitored in every experiment, namely:-

(i) The duration of contact between the silica rod and the molten metal.

(ii) The measurement of the thickness of the product layer.

(iii) The temperature of the reaction system.

In comparison with the latter two parameters, the error incurred in the measurement of the contact time between the silica rod and the melt was probably small. An experiment commenced when the silica rod was introduced into the liquid aluminium and was terminated by withdrawal of the partially reacted rod into the cooler regions of the furnace tube. The rate of cooling was considered to be sufficiently rapid that, relative to the total time of contact, the extent of reaction after removal from the melt would be negligibly small.

The measurement of the thickness of the reaction product layer is perhaps the most obvious source of error, especially for shorter reaction times. In the earlier stages of the reaction, the product layer consisted of a number of segments distributed around the periphery of the specimen, rather than a complete anular ring. The radial thickness of the reacted segments could vary by as much as $\pm$15% and consequently in order to minimise this as a possible source of error, the mean of a total of 32 measurements was taken, unreacted sections of the surface being ignored (see Section 3.4.1.) As a source of error, however, this rapidly diminished as reaction proceeded, since once a complete anular ring of reaction product had formed, the further progress of the reaction front appeared to occur much more "smoothly", producing a much more uniform thickness of reaction product.

Every effort was made in the design of the experimental apparatus to reduce the effect of temperature variations on the results obtained (Section 3.1.1.). The crucible containing the liquid aluminium was supported within a cylindrical steel pedestal of relatively large thermal mass and shielded from the furnace tube by a radiation shield, both measures being intended to minimise temperature fluctuations within the reaction system. The principal source of error is probably derived from the transparency of fused silica to infra-red radiation. It is possible that the silica rod may act as a "fibre optic" path for thermal radiation, producing an enhanced cooling effect when inserted into the melt. The magnitude of this effect is virtually impossible to assess. By surrounding the reaction crucible with a body of large thermal mass, combined with the high thermal conductivity of liquid aluminium, it was expected that this effect would be reduced to a minimum. The possible implications of this phenomenon with respect to the reaction mechanisms will be discussed in more detail in Section 5.1.3.1.

It is clearly impossible to make a realistic estimate of the overall error which might have been incurred in the experimental measurements made. Wherever possible measures have been taken to minimise all sources of error and the "close fit" of much of the data to a linear relationship has been taken as an indication of the effectiveness with which this has been achieved.

5.1.2. The rate of reaction

The reduction of silica by molten aluminium is somewhat unusual in that the rate of this process shows a significant drop in the temperature range 880°C to 1050°C. This is clearly shown in Figure 4.1.2.4, which shows the variation in the apparent reaction rate constant, k, for the process over the entire range of temperatures investigated in this work.

The apparent reaction rate constant, k, has been determined using equation (4.1.1.1.). The derivation of this relationship is as follows. The overall rate of reaction may be defined by the generalised expression,

$$-\left(\frac{dW_{SiO_2}}{dt}\right) = k.A_{cyl} \qquad 5.1.1.$$

where W is the mass of the reactant SiO_2 and A is the area over which the reaction is taking place, i.e. it is the area of the unreacted silica rod. If r_i is the radius of this rod and, therefore, of the reaction interface, then:

$$W_{SiO_2} = \rho_{SiO_2}.\pi r_i^2.l \quad ; \quad A_{cyl} = 2\pi r_i l$$

thus,

$$-\left(\frac{dW_{SiO_2}}{dt}\right) = -\rho_{SiO_2}.2\pi r_i^2 l.\frac{dr_i}{dt} = k.2\pi.r_i^2.l$$

which gives:

$$-\rho_{SiO_2}.\frac{dr_i}{dt} = k \qquad 5.1.2.$$

Integrating with boundary conditions:

$$t = 0 \quad \ldots\ldots\ r_i = r_o$$

$$t > 0 \quad \ldots\ldots\ 0 \leq r_i < r_o$$

i.e.

$$\int_{r_o}^{r_i} dr = -\frac{k}{\rho_{SiO_2}} \int_o^t dt$$

which gives:

$$\left[1 - \frac{r_i}{r_o}\right] = \frac{k.t}{\rho_{SiO_2} r_o} \qquad 5.1.3.$$

If R_x is the fraction of silica that has reacted, then:

$$R_x = \frac{r_o^2 - r_i^2}{r_o^2} = 1 - \left(\frac{r_i}{r_o}\right)^2$$

So, $r_i/r_o = (1 - R_x)^{0.5}$ and equation (5.1.3.) can be written as:

$$\left[1 - (1 - R_x)^{0.5}\right] = \frac{kt}{\rho_{SiO_2} . r_o}$$

A plot of $\left[1 - (1 - R_x)^{0.5}\right]$ against, t, should yield a straight line, the value of k, being obtainable from the gradient of the line. The data introduced in Section 4.1.2. has been plotted in this way and it can be seen that straight line relationships are obtained (Figures 4.1.2.1. and 4.1.2.3.). For each set of results, the best straight line has been obtained by regression analysis and both the regression equation and the standard deviation have been presented with the appropriate figure. In all cases a high degree of statistical correlation with a straight line relationship is observed. The slopes of these straight lines have been used to determine the values of k shown in Figure 4.1.2.4.

Experimentally determined linear plots of $\left[1 - \left(1 - R_x\right)^{0.5}\right]$ against t for reaction cylinders have in the past been taken to indicate the validity of expression (5.1.1.) and that k is the rate constant for some rate controlling step that occurs at the reaction interface.

Recently, however, a number of workers[65,86] have shown, theoretically, that this is not so. For a reacting cylinder, $\left[1 - \left(1 - R_x\right)^{0.5}\right]$ varies almost linearly with time, whatever the reaction mechanism. The linear plots and the calculated values of k are, however, a convenient means of representing the rate of the reaction, and therefore in this capacity they will continue to be used in this work.

Thus, Figure 4.1.2.4. shows that the reaction rate rises rapidly with temperature until about 880°C, when it drops drastically. It is not until ∿1050°C that the reaction rate starts again to increase consistently with temperature and temperatures in excess of ∿1250°C must be reached before the rate established at 860°C is surpassed.

Any heterogeneous reaction will involve a number of different steps, especially if one reactant and one product are solids. The fluid reactants must be brought to the reaction region by transport processes such as diffusion and convection and the fluid products removed. The actual reaction region will involve a chemical reaction step and often some solid-state diffusion process as well.

Each of these steps will have an intrinsic rate: the rate at which it would occur if the other steps were so fast as to provide no limit to the overall reaction rate. In fact, of course, the overall reaction will occur at the rate of the step or steps with the lowest intrinsic rate or rates.

The rates at which the steps occur vary with temperature, always increasing as the temperature increases, but not necessarily to the same extent. Thus the step with the slowest intrinsic rate at one temperature, and therefore the rate determining step at that temperature,

can speed up as the temperature increases more than the other steps. At a higher temperature, then, another step in the reaction becomes rate controlling and the characteristics of the reaction undergo a change.

This type of behaviour occurs when the overall reaction rate increases with temperature, and is not the type of behaviour that can explain the variation of reaction rates with temperature shown in Fig.4.1.2.4. Since rates of the individual reaction steps always increase with temperature, a drop in reaction rate can only occur if a new step is introduced into the reaction sequence, due to factors that are not kinetic. In order to examine what this step might be, the other steps in the reaction sequence must be examined.

At the reaction front, aluminium reacts with silica to produce alumina and silicon:

$$4\ Al + 3\ SiO_2 = 2\ Al_2O_3 + 3\ Si$$

The aluminium is liquid in the temperature range of interest but the silicon is solid. The silicon can only be removed from the reaction region after dissolving in the molten aluminium to form a liquid aluminium - silicon alloy. The composition of this alloy will be given by the liquidus line on the silicon rich side of the aluminium-silicon equilibrium phase diagram shown in Fig.2.1. Thus the reactant aluminium is provided for the reaction and the product silicon removed by counter-current diffusion through the liquid aluminium-silicon alloy in the pores of the product layer and in the boundary layer formed by convection outside the cylindrical rod.

Within the reaction zone, reacting silica and product alumina together with solid silicon, liquid aluminium-silicon alloy and any intermediate phases which may occur[+] will all be present at the same moment. Processes occurring in the reaction zone will thus include:

- the decomposition of the solid silica;
- the formation of solid silicon and alumina;
- the dissolution of solid silicon in the molten aluminium-silicon alloy;
- the formation and decomposition of any intermediate phases that may form.

There is no way of determining a priori the intrinsic rates at which any of these processes occur, but it is possible to estimate the rates at which the aluminium and the silicon counter diffuse through the porous product layer.

For the counter-diffusion of aluminium and silicon within a liquid alloy, Fick's first law can be written in the form:

$$J_{Si} = -C_T . D_{Si/Al} . \frac{\partial c^*_{Si}}{\partial x} + \left(J_{Si} + J_{Al} \right) C^* \qquad 5.1.4.$$

However, the fluxes of silicon and aluminium are linked by the stoichiometry of the reaction:

$$J_{Al} = -\frac{4}{3} J_{Si} \qquad 5.1.5.$$

[+] Free energy studies to evidenciate possible intermediate phases involved in the reaction system will be introduced later in this Chapter.

So that, equation (5.1.4.) can be rearranged as:

$$J_{Si} = - C_T \cdot D_{Si/Al} \cdot \frac{\partial C^*_{Si}}{\partial x} + \left(1 - \frac{4}{3}\right) J_{Si} \cdot C^*_{Si} \qquad 5.1.6.$$

or:

$$J_{Si} = \frac{-C_T \cdot D_{Si/Al}}{1 - \left(1 - \frac{4}{3}\right) C^*_{Si}} \cdot \frac{\partial C^*_{Si}}{\partial x} \qquad 5.1.7.$$

The significance of some of the symbols used in the equations may be more easily understood by reference to the following diagram:

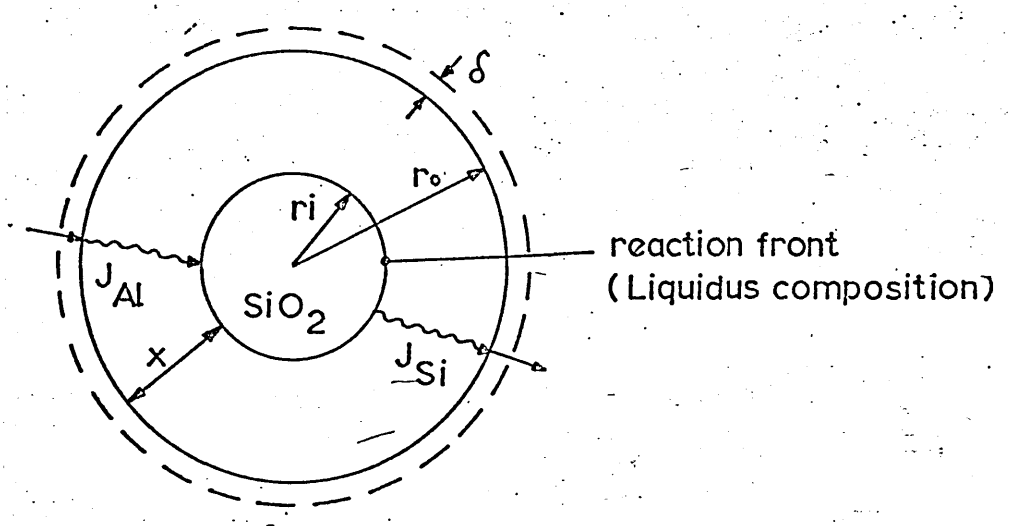

(These symbols are defined in Appendix A-5.1.)

A similar equation exists for the flux of aluminium.

Equation (5.1.7.) can be integrated by defining a new variable Y_{Si}, where Y_{Si} is given by[+]:

$$Y_{Si} = - \frac{\ln \left[1 - \left(1 - \frac{4}{3}\right)\right] C^*_{Si}}{\left(1 - \frac{4}{3}\right)} \qquad 5.1.8.$$

[+] For a variable $Z = Y(C^*)$ and if $C^* = F(X)$, the transformation $Z = Y(X)$ then becomes: $\frac{\partial Y}{\partial x} = \frac{\partial Y}{\partial C^*} = \frac{\partial C^*}{\partial x}$

so that equation (5.1.7) becomes:

$$J_{Si} = - C_T \cdot D_{Si/Al} \cdot \frac{\partial Y_{Si}}{\partial x} \qquad 5.1.9.$$

This equation will apply within the liquid surrounding the reacting silica rod and in the pores of the product layer. It cannot, in itself be integrated within the pores because their geometry cannot be specified. Diffusion through porous materials is normally treated, however, by defining an effective diffusion coefficient which can be related to the entire space occupied by the solid and the pores. This effective diffusion coefficient is given by:

$$D_{Si/Al\ eff.} = \frac{\gamma \cdot D_{Si/Al}}{\tau} \qquad 5.1.10.$$

where γ is the porosity of the solid product layer and is the fraction of the entire space available to the diffusion process. τ is called the tortuosity factor and is included since the actual diffusion flux cannot follow a straight path directly across the entire space but is constrained by the presence of the solid forming the pores to follow a tortuous and therefore, a longer path.

For an assemblage of randomly directed pores, the average path length must, by Pythagoras, be $\sqrt{2}$ times the straight-through path. Thus tortuosity factors are therefore, of the order of 1.4 for a system of randomly orientated pores.

Equation (5.1.9) can be written for diffusion within the porous solid as:

$$J_{Si} = - C_T \cdot \left(D_{Si/Al}\right)_{eff.} \cdot \frac{\partial Y_{Si}}{\partial x} \qquad 5.1.11.$$

In order to assess the rates at which the aluminium/silicon counter-diffusion process takes place and its importance in controlling the reaction, the use of equations (5.1.9) and 5.1.11.) becomes necessary to determine a hypothetical effective rate constant, defined by

equation (5.1.3.), for the first 75% of the reaction (i.e. until $r_i/r_o = 0.5$) and assuming the counter-diffusion step to be the slowest and therefore, rate controlling step.

Figure 5.1.1 shows a cross section of a reacting silica rod at a stage in the reaction. Counter-diffusion within the liquid alloy in the porous product layer (alumina) can be analysed by integrating equation (5.1.11.) across the porous product layer from r_i to r_o. As long as r_i lies in the range $r_o > r_i > 0.5r_o$, the average value of the gradient $\partial Y_{Si}/\partial x$ across the cylindrical shell is almost identical to its value halfway across the shell, i.e. at the radius $\left[\frac{1}{2}\left(r_i + r_o\right)\right]$. Thus the integration of equation (5.1.11.) can be carried out to give*:

$$j_{Si} = C_T \cdot \left(D_{Si/Al}\right)_{\text{eff.}} \cdot \frac{\pi\left[r_o - r_i\right]}{\left[r_o + r_i\right]} \cdot \left[\left(Y_{Si}\right)_i - \left(Y_{Si}\right)_o\right] \quad 5.1.12.$$

where j_{Si} is the molar flow of silicon per unit height of the cylinder; $\left(Y_{Si}\right)_i$ is to be calculated from the mole fraction of silicon in the liquid alloy in the reaction zone by using equation (5.1.8.). Since the reaction zone contains solid silicon, this mole fraction will be equal to the liquidus composition at the particular temperature being considered. $\left(Y_{Si}\right)_o$ is to be calculated from the composition of the alloy at the outer surface of the porous product layer which is not known. However, analysis of the mass convection processes occurring in the liquid surrounding the specimen can be elaborated, by assuming, that diffusion occurs through a thin stagnant layer of liquid surrounding the specimen, the thickness of this layer being represented by δ. With this assumption, the integration of equation (5.1.9.) gives:

---

*Elementary texts on Heat Transfer or Diffusion[87] show that the error resulting from the use of this equation only rises to be greater than 4% when r_i is smaller than $0.5r_o$.

$$j_{Si} = C_T \cdot \frac{\left(D_{Si/Al}\right)_{eff}}{\delta} \cdot \left[\left(Y_{Si}\right)_o - \left(Y_{Si}\right)\right]_b \qquad 5.1.13.$$

where $\left(Y_{Si}\right)_b$ is the mole fraction of silicon in the bulk molten alloy in the reacting crucible. The quotient $\left(D_{Si/Al}\right)_{eff}/\delta$ is more normally written as a mass transfer coefficient $\alpha_{Si/Al}$, so that equation (5.1.13.) becomes:

$$j_{Si} = 2\pi r_o . C_T . \alpha_{Si/Al}\left[\left(Y_{Si}\right)_o - \left(Y_{Si}\right)_b\right] \qquad 5.1.14.$$

Eliminating $\left(Y_{Si}\right)_o$ between equations (5.1.12.) and (5.1.14.) gives:

$$j_{Si} = \frac{C_T\left[\left(Y_{Si}\right)_i - \left(Y_{Si}\right)_b\right]}{\frac{1}{2\pi r_o . \alpha_{Si/Al}} + \frac{(r_o - r_i)}{\pi(r_o + r_i)\left[D_{Si/Al}\right]_{eff.}}} \qquad 5.1.15.$$

The silicon removed by the process described by equation (5.1.15.) is liberated from the moving reaction front; so it can be written:

$$j_{Si} = -2\pi r_i . \frac{dr_i}{dt} \cdot C_{SiO_2} \qquad 5.1.16.$$

Thus, eliminating j_{Si}, gives:

$$\left[\frac{r_i}{r_o . \alpha_{Si/Al}} + \frac{2r_i (r_i - r_i)}{(r_o + r_i)\left[D_{Si/Al}\right]_{eff}}\right]\frac{dr_i}{dt} = \frac{C_T\left[\left(Y_{Si}\right)_i - \left(Y_{Si}\right)_b\right]}{C_{SiO_2}} \qquad 5.1.17$$

This equation can be simplified before it is integrated. The value of $\alpha_{Si/Al}$ is unknown, since it depends on the concentration and velocity field within the molten aluminium in the crucible. For the moment, the definition of the Sherwood number[88] will merely be used:-

$$Sh = \alpha . d / D \qquad 5.1.18$$

Therefore,

$$\alpha_{Si/Al} = Sh . \left[D_{Si/Al} \right]_{eff.} / 2r_o \qquad 5.1.19.$$

Using this equation and equation (5.1.10.), gives equation (5.1.17.) as:

$$\left\{ \frac{2.r^*}{Sh} + \left[\frac{2.r^*.(1-r^*)}{(1+r^*)} \cdot \frac{\tau}{\gamma} \right] \right\} \frac{dr^*}{dt} = - \frac{D_{Si/Al} \cdot C_T \left[\left(Y_{Si} \right)_i - \left(Y_{Si} \right)_b \right]}{r_o^2 \cdot C_{SiO_2}} \qquad 5.1.20.$$

where $r^* = \frac{r_i}{r_o}$

Integrating equation (5.1.20.) over the period $t_{0.5}$, i.e. the time it would take the reaction interface to move from ($r_i = r_o$) to ($r_i = 0.5$), gives:

$$\int_{1.0}^{0.5} \left[\frac{2.r^*}{Sh} + \frac{2.\tau}{\gamma} \left(2 - r^* - \frac{2}{r^*+1} \right) \right] dr = - \frac{(D_{Si/Al})_{eff} \cdot C_T \left[(Y_{Si})_i - (Y_{Si})_b \right] t_{0.5}}{r_o^2 \cdot C_{SiO_2}} \qquad 5.1.21.$$

or

$$\frac{r^{*2}}{Sh} + \frac{2.\tau}{\gamma} \left[2r^* - \frac{r^*}{2} - 2 \ln(r^*+1) \right]_{0.5}^{1.0} = \frac{(D_{Si/Al})_{eff} \cdot C_T \left[(Y_{Si})_i - (Y_{Si})_b \right] t_{0.5}}{r_o^2 \cdot C_{SiO_2}} \qquad 5.1.22.$$

which gives

$$\frac{(D_{Si/Al})_{eff} \cdot C_T \left[(Y_{Si})_i - (Y_{Si\ b}) \right] t_{0.5}}{r_o^2 \cdot C_{SiO_2}} = \frac{0.75}{Sh} + 0.10 \frac{\tau}{\gamma} \qquad 5.1.23.$$

or

$$t_{0.5} = \frac{\left(\frac{0.75}{Sh} + 0.10 \frac{\tau}{\gamma} \right) . r_o^2 \cdot C_{SiO_2}}{(D_{Si/Al})_{eff} \cdot C_T \left[(Y_{Si})_i - (Y_{Si})_b \right]} \qquad 5.1.24$$

Comparing equation (5.1.24) with equation (5.1.3.), for $r_i = 0.5\ r_o$, gives the hypothetical apparent rate constant as:

$$k = \frac{(D_{Si/Al})_{eff} \cdot C_T \left[(Y_{Si})_i - (Y_{Si})_b \right] M_{SiO_2}}{\left(\frac{1.5}{Sh} + 0.2. \frac{\tau}{\gamma} \right) . r_o} \qquad 5.1.25.$$

where M_{SiO_2} is the relative molecular mass of silica $C_{SiO_2} = \frac{\rho_{SiO_2}}{M_{SiO_2}}$

Values of k can be calculated at different temperatures and compared with the values determined experimentally.

The micrographs presented elsewhere in section 4.3 show that columnar type cells tend to form in the product layer which suggests a low value of the tortuosity factor τ: about $\tau = 1.1$ would seem to be appropriate. The data in section 4.1.1 shows that the radius of a reacted rod shrinks by no more than 2%. This means that the volume occupied by the porous product layer (alumina) is some 4% less than that occupied by the silica from which it was formed. Since the theoretical reduction in volume is 19.1% the porosity of the product alumina must be about 15%.

Barinov[88], has measured the diffusion coefficient of silicon in molten aluminium, and quotes the followingequation from his results:

$$\left[\frac{(D_{Si/Al})_{eff}}{/cm^2.sec^{-1}/} \right] = 2.0 \times 10^{-3} \exp - \left(\frac{21.78\ kJ.mol^{-1}}{RT} \right) \qquad 5.1.26$$

The above data has been used to calculate the hypothetical rate constant k for cylinders 5.0mm in radius on the assumption that the molten aluminium in the crucible is so well stirred that $Sh \to \infty$. The details of these calculations are given in Appendix A.5.2. and the resulting values are shown by the dotted line in Fig.5.1.2.

The line shows that the hypothetical rate constants calculated from equation (5.1.25) on the assumption that the reaction is controlled by liquid phase diffusion processes are of the same order as those measured experimentally. Thus, it can be concluded that these diffusion processes do play a part in controlling the rateof the reaction in the low temperature region.

5.1.3 The reaction mechanisms

5.1.3.1 The low temperature mechanism

Since the experimental curve in Fig.4.1.2.4. increases more rapidly with temperature than that determined from diffusion theory, a "chemical step" at the reaction front is very likely to be an additional factor. The activation energy for such a step will be higher than that for liquid phase diffusion (see values in Table 4.1.2.2.), so its intrinsic reaction rate will increase more rapidly with temperature. Thus, as the temperature rises, the reaction front step will play a lesser and lesser role in determining the reaction rate, allowing the actual rate to approach the rate predicted considering liquid phase diffusion alone. Thus, the actual rate will increase more rapidly with temperature than the diffusion based rate, as is found to be the case.

A further factor tends to corroborate the suggestion that the reaction front step becomes less dominant as the temperature rises. Equation (5.1.3.) has been used to calculate the experimental values of the constant k. If this equation does apply, these values of k will naturally be independent of the size of the rod. Examination of Fig.5.1.2. shows that the three values of k determined from the experimental results obtained at 760°C for the three different sized rods are, in fact, virtually the same, whereas the values determined for 860°C differ.

However, the values at 860°C show a puzzling relationship with the size of the rod specimens. If, as is suggested by the similarity between the experimental and calculated values at 860°C, liquid phase diffusion was to be the dominant rate controlling process at 860°C, the experimental values of k should agree with equation (5.1.25.). This equation suggests that the values of k would vary inversely with the specimen radius whereas the lowest values at 860°C were obtained for the smallest rods. This is neither to be expected on the basis of reaction interface control, nor liquid phase diffusion control.

In calculating the diffusion theory values of k, it was assumed that the molten aluminium was sufficiently well stirred for the Sherwood number (Sh), to be very large. If this were not to be the case, the term involving the Sherwood number would contribute to the equation and reduce the value of k.

The liquid aluminium in the crucible is not stirred mechanically in the low temperature experiments but by convection. Silica is virtually transparent to infra-red radiation, so that the insertion of a silica rod into the aluminium bath will exert a considerable cooling effect. Section 4.3.2.1. has made reference to the observation that considerable heat flows along complete rods inserted from the top of the reactor into the crucible. Whereas the rods used in most of the experiments were shorter and were supported from within the reactor, considerable temperature differences existed along them (~80°C) and they would provide a "fibre optic" type path for thermal radiation from within the aluminium bath.

The heat radiated along the silica rods in this way, would have to be provided by thermal conduction and convection from within the alum-

inium bath, establishing differences in temperature between the bath as a whole and the surface of the silica rod. These temperature differences would produce natural convection flows within the bath and it is these flows that would determine the value of the Sherwood number of the mass transfer of silicon within the liquid. The larger the heat loss along the silica rod, the larger would be the temperature differences, convection flows and Sherwood number. It is logical, therefore, that the relative rotation rates such as those up to 35 rpm would exert no alteration to the general dynamic character of the reaction, since how otherwise were the rates of reaction of rotating experiments equivalent to those of experiments carried out under assumed static conditions and with any reaction system involved.

The thermal radiation flow along the rod will increase very rapidly with it's size. In the first place, the cross sectional area of the rod increases with the square of the radius, whereas the surface of the rod receiving heat from the bath increases with a somewhat lower power. Furthermore, the transfer of radiant heat depends upon geometric view factors which will be much greater for a 10 mm diameter rod immersed for 20 mm into the bath than for a 3 mm diameter rod also immersed 20 mm. Thus the temperature differences produced in the bath by the insertion of the longer rods will be much greater than those produced by the smaller rods. This means that the intensity with which thermally induced natural convection flows stir the aluminium in the crucible will increase very rapidly with the size of the rod specimens.

It is for this reason that a very large value of the Sherwood number was used in calculating the k values for the 10 mm diameter rod from equation (5.1.25.). The samereasoning suggests that the value of

the Sherwood number will decrease with the size of the rod increasing the contribution it makes to the divisor in equation (5.1.25.). The contribution to the reaction step made by convection in the aluminium in the bath could thus explain the relationship of reaction rate with specimen size found at 860°C.

Thus a likely picture emerges of the reaction mechanism at temperatures below 880°C. Three processes can contribute to controlling the reaction rate:

- mass convection within the aluminium bath;
- liquid phase counter diffusion of silicon and aluminium within the porous product layer (alumina);
- some step at the reaction front - either the formation of the solid silicon and alumina from the silica, or the dissolution of the solid silicon in the liquidus alloy.

Either of these processes play a lesser or greater role depending on the temperature or specimen (rod) diameter. In particular, the relative importance of the reaction front step diminishes as the temperature rises since its intrinsic rate increase more rapidly than the intrinsic rates of the other reactions. This is emphasised by the change of the silicon concentration in the liquidus alloy with rise in temperature.

For none of these processes can it be assumed that the intrinsic rate will fall as the temperature rises above ~880°C and certainly not enough to explain the observed five or six-fold fall in the reaction rate.

Clearly some additional process or processes must intrude into the reaction mechanism and for reasons that are not due to the kinetics of the various processes involved in the lower temperature reaction. Such additional processes can be associated with volume changes as indicated by the cracking in the microstructures.

5.1.3.2. High temperature mechanism

The rate of reaction drops drastically above ~880°C and starts to rise again above ~1050°C, as clearly shown in Fig.4.1.2.4. It then follows an exponential trend as predicted by the relationship between k and temperature. The microstructures produced at higher temperatures (from 1110 to 1265°C) and presented elsewhere in section 4.3.2, show the elongated (columnar) type of alumina cells produced in the coarse product layer. The microstructures have also shown a fine and, to some extent, unstable double layer reaction front which in turn transforms into the coarse matrix as the reaction progresses (Fig.4.3.1.31a). This evidence is consistent with the observed change in reaction rate at high temperatures compared to the reaction rate below 880°C. The sintering which has occurred behindthe reaction front has resulted in densification and shrinkage of the alumina phase. This has allowed radial paths to be maintained for the ingress of aluminium and the counter-flow of silicon dissolved from the reaction interface. Hence the rate of reaction is governed by the area of radial access which must be less than the effective area in the porous unsintered matrix produced at low temperatures in the reaction layer. It is unlikely from the results that any other event is making a significant contribution to the rate of reaction at high temperatures (>1100°C).

The reaction mechanism is therefore, controlled by the transport of the metallic phase to the inner reaction layers. The double layer effect has been produced at the reaction front prior to the onset of sintering. The development of coarsening progressively occurs as the reaction proceeds (Fig.4.3.1.30). As the sintering rate of the alumina increases with temperature so the pore network becomes more fully developed (see p.66) and the reaction rate increases.

The transitional events in the intermediate temperature range dramatically change the rate of reaction and, as shown by Figure 4.3.1.54, additional product phases have been detected. This is discussed in Section 5.1.3.4.

Since the conditions for the liquid aluminium in the crucible were the same as for the lower temperature reaction, i.e. without mechanical stirring, the same "fibre optic" type path for thermal radiation from within the fused silica rod may be expected to occur thus exerting a cooling effect during reaction. These temperature gradients produce natural convection flows ($Sh \rightarrow \infty$) within the aluminium and partly provide means for silicon transfer across the porous product layer. This must be postulated in order to accomplish an account for the relationship between the constant k and the size of the rod. As for the lower temperature reaction the experimental values of k would be expected to vary inversely with the diameter of the rod according to equation (5.1.25.). However, the lowest values at 1265^{o}C were obtained for the smallest rods. Mass convection within the aluminium bath must therefore, be assumed to contribute to the reaction mechanism and again its importance will be temperature and specimen (rod) size-dependent.

Solid state diffusion of aluminium across the solid silicon formed in the reaction zone must also be involved in the reaction mechanism, since how otherwise will the aluminium be available to react with the silica. This solid state diffusion step cannot in itself be rate controlling since the length of the diffusion path through the silicon will always be adjusted by the relative rates of formation and dissolution of silicon for the solid state diffusion step to occur at any rate required by the remainder of the reaction scheme. An aluminium reaction potential gradient will exist across the solid silicon, the relative activities of aluminium and silicon in contact with the silica and alumina being such as to satisfy the equilibrium conditions for the reaction involved. As the reaction progresses silicon must dissolve into the liquid aluminium-silicon alloy, the specific composition being given by the liquidus line. In view of the lateral morphology of the product layer and consequently of the interaction front the aluminium does not need to diffuse through the entire width of this front since it can move readily through silicon to the receding silica surface via the fissures maintained in the product layer.

The micrographs presented elsewhere in section 4.3.2. particularly in Fig.4.3.2.6. illustrate these effects. Accordingly the aluminium reaction gradient through solid silicon and the volume change between alumina and silica lead to the transformation of the reaction front with a marked growth texture as generally observed.

5.1.3.3. Effects of silicon, iron and manganese added to the aluminium on the mechanism of reaction

5.1.3.3.1. The aluminium-silicon alloys - silica reaction systems -

The results presented in Fig.4.1.5.a have shown that the relationship between the rate of reaction and temperature is the same as for the

aluminium-silica reaction system. This relationship is independent of the concentration of silicon in the starting liquid metal at least up to 15 atomic percent of silicon. The liquid phase presents the same identical potential as pure liquid aluminium, the reaction will thus be constrained by the dissolution of silicon in the liquidus alloy at the interface of the reaction front/coarse matrix. This is a satisfactory explanation for the linear increase in thickness of the product layer with time as previously demonstrated in sections 4.1.3., 4.3.2.1 and 5.1.3.

For the same reasons discussed earlier for the pure aluminium-silica reaction system, diffusion of aluminium across solid silicon in the reaction front must also take place with an aluminium reaction potential gradient existing between the two interfaces. Thereby, once equilibrium conditions are satisfied by the activity ratio between aluminium and silicon, other reactions such as the intermediate step described by equation (5.1.27) may thus be involved.

5.1.3.3.2. The aluminium-manganese and aluminium-iron alloys - silica reaction systems

As clearly shown in Figs. 4.1.5, b-c, the rates of reaction rise gradually with temperature, the reaction being slightly faster with iron present than with manganese. The explanation for this must lie on the thermodynamic-activity dependence of the reaction on the concentration of iron and manganese in the system and its effect on the counter-diffusing silicon and aluminium in the liquid phase through the columnated reaction product layer. In any case, both manganese and iron will attain local thermodynamic equilibrium thus effectively reducing the solubility of sil-

icon and therefore, reducing the rate of the reaction in proportion to the concentration of these elements dissolved in the liquid aluminium-silicon alloy. The equilibrium concentration is first attained at the interface, where the fine interaction front is selectively coarsened. Because liquid aluminium is the solute for iron and manganese, where equilibrium with solid silicon is attained the aluminium concentration will drop. This has previously been schematically suggested in section 4.3.2.2.

As mentioned earlier, due to the continued dissolution of silicon into the liquid alloy, there is also a variation in the silicon concentration between the saturated and the non-saturated liquid phase. The liquidus line for the binary aluminium-silicon phase diagram represents the saturation composition at a particular temperature. The effect of different concentrations of iron or manganese on this liquid line are discussed in section 4.3.2.2. and the diagrams presented in Figs. 5.1.4. and 5. show the effect on the saturated concentration in the temperature range studied. It is clear from these diagrams that the solubility of silicon in the liquid phase increases with increasing temperature and decreasing concentration of the third element, ie.iron or manganese. The rate of dissolution, according to equation (5.1.13) would be proportional to the rate of diffusion of silicon away from the interface down the silicon concentration gradient. Since a linear growth of the product layer was observed and since the morphology did not change significantly either with temperature or time of reaction, it may be proposed that neither iron nor manganese concentrations affect the overall mechanism of the reaction, only the rate.

5.1.3.4. The intermediate temperature reaction

As has been shown in the results there is a temperature range from approximately 860 to 1000°C where the reaction rate is indeterminate and inconsistent behaviour was obtained from repeat experiments.

However, the reaction sometimes proceeded to completion but the predominant feature of the reaction experiments was for the reaction to "arrest" at some stage. Microscopic examination of the samples has revealed various features but no explanation based on the evidence obtained has been possible and consequently the reasons for the scattered results are not known.

Several types of reactions have been postulated by many investigators to be participating, in one way or another, in the overall mechanism of the reaction between liquid aluminium and silica. These reactions were earlier introduced during the bibliographic review of pertinent works in the field and may be listed as follows:

1. $SiO_2 + 2AlO = Al_2O_3 + SiO$ $\quad \Delta G^o = -997.0 + 221 \times 10^{-3} T$ kJ mol^{-1}
2. $4\ Al + 3SiO_2 = 2Al_2O_3 + 3Si$ $\quad \Delta G^o = -767.0 + 144 \times 10^{-3} T$ kJ mol^{-1}
3. $Al + SiO = AlO + Si$ $\quad \Delta G^o = 165.0 - 6.7 \times 10^{-3} T$ kJ mol^{-1}
4. $4\ Al + SiO_2 = 2AlO + Si$ $\quad \Delta G^o = 483.0 - 284 \times 10^{-3} T$ kJ mol^{-1}
5. $2\ Al + SiO_2 = Al_2O + SiO$ $\quad \Delta G^o = 529.0 - 278 \times 10^{-3} T$ kJ mol^{-1}
6. $Si + SiO_2 = 2\ SiO$ $\quad \Delta G^o = 575.0 - 272 \times 10^{-3} T$ kJ mol^{-1}
7. $4\ Al + Al_2O_3 = 3\ Al_2O$ $\quad \Delta G^o = 1104.0 - 497 \times 10^{-3} T$ kJ mol^{-1}
8. $Al_2O_3 + 2\ Si = Al_2O + 2SiO$ $\quad \Delta G^o = 1196.0 - 486 \times 10^{-3} T$ kJ mol^{-1}
9. $Al + Al_2O_3 = 3\ AlO$ $\quad \Delta G^o = 1734.0 - 500 \times 10^{-3} T$ kJ mol^{-1}
10. $Al_2O_3 + Al_2O = 4\ AlO$ $\quad \Delta G^o = 1948.0 - 501 \times 10^{-3} T$ kJ mol^{-1}

The Gibbs free energy equations for these reaction as a function of temperature in the range 1000 to 1600 K were calculated by using data from references 3,91.92. For elemental aluminium and silica as the starting reacting species the only reaction thermo-dynamically favourable ($\Delta G^o < 0$; $1000 < T < 1600$ K) is reaction No.2.

Since elemental silicon and aluminium were detected everywhere within the reaction product layer and since no experimental evidence emerged to verify the existence or the stability of the sub-oxides of silicon and aluminium, there is thus no allowance for speculations to be made for reaction No.1, although by calculations, this reaction is thermodynamically more favourable than reaction No.2. Therefore the formation of gaseous sub-oxides such as Al_2O, AlO and/or SiO should be discarded as effective species taking part in the mechanism of the reaction.

However, Figs. 4.3.1.54 a-c have clearly shown a crystalline dense cubic phase precipitated in the near vicinity of the unreacted silica, i.e. within the reaction front at 980°C. The EDAX picture detecting silicon and aluminium in the cubes leads to the conclusion that an intermediate phase is formed. It has not been possible to elucidate this phase and it is somewhat speculative to postulate that it is a basis for a mechanism as it was not readily detected and was not present in all samples examined.

Chakraborty[89] found that during the alkali extraction of SiO_2 at 980°C, apart from amorphous silica, a crystalline cubic phase could be formed at all silica/alumina ratios. This was characterized as silica-alumina spinel with the same composition as mullite ($3\ Al_2O_3.2SiO_2$) and remained in intimate contact with the alumina during heating.

It if is assumed that the cubes presented in Figs. 4.3.1.54 b or c are of the same species as the ones identified by Chakraborty, then the additional process in the reaction system must be expressed as follows[90]:

$$Al_{Al/Si} + SiO_2 \rightarrow 3(3\ Al_2O_3.2\ SiO_2) + 8\ Al_{Al/Si} \rightarrow 13\ Al_2O_3 + 6\ Si_{Al/Si}$$

spinel

additional step

$$\Delta G^o = -1417.3 + 0.62\ T \quad /kJ.mol^{-1}/$$

The equilibrium constant for this additional step is given by:

$$k_{eq.} = \frac{a^{13}_{Al_2O_3} \cdot a^{6}_{Si_{Al/Si}}}{a^{3}_{spinel} \cdot a^{8}_{Al_{Al/Si}}}$$

Since the spinel and Al_2O_3 are pure, their activities are unity.

Hence:

$$k = \frac{a^{3}_{Si_{Al/Si}}}{a^{4}_{Al_{Al/Si}}}$$

An identical equation is obtained for the equilibrium constant for the reaction 4 Al + 3 SiO_2 = $3Al_2O_3$ + 3 Si, and thus values for the equilibrium constants of both processes may be calculated for a given interval of temperatures (1000 to 1600 K). The subsequent comparison is shown in Fig. 5.1.3. The details of these calculations are given in Appendix A-5.3.

Fig. 5.1.3. shows a critical temperature of an approximate value of 1062°C at the intersection of both stability lines. Above this temperature aluminium will be required to decompose the spinel phase and if the concentration of aluminium is eliminated then clearly the spinel phase will remain.

The other possible transition(s) in this temperature range are associated with the polymorphs of alumina as discussed in Chapter 2, section 2.3. It is possible that the volume changes associated with poly-

morphic transitions of the alumina from γ, κ and θ to α in this intermediate temperature range will affect the compactness of the reaction layers formed. At higher temperatures when sintering takes place together with the formation of the α form of alumina, shrinkage occurs and cracks form allowing access of the aluminium or aluminium alloy to the silica interface.

The incidence of the cubic phase as detected is limited and although it may have some significance in affecting the surface area of the 'active' interface it cannot be evidenced to postulate the arrest of the reaction in the intermediate temperature range.

The considerable differences in the rate of reaction in this intermediate zone can only reasonably therefore be attributed to physical restraint of the counterflows of the aluminium required for the reaction to continue and the solution of silicon metal produced at the interface, the oxides being retained as the product layer.

In the absence of confirmatory data from X-ray studies it is somewhat speculative to propose the polymorphic change in the alumina as being reduction rate controlling in this range, but it must be considered as one of the most likely explanations. The theoretical evaluation of mullite formation (or preliminary defect spinel) although feasible, and likely evidence for which has been found (Fig. 4.3.1.54 b and c), cannot be definitive as high concentrations would be necessary at the reaction interface to influence the kinetics of the process. No evidence of the high concentrations which would be required to suppress the reaction has been observed. It must also be remembered that the reaction front is advancing with respect to time and a stepped reaction rate would be likely

for the reaction to continue. The resultant barrier layers which would have had to be breached to allow more ingress of liquid aluminium should have been a prominent feature of the microstructure but were in fact totally absent. No evidence of such a mechanism has therefore, been found at the temperatures where the anomalous behaviour occurred.

The mechanism in this range of temperatures 860-1060°C requires further investigation to test the hypothesis presented here.

5.2 Practical implications

At the outset of the work it was envisaged that the investigation would make a contribution to knowledge of the potential for further reaction in steels of residual aluminium with silicate inclusions. This work has shown and, in a certain way, confirmed that if aluminium as deoxidant is added to liquid steel, the reaction potential of aluminium is such that it will reduce the pre-existing inclusions whenever silica is involved. Other sources than the deoxidation (or reoxidation) process itself, such as slag entrainment and refractory erosion which take place during the fabrication of steel, tapping and teeming processes, can also be responsible for the existence of silicate inclusions in the metallic bath. It is thought that this type of reaction can also occur in the solid ingot during heat treatment to the detriment of an aluminium refined grain metal structure, for example, at grain boundaries and defect sites. Eventually, on the metal side of the interface of the silica rich (or vitreous) inclusion/metal, aluminium segregates and, in turn, it will react with the inclusion.

However, the concentrations involved in steels are so dissimilar to those used in the present work that it is not appropriate to speculate in this field.

In other ways the work represents a significant appraisal of reaction mechanisms likely to be of importance in aluminium processing and silica fibre reinforced aluminium.

5.2.1. Aluminium processing

Consistently molten aluminium, particularly when required of high purity, runs the risk of contamination as a result of reacting with silica and silicates, used as furnace linings or even thermocouple sheaths[93]. This work has underlined the need to avoid the use of silica or silicate materials in contact with the molten aluminium if silicon contamination of the melt is to be avoided. Interestingly the reaction will be severe at the normal holding temperature but if the temperature of themolten aluminium was raised to 1000°C then contamination seems less likely. It is however, worth noting this fact as it would not be logical in the normal course of industrial practice. Obviously it is not practicable or desirable to consider such a superheat of aluminium during its processing particularly in the light of energy requirements.

5.2.2 Silica fibre reinforced aluminium

During the last two decades there has been periodic interest in the strengthening of aluminium by fibre reinforcement with silica. Whilst there is little load transfer when the composite is elastically deformed at room temperature, because the elastic moduli of aluminium and silica are so similar, at elevated temperatures, the lower coefficient of elasticity of the silica does give rise to appreciable load transfer to the strong silica fibres. Another practical advantage of the system is that the aluminium is strengthened and the density is reduced by the silica additions.

Two techniques have been developed for the fabrication of aluminium-silica fibre composites. The molten aluminium or aluminium alloy may be simply infiltrated between the silica fibres and allowed to solidify. An alternative technique has been developed by Rolls-Royce[50] in which newly drawn fibres are pre-coated by passing them continuously through a bead of molten aluminium, sometimes containing small additions of antimony or bismuth to control the chemical reaction between the silica and the aluminium. Fabrication is by hot pressing of suitably aligned coated fibres.

In all fibre refinforced systems, the achievement of adequate bonding at the fibre-matrix interface is a compromise. There must be sufficient affinity between fibre and matrix to ensure at least some mechanical keying so that load transfer can occur. Too great an affinity between the components, as is the case with aluminium and silica, can lead to thermal degradation. Chemical interaction of the aluminium and silica at elevated temperatures produces severe deterioration in the mechanical properties, probably as a result of volume changes occurring in the reaction zone leading to crack formation and thereby initiating premature failure.

If optimum mechanical properties are to be achieved and retained throughout service life of the component, it is imperative to minimise chemical interaction between the fibre and the matrix both during fabrication and during service. Clearly important practical conclusions can be drawn from the present work. The existence of a reaction rate minima in the temperature range 880-1050^{o}C might prove useful in limiting fibre-liquid interaction during the fabrication process. In addition it would

appear that dilution of the aluminium by alloying elements such as manganese, iron and silicon would certainly further reduce liquid-fibre reaction and might also improve the resistance to solid state chemical reaction between the fibre and the matrix. Unfortunately it would appear unlikely that there will be any practical opportunity to test the usefulness of these suggestions since commercial interest in aluminium-silica fibre composite materials as an engineering material has waned in recent years.

6. CONCLUSIONS AND SUGGESTIONS FOR FURTHER INVESTIGATIONS

The experimental technique developed to determine the rates of the reaction between liquid aluminium and vitreous silica at temperatures of practical importance was very satisfactory. The results show that aluminium as a strong deoxidant readily reacts with silica allowing it to be postulated that a similar reaction must occur during deoxidation practice of steelmaking, where secondary reactions take place between pre-existing silicate inclusions and dissolved aluminium.

The mechanism for these reactions has been clearly identified at temperatures below 860°C. The reaction is almost entirely diffusion controlled and maintained by transport of aluminium and silicon across the porous matrix. The porosity of the matrix is derived from the volume changes occurring during reaction.

Above ~880°C the process is abruptly discontinued and further progress of reaction is conditioned by a mechanism not fully elucidated but the polymorphs of alumina and the formation of a spinel type phase contribute. It is only as high as ~1050°C that the rate of reaction is gradually recovered by fissure formation as a result of sintering of the alumina phase and a consequent variation in the mechanism of reaction. The process is probably controlled by the transport of aluminium to the interaction front and limited by the saturated liquidus alloy present at the interface.

Additions of silicon up to 15 atomic percent to the liquid aluminium does not affect the rate of reaction whatsoever. Local equil-

ibrium of iron and manganese concentrations effectively reduces the solubility of silicon in the liquid metal phase, thereby reducing rates of counter-diffusion of silicon and aluminium and brings about a proportional reduction in the rate of reaction.

This work has not been exhaustive in its treatment of the reaction between liquid aluminium and vitreous silica. For instance, it would be of interest if the intercellular alumina spacing along the reaction product layer were measured for temperature and time conditions. With increasing temperature, the transport of silicon along the coarse matrix will become more important than its passage through the interaction front. A detailed study of the porosity and tortuosity factors would give means for solving exact equations in order to prescribe the flux of aluminium in porous cells of alumina. The mechanism in the intermediate temperature range 860-1060^{o}C must be evaluated conclusively.

The composition gradient of silicon, gradually dissolved in the liquid phase, for temperature and time conditions, needs more study to elucidate more fullythe aluminium and silicon counter-diffusion fluctuations in the reaction front. A more detailed interpretation of the behaviour of the interaction front at various times and temperatures could lead to a model describing the progress of reaction. This is notably absent from the literature at present.

The inhibiting effect of the increasing concentrations of both manganese or iron on aluminium may be attributed to the diminishing thermo-dynamic driving force behind the reaction, when aluminium is no longer the pure reacting agent. Available information concerning the effect of elements such as manganese and iron on the thermo-dynamic activity of liquid aluminium, when reacting with silica (and/or silicates), should be further investigated by more experimental work.

REFERENCES

1. KUBASCHEWSKI, O., "Thermochemistry of Metal-refractory Interactions", Rev. Hautes Temperat. et refract., t.3, 1966, p. 229-34.

2. GEIRNAHERT, G., "Meteaux Liquides, Compatibilites et Angles de Moillages", Bull. de la Soc. Franc. de Ceramique, n. 6, Jan-Mar. 1975, p. 7-51.

3. KUBASCHEWSKI, O., EVANS, E.L., "Metallurgical Thermochemistry", Pergamon Press, 1956.

4. PRABRIPUTALOONG K., PIGGOTT, M.R., "Thin Film Studies of the Reaction of Silica with Aluminium", J. of the Amer. Ceram. Soc., vol. 56, n. 4, 1973, p. 177-80.

5. HANSEN, M., "Constitution of Binary Alloys", 2nd ed., McGraw Hill, N.Y. 1958.

6. Ref. cit. in ref. n. 12, Journal of Instit. of Metals, 77, 1950, p. 498.

7. DEVEREUX, O.F., "Structure of Reaction Formed Alumina-silicon Cermets", Trans. of the Metall. Soc. AIME, vol. 242, May 1968, p. 795-99.

8. CISSE, J., BOLLING, G.F., KERR, H.W. "Simultaneous Refinement of Primary and Eutectic Silicon Hypereutectic Al-Si Alloys", Metall. Transactions, vol. 63, Mar. 1975, p. 195-97.

9. BOLLING, G.F., CISSE, J., COLE, G.S., U.S. PATENT n. 3607241.

10. GERSHINSKY, A.E., KHOROMENSKO, H.A., CHEREPOV, E.I., "Kinetics of Interaction Between Films of Al and SiO_2", Izv.Ak.N.SS52, Neorganicheskie Materialy, vol. 12, n.4, 1976, p. 627-30.

11. BREWER, L., SEARCY, A.W., "Gaseous Species of the Aluminium-alumina System", J. of the Amer. Ceram. Soc. 73, n. 11, 1951, p. 308.

12. VAN LANCKER, M., "Metallurgy of Aluminium Alloys", Chapman and Hall Ltd., London 1967.

13. GRUBE, G., SCHNEIDER, Z.A., ESCH, N., FLAD, M., Anorg. Chem., vol 1, 260, 1949, p.120

14. SCHAFER, H., SPEIDEL, H., Z. Elektrochem., 53 1949, p. 339-41.

15. BREWER. L., EDWARDS, R.K., J. Phys. Chem., vol. 58, 1954, p. 351

16. BREWER, L., GREENE, F.T., J. Phys. Chem. (Solids), 2, 1957, p. 286

17. HOLLAND, L., "The Properties of Glass Surfaces", Chapman and Hall, London, 1964

18. KOCHNEV, P.V., GOLD, P.V., Zh. Prikladnoie Khim., 21, 1948, p. 1249.

19. SOSMAN, R.B., "The Phases of Silica", New Brunswick, 1965 also "The Properties of Silica", Amer-Chem. Soc., Monogr. series n. 37. The Chem. Catalog. co., NY, 1927.

20. SMIRNOVA, T.P. DANILOVISH, V.S., AYUPOV, B.M., KUZNETZOV, F.A., "Mechanism of Thermal Oxidation of Silicon", Izv. Ak. SSSR, Neorgan. materialy, vol. 11, n. 8, 1975, p. 1374-76.

21. MARUMO, C., PASK J.A., "Reactions and Wetting Behaviour in the Aluminium-Fused Silica System". J. of Materials Sc., 12, 1977, p. 223-33

22. BRENNAN, J.J., PASK, J.A., Journal of the Amer. Ceram. Soc., vol. 51 4.10, 1958, p. 509

23. YANAGIDA, H., KROGER, F.A., "The system Al -O" J. of the Amer. Ceram. Soc., vol. 51, n. 12, 1968, p. 700-06

24. CHAMPION, J.H., KEENE, B.J., STILLWOOD, J.M., "Wetting of Aluminium Oxide by Molten Aluminium and Other Metals", J. of Materials Sc., 4, 1969, p. 39-49

25. PORTER, O.F., SCHISSEL, P., INGHRAM, M.G., J. Chem. Phys., 23, 1955, p. 339

26. ROOKSBY, H.P., "Oxides and Hydroxides of Aluminium and Iron" Chapter X in "The Xray Identification and Crystal Structures of Clay Minerals", G. Brown, Mineral. Soc., London, 1972.

27. DAY, M.K.B., HILL, V.J., "The Thermal Transformations of the Aluminas and Their Hydrates", J. Phys. Chem., vol 57, n. 12, 1953, p. 946-50.

28. NEWSOME, J. W., HEISER, H.W., RUSSEL, A.S., STUMPF, H.C., "Aluminia Properties", ALCOA, Res. Labs., Tech. pap. n. 10, 1960

29. STUMPF, H.C., RUSSEL, A.S., NEWSOME, J.W., TUCKER, L.M., "Thermal Transformation of Alumina Hydrates", Indust. Chem. Eng., vol. 42, n. 7, 1950, p. 1398-403

30. BYE, G.G., GAUVIN, D.G., "Crystallization of Metastable Aluminas in the Presence of V_2O_5". J. of the Amer. Ceram. Soc., vol. 57, n. 2, 1974, p. 55-57

31. BADKAR, P.A., BAILEY, H.E., "The Mechanism of Simultaneous Sintering and Phase Transformation in Alumina", J. Materials, Sc., vol. 11, n. 10, 1976, p. 1794-806

32. LIPPENS, B.C., PhD Thesis, Delft University, 1961; also "Physical and Chemical Aspects of Absorbents and Catalysts", ed. Liusen, BG. Academic Press, 1969.

33. BUDWORTH, D.W., "An introduction to Ceramic Science, Pergamon Press, 1970

34. SAALFELD, D.H., Clay Min. Bulletin, 3119, 1958, p. 249

35. LIPPENS, B.C., DE BOER, J.H. Acta Crystallograph. 17, 1964, p. 1312

36. KINGERY, W.D., BOWEN, H.K., UHLMANN, D.R., "Introduction to Ceramics", 2nd ed., John Wiley and Sons, 1976

37. ERVIN, G., Acta Crystallograph., 5, 1952, p. 105-08

38. BRINDLEY, G.W., "Hydroxides and Oxides of Aluminium", Progress in Ceramic Sc., vol. 3, ed. J. E. Burke, Pergamon Press, 1963.

39. CHRISTIAN, J.W., "The Theory of Transformation in Metals and Alloys", 1st. ed., Pergamon Press, Oxford, 1965

40. STRINGER, R.K., WARBIE, C.E., WILLIAMS, L. G., "Kinetics of Reactions in Ionic Systems", ed. Gray, T. Frechette, V.D., NY., Plenum Press, 1969

41. STIRLAND, D.J., THOMAS, H.G., MOORE, N.C., "Observations on Thermal Transformations in Alumina", Transactions of the Brit. Ceram. Soc., vol. 57, n. 2, 1958, p. 69-84

42. IIER, R.K., J. of the Amer. Ceram. Soc., 44, 1961, p. 618-24

43. SCOTT, B.A., HORSMAN, W.H., "Structural Changes During the Production of Corundum by Calcination of Gibbsite and Their Influence on Fabrication", c.f. in ref. n. 42 (Gauvin, D.G.)

44. GAUVIN, D.G., PhD Thesis, University of Sheffield, 1975.

45. SIMPKIN, G.T., PhD Thesis, University of Sheffield, 1971.

46. STANDAGE, A.E., GANI, M.S., "Reaction Between Vitreous Silica and Molten Aluminium", J. of the Amer, Ceram. Soc., vol. 50, n.2 1967, p. 101-05

47. PRABRIPUTALOONG, K., PIGGOTT, M.R., "The Reaction Between Silica and Aluminium", J. Electrochem. Soc., Solid State Sc. and Technol., vol. 1221, n. 3, 1974, p. 430-34

48. CHOU, N.T., ELDRIDGE, J.M. "Effects of Material and Processing Parameters on the Dielectric Strength of Thermally Grown SiO_2 Films", J. Electroch. Soc., Solid State Sc., vol. 117, n. 10, 1970, p. 287-93

49. GALANTE, F., GARDINI, A., MANFRE, G., Revista Stat. Sper. Vetro, n. 2, Mar-Apr., 1973, p. 49-54

50. SQUIRES, H.V., RAYSON, H.W., "Thermal Degradation of Silica Fiber Reinforced Aluminium", J. of Materials Science, 12, 1977, p. 1010-18

51. PICKERING, F.B., "Non-Metallic Inclusions Formed in Rimmed Steels", Jernkontoret Ann., 148, 11, 1964, p. 845-72

52. WAUDBY, P.E., SALTER, W.J.M., PICKERING, F.B., "Study on the Reaction Between Silicate Inclusions and Aluminium in Molten Iron", J. Iron and Steel Inst., July 1973, p. 486-92

53. STEPHENSON, I.M., GLADMAN, T., PICKERING, F.B., Swinden Labs., cit. in ref. 60 as private communication.

54. WAUDBY, P.E., PhD These, Sheffield Polytechnic, 1973.

55. SNOW, R.B., SHEA, J.S., Mechanisms of Erosion of Nozzles in Open-Wearth-Ladles", J. of the Amer. Ceram. Soc., vol. 32, 1949, p. 87-94.

56. BRONDYKE, K.T., "Effect of Molten Aluminium on Alumina-Silica Refractories". J. of the Amer. Ceram. Soc., vol. 36 n. 5, 1953, p. 171-74

57. HUMENIK, M., KINGERY, W.D., J. of the Americ. Ceram Soc., 37, n. 1, 1954, p. 18

58. PASK, J.A., "Glass-Metal "Interfaces" and Bonding" in "Modern Aspects of the Vitreous State", ed. J. Mackenzie, vol. 3, Butterworths, London, 1964.

59. MYSLIVEC, T., "Fyz. Chem. Zaklady ocelarstvi", 2 vyd. SNTL, Praha 1971

60. GIAZOV, V.M., VERTMAN, A.A., "Structure and Properties of Liquid Metals", ed. A. M. Samarin, Acad. Sc. USSR., Moscow, Baikov's Inst. of Metall., 1960, p. 121

61. ARRIDGE, R.G.C., BAKER, A.A., CRATCHIEY, D., "Metal Coated Fibers and Fibers Reinforced Metals". J. Sc. Instrum., GB, 41, 5, 1964, p. 259-61

62. PRABRIPUTALOONG, K., PIGGOTT, M.R., "Reduction of SiO_2 by Molten Al ", J. of the Amer. Ceram. Soc., 56 April 1973, p. 184-85

63. TAMMANN, G., Z.Anorg.Allg.Chem., 78, 1920, p. 111

64. PILLING, N.B., BEDWORTH, R.E., J. Inst. of Metals, 29, 1923, p. 529

65. SCHMALZRIED, H., "Solid State Reactions", Academic Press, 1974

66. JANDER, W., Z. Anorg. Allg. Chem., 1, 1927. p. 163

67. HULBERT, S.F., J. British Ceram. Soc., 6, 1969, p.11-20

68. HULBERT, S.F., POPOVITCH, M.J., "Kinetics and Mechanisms of the

Reaction Between TiO_2 and $CrCO_3$" in "Kinetics of Reactions in Ionic Systems", ed. Gray T., Frechette, V.D., Plenum Press, 1969

69. GARNER, W.E., "Chemistry of the Solid State", Butterworths, 1955

70. THEMELIS, N.T., PhD. Thesis, University Minnesota, 1961

71. SHARP, P.H., BRINDLEY, G.W., ACHAR, B.N.N., J. Amer. Ceram Soc. 49.1966, p. 379-82

72. LEVENSPIEL, O., "Chemical Reaction Engineering", 2nd. ed., John Wiley & Sons, 1972

73. McKEWAN, W. M., Trans. AIME, 212, 1958, p. 791-92

74. STALHANE, B., MALBERG, T., Jernkontorets Ann., 85, 1930, p. 1 and 609

75. SPENCER D.W., TOPLEY, B., J. Chem. Soc. 6: 2633, 1929

76. MELCHER, G., CAJADO, E.V., Bol. Assoc. Brasil. Metais, 5, 1949, p. 341

77. THEMELIS, N.T., GAUVIN, W.H., The Can. Min. Metall. Boll., 55, 1962, p. 444-56

78. LANGMUIR, I., J. Chem. Soc. 38 : 2263, 1917

79. JACOBS, P.W.M., "Kinetics of Thermal Decomposition of Solids" in "Kinetics of Reactions in Ionic Systems", ed. Gray, T., Frechette, V.D., Plenum Press, 1969.

80. MONDOLFO, L.F., "Aluminium alloys, Structures and Properties," Butterworths, 1976

81. PYE UNICAM, "Manganese and Iron in Aluminium Alloys" Cambridge, 1961

82. N.N., "Analysis of Aluminium and its Alloys", The Brit.Al,Co.,1961

83. CULLITY,B.D.. "Elements of X-ray Diffraction", Addison-Wesley, Publish.,Co., 1967

84. HEARLE,J.W.S.,SPARROW,J.T.,CROSS,P.M., "The Use of the Scanning-Electron Microscope", Pergamon Press,1974

85. LEWIS,D.B., Private communication

86. HILLS,A.W.D., "The Importance of Macroscopic Transport Phenomena in Gas/Solid Reactions",in "Heterogeneous Kinetics at Elevated Temperatures", Plenum Press, 1970

87. GEIGER,G.H.,POIRIER,P.R., "Transport Phenomena in Metallurgy", Addison-Wesley,1973, p.525

88. BARINOV,G.I., "Dissolution Kinetics of Metals in Liquid Aluminium", Tekcnolog.Materia'ly, 197o,Elektrotekcn.Tr.

89. CHAKRABORTY,A.K., J.Amer.Ceram.Soc.,vol.62,n.3-4,1979,p.120-24

90. ROBIE,R.A.,WALDBAUM,D.R., Geological Survey Bull.,n.1259, US Governm.Print.Off.,Washington,1968

91. ALCOCK,C.B., "Formation of Volatile Oxides by Furnace Construction Materials", Trans.Brit.Ceram.Soc., 60.n.2.1961.p.147-64

92. ELLIOTT,J.T.,GLEISER,M., "Thermochemistry for Steelmaking",vol.1, Addison-Wesley,1968

93. PRICE,R.F., Private communication

Table 2.1. - Nomenclature of transition aluminas.[26,41]

Great Britain	USA	Germany	France
delta	gamma	gamma	gamma
delta + theta	delta	delta	delta
gamma	eta	eta	eta
theta	theta		theta
	iota		
chi + gamma	chi	chi	chi + gamma
kappa + theta	kappa	kappa	kappa + delta
alpha	alpha	alpha	alpha

Table 3.1. Some chemical and physical properties of the materials used in the preliminary experiments.

Protective inert gas	(Commercial argon, BOC) purity/mass %/ : 99.999 flow rate/cm^3/min/ : = 150
Aluminium	(British Aℓ.Co) chemical analysis/mass %/; Aℓ-99.998; Fe-0.0005; Si-0.0005; Cu-0.0005 mass/g/: 35.0 - 40.0
Silica rods	(Vitreosil - R) Spectrographic analysis/mass % of oxides, mainly Fe_2O_3/: 0.03 optical character: transparent (dense, non-porous) preliminary heat treatment: annealing in air at 1280°C for several hours.
Crucibles	(Purox Recrystallized alumina): H : D = 40:30 mm

Table 3.2. Outline of the preliminary experimental programme

Diameter of the rod	Temperature	Immersion time
mm	°C	min
3.0	760	0.5 - 30
	815	0.5 - 30
	840	1.0 - 25
	860	1.0 - 15
5.0	760	0.5 - 30
	815	1.0 - 40
	840	1.0 - 30
	860	1.0 - 30
	920	5.0 - 90
	980	10.0 - 120
10.0	760	2.0 - 60
	815	2.0 - 60
	840	1.0 - 45
	860	1.0 - 45
	920	10.0 - 120
	980	15.0 - 120

Table 3.3 : Outline of fabrication procedures and some characteristics of metallic starting and produced materials.

Fabrication of alloys

Metals used:

Aluminium/Super pure, Brit. Aℓ, Co/chem. composition/mass %/:
Aℓ-99.998; Fe-0.0005; Si-0.0005; Cu-0.0005

Manganese/electrolytic, Midgley, Sheffield/chem. composition/mass %/:
Mn-99.99; Fe-0.008

Iron/Japanese electrolytic, Derby and Co. Ltd./chem. composition/mass %/:
Cu-0.004; Fe-99.9; C-0.005; P-0.004; S-0.005; Si-0.005; Mn-0.005

Silicon/Watsons, "Metallurgists", Dronfield/chem. composition/mass %/:
Si-98.0; Fe-0.4; Ca-0.2; Aℓ-0.3

Mass per cast of each fabricated alloy/kg/: 4.0

Desired chemical composition/mass %/

Aℓ-5; 10; 15 atomic % Mn: 9.68; 18.45; 26.4 mass %, respectively
Aℓ-5; 10; 15 atomic % Fe: 9.83; 18.54; 26.8 mass %, respectively
Aℓ-5; 10; 15 atomic % Si: 5.23; 10.44; 15.6 mass %, respectively

Crucibles used:

Thermax G 10
Chem. composition/mass %/: SiO_2-1.8; FeO-1.3; $Aℓ_2O_3$-10.0; CaO-2.0; Magnesite - 84.6

Pure magnesia

Protective argon during melting/comm. purity Ar, BOC/cm^3/min/: 1500 - 2000

/cont....

... cont./Table 3.3.

Pouring temperature/°C/: Aℓ - Mn alloys - 1050 - 1150
Aℓ - Fe alloys - 1050 - 1150
Aℓ - Si alloys - 900 - 1000

Liquid metal poured into cold water

Actual chemical analysis of aluminium-alloys fabricated

Alloys: Aℓ-5; 10; 15 atomic % Mn
Method: atomic absorption/stan.instr.conditions cit.in ref.81
chemical analysis/mass %/: 9.52; 18.73; 24.28, respectively.
Aℓ-5; 10; 15 atomic % Fe
Method: atomic absorption/stan.instr.conditions cit.in ref.81
chemical analysis/mass %/: 9.90; 18.80; 27.21, respectively.
Aℓ-5; 10; 15 atomic % Si
Method: Gravimetric Regelsberger.[82]
chemical analysis/mass %/: 5.4; 10.2; 15.8, respectively.

with pure aluminium and aluminium-manganese, iron, silicon alloys at elevated temperatures.

Metal system	Diameter of the silica rod	Temperature	Immersion time
	mm	°C	min
Al	3.0/static/	1110	2.5 - 60
		1170	5 - 30
		1220	2.5 - 20
		1265	1 - 15
	5.0/static/	1110	10 - 90
		1170	5 - 45
		1220	5 - 30
		1265	1 - 15
	10.0/static/	1110	20 -180
		1170	10 - 90
		1220	10 - 60
		1265	2 - 25
	10.0/ rotating/ rpm = 5,15,35	1170	10 - 90
		1265	2 - 20
Al-5 atomic % Mn	10.0/static/	1110	30 -180
		1170	5 -120
		1220	5 - 60
		1265	2 - 35
	10.0/ rotating/ rpm = 5,15,35	1170	5 -120
		1265	5 - 35
Al-10 atomic % Mn	10.0/static/	1110	30 -240
		1170	15 -210
		1220	10 -150
		1265	5 - 75
Al-15 atomic % Mn	10.0/static/	1110	45 -240
		1170	30 -210
		1220	20 -180
		1265	10 - 90
Al-5 atomic % Fe	10.0/static/	1110	20 -210
		1170	25 -120
		1220	5 - 60
		1265	5 - 30

/cont....

...cont./ Table 3.4.

Metal System	Temperature of the silica rod.	Temperature	Immersion time
	mm	°C	min
Aℓ-5 atomic % Fe	10.0 /rotating/ rpm=5,15,35	1170 1265	5 -120 5 -45
Aℓ-10 atomic % Fe	10.0 /static/	1110 1170 1220 1265	15 -270 15 -240 10 -120 5 -75
Aℓ-15 atomic % Fe	10.0 /static/	1110 1170 1220 1265	20 -240 45 -210 20 -180 5 -120
Aℓ-5 atomic % Si	10.0 /static/	1110 1170 1220 1265	10 -180 5 -90 10 -60 2 -30
Aℓ-10 atomic % Si	10.0 /static/	1110 1170 1220 1265	10 -180 5 -75 4 -45 5 -30
Aℓ-15 atomic % Si	10.0 /static/	1110 1170 1220 1265	10 -180 10 -60 5 -45 5 -25

Table 3.5. Etching (and leaching) solutions used for specimens to be submitted to x-ray diffraction analysis and optical and Scanning -electron microscope (SEM) examination

X-ray diffraction analysis		
Metal to be etched	Etchant	Time( )
aluminium	A. 5 ml (40%) hydrofluoric acid + 95 ml distilled water	10 min
aluminium-silicon alloys	B. 10 ml sodium hydroxide + + 90 ml distilled water	15 min
	A as above	5 min
aluminium-manganese and aluminium iron alloys	C. 5 ml (40%) hydrofluoric acid + + 10 ml conc. hydrochloric acid + + 15 ml conc. nitric acid + + 70 ml distilled water	15 min

SEM - examination		
Metal to be etched	Etchant	Time
Aluminium	A (as above)	3 min
aluminium-silicon alloys	B (as above)	5 min
	A (as above)	2 min
aluminium-manganese and aluminium-iron alloys	A (as above)	3 min
	6 % bromine alcohol	12 min

Table 4.1.2.1. Experimental results: the kinetics of reaction between liquid pure aluminium and vitreous silica.
Diameter of the silica rod: 3.0 mm

Temperature	Immersion time	Product layer thickness	Percentage conversion
t^o	t	$\Delta r = r_o - r_i$	$1-(1-R_x)^{0.5}$
^oC	min	mm	%
760	0.5	0.01	0.67
	1.	0.02	1.33
	2.	0.04	2.67
	5.	0.08	5.33
	5.	0.09	6.00
	7.	0.11	7.33
	10.	0.15	10.00
	15.	0.21	14.00
	20.	0.27	18.00
	25.	0.33	22.00
	25 •	0.35	23.33
	30.	0.38	25.33
	30.	0.39	26.00
^oC	min	mm	%
815	0.5	0.03	2.00
	1.	0.05	3.33
	5.	0.25	16.67
	5.	0.22	14.67
	5.	0.23	15.33
	10.	0.45	30.00
	10.	0.42	28.00
	10.	0.43	28.67
	15.	0.62	41.33
	15.	0.61	40.67
	20.	0.84	56.00
	25. *	1.08	72.00
	30.	1.31	87.33

* Fig. 4.3.1.9 ; F - 32
• Fig. 4.3.1.15; F - 35

/cont ···

..cont/Table 4.1.2.1.kinetics pure aluminium - silica reaction system. Diameter of the silica rod: 3.0 mm

Temperature	Immersion time	Product layer thickness	Percentage conversion
t^o	t	$\Delta r = r_o - r_i$	$1-(1-R_x)^{0.5}$
^oC	min	mm	%
840	1.	0.09	6.00
	2.	0.18	12.00
	5.	0.48	32.00
	5.	0.40	26.67
	5.	0.37	24.67
	7.	0.52	34.67
	10. •	0.81	54.00
	10.	0.77	51.33
	12. o	0.88	58.67
	15.	1.15	76.67
	20.	1.45	96.67
	20.	1.48	98.67
	25.	1.50	100.00
^oC	min	mm	%
860	1.	0.11	7.33
	2. *	0.18	12.00
	2.	0.20	13.33
	5.	0.58	38.67
	7.	0.72	48.00
	10.	1.10	73.33
	10.	1.05	70.00
	10.	1.02	68.00
	12.5	1.26	84.00
	15.	1.47	98.00
	15.	1.49	99.33

* Fig. 4.3.1.6. ; F - 30
• Fig. 4.3.1.8.,a.; F - 31
o Fig. 4.3.1.14. ; F - 34

/cont ...

..cont/Table 4.1.2.1.kinetics pure aluminium - silica reaction system. Diameter of the silica rod: 3.0 mm

Temperature	Immersion time	Product layer thickness	Percentage conversion
t^{o}	t	$\Delta r = r_o - r_i$	$1-(1-R_x)^{0.5}$
^{o}C	min	mm	%
1110	2.5	0.09	6.00
	5	0.18	12.00
	10	0.29	19.33
	10 ×	0.32	21.33
	15 *	0.40	26.67
	40 •	1.05	70.00
	50	1.31	87.33
	60	1.50	100.00
^{o}C	min	mm	%
1170	5	0.30	19.8
	10	0.61	40.67
	10 o	0.58	38.67
	15	0.87	58.00
	20	1.10	73.30
	20	1.14	74.00
	25 +	1.40	93.30
	30	1.50	100.0

• Fig. 4.3.1.30 ; F - 43

\+ Fig. 4.3.1.34 ; F - 45

o Fig. 4.3.1.35 ; F - 45

* Fig. 4.3.1.38 ; F - 47

× Fig. 4.3.1.49 ; F - 54

/cont ...

..cont/Table 4.1.2.1. kinetics pure aluminium - silica reaction system. Diameter of the silica rod: 3.0 mm

Temperature	Immersion time	Product layer thickness	Percentage conversion
t^o	t	$\Delta r = r_o - r_i$	$1-(1-R_x)^{0.5}$
°C	min	mm	%
1220	2.5	0.21	14.00
	2.5	0.25	16.67
	5 •	0.41	27.33
	5	0.39	26.00
	15	1.16	77.33
	15	1.19	79.33
	20	1.50	100.00
°C	min	mm	%
1265	1. *	0.06	4.00
	2.	0.21	14.00
	4	0.39	26.00
	5.	0.48	32.00
	12.	1.20	80.00
	15.	1.50	100.00
	15.	1.50	100.00

* Fig. 4.3.1.27 ; F - 41

• Fig. 4.3.1.29,b ; F - 42

/cont ...

..cont/Table 4.1.2.1. kinetics pure aluminium - silica reaction system. Diameter of the silica rod: 5.0 mm

Temperature	Immersion time	Product layer thickness	Percentage conversion
t^o	t	$\Delta r = r_o - r_i$	$1-(1-R_x)^{0.5}$
°C	min	mm	%
760	0.5	0.01	0.40
	1.	0.02	0.80
	2.	0.03	1.20
	5.	0.06	2.40
	5.	0.05	2.00
	10.	0.15	6.00
	10.	0.17	6.80
	15.	0.20	8.00
	15.	0.19	7.60
	20.	0.24	9.60
	20.	0.26	10.40
	25.	0.32	12.80
	30.	0.40	16.00
°C	min	mm	%
815	1.	0.04	1.60
	2.	0.10	4.00
	5.	0.21	8.40
	5.	0.22	8.80
	10.	0.47	18.80
	10. *	0.50	20.00
	10.	0.51	20.40
	15.	0.77	30.80
	20.	1.05	42.00
	25.	1.40	56.00
	30. •	1.55	62.00
	40 o	2.05	82.00

• Fig.4.3.1.7 ; F - 30
* Fig.4.3.1.13 ; F - 34
o Fig.4.3.1.18 ; F - 37

/cont ...

..cont/Table 4.1.2.1. kinetics pure aluminium - silica reaction system. Diameter of the silica rod: 5.0 mm

Temperature	Immersion time	Product layer thickness	Percentage conversion
t^{o}	t	$\Delta r = r_o - r_i$	$1-(1-R_x)^{0.5}$
^{o}C	min	mm	%
840	1.	0.07	2.80
	2.	0.15	6.00
	5.	0.35	14.00
	10. •	0.84	33.60
	15. +	1.21	48.40
	20.	1.54	61.60
	25. o	2.00	80.00
	30.	2.50	100.00
^{o}C	min	mm	%
860	1.	0.14	5.60
	2. *	0.23	9.20
	5. *	0.63	25.20
	5.	0.58	23.20
	10.	1.19	47.60
	10.	1.11	44.40
	15.	1.67	66.80
	20.	2.16	86.40
	20.	2.22	88.80
	20. *	2.18	87.20
	25.	2.42	96.80
	25.	2.45	98.00
	30. *	2.50	100.00

* Fig.4.3.1.1. ; F - 28

• Fig.4.3.1.8.,b; F - 31

o Fig.4.3.1.10. ; F - 32

\+ Fig.4.3.1.20,a-c to 25; F - 38 to 40

/cont ...

..cont/Table 4.1.2.1. kinetics pure aluminium - silica reaction system. Diameter of the silica rod: 5.0 mm

Temperature	Immersion time	Product layer thickness	Percentage conversion
t^{o}	t	$\Delta r = r_o - r_i$	$1-(1-R_x)^{0.5}$
^{o}C	min	mm	%
920	5	0.08	3.23
	5	0.82	32.80
	5	1.00	40.00
	10	-	-
	10	1.28	51.20
	20	-	-
	20	0.60	24.00
	20	1.25	50.00
	30	1.70	68.00
	30	2.50	100.00
	40	0.96	38.40
	40 x	2.00	80.00
	60	2.50	100.00
	60	2.22	88.80
	60	1.74	69.60
	90	1.80	72.00
	90	2.15	86.00
	90	2.23	89.20
^{o}C	min	mm	%
980	10	0.26	10.40
	10	0.71	28.40
	20	-	-
	20	0.16	6.40
	20	0.51	20.40
	30	0.36	14.40
	30	1.27	50.80
	45	1.19	47.60
	45	1.95	78.00
	60	0.17	6.80
	60	0.79	31.60
	90	0.45	18.00
	90	1.10	44.00
	90	0.96	38.40
	90 o	1.85	74.00
	120 •	1.01	40.40
	120	1.80	72.00
	120	2.50	100.00

x Fig. 4.3.1.50 ; F - 55

o Fig. 4.3.1.52 ; F - 56

• Fig. 4.3.1.54,a;F - 57

/cont ...

..cont/Table 4.1.2.1. kinetics pure aluminium - silica reaction system. Diameter of the silica rod: 5.0 mm

Temperature	Immersion time	Product layer thickness	Percentage conversion
t^o	t	$\Delta r = r_o - r_i$	$1-(1-R_x)^{0.5}$
^oC	min	mm	%
1110	10	0.26	10.40
	20	0.45	18.00
	40	1.12	44.80
	50	1.40	56.00
	70	1.91	76.40
	90	2.34	93.60
^oC	min	mm	%
1170	5 •	0.33	13.00
	10	0.57	22.67
	20	1.06	42.31
	30 x	1.55	62.00
	45 *	2.50	100.00
^oC	min	mm	%
1220	5	0.46	18.30
	10	0.80	32.00
	15 +	1.29	51.67
	20	1.70	68.00
	30	2.44	97.40
^oC	min	mm	%
1265	1	0.10	4.00
	5	0.74	29.60
	7.5	1.06	42.50
	10 o	1.41	56.30
	15	2.19	86.70

* Fig.4.3.1.26 ; F - 41

• Fig.4.3.1.29,a;F - 42

\+ Fig.4.3.1.32; F - 44

o Fig.4.3.1.36; F - 46

x Fig.4.3.1.39; F - 48

/cont...

..cont/Table 4.1.2.1. kinetics pure aluminium - silica reaction system. Diameter of the silica rod: 10.0 mm

Temperature	Immersion time	Product layer thickness	Percentage conversion
t^{o}	t	$\Delta r = r_o - r_i$	$1-(1-R_x)^{0.5}$
^{o}C	min	mm	%
760	2.	0.03	0.60
	5.	0.05	1.00
	10.	0.13	2.60
	15.	0.22	4.40
	20.	0.29	5.80
	20.	0.30	6.00
	25.	0.41	8.20
	25.	0.39	7.80
	30.	0.48	9.60
	45.	0.65	13.00
	60	0.90	18.00
^{o}C	min	mm	%
815	2. *	0.11	2.20
	5.	0.30	6.00
	5.	0.28	5.60
	5. •	0.27	5.40
	10.	0.45	9.00
	15. o	0.68	13.60
	20.	0.87	17.40
	20.	0.89	17.80
	20.	0.90	18.00
	25.	1.25	25.00
	25.	1.22	24.40
	30.	1.53	30.60
	30.	1.50	30.00
	30.	1.49	29.80
	45.	2.10	42.00
	60.	2.85	57.00

* Fig.4.3.1.2.; F - 29
• Fig.4.3.1.4.; F - 29
o Fig.4.3.1.5.; F - 30

/cont...

..cont/Table 4.1.2.1. kinetics pure aluminium - silica reaction system. Diameter of the silica rod: 10.0 mm

Temperature	Immersion time	Product layer thickness	Percentage conversion
t^o	t	$\Delta r = r_o - r_i$	$1-(1-R_x)^{0.5}$
^oC	min	mm	%
840	1	0.14	2.80
	2	0.26	5.20
	5	0.36	7.20
	5	0.41	8.20
	10 *	0.86	17.20
	15	1.15	23.00
	15	1.25	25.00
	20	1.67	33.40
	20 •	1.54	30.80
	25	2.00	40.00
	30	2.54	50.80
^oC	min	mm	%
860	1 ⊙	0.09	1.80
	5	0.67	13.40
	5 ⊙	0.65	13.00
	10 ⊙	1.13	22.60
	15	1.86	37.20
	15	1.83	36.60
	15	1.80	36.00
	20	2.36	47.20
	25	2.80	56.00
	25	2.93	58.60
	30	3.50	70.00
	30	3.45	69.00
	45	5.00	100.00

* Fig.4.3.1.8,c; F - 31

• Fig.4.3.1.11.; F - 32

⊙ Fig.4.31.12,a-c; F - 33

/cont ...

..cont/Table 4.1.2.1. kinetics pure aluminium - silica reaction system. Diameter of the silica rod: 10.0 mm

Temperature	Immersion time	Product layer thickness	Percentage conversion
t^{o}	t	$\Delta r = r_o - r_i$	$1-(1-R_x)^{0.5}$
°C	min	mm	%
920	10	-	-
	10	0.59	11.80
	10	0.71	14.20
	20	0.30	6.00
	20	2.92	58.40
	30	2.50	50.00
	30	4.20	84.00
	30	5.00	100.00
	60	0.69	13.80
	60	2.43	48.60
	60	4.51	90.20
	90	2.50	50.00
	90 x	3.82	76.40
	120	3.80	76.00
	120	4.77	95.40
	120	5.00	100.00
°C	min	mm	%
980	15	0.46	9.20
	15	0.62	12.40
	20	-	-
	20	0.31	6.20
	20 +	0.50	10.00
	30	0.63	12.60
	30	2.02	40.40
	45	0.35	7.00
	45	1.17	23.40
	45	3.46	69.20
	60	0.92	18.40
	60	2.20	44.00
	60	2.40	48.00
	90	0.73	14.60
	90	1.20	24.00
	90	1.92	38.40
	120	1.83	36.60
	120 o	3.29	65.80

x Fig. 4.3.1.51; F - 56
o Fig. 4.3.1.53; F - 56
+ Fig. 4.3.1.54,c; F - 57

/cont ...

...cont/Table 4.1.2.1. kinetics pure aluminium - silica reaction system. Diameter of the silica rod: 10.0 mm

Temperature	Immersion time	Product layer thickness	Percentage conversion
t^{o}	t	$\Delta r = r_o - r_i$	$1-(1-R_x)^{0.5}$
^{o}C	min	mm	%
1110	20. +	0.59	11.80
	20.	0.60	12.00
	30.	0.90	18.00
	120. o	3.52	70.40
	150.	4.68	93.60
	160.	4.82	96.40
	180.	5.00	100.00
^{o}C	min	mm	%
1170	10.	0.49	9.80
	15.	0.79	15.80
	15.	0.71	14.20
	30. •	1.57	31.40
	45.	2.45	49.00
	70.	3.96	79.20
	70.	4.10	82.00
	80.	4.81	96.20
	90.	5.00	100.00

• Fig. 4.3.1.31,a-b; F - 43
o Fig. 4.3.1.33,a-b; F - 45
+ Fig.4.3.1.42,a-c ; F - 50

/cont ...

..cont/Table 4.1.2.1. kinetics pure aluminium - silica reaction system. Diameter of the silica rod: 10.0 mm

Temperature	Immersion time	Product layer thickness	Percentage conversion
t^o	t	$\Delta r = r_o - r_i$	$1-(1-R_x)^{0.5}$
^oC	min	mm	%
1220	10.	0.90	17.90
	15. •	1.26	25.20
	30.	2.30	46.00
	45. +	3.95	79.00
	50.	4.26	85.20
	55. x	4.69	93.80
	60.	5.00	100.00
^oC	min	mm	%
1265	2. *	0.39	7.80
	4.	0.62	12.40
	6.	0.75	15.00
	10.	1.79	35.80
	15. o	2.76	55.20
	20.	3.65	73.00
	25.	4.69	93.80
	25.	4.73	94.60

* Fig.4.3.1.28; F - 41
• Fig.4.3.1.29; F - 42
o Fig.4.3.1.37; F - 46
\+ Fig.4.3.1.43,a-c; F - 51
x Fig.4.3.1.48; F - 54

Table 4.1.2.2.: Experimental results: measured and calculated constants for reaction between liquid pure aluminium and vitreous silica.

Rod diameter	Silica density	Temperature	1/T	Reaction rate constant		Regression line equation			Activation Energy
						$y = mx + c$ $\log k = -E/2.3RT + \log k_o$			
d_o	ρ_{SiO_2}	t		slope	k				E
m	$kg \times m^{-3}$	^oC	$K^{-1} \times 10^{-4}$	sec^{-1}	$kg \times m^{-2} \times sec^{-1}$	m	C	r	$kJ \times mol^{-1}$
3.0×10^{-3}	2.2×10^{3}	760	9.68	1.4×10^{-4}	4.62×10^{-4}				
		815	9.19	4.8×10^{-4}	15.84×10^{-4}				
		840	8.98	8.0×10^{-4}	26.40×10^{-4}				
		860	8.83	11.0×10^{-4}	36.30×10^{-4}	-10590.1	+6.92	1.00	202.61
		1110	7.23	2.8×10^{-4}	9.24×10^{-4}				
		1170	6.93	6.0×10^{-4}	19.80×10^{-4}				
		1220	6.70	8.2×10^{-4}	27.06×10^{-4}				
		1265	6.50	11.3×10^{-4}	37.29×10^{-4}	-8155.5	+1.86	0.98	156.49

/cont....

...cont./

TABLE 4.1.2.2.: Experimental results: measured and calculated constants for reaction between liquid pure aluminium and vitreous silica.

Rod diameter	Silica density	Temperature	1/T	Reaction rate constant		Regression line equation			Activation Energy
						$y=mx + c$ $\log k = -E/2.3RT + \log k_o$			
d_o	ρ_{SiO_2}	t		slope	k				E
m	kg x m^{-3}	^oC	$K^{-1} \times 10^{-4}$	sec^{-1}	kg x m^{-2} x sec^{-1}	m	C	r	kJ x mol^{-1}
5.0×10^{-3}	2.2×10^{3}	760	9.68	0.9×10^{-4}	4.95×10^{-4}				
		815	9.19	3.5×10^{-4}	19.25×10^{-4}				
		840	8.98	5.3×10^{-4}	29.15×10^{-4}				
		860	8.83	6.7×10^{-4}	36.85×10^{-4}	-10571.8	+5.46	0.99	199.44
		920	8.38	0.9×10^{-4}	4.95×10^{-4}				
		980	7.98	0.7×10^{-4}	3.85×10^{-4}	+2254.4	-6.69	1.00	43.15
		1110	7.23	1.8×10^{-4}	9.90×10^{-4}				
		1170	6.93	3.6×10^{-4}	19.70×10^{-4}				
		1220	6.70	5.4×10^{-4}	29.50×10^{-4}				
		1265	6.50	9.7×10^{-4}	53.5×10^{-4}	-9769.4	+4.05	0.98	186.85

/cont....

....cont./

Table 4.1.2.2.: Experimental results: measured and calculated constants for reaction between liquid pure aluminium and vitreous silica.

Rod diameter	Silica density	Temperature	1/T	Reaction rate constant		Regression line equation			Activation Energy
						$y=mx + c$ $\log k = -E/2.3RT + \log k_o$			
d_o	ρ_{SiO_2}	d		slope	k				E
m	$kg \times m^{-3}$	^oC	$K^{-1} \times 10^{-4}$	sec^{-1}	$kg \times m^{-2} \times sec^{-1}$	m	C	r	$kJ \times mol^{-1}$
10.0×10^{-3}	2.2×10^{3}	760	9.68	0.5×10^{-4}	5.50×10^{-4}				
		815	9.19	1.6×10^{-4}	17.60×10^{-4}				
		840	8.98	2.7×10^{-4}	29.70×10^{-4}				
		860	8.83	3.8×10^{-4}	43.15×10^{-4}	-10491.4	+6.89	1.00	200.64
		920	8.38	0.9×10^{-4}	9.90×10^{-4}				
		980	7.98	0.6×10^{-4}	6.60×10^{-4}	+4387.0	-6.68	1.00	83.90
		1110	7.23	1.0×10^{-4}	11.00×10^{-4}				
		1170	6.93	2.1×10^{-4}	23.10×10^{-4}				
		1220	6.70	2.9×10^{-4}	31.90×10^{-4}				
		1265	6.50	6.4×10^{-4}	70.40×10^{-4}	-10483.1	+4.61	1.00	200.48

Table 4.1.3. Experimental results: the kinetics of reaction between liquid aluminium - silicon alloys and vitreous silica.
Al - 5.0 atomic % Si;

Temperat.	Immersion time	Product layer thickness	Percentage conversion
t^o	t	$\Delta r = r_o - r_i$	$1-(1-R_x)^{0.5}$
°C	min	mm	%
1110	10	0.26	5.20
	15	0.48	9.60
	20	0.54	10.80
	20	0.59	11.80
	30	0.71	14.20
	45	1.17	23.40
	45	0.98	19.60
	60	1.45	29.00
	60	1.57	31.40
	90	2.54	50.80
	120	3.47	69.40
	120	3.40	68.00
	150	4.62	92.40
	180	5.00	100.00
	180	4.90	98.00
°C	min	mm	%
1170	5	0.24	4.80
	10	0.44	8.80
	10	0.50	10.00
	15	0.98	19.60
	20	1.07	21.40
	25	1.22	24.40
	30	1.56	31.20
	30	1.43	28.60
	45	2.21	44.20
	60	3.65	73.00
	60	3.60	72.00
	90	5.00	100.00
	90	5.00	100.00

/cont . . .

..cont/Table 4.1.3. kinetics aluminium - 5.0 atomic % silicon- silica reaction system.

Temperat.	Immersion time	Product layer thickness	Percentage conversion
t^o	t	$\Delta r = r_o - r_i$	$1-(1-R_x)^{0.5}$
^oC	min	mm	%
1220	10	0.92	18.40
	20	1.61	32.20
	30	2.04	40.80
	45	4.10	82.00
	50	4.20	84.00
	55	4.41	88.20
	60	5.00	100.00
^oC	min	mm	%
1265	2	0.35	7.00
	4	0.64	12.80
	5	0.67	13.40
	7	0.97	19.40
	10	1.75	35.00
	12	2.01	40.20
	15	2.80	56.00
	20	3.62	72.40
	20	3.70	72.40
	25	4.73	74.00
	30	5.00	100.00
	30	5.00	100.00

/cont . . .

..cont/Table 4.1.3. kinetics aluminium - 10.0 atomic % silicon - silica reaction system.

Temperat.	Immersion time	Product layer thickness	Percentage conversion
t^{o}	t	$\Delta r = r_o - r_i$	$1-(1-R_x)^{0.5}$
^{o}C	min	mm	%
1110	10	0.23	4.60
	20	0.57	11.40
	30	0.64	12.80
	45	0.93	18.60
	45	0.85	17.00
	45	1.09	21.80
	60	1.65	33.00
	60	1.33	26.00
	60	1.42	28.40
	90	2.36	47.20
	105	3.11	62.20
	120	3.59	71.80
	150	4.40	88.00
	150	4.21	84.20
	180	5.00	100.00
	180	5.00	100.00
^{o}C	min	mm	%
1170	5	0.14	2.80
	10	0.47	9.40
	15	0.72	14.40
	15	0.95	19.00
	20	1.14	22.80
	25	1.19	23.80
	30	1.47	29.40
	45	2.30	46.00
	45	2.46	49.20
	55	3.06	61.20
	75	4.22	84.40

/cont . . .

..cont/Table 4.1.3. kinetics aluminium - 10.0 atomic % silicon - silica reaction system.

Temperat.	Immersion time	Product layer thickness	Percentage conversion
t^o	t	$\Delta r = r_o - r_i$	$1-(1-R_x)^{0.5}$
^oC	min	mm	%
1220	4	0.32	6.40
	7	0.83	16.60
	10	1.10	22.00
	10	0.92	18.40
	15 x	1.25	25.00
	20	1.41	28.20
	25	1.80	36.00
	30	2.56	51.20
	35	2.71	54.20
	45	3.80	76.00
^oC	min	mm	%
1265	5	0.49	9.80
	10	1.60	32.00
	10	1.45	29.00
	10	1.48	29.60
	15	2.59	51.80
	20	3.32	66.40
	25	4.32	86.40
	30	5.00	100.00

x Fig.4.3.2.1; F - 58

/cont . . .

..cont/Table 4.1.3. kinetics aluminium - 15.0 atomic % silicon - silica reaction system.

Temperat.	Immersion time	Product layer thickness	Percentage conversion
t^{o}	t	$\Delta r = r_o - r_i$	$1-(1-R_x)^{0.5}$
^{o}C	min	mm	%
1110	10	0.05	1.00
	20	0.41	8.20
	20	0.24	4.80
	30	0.54	10.80
	45	0.88	17.60
	45	0.47	9.40
	45	0.60	12.00
	60	0.97	19.40
	60	1.40	28.00
	90	2.35	47.00
	90	2.55	51.00
	90	2.10	42.00
	120	3.11	62.20
	150	4.30	86.00
	180	4.55	91.00
	180	5.00	100.00
	180	4.88	97.60
^{o}C	min	mm	%
1170	10	0.19	3.80
	10	0.12	2.40
	12	0.42	8.40
	15	0.82	16.40
	15	0.70	14.00
	20	0.95	19.00
	25	1.19	23.80
	30	1.57	31.40
	45	2.47	49.40
	45	2.07	41.40
	45	2.23	44.60
	60	3.26	65.20
	60	3.10	62.00

/cont . . .

..cont /Table 4.1.3. kinetics aluminium - 15.0 atomic % silicon - silica reaction system

Temperat.	Immersion time	Product layer thickness	Percentage conversion
t^{o}	t	$\Delta r = r_o - r_i$	$1-(1-R_x)^{0.5}$
^{o}C	min	mm	%
1220	5	0.31	1.00
	10	0.74	14.80
	10	0.85	17.00
	15	1.10	22.00
	20	1.57	31.40
	25	1.83	36.60
	25	2.00	40.00
	25	1.71	34.20
	25	1.76	35.20
	30	2.47	49.40
	35	2.85	57.00
	45	3.71	74.20
^{o}C	min	mm	%
1265	5	0.69	13.80
	5	0.67	13.40
	10	1.46	29.20
	15	2.51	50.20
	15	2.44	48.80
	15	2.45	49.00
	20	3.20	64.00
	25	4.32	86.40
	25	5.00	100.00

Table 4.1.4.1. Experimental results: the kinetics of reaction between liquid aluminium - manganese alloys and vitreous silica.

Al - 5.0 atomic % Mn;

Temperat.	Immersion time	Product layer thickness	Percentage conversion
t^o	t	$\Delta r = r_o - r_1$	$1-(1-R_x)^{0.5}$
°C	min	mm	%
1110	30	0.41	8.20
	30	0.46	9.20
	45	0.78	15.10
	60	1.00	20.00
	60	1.29	25.80
	90	2.07	41.30
	90	1.96	39.20
	120	2.45	49.00
	150	3.48	69.50
	150	3.65	73.00
	160	3.71	74.20
	180	4.13	82.60
°C	min	mm	%
1170	5	0.24	4.8
	10	0.16	3.2
	10	0.23	4.5
	10	0.38	7.6
	15	0.74	14.8
	20	0.59	17.7
	25	0.97	19.4
	30	1.05	21.0
	30	1.47	29.4
	45	1.90	38.0
	60	2.77	55.3
	60	2.43	48.4
	75	2.97	59.3
	90	3.55	71.0
	90	3.90	78.0
	90	3.98	79.5
	105	4.40	88.0
	105	4.47	89.3
	120	5.00	100.0

/cont..

..cont/Table 4.1.4.1. kinetics aluminium - 5.0 atomic % manganese - silica reaction system.

Temperat.	Immersion time	Product layer thickness	Percentage conversion
t^{o}	t	$\Delta r = r_o - r_i$	$1-(1-R_x)^{0.5}$
^{o}C	min	mm	%
1220	5	0.51	10.20
	10	0.77	15.30
	15	1.43	28.60
	20	1.70	34.00
	30 ▫	2.30	46.00
	40	3.39	67.80
	45	3.83	76.60
	50	3.95	79.00
	60	4.81	96.20
	60	5.00	100.00
^{o}C	min	mm	%
1265	2	0.33	6.5
	5	0.74	14.7
	10	1.07	21.4
	10	1.18	23.5
	15	2.25	44.9
	20	2.90	58.0
	30	3.88 ●	77.6
	30	4.07	81.3
	35	5.00	100.0

▫ Fig.4.3.2.6,d; F - 64
● Fig.4.3.2.7,c; F - 66

/cont. . .

..cont/Table 4.1.4.1. kinetics aluminium - 10.0 atomic % manganese - silica reaction system.

Temperat.	Immersion time	Product layer thickness	Percentage conversion
t^{o}	t	$\Delta r = r_o - r_i$	$1-(1-R_x)^{0.5}$
^{o}C	min	mm	%
1110	30	0.18	4.5
	45	0.34	6.8
	60	0.39	7.8
	80	0.66	13.1
	80	0.80	16.0
	90	0.88	17.5
	120	0.99	19.7
	150	1.08	21.5
	150	1.25	25.0
	180	1.55	31.0
	210	1.95	39.0
	240	2.02	40.4
^{o}C	min	mm	%
1170	15	0.25	5.0
	20	0.16	3.1
	20	0.27	5.3
	25	0.29	5.8
	30	0.45	9.0
	45	0.69	13.7
	60	1.02	20.3
	60	0.82	16.4
	90	1.42	28.4
	90	1.80	36.0
	90	1.76	35.2
	105	2.00	40.0
	120	2.24	44.8
	150	3.02	60.4
	180	3.48	69.6
	210	4.49	89.7

/ cont...

..cont/Table 4.1.4.1. kinetics aluminium - 10.0 atomic % manganese - silica reaction system.

Temperat.	Immersion time	Product layer thickness	Percentage conversion
t^o	t	$\Delta r = r_o - r_i$	$1-(1-R_x)^{0.5}$
^oC	min	mm	%
1220	10	0.29	5.8
	20	0.50	10.0
	30	0.92	18.4
	45	1.20	24.0
	45	1.47	29.3
	60	1.80	36.0
	75	2.29	45.8
	90	3.05	61.0
	90	3.29	65.8
	105	3.67	73.3
	120 +	3.75	75.0
	120	4.28	85.5
	150	5.00	100.0
^oC	min	mm	%
1265	5	0.29	5.7
	10	0.66	13.2
	15	1.27	25.4
	20	1.46	29.2
	30	2.10	42.0
	45	3.22	64.3
	60	4.64	92.8
	60	4.18	83.5
	75	5.00	100.0

+ Fig.4.3.2.5,a-b; F - 60

/cont . . .

..cont/Table 4.1.4.1. kinetics aluminium - 15.0 atomic % manganese - silica reaction system.

Temperat.	Immersion time	Product layer thickness	Percentage conversion
t^{o}	t	$\Delta r = r_o - r_i$	$1-(1-R_x)^{0.5}$
^{o}C	min	mm	%
1110°C	45	0.14	2.8
	60	0.05	1.0
	75	0.05	1.0
	75	0.15	3.0
	90	0.05	1.0
	90	0.10	2.0
	105	0.19	3.8
	105	0.40	8.0
	120	0.23	4.6
	120	0.45	9.0
	150	0.15	3.0
	150	0.39	7.7
	150	0.47	9.3
	180	0.45	8.9
	210	0.44	8.8
	210	0.83	16.5
	240	0.23	11.5
	240	0.42	8.3
	240	0.87	17.4
^{o}C	min	mm	%
1170	30	0.05	1.0
	45	0.05	1.0
	45	0.31	6.2
	60	0.29	5.8
	75	0.92	18.4
	90	1.05	21.0
	90	1.23	24.5
	105	1.19	23.8
	120	1.20	24.0
	120	1.45	29.0
	120	1.57	31.4
	150	2.18	43.5
	180	2.25	45.0
	180	2.12	42.4
	210	2.97	59.4

/cont . . .

..cont/Table 4.1.4.1. kinetics aluminium - 15.0 atomic % manganese - silica reaction system.

Temperat.	Immersion time	Product layer thickness	Percentage conversion
t^{o}	t	$\Delta r = r_o - r_i$	$1-(1-R_x)^{0.5}$
°C	min	mm	%
1220	20	0.05	1.0
	30	0.57	11.4
	45	0.70	14.0
	60	1.32	26.4
	75	1.60	32.0
	75	1.85	37.0
	90	2.26	45.1
	105	2.90	58.0
	120	3.15	63.0
	120	2.71	54.3
	150	3.75	75.0
	150	4.21	84.2
	180	4.52	90.3
°C	min	mm	%
1265	10	0.36	7.2
	20	0.87	17.4
	30	1.49	29.8
	45	2.20	44.0
	60 o	2.76	55.2
	75	3.67	73.4
	75	3.75	75.0
	90	5.00	100.0

o Fig. 4.3.2.3.; F - 59

Table 4.1.4.2. Experimental results: the kinetics of the reaction between liquid aluminium - iron alloys and vitreous silica. Al - 5.0 atomic % Fe;

Temperat.	Immersion time	Product layer thickness	Percentage conversion
t^o	t	$\Delta r = r_o - r_i$	$1-(1-R_x)^{0.5}$
^oC	min	mm	%
1110	20	0.23	4.5
	30	0.55	11.0
	30	0.42	8.4
	30	0.33	6.5
	60	0.90	18.0
	60	1.20	24.0
	120	2.87	57.4
	150	3.75	75.0
	150	3.34	66.8
	160	4.15	83.0
	180	4.25	85.0
	210	5.00	100.0
	210	5.00	100.0
^oC	min	mm	%
1170	25	0.83	16.5
	25	1.12	22.3
	30	1.27	25.4
	45	1.84	36.8
	45	1.75	35.0
	45	1.79	35.7
	60	2.10	41.9
	75	2.78	55.5
	80	3.15	63.0
	90	3.50	70.0
	90	3.72	74.3
	105 x	4.30	85.9
	120	5.00	100.0

x 4.3.2.2; F - 59

/cont . . .

..cont/Table. 4.1.4.2. kinetics aluminium - 5.0 atomic % iron-silica reaction system.

Temperat.	Immersion time	Product layer thickness	Percentage conversion
t^{o}	t	$\Delta r = r_o - r_i$	$1-(1-R_x)^{0.5}$
^{o}C	min	mm	%
1220	5	0.49	9.70
	10	0.75	15.00
	10	0.72	14.30
	15	1.41	28.20
	20	1.69 •	33.80
	25	1.80	35.90
	25	1.8	36.20
	30	2.27	45.40
	45	3.76	75.20
	45	3.75	75.00
	60	5.00	100.00
	60	5.00	100.00
^{o}C	min	mm	%
1265	5	0.81	16.10
	10	1.12	22.40
	15	2.11	42.10
	15	2.07	41.30
	20	2.88	57.50
	20	2.92	58.40
	20	2.87	57.30
	25	3.32	66.40
	30	3.79	75.80
	30	3.92	78.40

• Fig. 4.3.2.6,a; F - 61

/cont . . .

..cont/Table 4.1.4.2. kinetics aluminium - 10.0 atomic % iron - silica reaction system.

Temperat.	Immersion time	Product layer thickness	Percentage conversion
t^{o}	t	$\Delta r = r_o - r_i$	$1-(1-R_x)^{0.5}$
^{o}C	min	mm	%
1110	15	-	-
	15	-	-
	20	-	-
	20	0.04	1.00
	30	0.16	3.10
	30	0.20	4.00
	45	0.29	5.70
	60	0.38	7.50
	60	0.27	5.40
	70	0.43	8.60
	80	0.75	14.90
	90	0.77	15.30
	90	0.58	11.60
	120	0.98	19.50
	150	1.10	22.00
	150	1.11	22.20
	180	1.59	31.70
	210	1.80	36.00
	240	1.95 o	38.90
	240	2.03	40.60
	270	2.48	49.50
^{o}C	min	mm	%
1170	15	0.23	4.60
	20	0.24	4.80
	25	0.32	6.40
	30	0.42	8.40
	30	0.37	7.40
	45	0.68	13.60
	60	0.95	19.00
	60	0.93 ●	18.60
	60	0.97	19.40
	90	1.67	33.40
	105	1.99	39.80
	120	2.20	44.00
	150	2.82	56.40
	150	2.80	56.00
	180	3.32	66.40
	240	4.42	88.40
	240	4.55	91.00

o Fig.4.3.2.4. ; F - 59

● Fig. 4.3.2.7,a; F - 65

/cont . . .

..cont/Table 4.1.4.2. kinetics aluminium - 10.0 atomic % iron - silica reaction system.

Temperat.	Immersion time	Product layer thickness		Percentage conversion
t^o	t	$\Delta r = r_o - r_i$		$1-(1-R_x)^{0.5}$
^oC	min	mm		%
1220	10	0.32		6.40
	15	0.46		9.20
	20	0.48		9.60
	25	0.73		14.60
	30	0.89		17.80
	35	1.07		21.40
	45	1.31	x	26.20
	60	1.75		35.00
	60	1.73		34.60
	75	2.31	o	46.20
	90	3.18		63.60
	105	3.60		72.00
	105	3.56		71.20
	120	4.22		84.20
^oC	min	mm		%
1265	5	0.27		5.40
	10	0.68		13.60
	15	1.25		25.00
	20	1.43		28.60
	25	1.64		32.80
	30	2.08		41.60
	40	2.63		52.60
	45	3.16		63.20
	60	4.09		81.80
	75	4.91		98.20

x Fig.4.3.2.6,b; F -62

o Fig.4.3.2.7,b; F - 65

/cont . . .

..cont/Table 4.1.4.2. kinetics aluminium - 15.0 atomic % iron - silica reaction system.

Temperat.	Immersion time	Product layer thickness	Percentage conversion
t^{o}	t	$\Delta r = r_o - r_i$	$1-(1-R_x)^{0.5}$
^{o}C	min	mm	%
1110	20	-	-
	30	-	-
	45	-	-
	45	0.05	1.00
	60	0.05	1.00
	90	0.08	2.00
	90	0.05	1.00
	120	0.12	2.40
	120	0.05	1.00
	120	0.17	3.40
	150	0.29	5.80
	240	0.33	6.60
	240	0.52	10.40
^{o}C	min	mm	%
1170	45	0.05	1.00
	45	0.11	2.20
	60	0.13	2.60
	60	0.12	2.40
	60	0.18	3.60
	75	0.64	12.80
	90	0.85	17.00
	105	1.07	21.40
	120	0.98	19.60
	150	1.81	36.20
	180	2.02	40.40
	180	1.93	38.60
	210	2.90	58.00
	210	2.77	55.40

/cont . . .

..cont/Table 4.1.4.2. kinetics aluminium - 15.0 atomic % iron - silica reaction system.

Temperat.	Immersion time	Product layer thickness	Percentage conversion
t^{o}	t	$\Delta r = r_o - r_i$	$1-(1-R_x)^{0.5}$
^{o}C	min	mm	%
1220	20	-	-
	30	0.22	4.40
	45	0.48	9.60
	45	0.51	10.20
	60	0.88	17.60
	90	1.19	23.80
	90	1.30 •	26.00
	120	2.21	44.20
	120	2.45	49.00
	120	2.35	47.00
	150	3.14	62.80
	180	3.90	78.00
	180	4.13	82.60
^{o}C	min	mm	%
1265	5	0.05	1.00
	10	0.21	4.20
	15	0.38	7.60
	15	0.45	9.00
	20	0.74	14.80
	20	0.76	15.10
	30	1.17	23.40
	45	1.86	37.20
	60	2.50	50.00
	60	2.42	48.40
	75	3.10	62.00
	75	3.02	60.40
	90	3.74	74.80
	120	5.00	100.00
	120	5.00	100.00

• Fig.4.3.2.6,c; F - 63

Table 4.1.5.a.: Experimental results: measured and calculated kinetic constants for reaction between liquid aluminium-silicon alloys and vitreous silica.

Al-Si	Rod diameter	Silica density	Temperature	1/T	Reaction rate constant		Regression line equation			Activation energy
concentration	d_o	ρ_{SiO_2}	t		Slope	k	$y = mx + c$ $\log k = -E/2.3RT + \log k_o$			E
atomic % Si	m	kg x m^{-3}	^oC	$K^{-1} \times 10^{-4}$	sec^{-1}	kg x m^{-2} x sec^{-1}	m	C	r	kJ x mol^{-1}
5.0	10×10^{-3}	2.2×10^3	1110	7.23	1.0×10^{-4}	11.00×10^{-4}				
			1170	6.93	1.9×10^{-4}	20.90×10^{-4}				
			1220	6.70	2.8×10^{-4}	30.80×10^{-4}				
			1265	6.50	5.6×10^{-4}	61.60×10^{-4}	-9877.6	+4.17	1.00	188.90
10.0	10×10^{-3}	2.2×10^3	1110	7.23	1.0×10^{-4}	11.00×10^{-4}				
			1170	6.93	1.9×10^{-4}	20.90×10^{-4}				
			1220	6.70	2.6×10^{-4}	28.60×10^{-4}				
			1265	6.50	6.3×10^{-4}	69.30×10^{-4}	-10308.6	+4.47	0.99	197.15
15.0	10×10^{-3}	2.2×10^3	1110	7.23	1.0×10^{-4}	11.00×10^{-4}				
			1170	6.93	1.9×10^{-4}	20.90×10^{-4}				
			1220	6.70	2.8×10^{-4}	30.80×10^{-4}				
			1265	6.50	6.4×10^{-4}	70.40×10^{-4}	-11207.8	+4.64	0.99	201.61

Table 4.1.5.b.: Experimental results: measured and calculated kinetic constants for reaction between liquid aluminium-manganese alloys and vitreous silica.

Al-Mn	Rod diameter	Silica density	temp-erature	$^1/_T$	Reaction rate constant		Regression line equation			Activation Energy
concentration	d_o	ρ_{SiO_2}	t^o		Slope	k	$y = mx + c$ $\log k = -E/2.3RT + k_o$			E
Atomic % Mn	mm	$kg\text{-}m^{-3}$	^oC	$K^{-1}.10^{-4}$	Sec	$kg.m^{-2}.Sec^{-1}$	m	c	r	$kJ.mol^{-1}$
5.0	static	2.2×10^3	1110	7.23	0.8×10^{-4}	8.80×10^{-4}				
	10×10^{-3}		1170	6.93	1.4×10^{-4}	15.40×10^{-4}				
			1220	6.70	2.7×10^{-4}	29.70×10^{-4}				
			1265	6.50	4.5×10^{-4}	49.50×10^{-4}	-10399.3	+4.44	1.00	198.88
10.0	static	2.2×10^3	1110	7.23	0.3×10^{-4}	3.30×10^{-4}				
	10×10^{-3}		1170	6.93	0.7×10^{-4}	7.70×10^{-4}				
			1220	6.70	1.1×10^{-4}	12.16×10^{-4}				
			1265	6.50	2.4×10^{-4}	26.40×10^{-4}	-11944.8	+5.15	0.98	228.48
15.0	static	2.2×10^3	1110	7.23	0.1×10^{-4}	1.10×10^{-4}				
	10×10^{-3}		1170	6.93	0.5×10^{-4}	5.50×10^{-4}				
			1220	6.70	0.9×10^{-4}	9.90×10^{-4}				
			1265	6.50	1.7×10^{-4}	18.70×10^{-4}	-16566.4	+8.09	0.96	316.82

Table 4.1.5.c.: Experimental results: measured and calculated kinetic constants for reaction between liquid aluminium-iron alloys and vitreous silica.

Al-Fe	Rod diameter	Silica density	temp-erature	$^1/_T$	Reaction rate constant		Regression line equation $y = mx + c$ $\log k = -E/2.3RT + k_o$			Activation Energy
concentration	d_o	ρ_{SiO_2}	t^o		Slope	k				E
Atomic % Fe	mm	$kg\text{-}m^{-3}$	^oC	$K^{-1}.10^{-4}$	Sec	$kg.m^{-2}.Sec^{-1}$	m	c	r	$kJ.mol^{-1}$
5.0	static	2.2×10^3	1110	7.23	0.9×10^{-4}	9.90×10^{-4}				
	10×10^{-3}		1170	6.93	1.3×10^{-4}	14.30×10^{-4}				
			1220	6.70	2.6×10^{-4}	28.60×10^{-4}				
			1265	6.50	4.3×10^{-4}	47.30×10^{-4}	-9515.3	+3.83	0.97	182.01
10.0	static	2.2×10^3	1110	7.23	0.3×10^{-4}	3.30×10^{-4}				
	10×10^{-3}		1170	6.93	0.7×10^{-4}	7.70×10^{-4}				
			1220	6.70	1.2×10^{-4}	13.20×10^{-4}				
			1265	6.50	2.2×10^{-4}	24.22×10^{-4}	-11694.0	+4.98	1.00	223.64
15.0	static	2.2×10^3	1110	7.23	0.07×10^{-4}	0.77×10^{-4}				
	10×10^{-3}		1170	6.93	0.50×10^{-4}	5.50×10^{-4}				
			1220	6.70	0.80×10^{-4}	8.80×10^{-4}				
			1265	6.50	1.50×10^{-4}	16.50×10^{-4}	-17746.6	+8.84	0.95	339.39

Table 4.1.6.: Experimental results: kinetics of the reaction between liquid pure aluminium and vitreous silica under rotating conditions of the silica rod. ϕ_{rod} = 10 mm; rotation per minute: 5,15,35.

Temperat.	Rotations per minute	Immersion time	Product layer thickness	Percentage conversion
t^o		t	$\Delta r = r_o - r_i$	$1-(1-R_x)^{0.5}$
^oC	rpm	min	mm	%
1170	5	15	0.83	17.00
		30	1.54	31.00
		45	2.48	50.00
		80	4.80	96.00
	15	35	2.02	40.00
		50	3.00	60.00
		90	5.00	100.00
	35	10	0.48	9.60
		30	1.56	31.00
		60	3.54	71.00
^oC	rpm	min	mm	%
1265	5	2.	0.42	8.40
		5.	0.53	10.60
		10.	1.75	35.00
		15.	2.70	54.00
		20.	3.73	76.60
	15	1.	0.19	3.80
		2.	0.44	8.80
		5.	0.56	11.20
		10.	1.84	36.80
	35	2.	0.48	9.60
		10.	1.80	36.00
		20.	3.70	74.00

/cont...

Table 4.1.6.: Kinetics Al-5 atomic % Mn - SiO_2 system under rotating conditions of the silica rod. ϕ_{rod} = 10 mm.
Rotations per minute: 5, 15, 35.

Temperat.	Rotations per min	Immersion time	Product layer thickness	Percentage conversion
t^o	rpm	t	$\Delta r = r_o - r_i$	$1-(1-R_x)^{0.5}$
^oC		min	mm	%
1170	5	10	0.32	6.40
		15	0.49	9.80
		20	0.71	14.30
		30	1.10	22.00
		60	2.45	49.00
		90	3.80	76.00
	15	5	0.28	5.60
		10	0.56	11.20
		20	0.68	13.50
		30	1.03	20.50
		75	2.97	59.40
		90	3.66	73.10
		105	4.45	89.00
		120	5.00	100.00
	35	15	0.58	11.30
		25	0.99	19.80
		35	1.42	28.40
		45	1.70	34.00
		60	2.65	53.00
		105	4.29	85.90
		120	4.90	98.00
1265	5	5	0.89	17.9
		10	1.21	24.2
		15	2.28	45.6
		20	2.76	55.3
		25	3.50	70.00
		30	4.12	82.70
	15	5	0.83	16.5
		10	1.25	25.0
		15	2.36	47.2
		15	2.27	45.4
		20	2.90	58.0
		25	3.36	67.3
		35	5.00	100.0
	35	5	0.76	15.3
		10	1.19	23.8
		15	2.32	46.4
		20	2.79	55.8
		25	3.45	69.0
		25	3.30	66.0
		30	4.27	85.4
		35	5.00	100.0
		35	5.00	100.0

/cont...

....cont./Table 4.1.6.: kinetics Al-5 atomic % Fe - SiO_2 system under rotating conditions of the silica rod. ϕ_{rod} = 10 mm.
Rotations per minute: 5, 15, 35.

Temperat.	Rotations per min	Immersion time	Product layer thickness	Percentage conversion
t^o	rpm	t	$\Delta r = r_o - r_i$	$1-(1-R_x)^{0.5}$
^oC		min	mm	%
1170	5	10	0.46	9.20
		15	0.67	13.40
		25	1.17	23.50
		30	1.29	25.80
		90	3.82	76.40
		105	4.18	83.70
		120	4.87	97.50
	15	5	0.23	4.70
		15	0.74	14.90
		20	0.89	17.80
		30	1.15	23.00
		45	1.62	32.50
		105	4.06	81.30
		120	5.00	100.00
		120	5.00	100.00
	35	10	0.43	8.70
		20	0.90	18.00
		30	1.23	24.70
		60	2.31	46.30
		75	2.97	59.40
		90	2.97	77.30
1265	5	5	0.57	11.40
		10	1.23	24.70
		15	1.96	39.30
		30	4.12	82.50
		45	5.00	100.00
	15	5	0.71	14.30
		10	1.02	20.50
		20	2.67	53.40
		30	3.87	77.50
		40	5.00	100.00
	35	10	1.32	26.40
		20	2.64	52.80
		30	3.95	79.00
		40	5.00	100.00

Table 4.1.7.: Experimental results: measured and calculated kinetic constants for the reaction between liquid pure aluminium and aluminium alloys and vitreous silica, under rotating conditions of the silica rod. ϕ_{rod} = 10 mm; ρ_{SiO_2} = 2.2 x 10^{-3} kg.m^{-3}

Molten Metal	Rotation	Temperature	$1/T$	Reaction rate constant		regression line equation $y = mx + c$, $\log k = -E/2.3RT + \log k_o$			Activation energy
				Slope	k				E
	rpm	t^o C	$K^{-1} \times 10^{-4}$	sec^{-1}	$kg.m^{-2}.sec^{-1}$	m	C	r	$kJ.mol^{-1}$
Aℓ	5	1170	6.93	2.1 x 10^{-4}	23.10 x 10^{-4}				
		1265	6.50	6.6 x 10^{-4}	72.60 x 10^{-4}	-11893.9	+5.61	1.00	227.47
	15	1170	6.93	2.2 x 10^{-4}	24.20 x 10^{-4}				
		1265	6.50	5.9 x 10^{-4}	64.90 x 10^{-4}	-10000.7	+4.32	1.00	191.41
	35	1170	6.93	2.1 x 10^{-4}	23.10 x 10^{-4}				
		1265	6.50	6.0 x 10^{-4}	66.00 x 10^{-4}	-10651.2	+4.74	1.00	203.70
Aℓ-5 at % Mn	5	1170	6.93	1.5 x 10^{-4}	16.50 x 10^{-4}				
		1265	6.50	4.5 x 10^{-4}	49.50 x 10^{-4}	-11116.2	+4.94	1.00	213.17
	15	1170	6.93	1.4 x 10^{-4}	15.40 x 10^{-4}				
		1265	6.50	4.7 x 10^{-4}	51.70 x 10^{-4}	-12287.4	+5.70	1.00	234.99
	35	1170	6.93	1.6 x 10^{-4}	17.60 x 10^{-4}				
		1265	6.50	4.6 x 10^{-4}	50.60 x 10^{-4}	-10714.4	+4.67	1.00	209.91
Aℓ-5 at % Fe	5	1170	6.93	1.3 x 10^{-4}	14.31 x 10^{-4}				
		1265	6.50	4.4 x 10^{-4}	48.40 x 10^{-4}	-12370.1	+5.73	1.00	236.57
	15	1170	6.93	1.3 x 10^{-4}	14.31 x 10^{-4}				
		1265	6.50	4.1 x 10^{-4}	45.10 x 10^{-4}	-11653.6	+5.23	1.00	222.87
	35	1170	6.93	1.3 x 10^{-4}	14.31 x 10^{-4}				
		1265	6.50	4.3 x 10^{-4}	47.30 x 10^{-4}	-12136.8	+5.57	1.00	232.11

Table 4.2.1. Experimental results: x - ray diffraction data for aluminium and silicon.

standard phases						ASTM*			
aluminium			silicon			aluminium		silicon	
2θ	d	i	2θ	d	i	d	I	d	I
36.95	2.43	1	28.39	3.14	1	2.34	1	3.14	1
44.06	2.27	4	47.82	1.90	2	2.02	2	1.92	2
47.56	2.11	2	54.81	1.67	3	1.43	4	1.64	3
51.68	1.95	5	74.64	1.27	4	1.22	3	1.11	4
70.20	1.47	3	83.18	1.16	3	-	-	-	-
75.37	1.38	3	116.81	0.90	4	-	-	-	-

* ASTM -"Fink Inorg.Ind. Powder Diffrac.File", ed. Smith,JV. et al. ASTM, 1967 .

i = order of intensity of lines in the film

I = relative intensity

Table 4.2.2.: X - ray diffraction data for standard polymorphs of alumina.

Standard polymorphs of alumina/prepared/																ASTM*									
γ			δ			θ			θ+κ			α				γ		δ		θ		θ+κ		α	
2θ	d	i	2θ	d	i	2θ	d	i	2θ	d	i	2θ	d	i		d	I	d	I	d	I	d	I	d	I
																						6.21	30		
																				5.20	30				
																		5.02	30						
																4.56	40								
																		9.55	30						
							4.52	2																	
																				4.50	60	4.50	20		
																						4.20	10		
																		4.07	20						
																				3.53	20				
																								3.49	75
																						3.04	40		
																		2.87	40						
																				2.85	80				
									31.93	2.82	1														
						31.96	2.80	1								2.80	20								
									32.08	2.79	2											2.79	60		
						32.64	2.74	1																	
																		2.73	80						
																				2.72	80				
																						2.70	20		
																		2.58	30						
									34.91	2.57	3											2.57	80		
																				2.56	30				
																								2.55	90
									35.34	2.54	2														
																		2.43	60	2.43	80				
						37.31	2.41	3														2.41	30		
																2.39	80								

..cont./

..cont/ Table 4.2.2.

Standard polymorphs of alumina/prepared															ASTM*									
γ			δ			θ			θ+κ			α			γ		δ		θ		θ+κ		α	
2θ	d	i	2θ	d	i	2θ	d	i	2θ	d	i	2θ	d	i	d	I	d	I	d	I	d	I	d	I
																							2.38	40
			38.13	2.36	5																			
												38.30	2.35	2										
									38.47	2.34	2													
						38.81	2.32	2													2.32	40		
																			2.31	60				
39.17	2.30	2				39.17	2.30	2				39.17	2.30	3										
			39.34	2.29	2																			
															2.28	50	2.28	40						
																			2.26	10				
						40.07	2.25	3																
																	2.24	60						
																	2.19	80						
																							2.17	1
																					2.16	10		
									42.23	2.14	3													
																			2.11	60	2.11	80		
												43.09	2.10	1										
																							2.09	100
						43.73	2.07	3																
																					2.06	30		
44.64	2.03	2																						
																			2.01	80				
			45.58	1.99	3																1.99	40		
									45.83	1.98	2				1.98	100								

..cont/

..cont/ Table 4.2.2.

Standard polymorphs of alumina/prepared/															ASTM*									
γ			δ			θ			θ + κ			α			γ		δ		θ		θ + κ		α	
2θ	d	i	2θ	d	i	2θ	d	i	2θ	d	i	2θ	d	i	d	I	d	I	d	I	d	I	d	I
																							1.96	02
																	1.95	30			1.95	20		
																	1.91	20	1.91	40				
																					1.87	60		
																					1.82	60		
																	1.80	20	1.80	20				
																					1.74	20	1.74	45
																			1.73	10				
												54.28	1.69	2										
									56.08	1.64	4										1.64	60		
						56.30	1.634	2																
			58.83	1.62	4							56.83	1.62	1										
																			1.61	20				
																							1.60	80
																							1.55	90
																	1.54	40	1.54	60	1.54	10		
															1.52	30								
																	1.51	30					1.51	08
																	1.49	40	1.49	40	1.49	30		
																	1.45	30	1.45	40	1.45	30		
																			1.43	10	1.43	80		
									65.76	1.42	2													
												66.29	1.41	2										
																							1.404	30
			66.82	1.40	1										1.40	100	1.40	60	1.40	60				

..cont /

..cont/ Table 4.2.2.

Standard polymorphs of alumina/prepared/															ASTM*									
γ			δ			θ			θ+κ			α			γ		δ		θ		θ+κ		α	
2θ	d	i	2θ	d	i	2θ	d	i	2θ	d	i	2	d	i	d	I	d	I	d	I	d	I	d	I
									66.98	1.397	1													
67.37	1.39	1															1.39	100	1.39	100	1.39	100		
												67.92	1.38	2										
						6 .20	1.375	1																
																							1.37	50
																					1.35	30		
																	1.29	20						
															1.14	20								

Table 4.2.3. : X - ray diffraction data for selected reaction specimens. Pure Al - SiO_2 reaction system.

reaction specimens																		standard phases						
temperature /°C/																		alumina polymorphs					Al	S
760										860				920										
reaction time /min/																								
2 + 5 + 10		30*		60		(1 + 5)*		20 + 25		45*		20		60*		120		γ	δ	θ	θ+κ	α		
2θ	d	2θ	d	2θ	d	2θ	d	2θ	d	2θ	d	2θ	d	2θ	d	2θ	d	d - spacing						
27.97	3.19																							
				28.70	3.11																			3.
												28.80	3.10	28.80	3.10									
										28.99	3.08													
																					2.82			
31.96	2.80																			2.80				
																				2.79				
		34.77	2.58																2.74					
																						2.57		
								35.05	2.56															
35.21	2.55			35.19	2.55																			
						35.34	2.54														2.54			
												35.60	2.52			35.63	2.52							
										35.79	2.51			35.77	2.51									
		36.84	2.44																					
																				2.41				
		37.80	2.38																					
				37.96	2.37											37.96	2.37							
										38.13	2.36	38.13	2.36						2.36					
																						2.35		
38.45	2.34													38.47	2.34						2.34		2.34	
						38.67	2.33																	

* Etched in 5.0 ml (40%) HF + 95 ml destil.water for 5 to 15 min.

..cont/

..cont/ Table 4.2.3.

reaction specimens																		standard phases						
temperature /°C/																		alumina polymorphs					Al	Si
760						860						920												
reaction time /min/																								
2 + 5 + 10		30*		60		(1 + 5)*		20 + 25		45*		20		60*		120		γ	δ	θ	θ+κ	α		
2θ	d	2θ	d	2θ	d	2θ	d	2θ	d	2θ	d	2θ	d	2θ	d	2θ	d	d - spacing						
												38.81	2.32								2.32			
38.96	2.31							38.99	2.31															
																		2.30			2.30	2.30		
		39.34	2.29																2.29					
																							2.27	
																				2.25				
40.45	2.23																							
								38.33	2.15															
																					2.14			
				42.85	2.11																		2.11	
43.07	2.10	43.07	2.10			43.10	2.10											-				2.10		
												43.29	2.09			43.31	2.09							
								43.51	2.08															
						43.75	2.07			43.70	2.07			43.73	2.07					2.07				
43.95	2.06																							
																		2.03						
										44.87	2.02													
		45.11	2.01									45.	2.01											
45.34	2.00			45.	2.00			45.34	2.00															
						45.58	1.99									45.61	1.99		1.99					
																					1.98			
																							1.95	
								47.09	1.93															
47.61	1.91																							
				47.88	1.90					47.91	1.90			47.87	1.90									1.90

..cont/

..cont/ Table 4.2.3.

reaction specimens																		standard phases						
temperature /°C/																		alumina polymorphs					Al	Si
760						860						920												
reaction time /min/																								
2 + 5 + 10		30*		60		(1 + 5)*		20 + 25		45*		20		60*		120		γ	δ	ϑ	κ ϑ	α		
2ϑ	d	2ϑ	d	2ϑ	d	2ϑ	d	2ϑ	d	2ϑ	d	2ϑ	d	2ϑ	d	2ϑ	d	d - spacing						
												48.14	1.89											
																53.93	1.70							
																						1.69		
54.63	1.68																							
																								1.67
								56.08	1.64												1.64			
56.45	1.63			56.45	1.63															1.63				
																			1.62			1.62		
						57.22	1.61																	
		57.63	1.60											57.61	1.60	57.60	1.60							
										57.81	1.595													
												58.00	1.59											
												61.85	1.50	61.87	1.50									
																							1.47	
				65.2	1.43			65.24	1.43															
																					1.42			
66.29	1.41					66.29	1.4							66.29	1.41							1.41		
		66.82	1.40					66.79	1.40	66.82	1.40					66.81	1.40		1.40					
				67.11	1.395							67.09	1.395	67.06	1.395						1.397			
67.39	1.39					67.37	1.39											1.39				1.38	1.38	
																				1.375				
				68.52	1.37					68.49	1.37													
												68.77	1.365											
																								1.27
										70.85	1.23													

..cont/

..cont/ Table 4.2.3.

reaction specimens																		standard phases						
temperature /°C/																		alumina polymorphs					Al	Si
980						1110						1265												
reaction time /min/																								
15 + 20		60		90*		20		30		150*		2 + 4 + 6		15*		25		γ	δ	θ	θ+κ	α		
2θ	d	2θ	d	2θ	d	2θ	d	2θ	d	2θ	d	2θ	d	2θ	d	2θ	d	d - spacing						
																								3.14
				28.61	3.12							28.61	3.12											
28.80	3.10																							
																					2.82			
																				2.80				
																					2.79			
																				2.79				
										34.11	2.58													
																34.91	2.57					2.57		
												35.23	2.55	35.19	2.55									
				35.34	2.54																2.54			
		35.48	2.53					35.4	2.53															
35.77	2.51																							
																							2.43	
																				2.41				
		37.96	2.37																					
										38.13	2.36								2.36					
												38.	2.35			38.30	2.35					2.35		
								38.47	2.34												2.34			
38.31	2.32																				2.32			
				38.96	2.31			38.99	2.31			38.99	2.31	39.02	2.31	38.95	2.31							
		39.17	2.30															2.30			2.30	2.30		
																			2.29					

* Etched in 5.0 ml (40%) HF + 95 ml dest.water for 5 to 15 min.

..cont./

..cont/ Table 4.2.3.

reaction specimens																		standard phases						
temperature /°C/																		alumina polymorphs					Al	Si
980							1110					1265												
reaction time /min/																								
15 + 20		60		90*		20		30		150*		2 + 4 + 6		15*		25		γ	δ	θ	θ + κ	α		
2θ	d	2θ	d	2θ	d	2θ	d	2θ	d	2θ	d	2θ	d	2θ	d	2θ	d	d - spacing						
																							2.27	
																				2.25				
																					2.14			
		42.89	2.11					42.86	2.11			42.81	2.11										2.11	
										43.07	2.10					43.09	2.10					2.10		
43.29	2.09			43.29	2.09									43.33	2.09									
																				2.07				
												43.95	2.06											
																		2.03						
														44.87	2.02									
								45.11	2.01	45.14	2.01													
45.34	2.00																							
																			1.99					
																					1.98			
																							1.95	
		47.61	1.91																					
47.92	1.90							47.87	1.90			47.83	1.90											
		53.61	1.71							53.59	1.71													
				53.93	1.70											53.90	1.70							
																						1.69		
																								1.67
																					1.64			
																				1.63				
														56.83	1.62									
57.19	1.61	57.20	1.61							57.22	1.61					57.20	1.61		1.62			1.62		
				57.60	1.60			57.61	1.60															
												61.85	1.50											

..cont/

..cont/ Table 4.2.3.

reaction specimens																		standard phases						
temperature /°C/																								
980						1110						1265						alumina polymorphs					Al	Si
reaction time /min/																								
15 + 20		60		90*		20		30		150*		2+ 4 + 6		15*		25								
	d		d		d		d		d		d		d		d		d	d - spacings						
																						1.47		
																					1.42			
		66.29	1.41	66.31	1.41																	1.41		
										66.84	1.40					66.84	1.40		1.40					
																					1.397			
67.35	1.39	67.37	1.39					67.38	1.39			67.37	1.39					1.39						
																						1.38	1.38	
																				1.375				

..cont./

Table 4.2.4.1. : X -ray diffraction data for selected specimens. Al - 5, 10, 15 atomic % Mn SiO_2 reaction system.

reaction specimens																standard phases						
Al - 5 at % Mn						Al - 10 at % Mn						Al - 15 at % Mn										
temperature /°C/																						
1265						1220						1220				alumina polymorphs					Al	Si
reaction time /min/																						
5 + 10		45*		75		(10 + 20)*		75		90		(30 + 45)*		120		γ	δ	θ	θ+κ	α		
2θ	d	2θ	d	2θ	d	2θ	d	2θ	d	2θ	d	2θ	d	2θ	d	d - spacings						
45.80	2.57							45.83	2.57											2.57		
				35.04	2.56							35.06	2.56									
		35.18	2.55			35.20	2.55			35.22	2.55			35.19	2.55							
																			2.54			
38.11	2.36	38.09	2.36			38.15	2.36							38.13	2.36		2.36					
																				2.35		
				38.42	2.34			38.46	2.34										2.34			
																			2.32			
						38.97	2.31							39.01	2.31							
39.18	2.30											39.15	2.30			2.30			2.30	2.30		
								39.34	2.29								2.29					
																					2.27	
																		2.25				
																			2.14			
												42.85	2.11								2.11	
43.06	2.10			43.06	2.10					43.09	2.10			43.08	2.10					2.10		
		43.30	2.09			43.30	2.09	43.2	2.09													
																		2.07				
46.31	2.00					46.30	2.00															
																	1.99					
																			1.98			
																					1.95	
																						1.90
								53.60	1.71													

T - 61

* Etched in etchant C referred to in Table 3.5 for 10 to 15 min.

..cont/

..cont/ Table 4.2.4.1.

reaction specimens																standard phases						
Al - 5 at % Mn						Al - 10 at % Mn						Al - 15 at % Mn										
temperature /°C/																						
1265						1220						1220										
reaction time /min/																alumina polymorphs					Al	Si
5 + 10		45*		75		(10 + 20)*		75		90		(30 + 45)*		120		γ	δ	θ	θ+κ	α		
2θ	d	2θ	d	2θ	d	2θ	d	2θ	d	2θ	d	2θ	d	2θ	d	d - spacings						
		53.95	1.70			53.95	1.70							53.93	1.70							
												54.30	1.69							1.69		
																						1.67
																			1.64			
																		1.63				
56.82	1.62													56.80	1.62		1.62			1.62		
				57.19	1.61					57.19	1.61											
		57.63	1.60			57.60	1.60	57.60	1.60													
																					1.47	
																			1.42			
																				1.41		
		66.83	1.40	66.78	1.40			66.80	1.40	66.80	1.40			66.78	1.40		1.40					
																			1.397			
67.09	1.39					67.08	1.39					67.05	1.39									
		67.94	1.38			67.90	1.38	67.89	1.38	67.92	1.38									1.38	1.38	
																		1.375				
												68.10	1.37									

Table 4.2.4.2. : X - ray diffraction data for selected specimens. Al - 5, 10, 15 atomic %Fe - SiO_2 reaction system.

Reaction specimens																standard phases						
Al - 5 at % Fe						Al - 10 at % Fe						Al - 15 at % Fe										
temperature /°C/																						
1170						1170						1220										
reaction time /min/																alumina polymorphs					Al	Si
10+15+20		90		120*		20 + 25		90*		210		30 + 45		120		180		γ	δ	θ	θ+κ	α		
2θ	d	2θ	d	2θ	d	2θ	d	2θ	d	2θ	d	2θ	d	2θ	d	2θ	d	d - spacing						
						34.9	2.57							34.90	2.57							2.57		
		35.03	2.56	35.00	2.56					35.01	2.56													
								35.20	2.55							35.16	2.55							
35.40	2.54											35.40	2.54								2.54			
																				2.41				
										3	2.37					37.97	2.37							
38.09	2.36	38.14	2.36					38.10	2.36			38.14	2.36						2.36					
				38.26	2.35									38.22	2.35							2.35		
38.50	2.34					38.50	2.34														2.34			
																					2.32			
								39.00	2.31							38.96	2.31							
		39.20	2.30			39.19	2.30														2.30	2.30		
																			2.29					
																							2.27	
																				2.25				
42.85	2.11																						2.11	
				43.03	2.10					43.06	2.10			43.08	2.10	43.06	2.10					2.10		
		43.31	2.09			43.33	2.09	43.31	2.09			43.30	2.09											
																				2.07				
														53.30	1.72									
53.60	1.71							53.58	1.71															
				53.96	1.70							53.95	1.70											
																						1.69		
																								1.67

* Etched in etchant C referred to in Table 3.5, for 10 to 15 min.

..cont/

..cont/ Table 4.2.4.2.

Reaction specimens																		standard phases						
Al - 5 at % Fe						Al - 10 at % Fe						Al - 15 at % Fe												
temperature /°C/																								
1170						1170						1220												
reaction time /min/																		alumina polymorphs					Al	Si
10 + 15 + 25		90		120*		20 + 25		90*		240		30 + 45		120		180		γ	δ	θ	θ+κ	α		
2θ	d	2θ	d	2θ	d	2θ	d	2θ	d	2θ	d	2θ	d	2θ	d	2θ	d	d - spacing						
																				1.63				
																			1.62			1.62		
		57.20	1.61			57.25	1.61							57.23	1.61									
57.63	1.60			57.58	1.60			57.57	1.60			57.60	1.60											
										58.03	1.59					58.00	1.59							
																					1.42			
						66.31	1.41															1.41		
66.85	1.40	66.80	1.40	66.81	1.40			66.87	1.40	66.81	1.40	66.82	1.40			66.84	1.40							
														66.93	1.398						1.397			
																		1.39						
		67.90	1.38	67.95	1.38					67.80	1.38			67.90	1.38	67.91	1.38					1.38	1.38	
								68.10	1.377											1.375				

Fig. 2.1. - the aluminium-silicon equilibrium phase diagram
(after Hansen, M.[5])

Fig. 2.2. - temperature dependence of the time required to initiate reaction between aluminium and silica

+ pure aluminium; first observation of reaction layer

■ pure aluminium; extrapolated time for zero time thickness

o pure aluminium; (from ref.46)

x Al-0.38 % Bi (from ref. 46)
(after Squires, H.V., Rayson, H.W.[50])

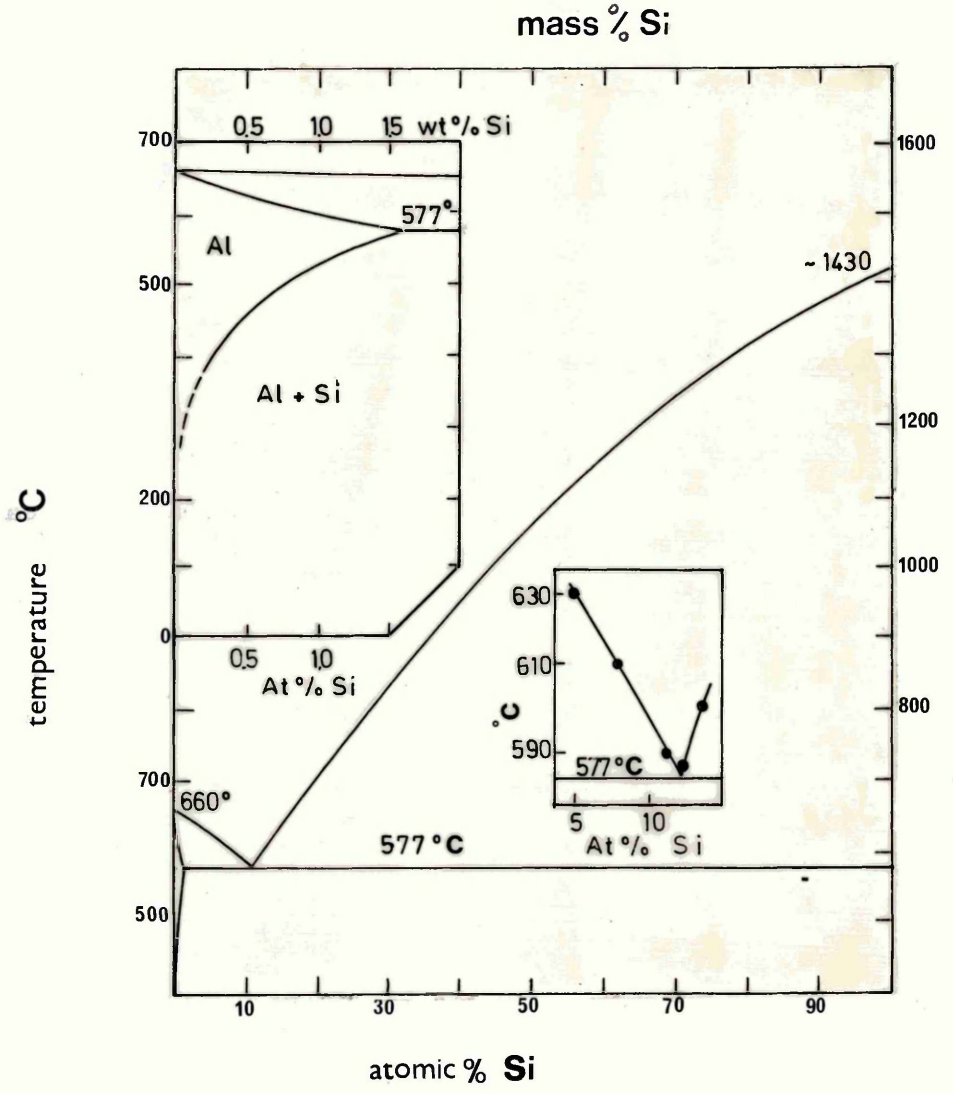
mass % Si
0.5
1.0
1.5 wt% Si
577°
Al
Al + Si
~1430
660°
577 °C
0.5
1.0
At % Si
630
610
590
°C
577°C
5
10
At % Si
temperature °C
700
500
200
0
700
500
1600
1200
1000
800
10
30
50
70
90
atomic % Si

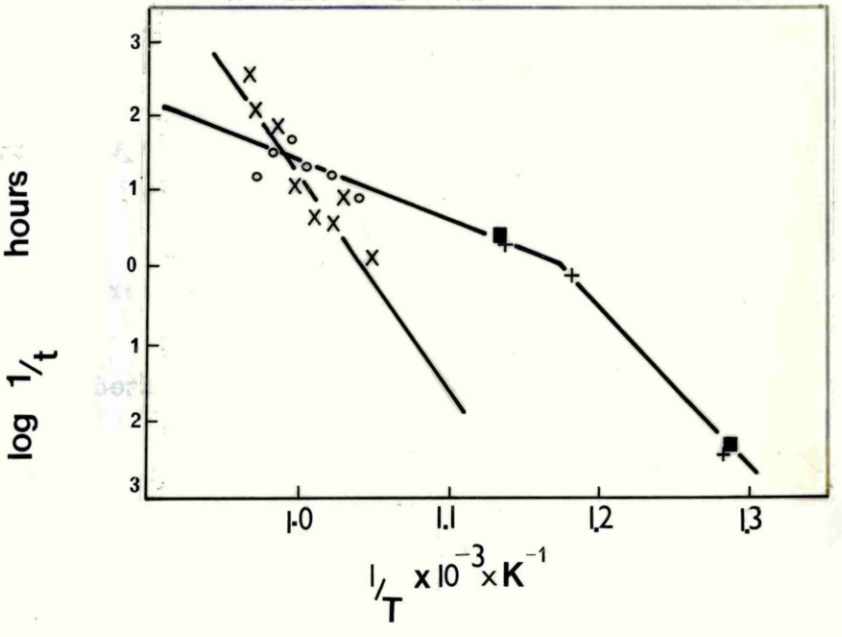
log 1/t hours
3
2
1
0
1
2
3
1.0
1.1
1.2
1.3
1/T x 10⁻³ x K⁻¹

Fig. 2.3. - change in wetting behaviour of liquid aluminium in contact with silica surface at two different temperatures.
(after Marumo, C., Pask, J.A.[21])

Fig. 2.4. - a. : electron-microprobe analysis /in mass % of a cross-section of an aluminium-silica specimen after reaction at 1000°C for one hour;

b. : calculated ionic species profiles based on a constant number of oxygen ions using mass % concentration data obtained from a.

(after Marumo, C., and Pask, J.A.[21])

Fig. 2.5. - general forms of a conversion process in a heterogeneous reacting system:

R_s represents the extent of the initial period (I)

t_o marks the end of the induction period (II)

R_i, t_i are the co-ordinates of the point of inflection separating the acceleratory period (III) from the deceleratory period (IV).

R_f is the fractional conversion related to almost complete reaction

(after Jacobs, P.W.M.[79])

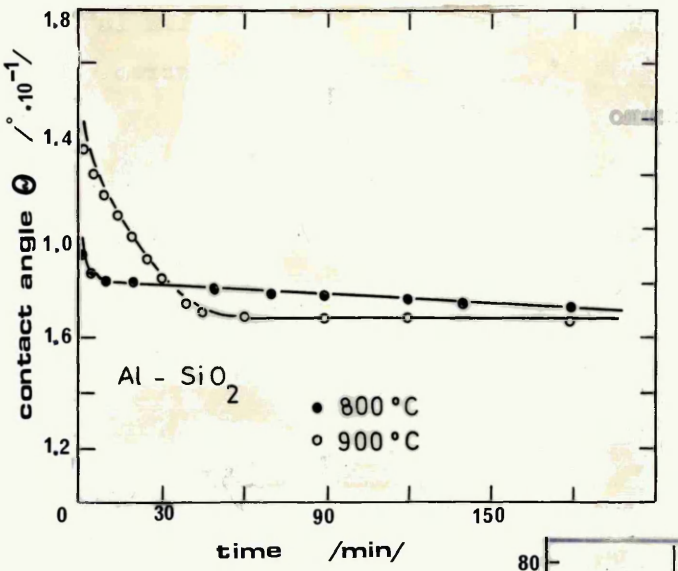
contact angle θ /°.10⁻¹/
1,8
1,4
1,0
1,6
1,2
Al - SiO2
● 800 °C
○ 900 °C
0
30
90
150
time /min/

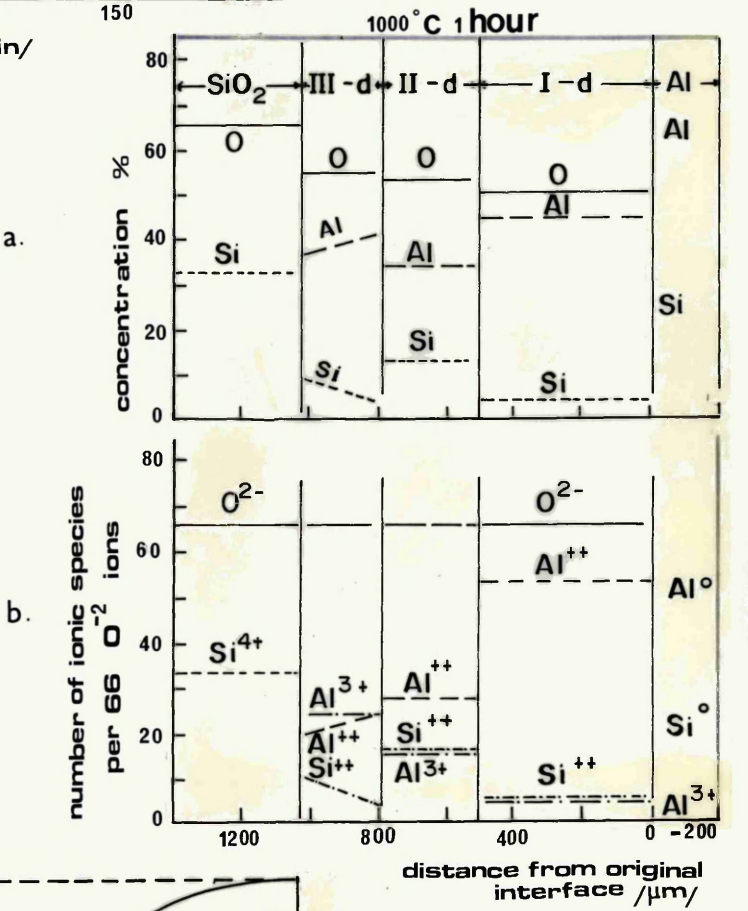
1000°C 1 hour
a.
b.
SiO2
III -d
II -d
I -d
Al
O
Si
concentration %
number of ionic species per 66 O-2 ions
O2-
Si4+
Al3+
Al++
Si++
Al°
Si°
1200
800
400
0 -200
distance from original interface /μm/

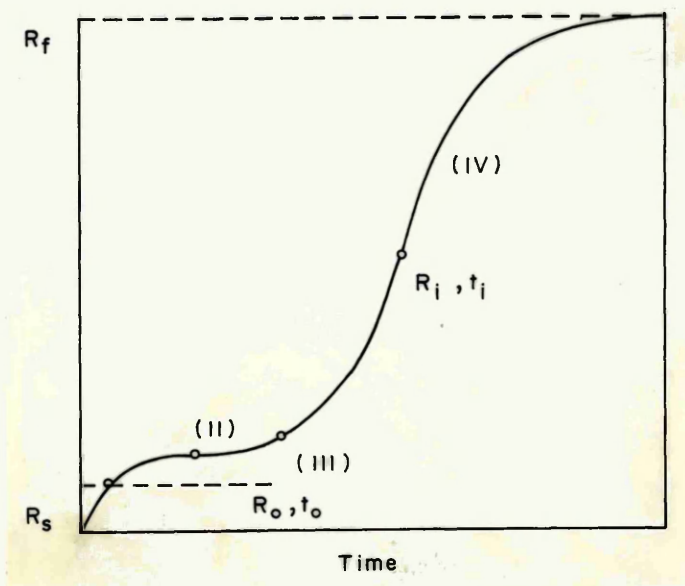
Rf
Rs
(II)
(III)
(IV)
Ri , ti
Ro , to
Time

Fig. 2.6. : reported activation energy values by different investigators in the field of interaction between silica and aluminium. Conversion to same units had to be made.

(1) after Prabriputaloong, K., Piggott, M.R.[4]

(2) after Standage, A.E., Gani, M.S.[46]

(3) after Squires, H.V., Rayson, H.W.[50]

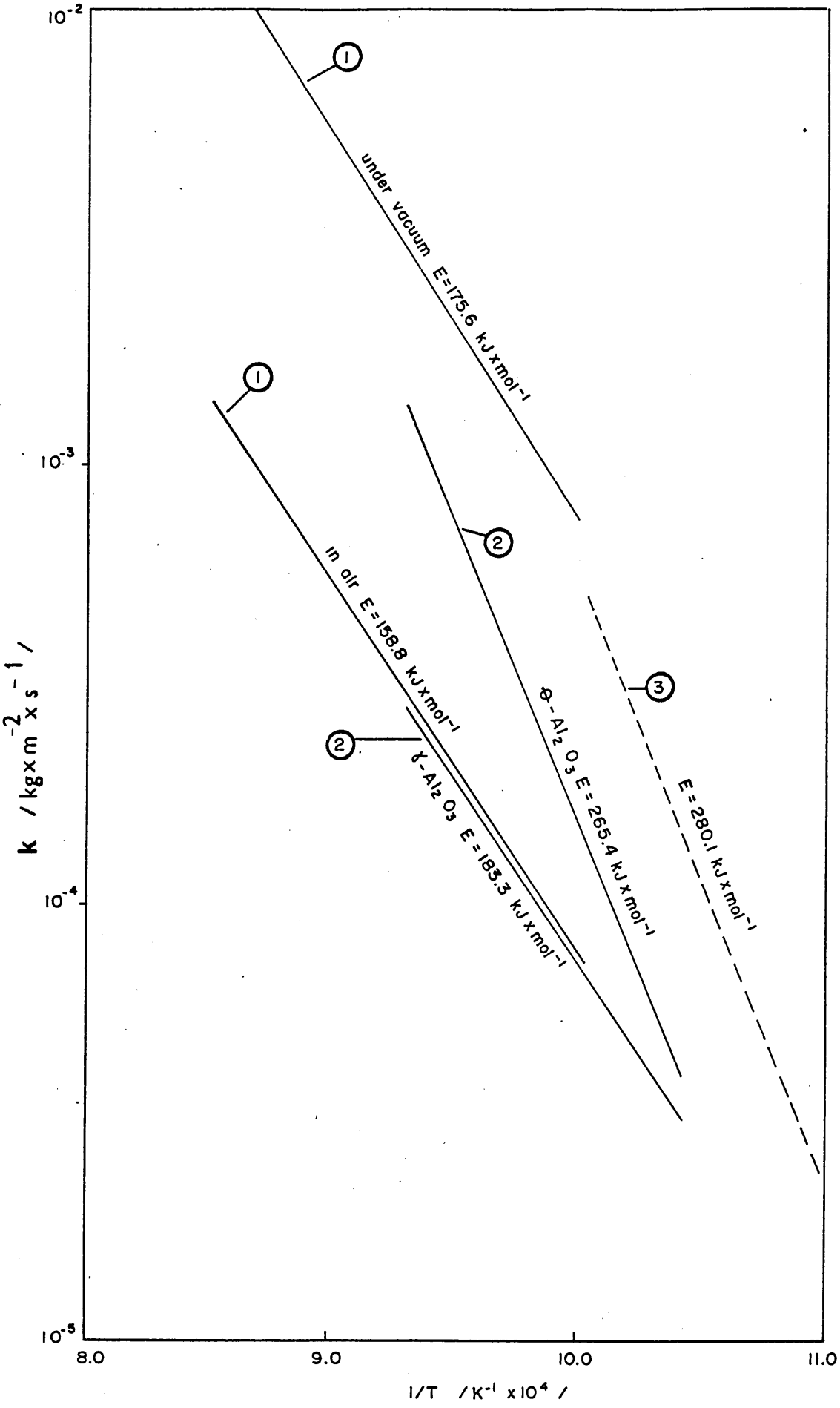
10-2
10-3
10-4
10-5
8.0
9.0
10.0
11.0
k / kg x m-2 x s-1 /
1/T /K-1 x 10-4 /
1
under vacuum E=175.6 kJ x mol-1
1
in air E=158.8 kJ x mol-1
2
γ-Al2O3 E=183.3 kJ x mol-1
2
Θ-Al2O3 E=265.4 kJ x mol-1
3
E=280.1 kJ x mol-1

Fig. 2.7. The aluminium-rich end of the aluminium-manganese binary phase diagram.
(after Mondolfo, L.F.[80])

Fig. 2.8. The aluminium-rich end of the aluminium-iron binary phase diagram.
(after Mondolfo, L.F.[80])

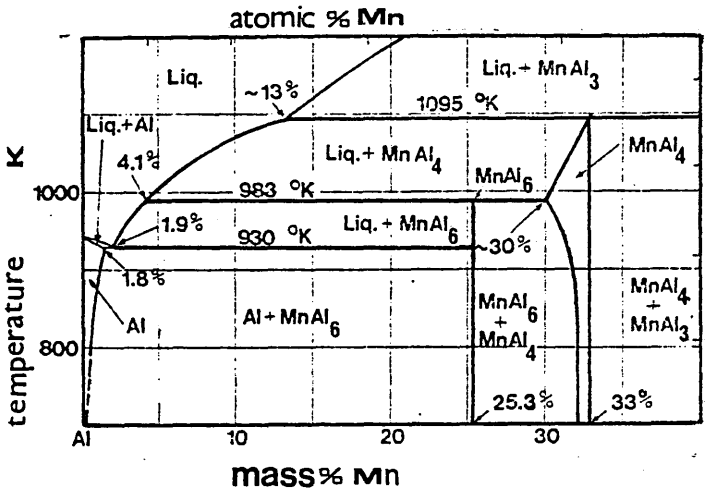
atomic % Mn
Liq.
~13%
Liq.+ MnAl3
1095 °K
Liq.+Al
4.1%
Liq.+ MnAl4
MnAl6
MnAl4
983 °K
1000
1.9%
930 °K
Liq.+ MnAl6
~30%
1.8%
Al
Al+ MnAl6
MnAl6 + MnAl4
MnAl4 + MnAl3
800
25.3%
33%
temperature K
Al
10
20
30
mass% Mn

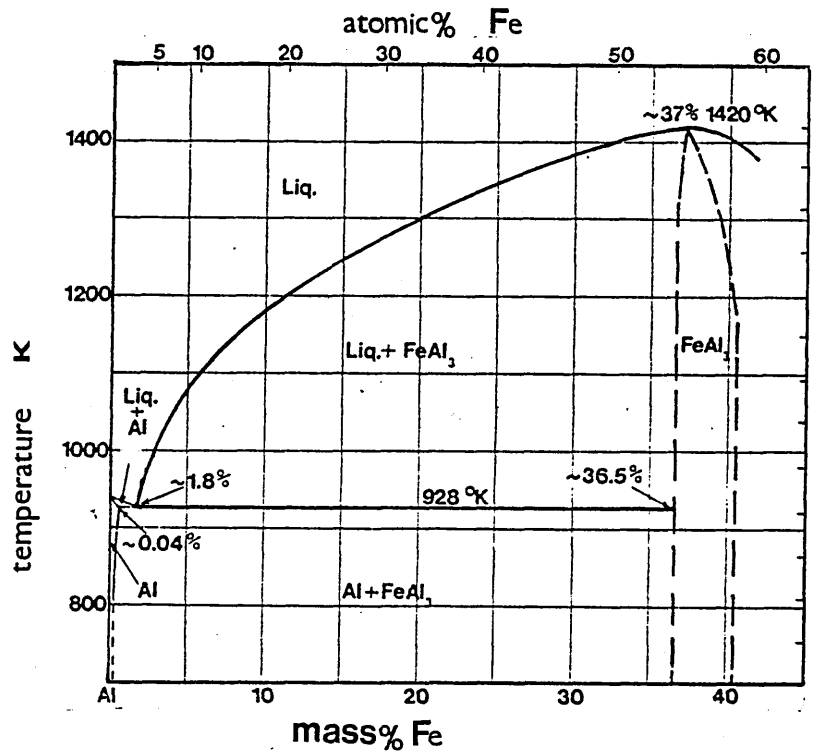
atomic% Fe
5
10
20
30
40
50
60
~37% 1420°K
1400
Liq.
1200
Liq.+ FeAl3
FeAl3
Liq. + Al
1000
~1.8%
928 °K
~36.5%
~0.04%
Al
800
Al+FeAl3
temperature K
Al
10
20
30
40
mass% Fe

Fig. 2.9. Phase distribution at the aluminium corner of the aluminium-manganese-silicon ternary diagram.
(after Mondolfo, L.F.[80])

Fig. 2.10. Phase distribution in the solid aluminium corner of the aluminium-iron-silicon ternary diagram.
(after Mondolfo, L.F.[80])

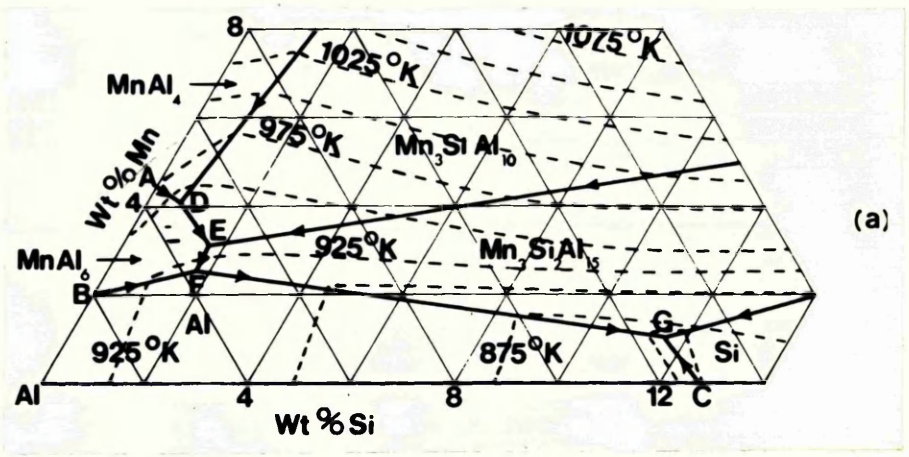
8
1025 °K
1075 °K
MnAl4
975 °K
Mn3SiAl10
Wt % Mn
4
D
E
(a)
MnAl6
925 °K
Mn3Si2Al15
B
F
Al
G
925 °K
875 °K
Si
Al
4
8
12
C
Wt % Si

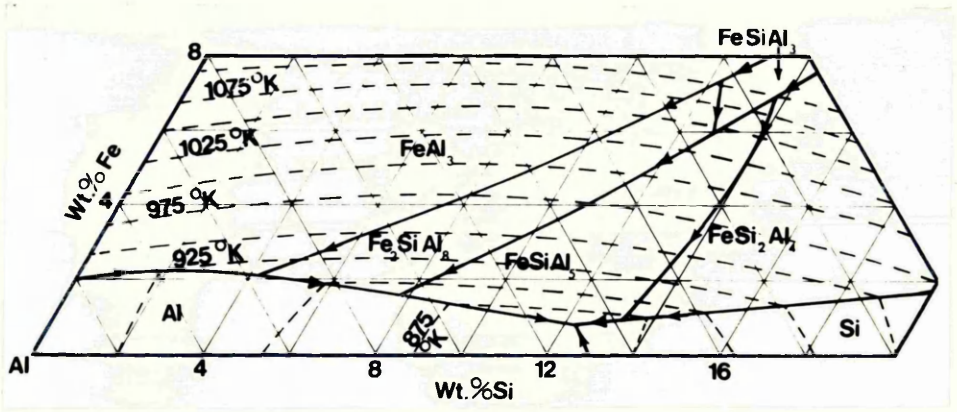
FeSiAl3
8
1075 °K
1025 °K
FeAl3
Wt.% Fe
4
975 °K
925 °K
Fe2SiAl8
FeSiAl5
FeSi2Al4
Al
875 °K
Si
Al
4
8
12
16
Wt.%Si

Fig. 3.1. - equipment used in the preliminary experiments for reaction between vitreous silica and molten aluminium .

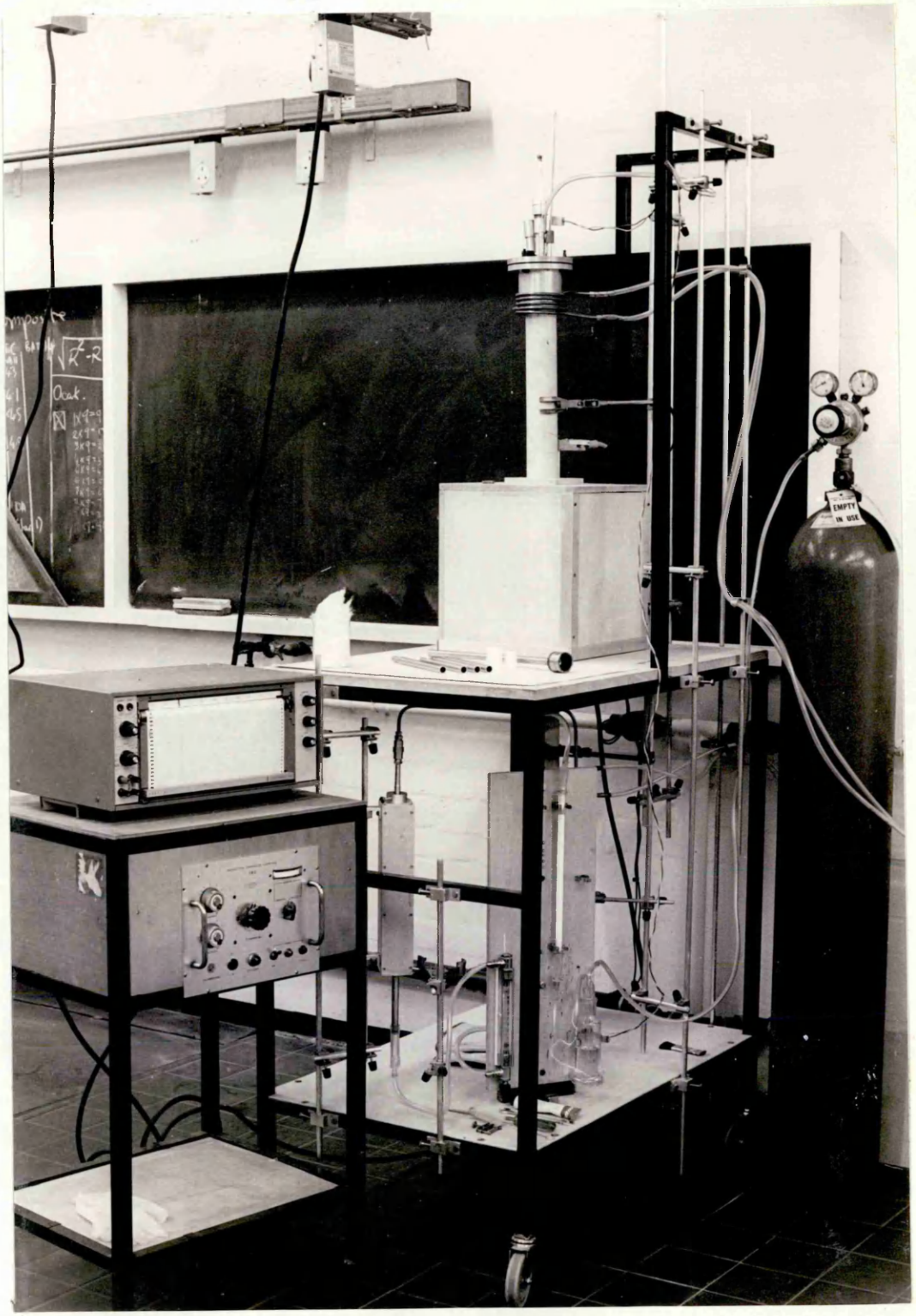
EMPTY
IN USE

Fig. 3.2. - flow diagram of the reactor and gas purifying system for preliminary studies.

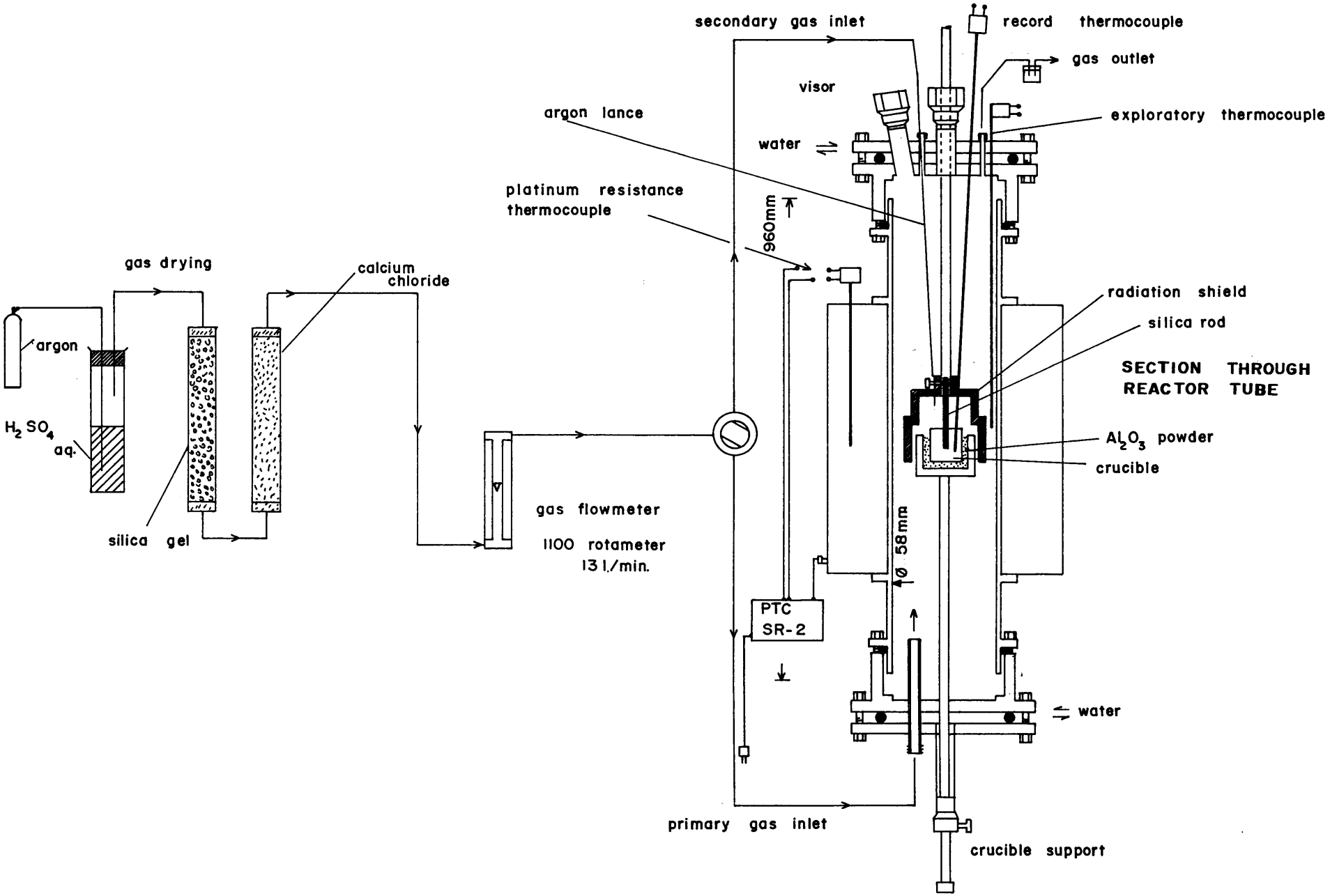
secondary gas inlet
record thermocouple
gas outlet
visor
argon lance
exploratory thermocouple
water
platinum resistance thermocouple
960mm
gas drying
calcium chloride
argon
radiation shield
silica rod
SECTION THROUGH REACTOR TUBE
H_2SO_4 aq.
Al_2O_3 powder
crucible
silica gel
gas flowmeter
1100 rotameter
13 l./min.
58mm
PTC SR-2
water
primary gas inlet
crucible support

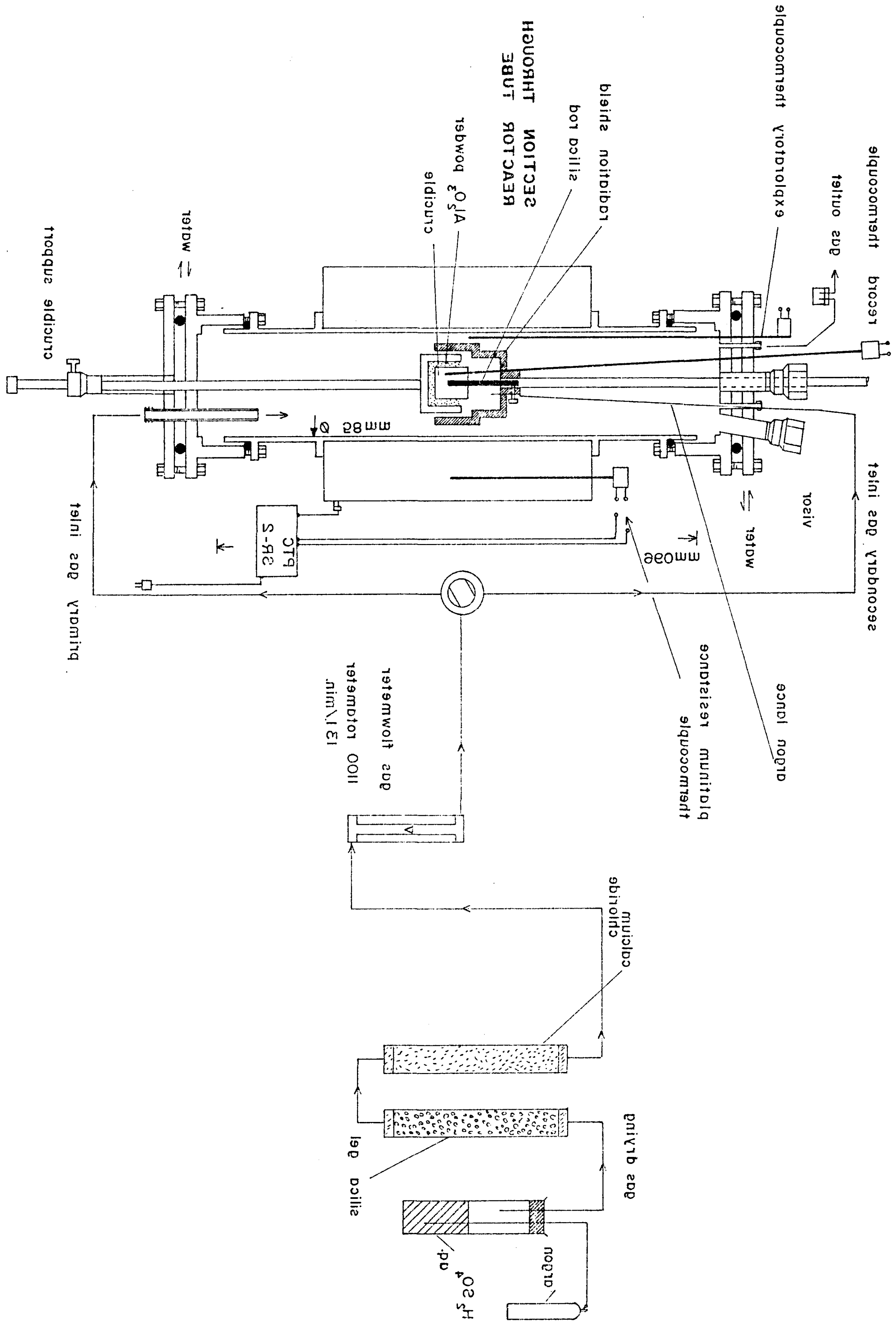
SECTION THROUGH REACTOR TUBE
crucible support
water
primary gas inlet
PTC SR-2
960mm
Ø 58mm
water
visor
secondary gas inlet
record
thermocouple
gas outlet
exploratory thermocouple
radiation shield
silica rod
Al_2O_3 powder
crucible
argon lance
platinum resistance thermocouple
gas flowmeter
1100 rotameter
13 l/min.
calcium chloride
silica gel
gas drying
argon
H_2SO_4 aq.

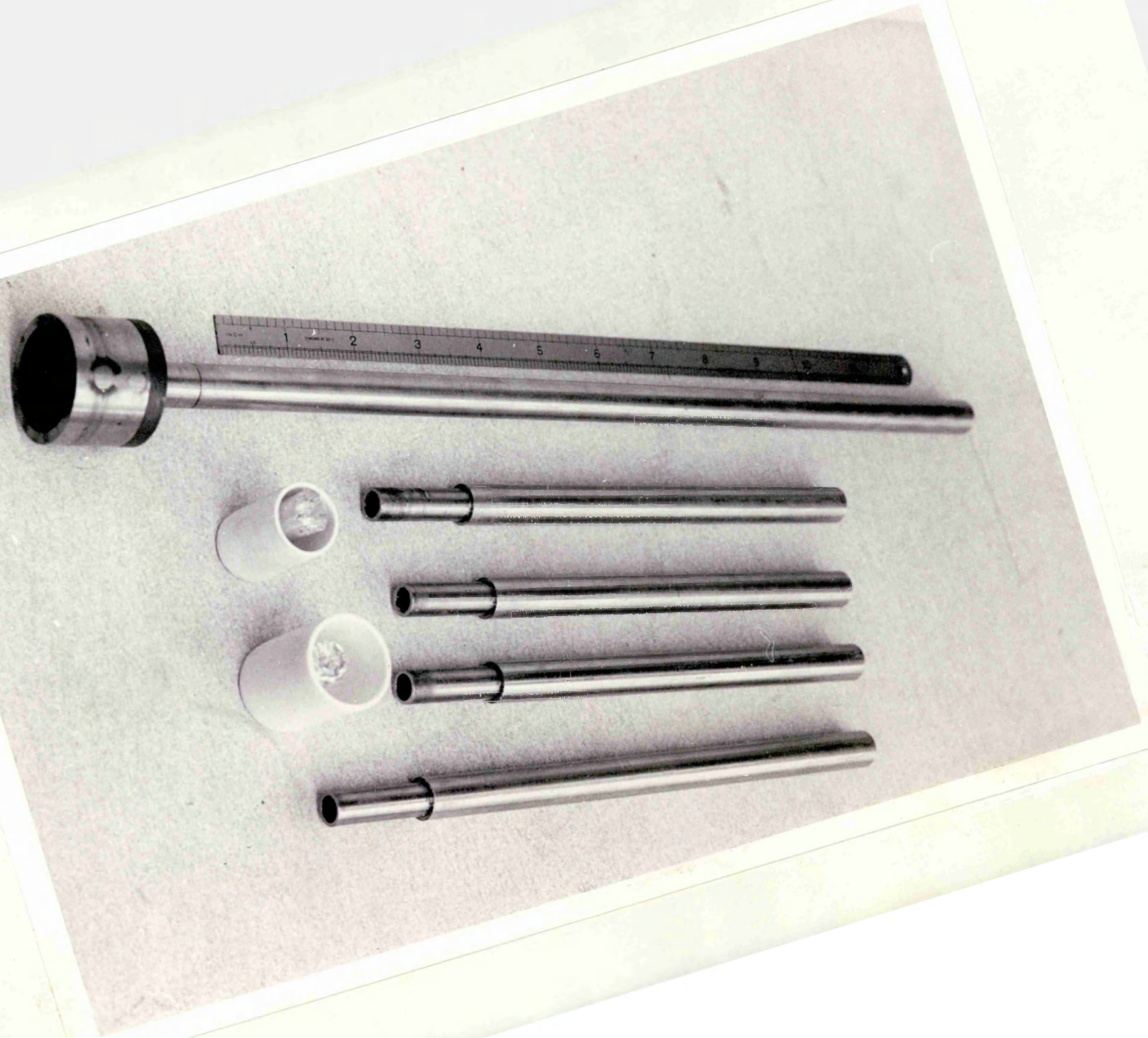

Fig. 3.4. - modified equipment for studies on reaction between silica and liquid pure aluminium and aluminium alloy at higher temperatures.

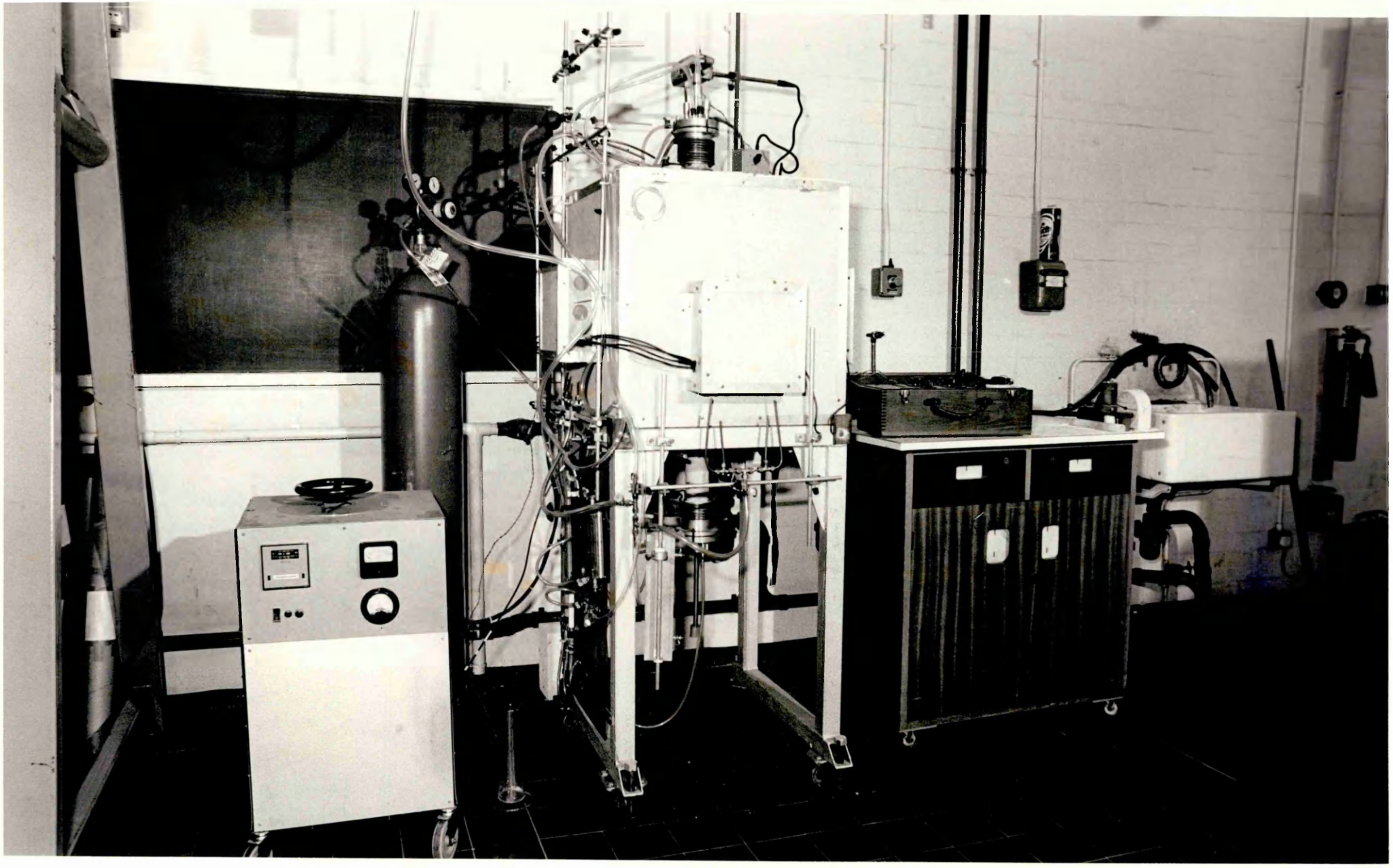

Fig. 3.5. - scheme of high temperature apparatus .

(a) - Furnace: "crystalon" hot rods heating elements - insulating brick structure

(b) - Eurotherm "on/off" switch control wiring diagram

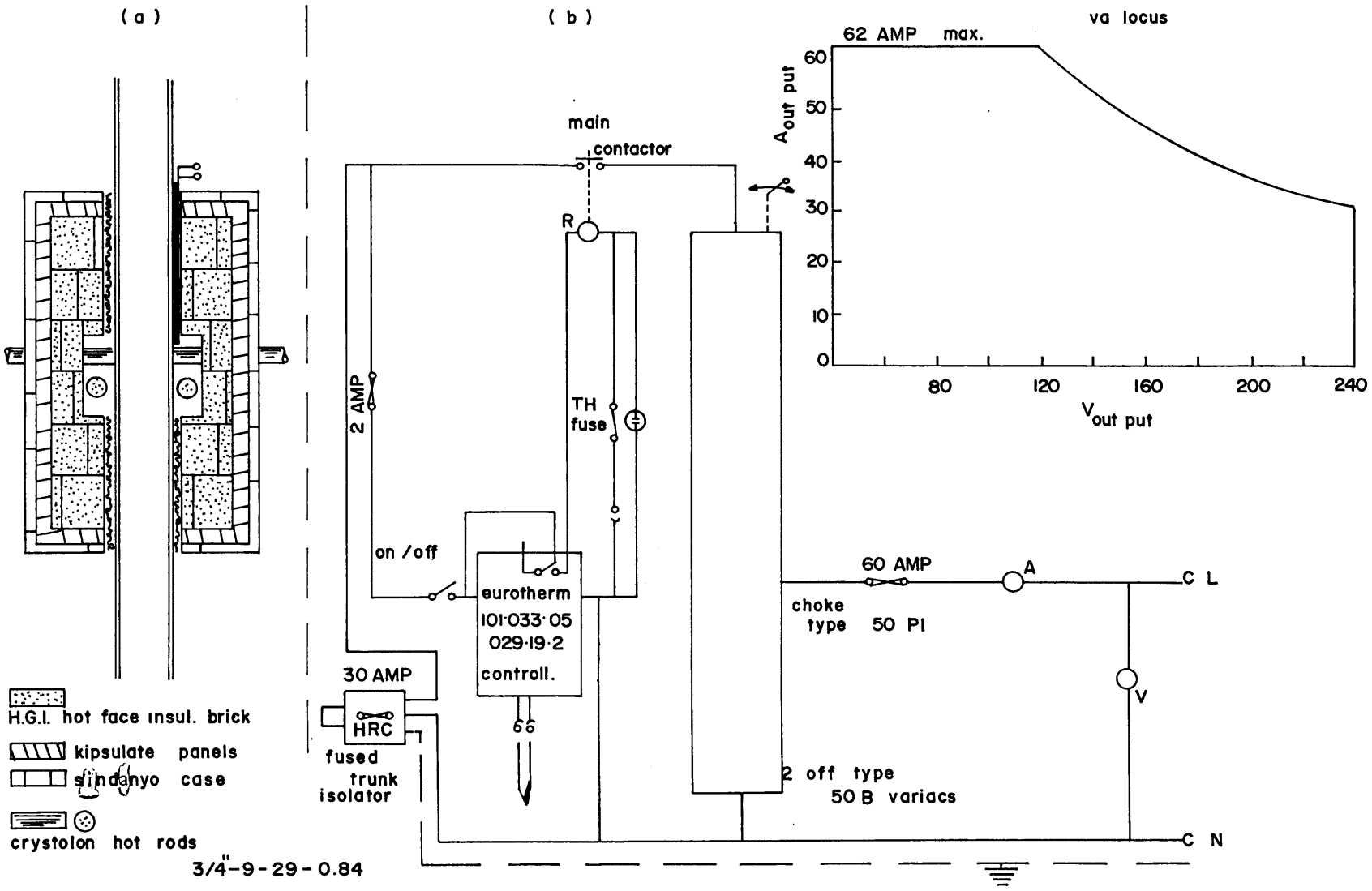
(a)
(b)
va locus
62 AMP max.
A out put
V out put
60
50
40
30
20
10
0
80
120
160
200
240
main
contactor
R
2 AMP
TH
fuse
on /off
eurotherm
101·033·05
029·19·2
controll.
60 AMP
A
C L
choke
type 50 PI
V
30 AMP
HRC
fused
trunk
isolator
2 off type
50 B variacs
C N
H.G.I. hot face insul. brick
kipsulate panels
sindanyo case
crystolon hot rods
3/4"-9-29-0.84

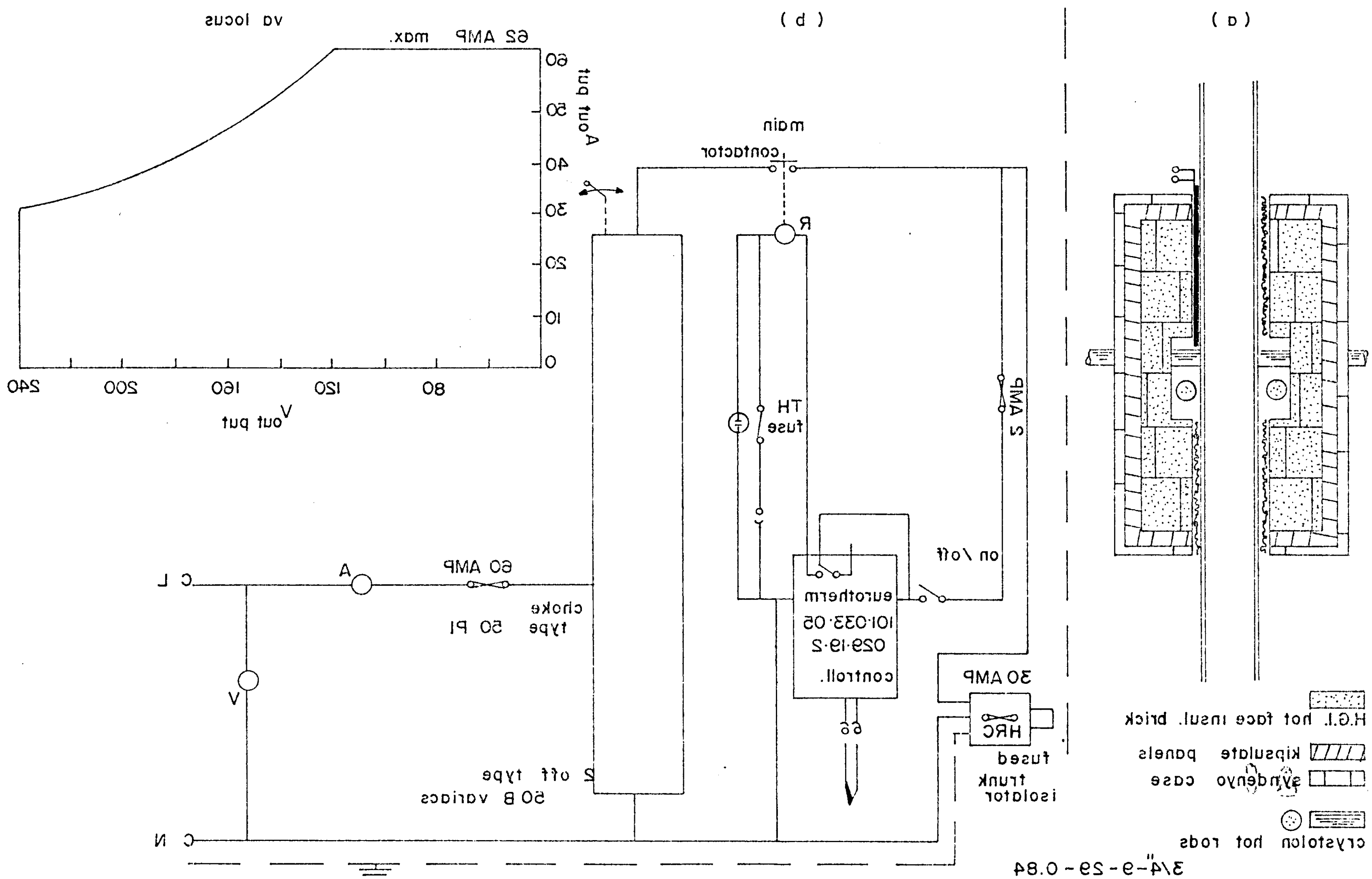

(a)
(b)
va locus
62 AMP max.
$A_{out\ put}$
$V_{out\ put}$
0
10
20
30
40
50
60
80
120
160
200
240
main
contactor
R
TH
fuse
2 AMP
on /off
eurotherm
101·033·05
029·19·2
controll.
30 AMP
HRC
fused
trunk
isolator
60 AMP
A
choke
type 50 PI
C L
V
C N
2 off type
50 B variacs
H.G.I. hot face insul. brick
kipsulate panels
syndenyo case
crystolon hot rods
3/4"-9-29-0.84

Fig. 3.6. - schematic section of reactor readapted for higher temperature experiments .

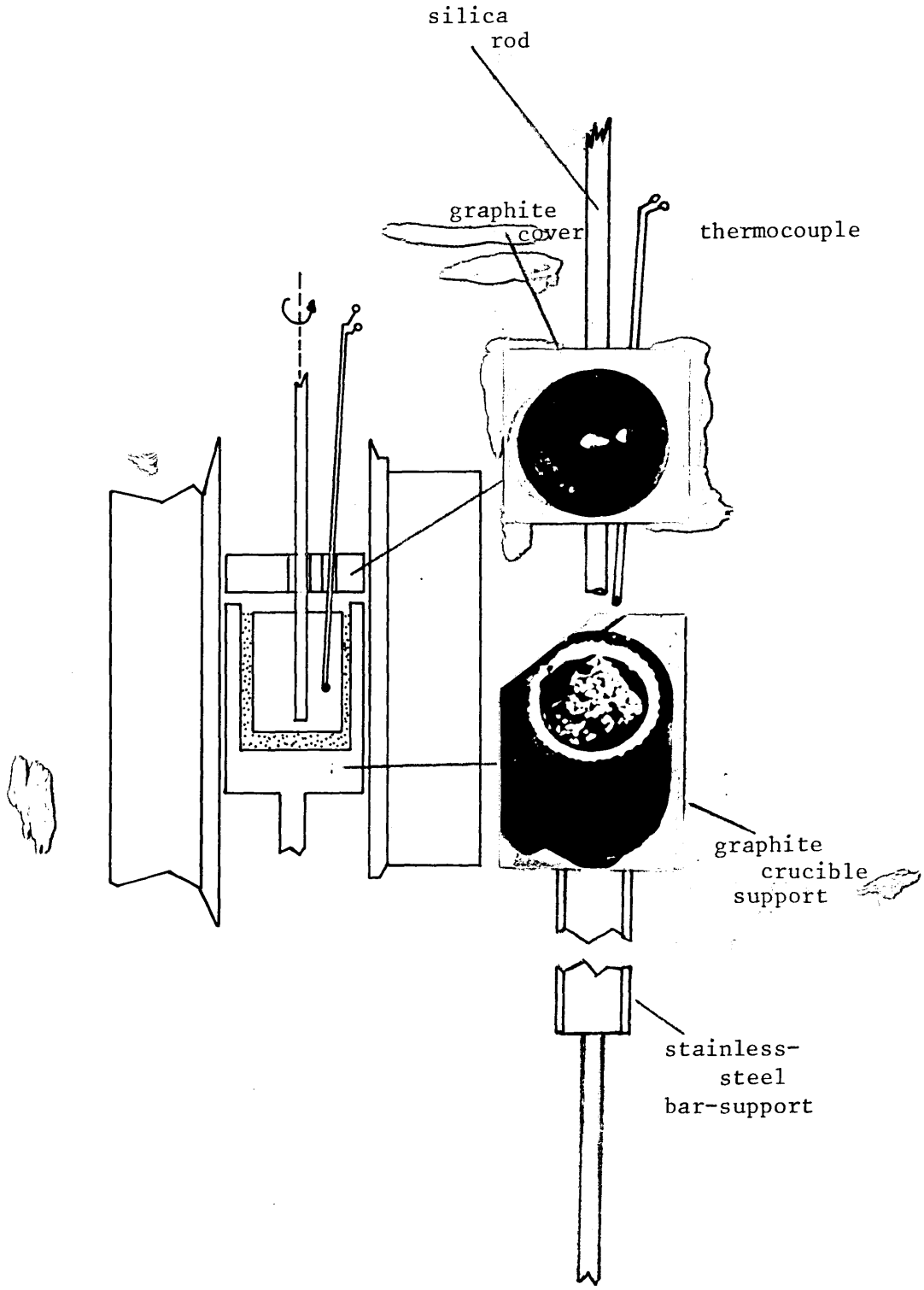
silica
rod
graphite
cover
thermocouple
graphite
crucible
support
stainless-
steel
bar-support

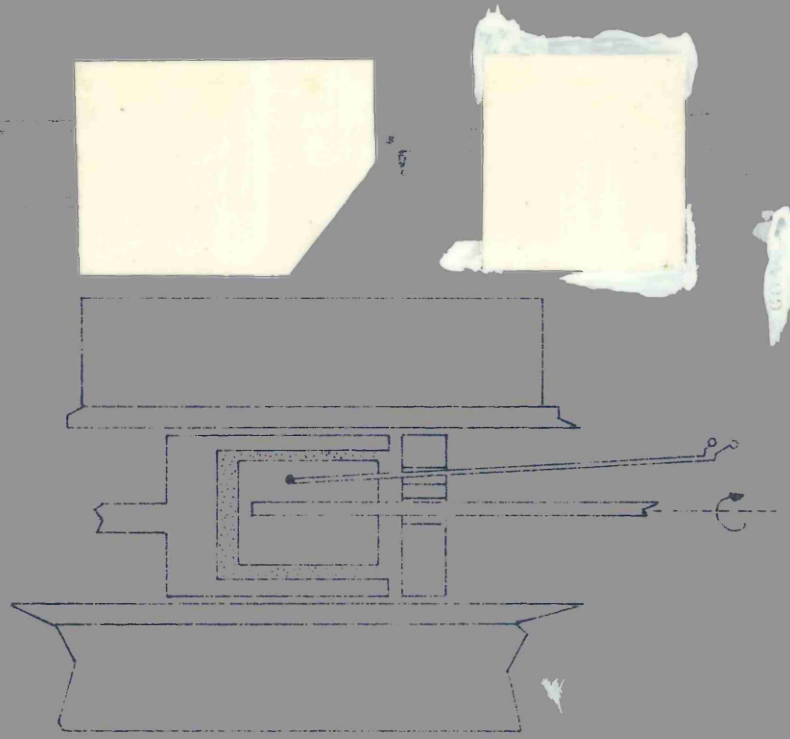

Fig.3.7 - variable speed "Gallenkamp" stirrer for rotation of the silica rod immersed in the molten metal .

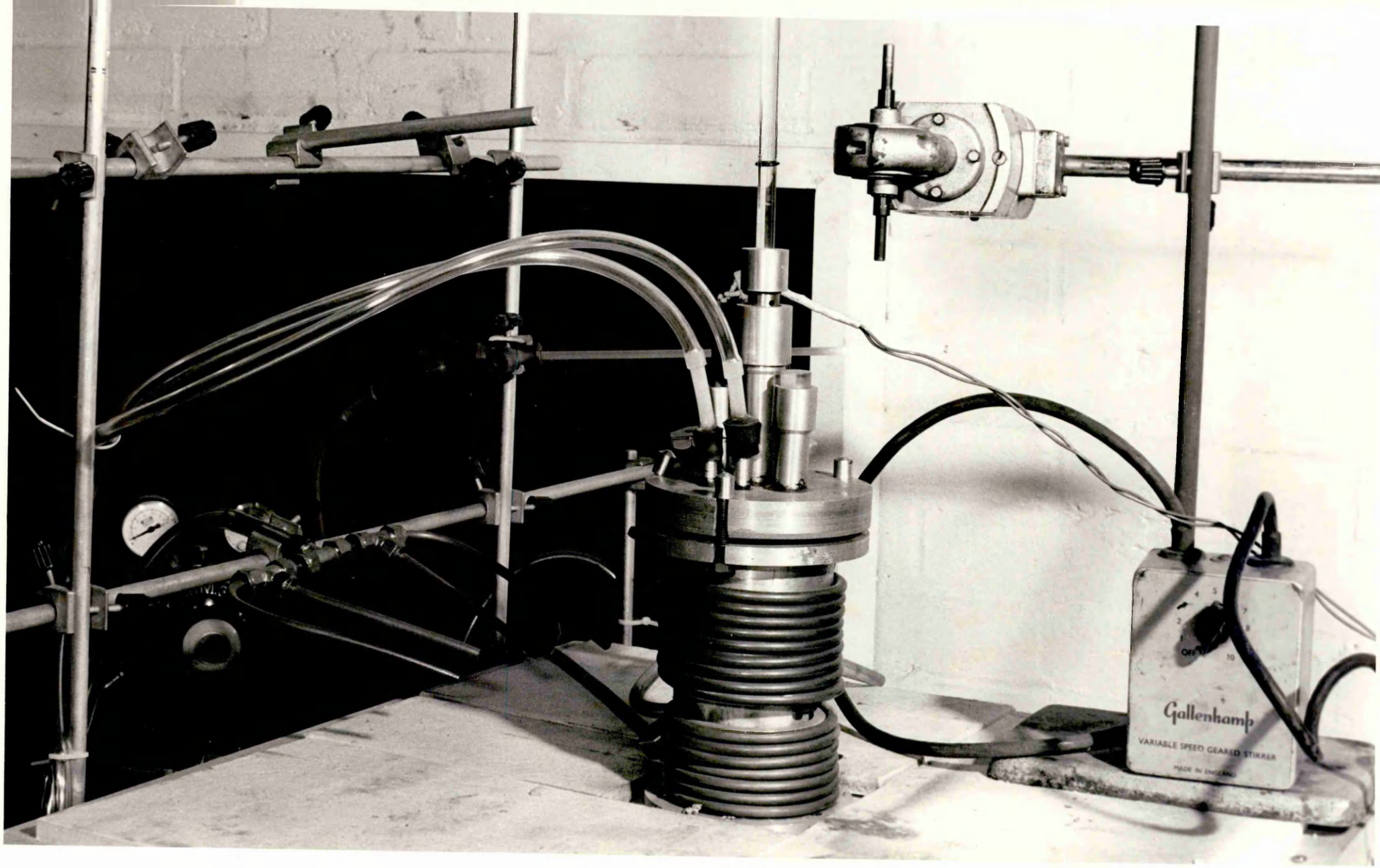
Gallenkamp
VARIABLE SPEED GEARED STIRRER
MADE IN ENGLAND

Fig. 3.8. a - d - schematic representation of different sectional configurations of the product layer formed during reaction :

(a) vertical section with representative cut for measurement
(b) non-uniform product layer
(c) uniform product layer
(d) irregular product layer

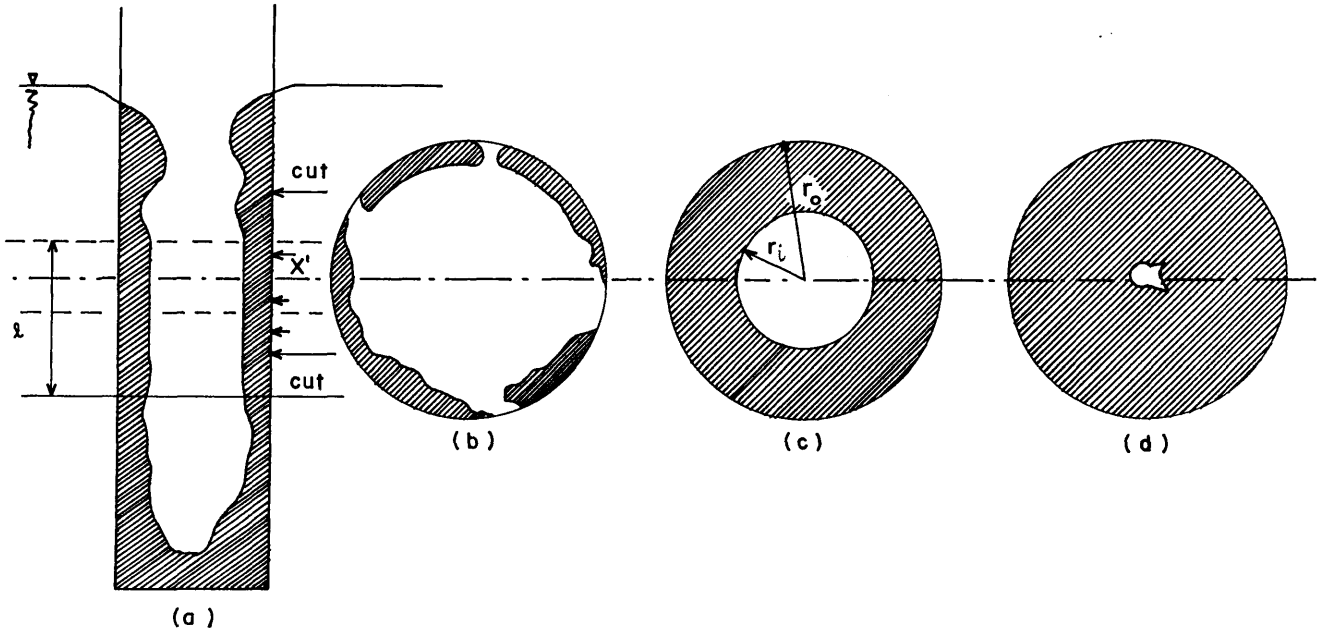
cut
X'
ℓ
cut
(a)
(b)
r_o
r_i
(c)
(d)

cut
x'
cut
ℓ
r_o
r
(a)
(b)
(c)
(d)

FIG. 4.1.2.1 - reaction between liquid pure aluminium and vitreous silica at different temperatures varying from 760 to 860°C.

Percentage of the product layer formed expressed as the left hand side of equation 4.1.1.1 versus time.

DIAMETER	FIGURE	TEMPERATURE	REGRESSION LINE EQUATION (y=mx + c)	STANDARD DEVIATION (σ)
3.0 mm	(a)	● 760°C	0.84x + 1.10	0.65
		⊙ 815°C	2.86x + 0.43	1.39
		⊘ 840°C	4.30x + 6.37	5.82
		○ 860°C	6.63x + 1.68	2.85
5.0 mm	(b)	● 760°C	0.51x + 0.21	0.63
		⊙ 815°C	2.12x - 0.99	1.93
		⊘ 840°C	3.29x - 1.08	1.93
		○ 860°C	3.63x + 1.31	1.03
10.0mm	(c)	● 760°C	0.30x - 0.10	0.44
		⊙ 815°C	0.95x + 0.29	1.17
		⊘ 840 °C	1.61x + 0.46	1.35
		○ 860°C	2.22x + 1.94	1.48

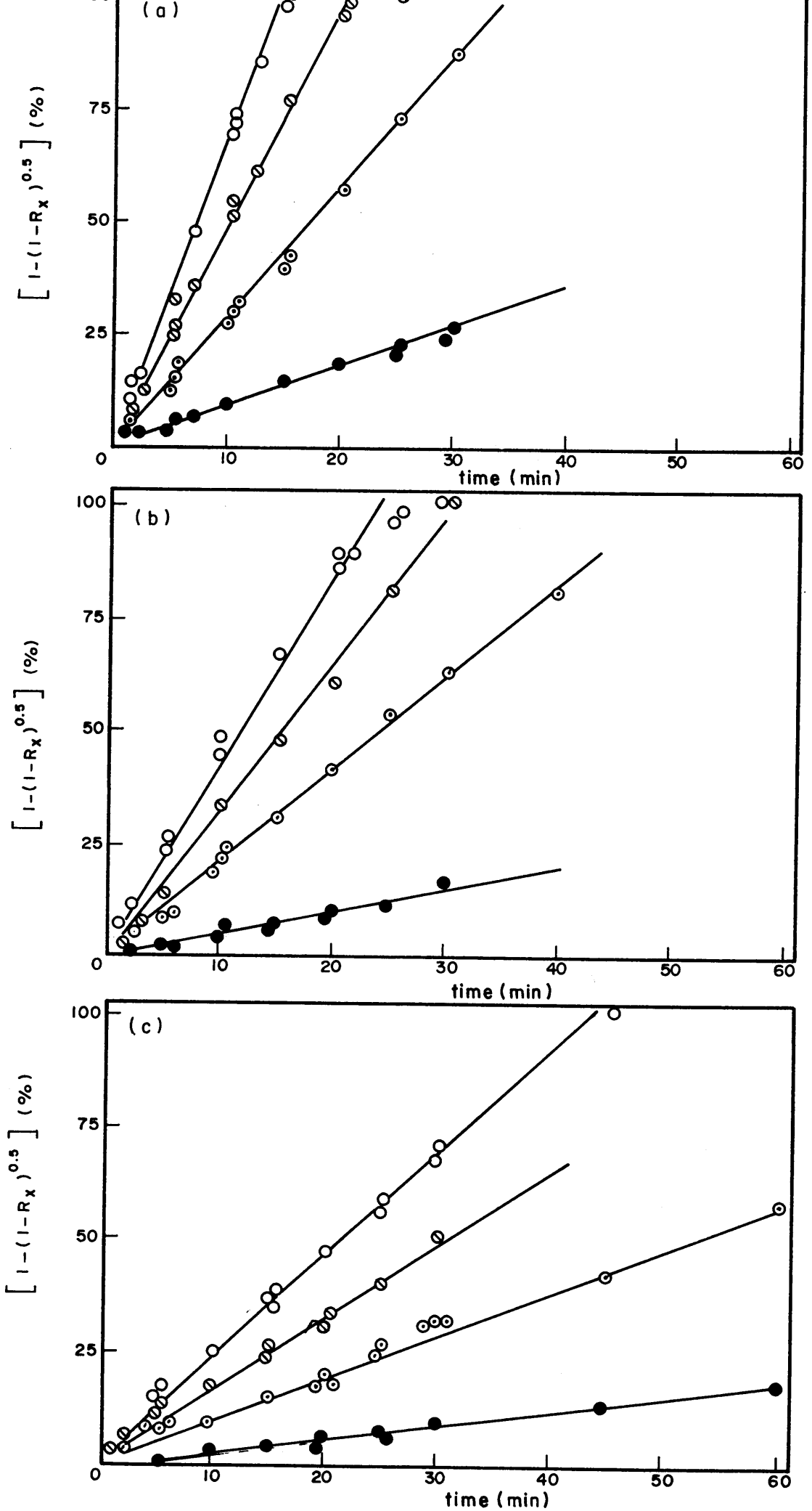
(a)
(b)
(c)
$[1-(1-R_x)^{0.5}]$ (%)
time (min)
0
10
20
30
40
50
60
25
50
75
100

(a)
(b)
(c)
time (min)
0
10
20
30
40
50
60
25
50
75
100

FIG. 4.1.2.2 - reaction between liquid pure aluminium and vitreous silica at different temperatures: 920 and 980°C.

Percentage of the product layer formed expressed as the left hand side of equation 4.1.1.1. versus time

original diameter of the rod:

(a) 5.0 mm

(b) 10.0 mm

temperatures:

O 920°C

● 980°C

x reference plot at 860°C

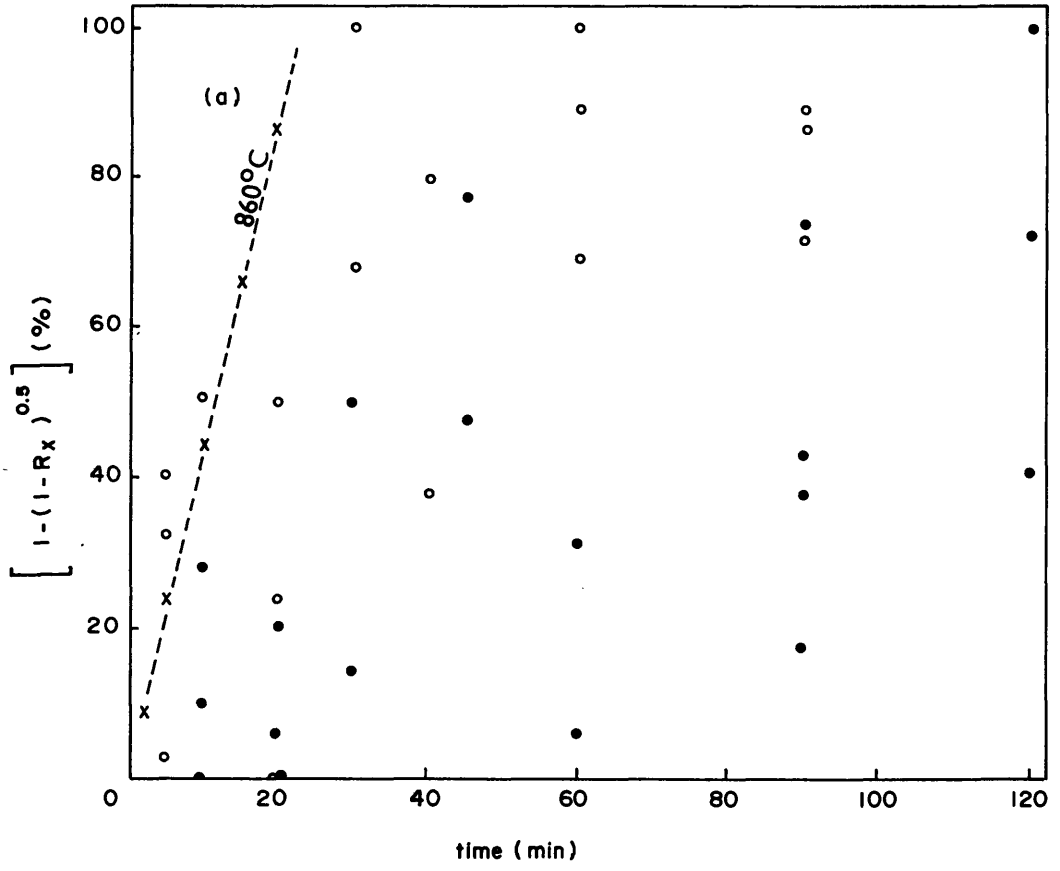
(a)
860°C
$\left[1-(1-R_x)^{0.5}\right]$ (%)
time (min)
0
20
40
60
80
100
120

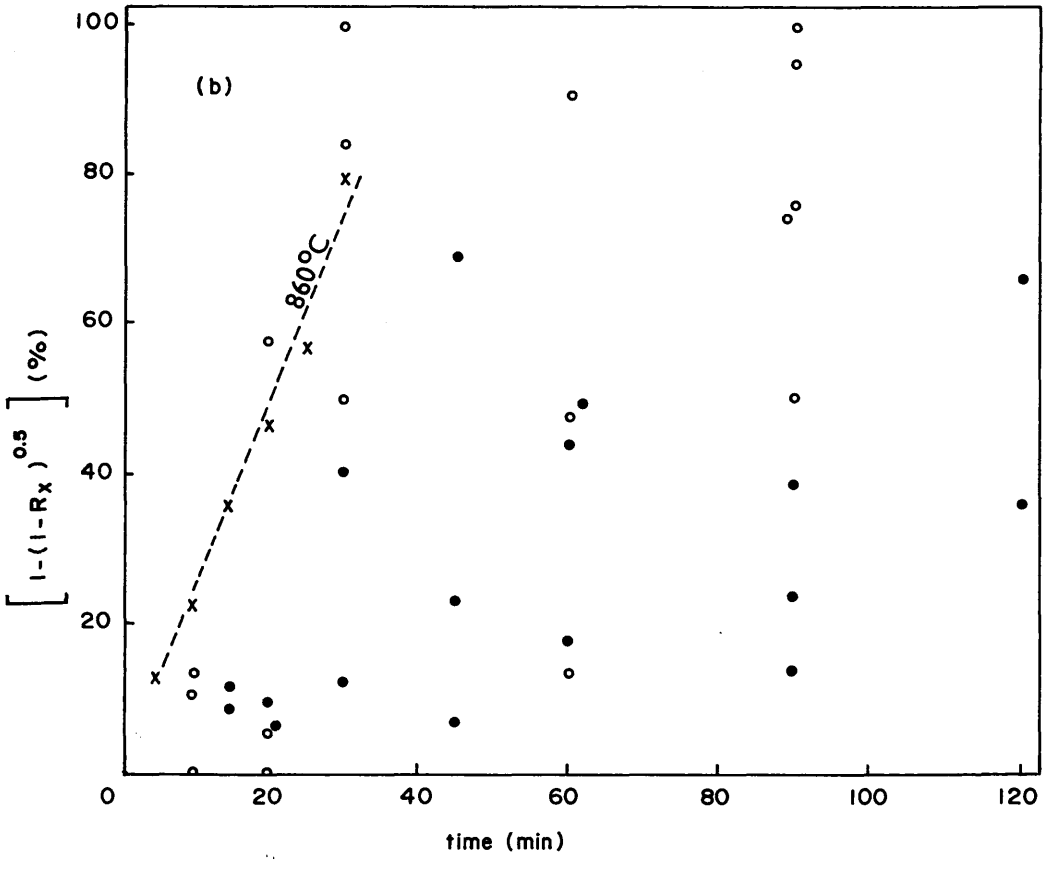
(b)
860°C
$\left[1-(1-R_x)^{0.5}\right]$ (%)
time (min)
0
20
40
60
80
100
120

(a)
$C_{0.98}$
$[1-(1-R_x)^{0.5}]$ (%)
time (min)
0
20
40
60
80
100
120

(b)
$C_{0.98}$
$[1-(1-R_x)^{0.5}]$ (%)
time (min)
0
20
40
60
80
100
120

FIG. 4.1.2.3 - reaction between liquid pure aluminium and vitreous silica at different temperatures varying from 1110 to 1265°C.

Percentage of the product layer formed expressed as the left hand side of equation 4.1.1.1 versus time.

DIAMETER	FIGURE	TEMPERATURE	REGRESSION LINE EQUATION ($y = mx + c$)	STANDARD DEVIATION (σ)
3.0 mm	(a)	● 1110°C	1.65x + 3.21	1.56
		⊖ 1170°C	3.30x + 6.47	3.40
		⊗ 1220°C	4.59x + 2.68	5.18
		○ 1265°C	6.67x - 1.25	1.45
5.0 mm	(b)	● 1110°C	1.07x - 0.22	2.82
		⊖ 1170°C	2.15x + 0.61	2.75
		⊗ 1220°C	3.22x + 1.99	1.89
		○ 1265°C	5.84x - 1.16	1.96
10mm	(c)	● 1110°C	0.58x + 0.66	3.74
		⊖ 1170°C	1.18x - 2.83	2.48
		⊗ 1220°C	1.70x - 0.52	2.63
		○ 1265°C	3.88x - 3.44	2.53

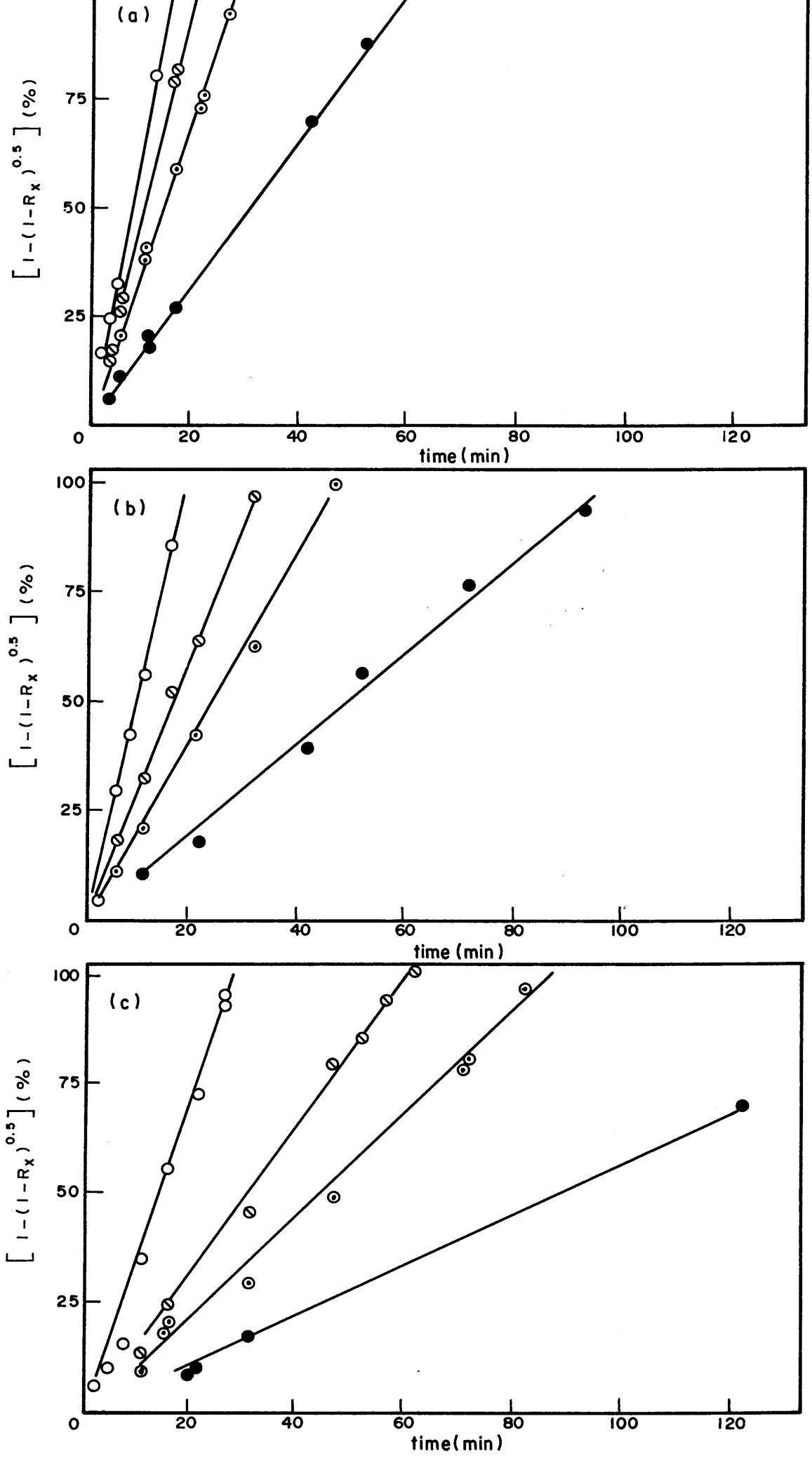
(a)
(b)
(c)
$[1-(1-R_x)^{0.5}]$ (%)
time (min)
0
20
40
60
80
100
120
25
50
75

(a)
(b)
(c)
time (min)
0
20
40
60
80
100
120
25
50
75
100

FIG. 4.1.2.4 - reaction between liquid pure aluminium and vitreous silica calculated values of the reaction rate constant /k/ for different diameter of the silica rod versus temperature

experimental temperature range /°C/	diameter of the silica rod /mm/
760 - 860	● 3.0 ▲ 5.0 ▼ 10.0
920 - 980	▲ 5.0 ▽ 10.0
1110 - 1265	O 3.0 Δ 5.0 ▽ 10.0

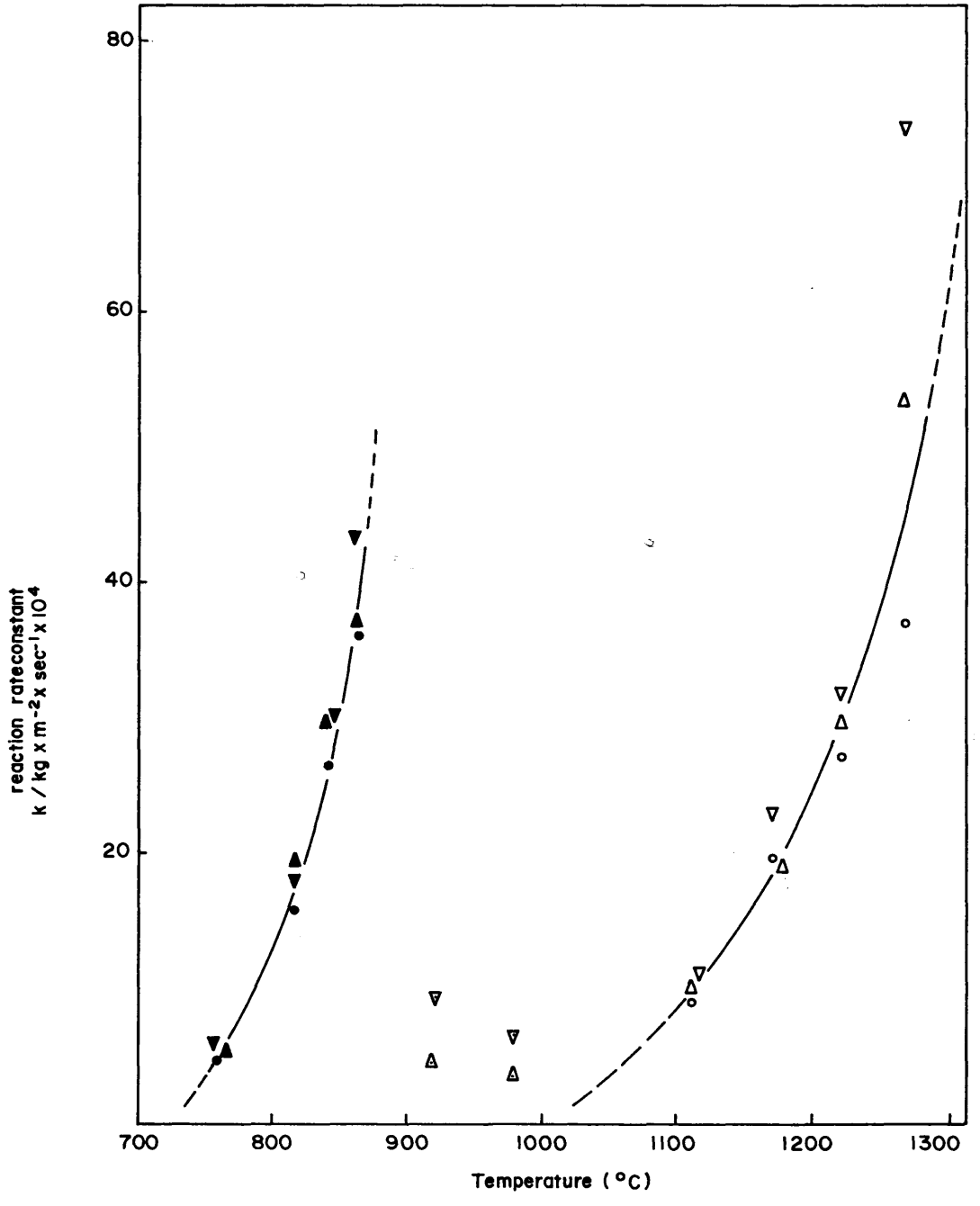
80
60
40
20
700
800
900
1000
1100
1200
1300
reaction rateconstant
k / kg x m⁻² x sec⁻¹ x 10⁴
Temperature (°C)

80
60
40
20
700
800
900
1000
1100
1200
1300
Temperature (°C)
reaction rate constant
k \ kg x m x sec.-1 x s-1 x 10 4

FIG. 4.1.2.5 - application of Arrhenius equation 4.1.2.1 to experimental results of reaction between liquid pure aluminium and vitreous silica for activation energy E/kJ x mol^{-1}/determination

experimental temperature range /°C /	silica rod diameter /mm/	activation energy E / kJ x mol^{-1} /
760 - 860	● 3.0	202.61
	▲ 5.0	199.44
	▼ 10.0	200.64
920 - 980	▲ 5.0	43.15
	▽ 10.0	83.90
1110 - 1265	O 3.0	156.49
	Δ 5.0	186.85
	▽ 10.0	200.48

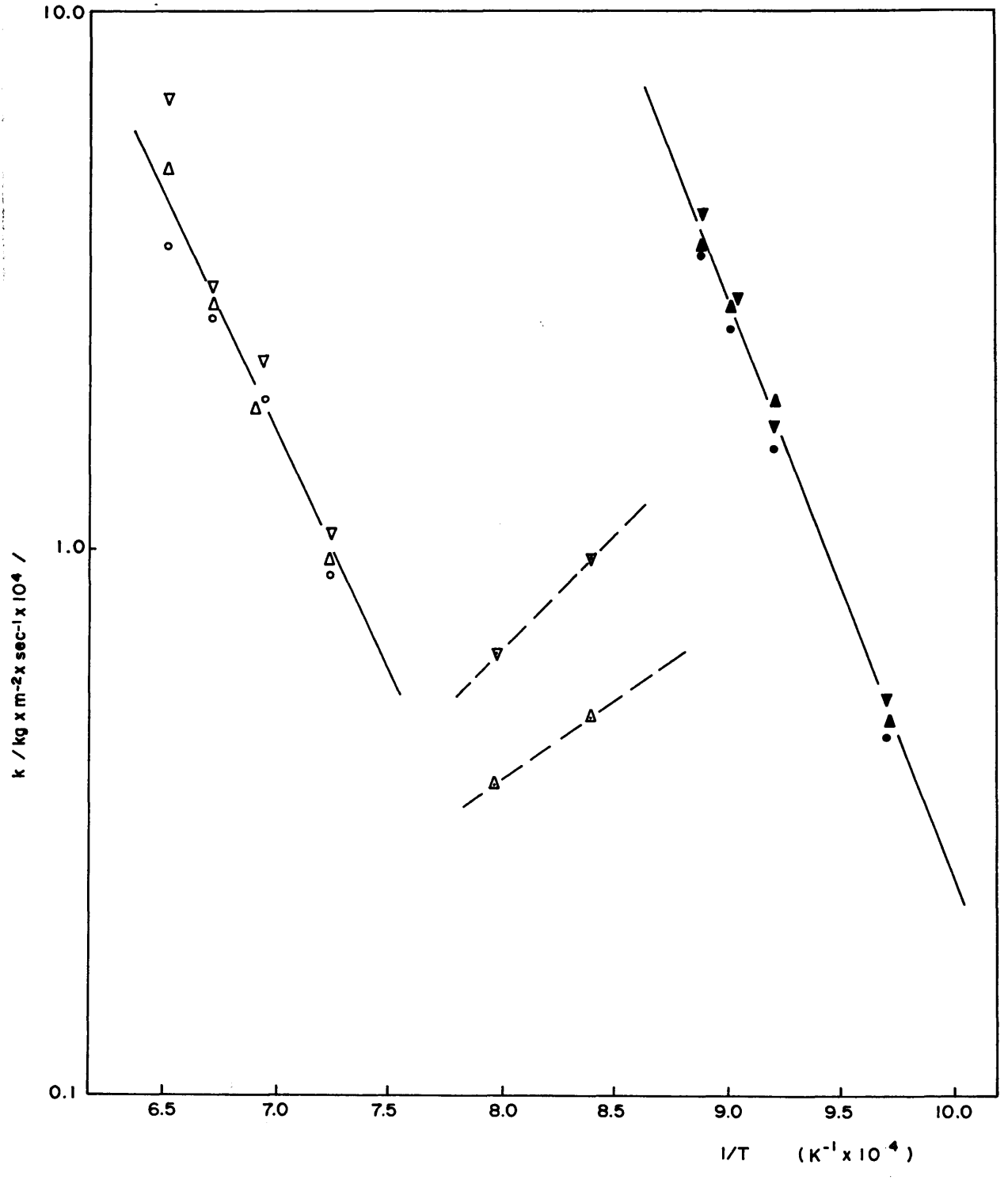
10.0
1.0
0.1
k / kg x m-2x sec-1 x 104 /
6.5
7.0
7.5
8.0
8.5
9.0
9.5
10.0
1/T (K-1 x 10-4)

0.01
0.1
1.0
1.0
9.5
9.0
8.5
8.0
7.5
7.0
6.5
1/T (K⁻¹ x 10⁴)
K (Kg x m⁻³ x sec⁻¹ x 10⁴)

FIG. 4.1.2.6 - correlation between rate of reaction and the reciprocal diameter of the silica rods, according to equation 4.1.1.1.

(a) temperature range: 760 - 860°C

(b) temperature range: 1110 - 1265°C

(see next page)

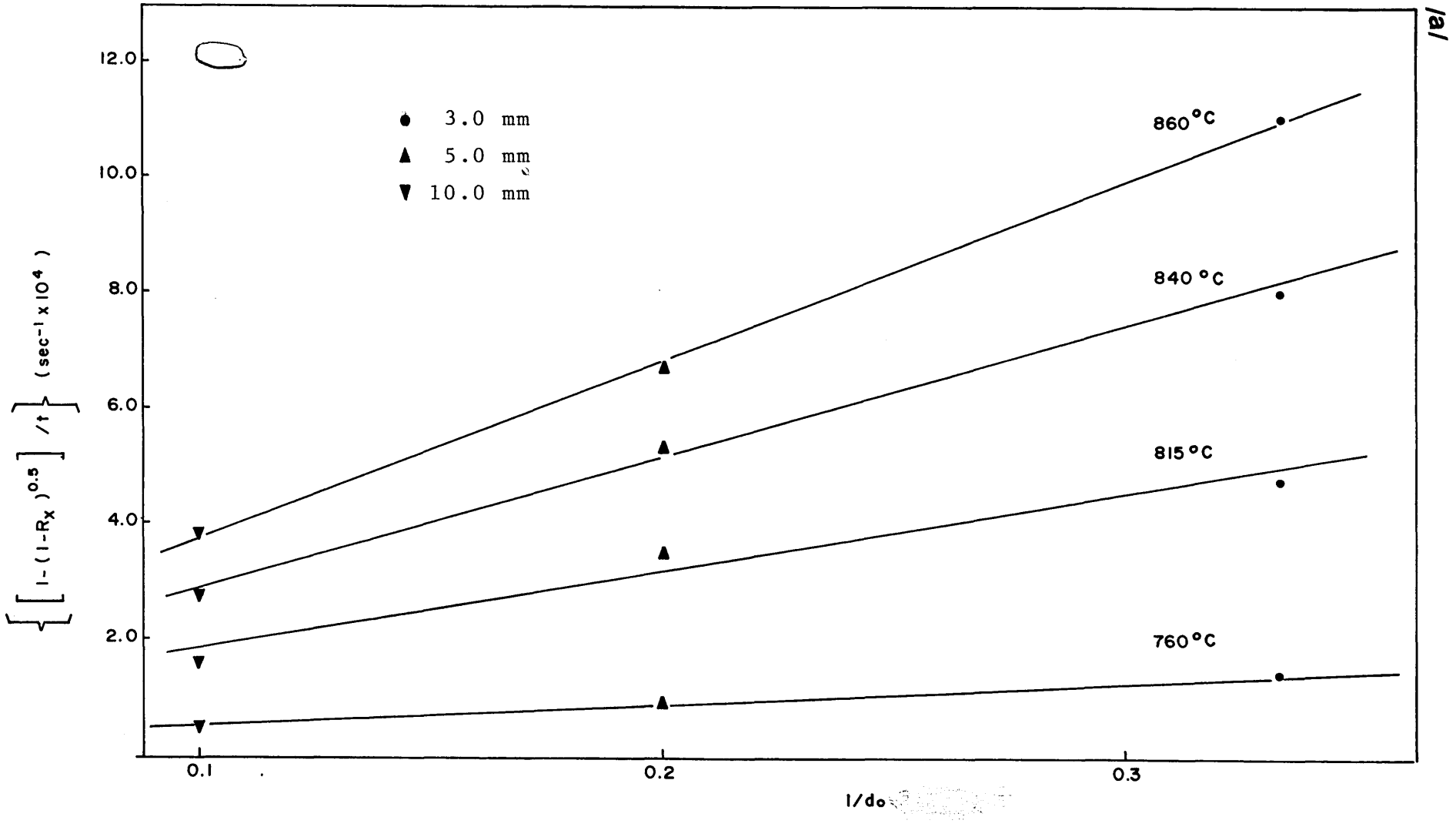
12.0
10.0
8.0
6.0
4.0
2.0
0.1
0.2
0.3
1/do
3.0 mm
5.0 mm
10.0 mm
860°C
840°C
815°C
760°C
[1-(1-Rx)^0.5]/t (sec^-1 x 10^4)

(a)
0.01 mm
0.2 mm
3.0 mm
25.0°C
18.2°C
10.4°C
3.8°C
0.5
1.0
1.5
2.0
2.5
3.0
$10^4 \times (sec^{-1})$
$\left\{ \frac{1}{2.0} \left[(1-R_x)^{-1} - 1 \right] \right\}$

(a)

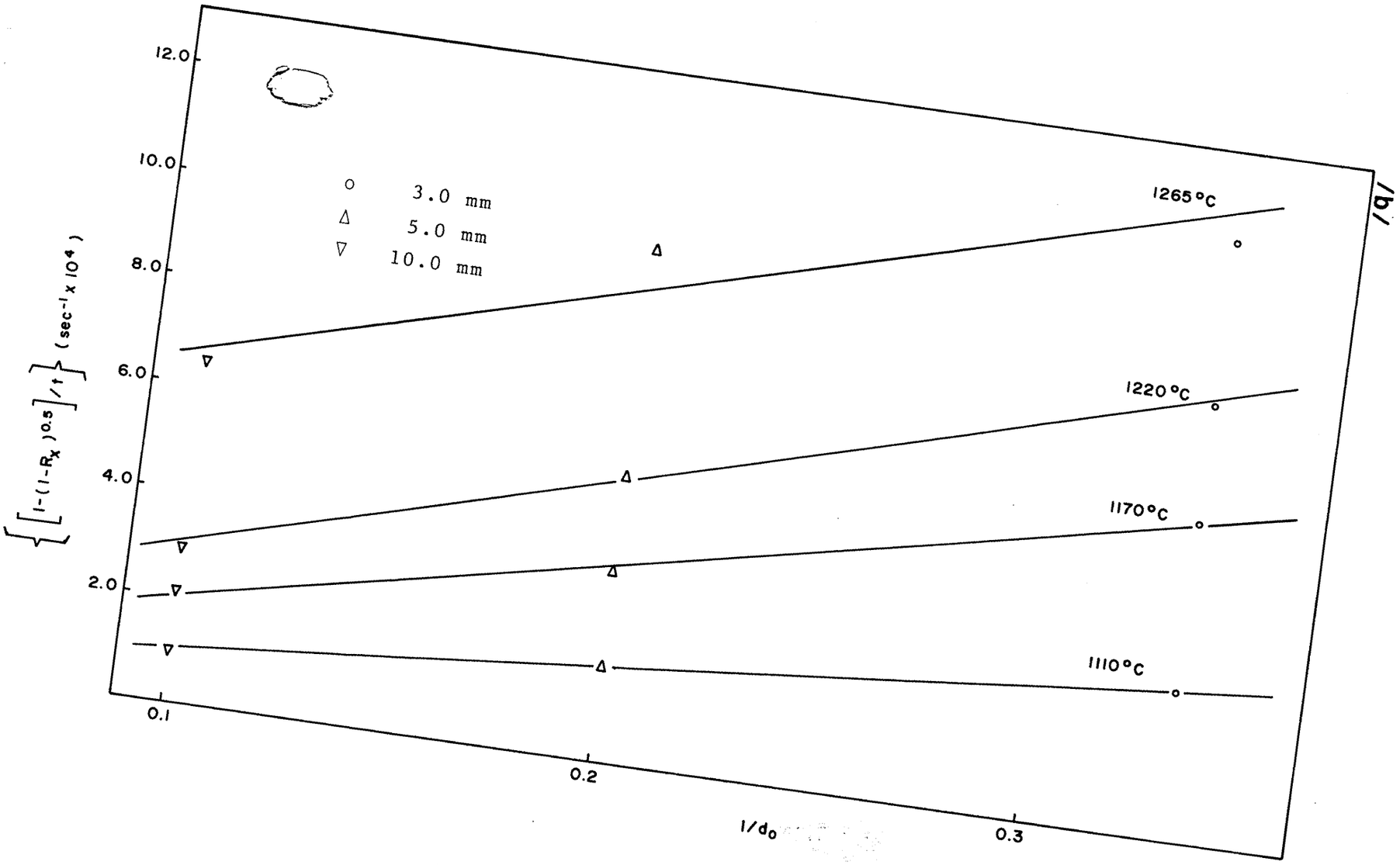
12.0
10.0
8.0
6.0
4.0
2.0
0.1
0.2
0.3
$1/d_o$
$\left\{\left[\left[1-(1-R_x)^{0.5}\right]/t\right\}$ (sec^{-1} x 10^4)
○ 3.0 mm
△ 5.0 mm
▽ 10.0 mm
1265 °C
1220 °C
1170 °C
1110 °C
/g/

1.0
0.5
0.3
1150°C
1200°C
1250°C
1300°C
10.0 mm
2.0 mm
0.3 mm
(d)

FIG. 4.1.3 - reaction between liquid aluminium - silicon alloys and vitreous silica at different temperatures varying from 1110 to 1265°C. Precentage of the product layer formed expressed as the left hand side of equation 4.1.1.1 versus time.

Original diameter of the silica rod=10.0mm

ATOMIC % SILICON	FIGURE	TEMPERATURE	REGRESSION LINE EQUATION (y = mx + c)	STANDARD DEVIATION
5.0	(a)	● 1110°C	0.58x - 1.71	3.29
		⊖ 1170°C	1.15x - 1.96	3.56
		⊘ 1220°C	1.69x - 1.46	5.42
		○ 1265°C	3.35x - 0.07	4.66
10.0	(b)	● 1110°C	0.59x - 4.75	2.05
		⊖ 1170°C	1.13x - 2.11	2.28
		⊘ 1220°C	1.55x + 2.17	3.76
		○ 1265°C	3.63x - 6.02	2.38
15.0	(c)	● 1170°C	0.59x - 8.61	4.83
		⊖ 1170°C	1.14x - 4.93	2.91
		⊘ 1220°C	1.73x - 4.43	2.86
		○ 1265°C	3.92x - 8.33	4.97

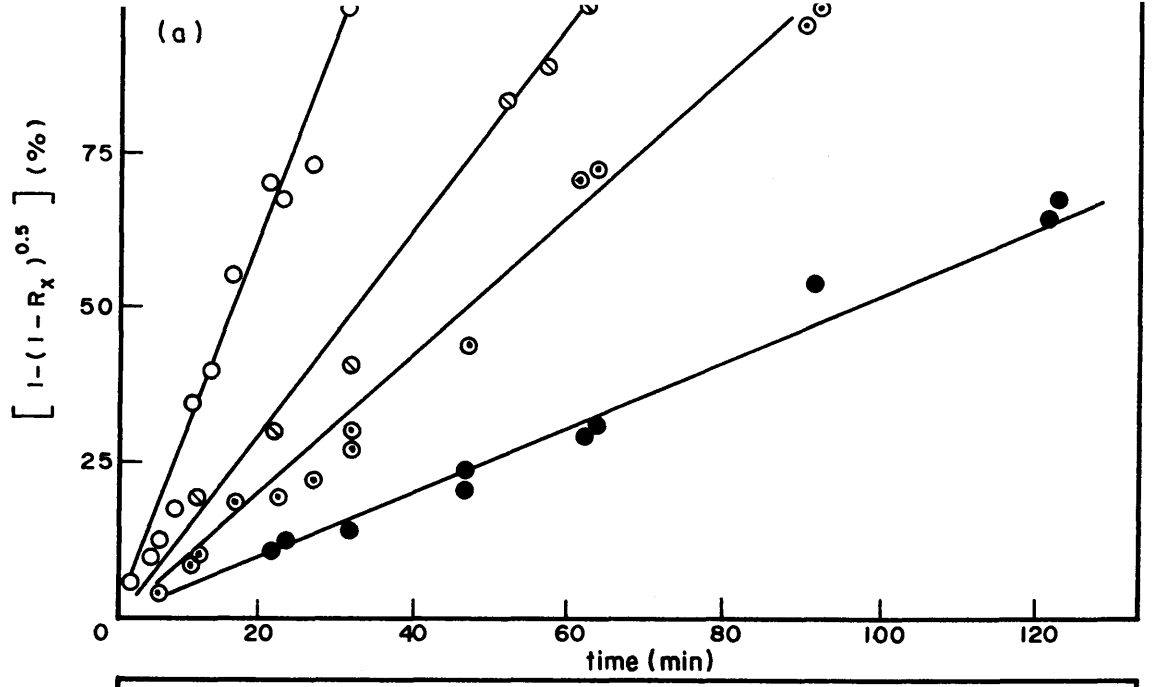
(a)
$[1-(1-R_x)^{0.5}]$ (%)
0
25
50
75
20
40
60
80
100
120
time (min)

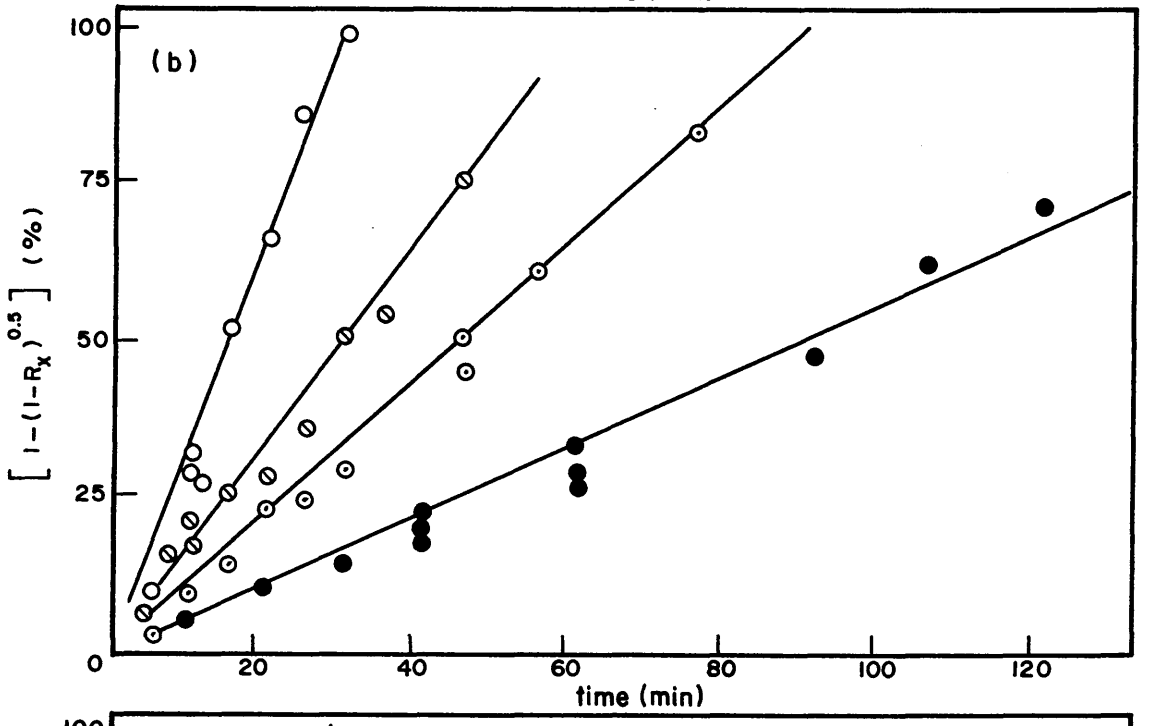
(b)
$[1-(1-R_x)^{0.5}]$ (%)
0
25
50
75
100
20
40
60
80
100
120
time (min)

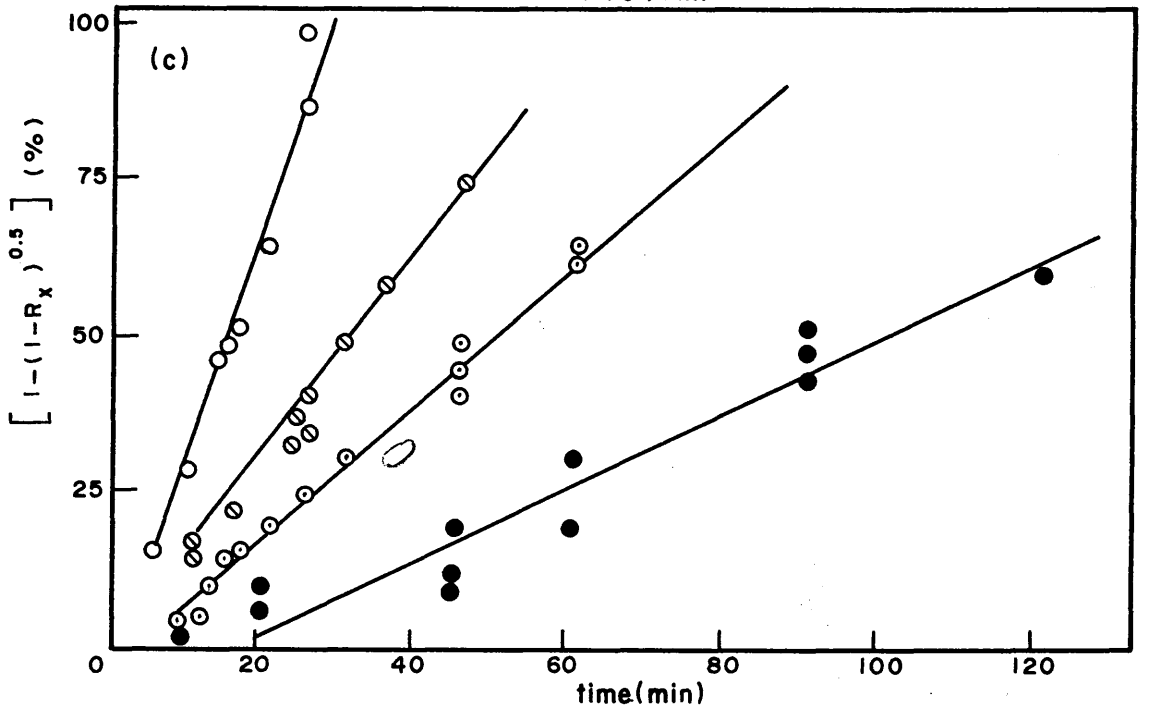
(c)
$[1-(1-R_x)^{0.5}]$ (%)
0
25
50
75
100
20
40
60
80
100
120
time (min)

(a)
(b)
(c)
time (min)
0
20
40
60
80
100
120
25
50
75
100

FIG. 4.1.4.1 - reaction between liquid aluminium - manganese alloys and vitreous silica at different temperatures varying from 1110 to 1265°C. Percentage of the product layer formed expressed as the left hand side of equation 4.1.1.1 versus time.

Original diameter of the silica rod=10.0mm

ATOMIC % MANGANESE	FIGURE	TEMPERATURE	REGRESSION LINE EQUATION (y = mx + c)	STANDARD DEVIATION (σ)
5.0	(a)	● 1110°C	0.51x - 6.89	2.51
		⊖ 1170°C	0.85x - 0.96	3.09
		⊗ 1220°C	1.61x + 1.58	3.45
		○ 1265°C	2.78x - 0.98	4.04
10.0	(b)	● 1110°C	0.18x - 0.76	2.22
		⊖ 1170°C	0.43x - 5.08	2.72
		⊗ 1220°C	0.70x - 3.37	3.70
		○ 1265°C	1.39x + 1.12	3.90
15.0	(c)	● 1110°C	0.06x - 2.07	3.09
		⊖ 1170°C	0.31x - 8.81	3.72
		⊗ 1220°C	0.57x - 8.13	4.18
		○ 1265°C	1.09x - 4.78	3.00

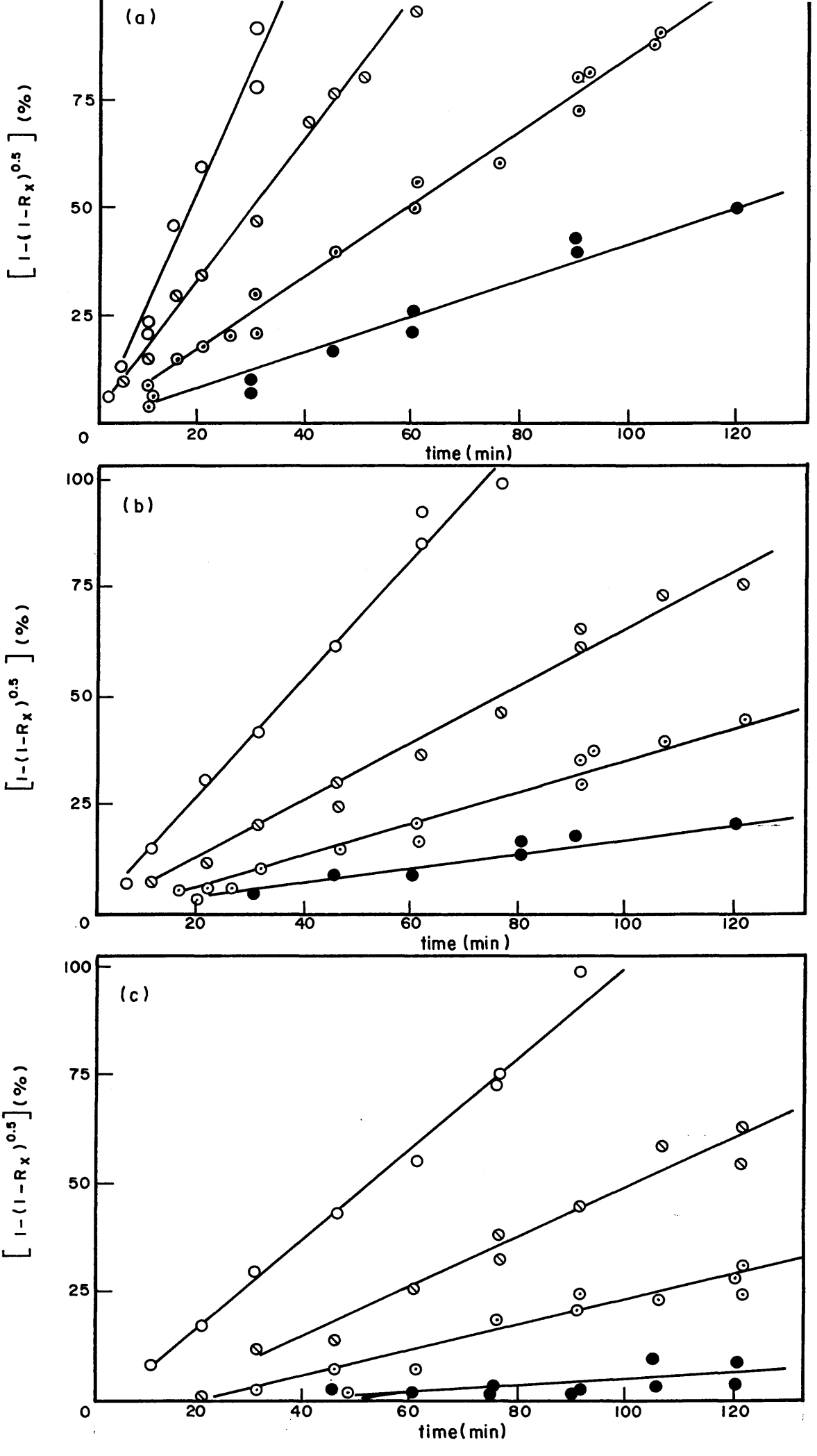
(a)
(b)
(c)
$[1-(1-R_x)^{0.5}]$ (%)
time (min)
0
20
40
60
80
100
120
25
50
75

(a)
(b)
(c)
time (min)
0
20
40
60
80
100
120
25
50
75
100
$[s_{2,0}(x_R-1)^{-1}]$ (%)

FIG. 4.1.4.2 - reaction between liquid aluminium - iron alloys and vitreous silica at different temperatures varying from 1110 to 1265°C. Percentage of the product layer formed expressed as the left hand side of equation 4.1.1.1 versus time.

Original diameter of the silica rod=10.0mm

ATOMIC % IRON	FIGURE	TEMPERATURE	REQUESSION LINE EQUATION ($y = mx + c$)	STANDARD DEVIATION (σ)
5.0	(a)	● 1110°C	0.52x - 7.22	3.64
		⊖ 1170°C	0.82x - 1.95	3.02
		⊗ 1220°C	1.68x - 1.51	2.95
		○ 1265°C	2.55x + 3.03	3.43
10.0	(b)	● 1110°C	0.18x - 3.02	1.96
		⊖ 1170°C	0.39x - 3.13	1.25
		⊗ 1220°C	0.71x - 3.95	2.63
		○ 1265°C	1.32x + 1.48	6.20
15.0	(c)	● 1110°C	0.04x - 2.03	1.52
		⊖ 1170°C	0.32x -14.61	3.31
		⊗ 1220°C	0.52x -14.96	3.85
		○ 1265°C	0.86x - 3.29	1.33

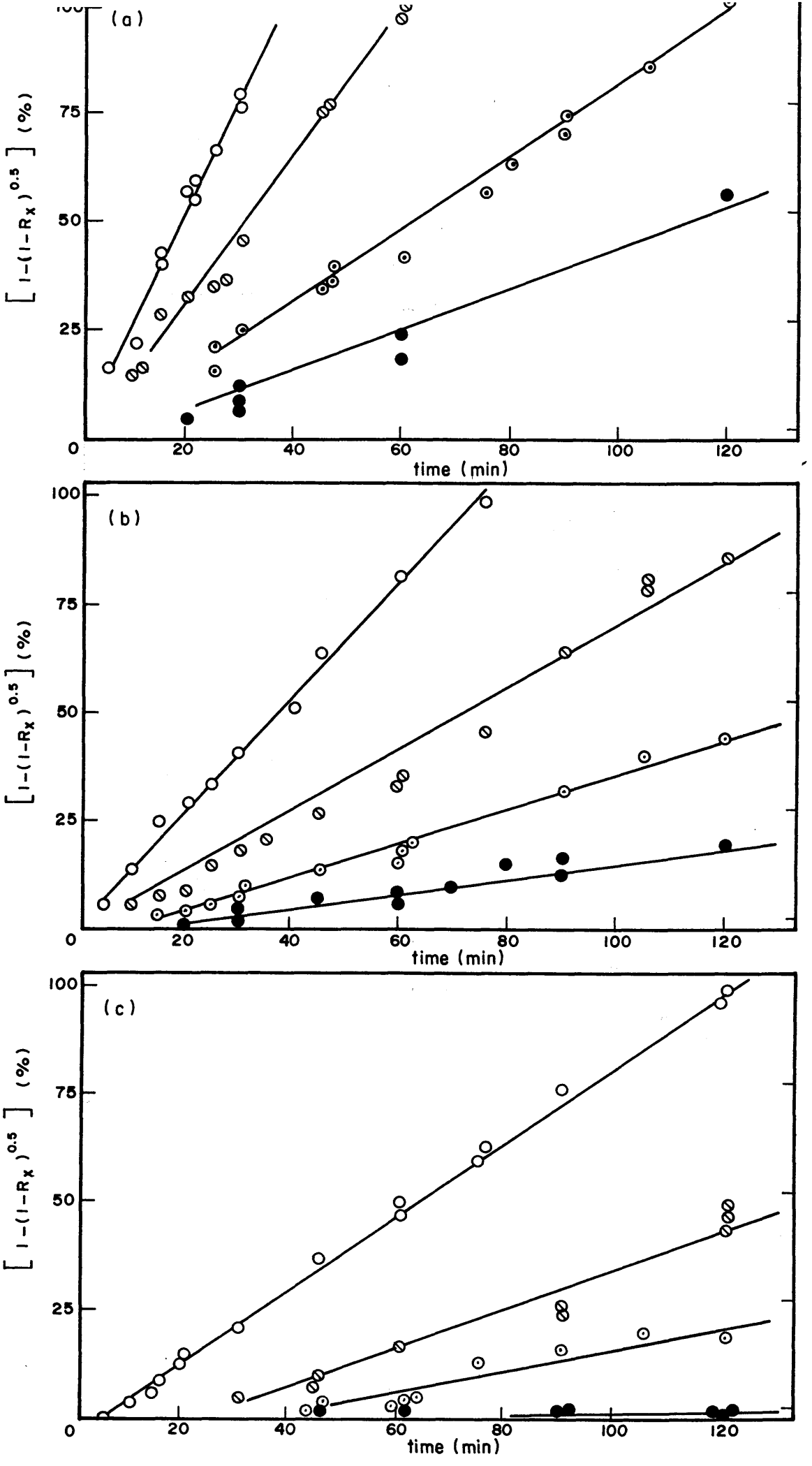
(a)
(b)
(c)
$[1-(1-R_x)^{0.5}]$ (%)
time (min)
0
25
50
75
100
20
40
60
80
100
120

(a)
(b)
(c)
time (min)
0
20
40
60
80
100
120
25
50
75
100
$[1-(1-x_B)^{-1}]$ (%)

FIG. 4.1.5. - reaction between liquid aluminium - silicon, manganese, iron alloys and vitreous silica: measured values of the reaction rate constant /k/ for different experimental contents of silicon, manganese and iron in the aluminium versus temperature.

(a) aluminium-silicon alloys:
- O 5 at % Si
- ⊘ 10 at % Si
- ⊙ 15 at % Si
- ● pure aluminium (reference plot)

(b) aluminium-manganese alloys:
- O 5 at % Mn
- ⊘ 10 at % Mn
- ⊙ 15 at % Mn

(c) aluminium-iron alloys:
- O 5 at % Fe
- ⊘ 10 at % Fe
- ⊙ 15 at % Fe

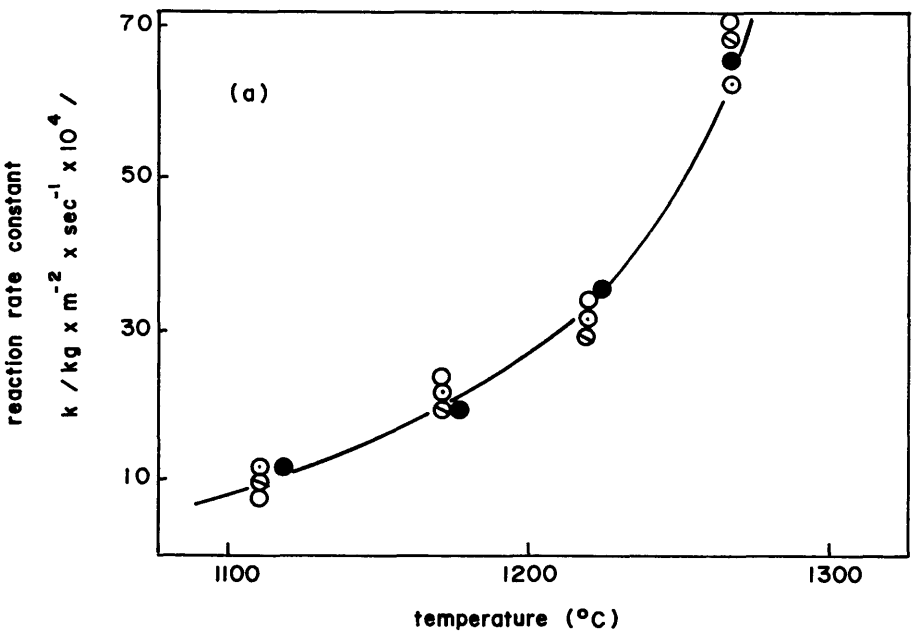
(a)
reaction rate constant
k / kg x m^{-2} x sec^{-1} x 10^{4} /
70
50
30
10
1100
1200
1300
temperature (°C)

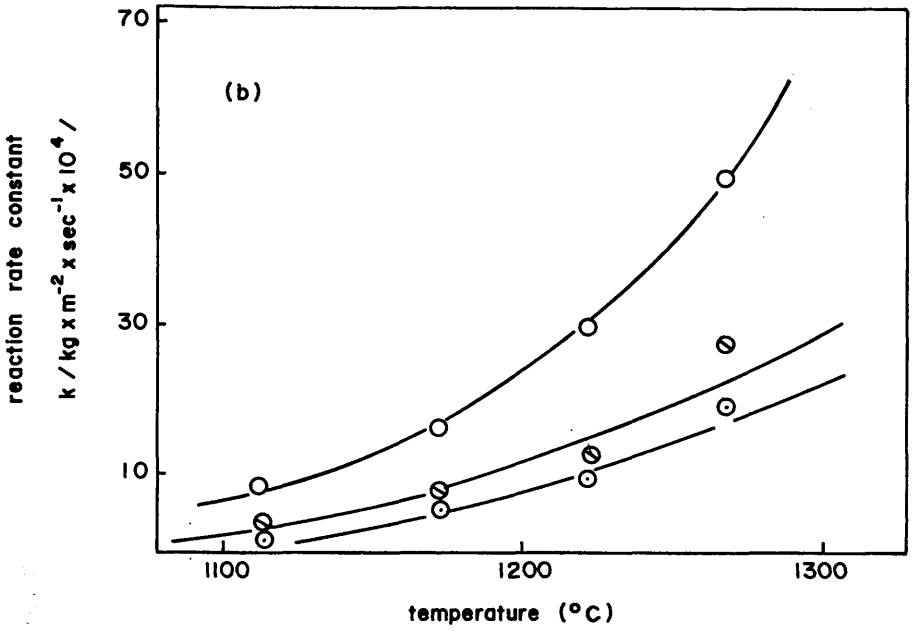
(b)
reaction rate constant
k / kg x m^{-2} x sec^{-1} x 10^{4} /
70
50
30
10
1100
1200
1300
temperature (°C)

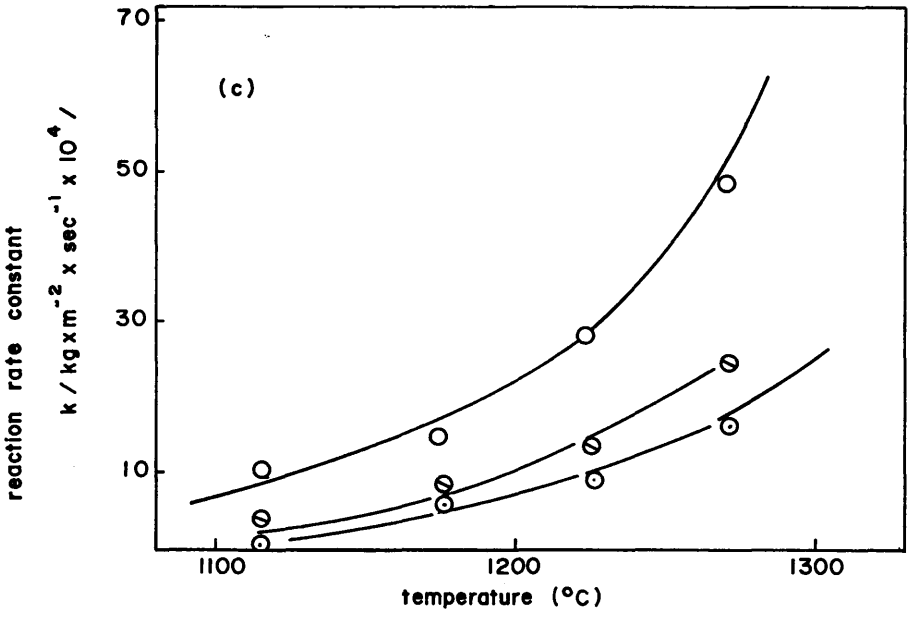
(c)
reaction rate constant
k / kg x m^{-2} x sec^{-1} x 10^{4} /
70
50
30
10
1100
1200
1300
temperature (°C)

(a)
(b)
(c)
reaction rate constant
K \ kg x m^-3 x sec^-1 x 10^4 \ K
temperature (°C)
1100
1200
1300
10
30
50
70

FIG. 4.1.6. - application of Arrhenius equation 4.1.2.1. to experimental results of reaction between liquid aluminium alloys with silicon, manganese, iron and vitreous silica for activation energy E/kJ x x mol^{-1}/determination.

Temperature range /°C/	element content /at%/		activation energy E/kJ x mol^{-1}/
1110-1265	Silicon: O —	5.0	188.90
	⊘ —	10.0	197.15
	⊙ —	15.0	201.61
	Manganese: Δ —	5.0	198.88
	▲ —	10.0	228.48
	▲ —	15.0	316.82
	Iron: ∇ —	5.0	182.01
	▽ —	10.0	223.64
	▽ —	15.0	339.39

Experiments under rotating conditions:
/average reaction rate constant values from different r.p.m. at temperatures/

x pure aluminium
\+ aluminium - 5 at%Mn
* aluminium - 5 at%Fe

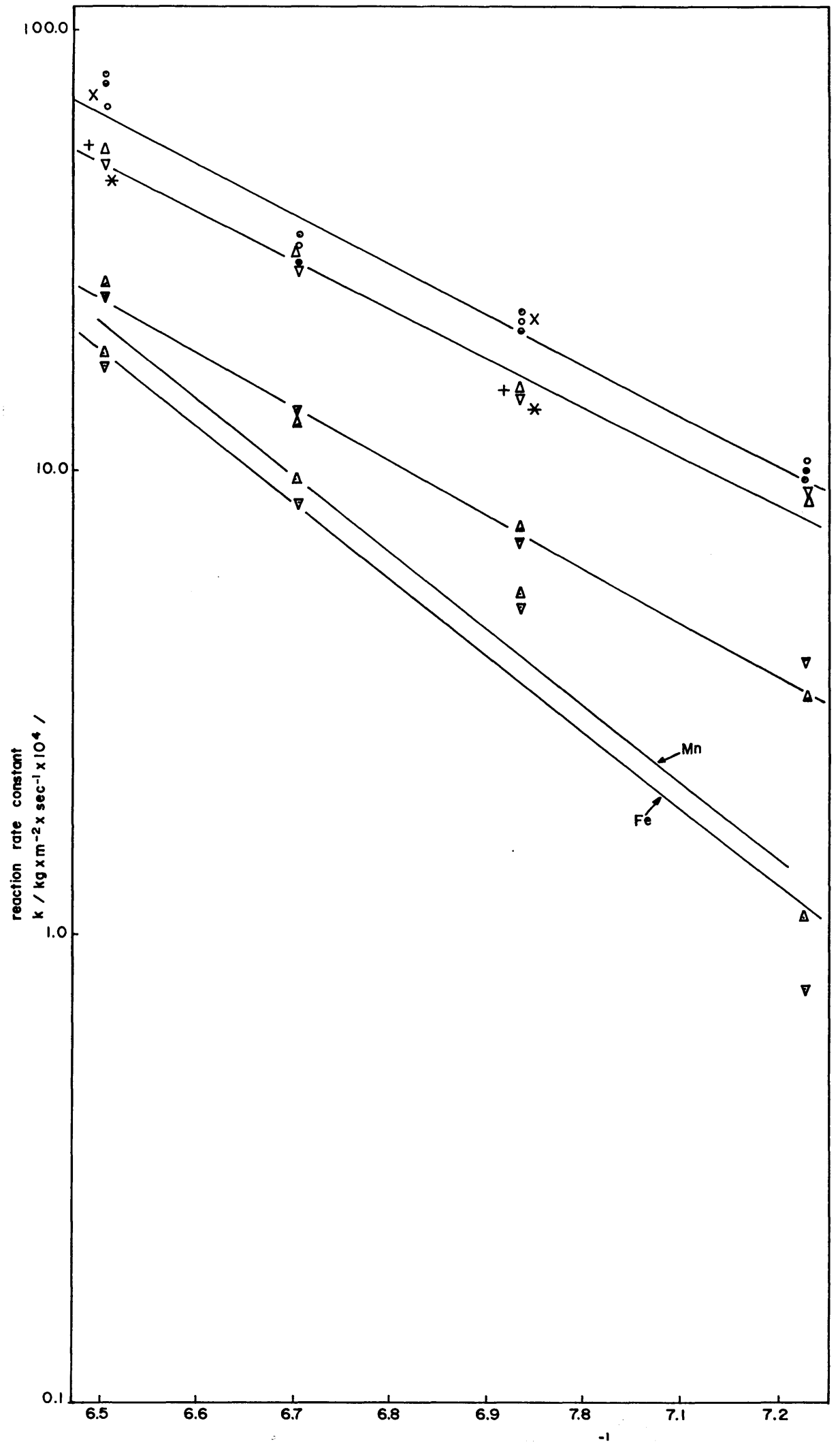
100.0
10.0
1.0
0.1
reaction rate constant
k / kg x m⁻² x sec⁻¹ x 10⁴ /
Mn
Fe
6.5
6.6
6.7
6.8
6.9
7.8
7.1
7.2
-1

Reaction rate constant
$k \times kg \times m^{-3} \times sec^{-1} \times 10^{+4}$

FIG. 4.1.7.a,b - reaction between liquid pure aluminium and vitreous silica carried out under rotating conditions of the silica rod. Percentage of the product layer formed expressed as the left hand side of equation 4.1.1.1. versus time.

Original diameter of the silica rod=10.0mm

RATATIONS PER MINUTE	FIGURE	TEMPERATURE	REQUESSION LINE EQUATION (y = mx + c)	STANDARD DEVIATION (σ)
0 5.0	(a)	1170°C	1.23x - 3.96	2.68
	(b)	1265°C	3.96x - 4.15	4.13
⊘ 15.0	(a)	1170°C	1.07x + 4.12	2.88
	(b)	1265°C	3.52x + 0.71	4.73
● 35.0	(a)	1170°C	1.24x - 4.01	2.58
	(b)	1265°C	3.59x + 1.61	1.95

reference plot for comparison: ⊘ static silica rod

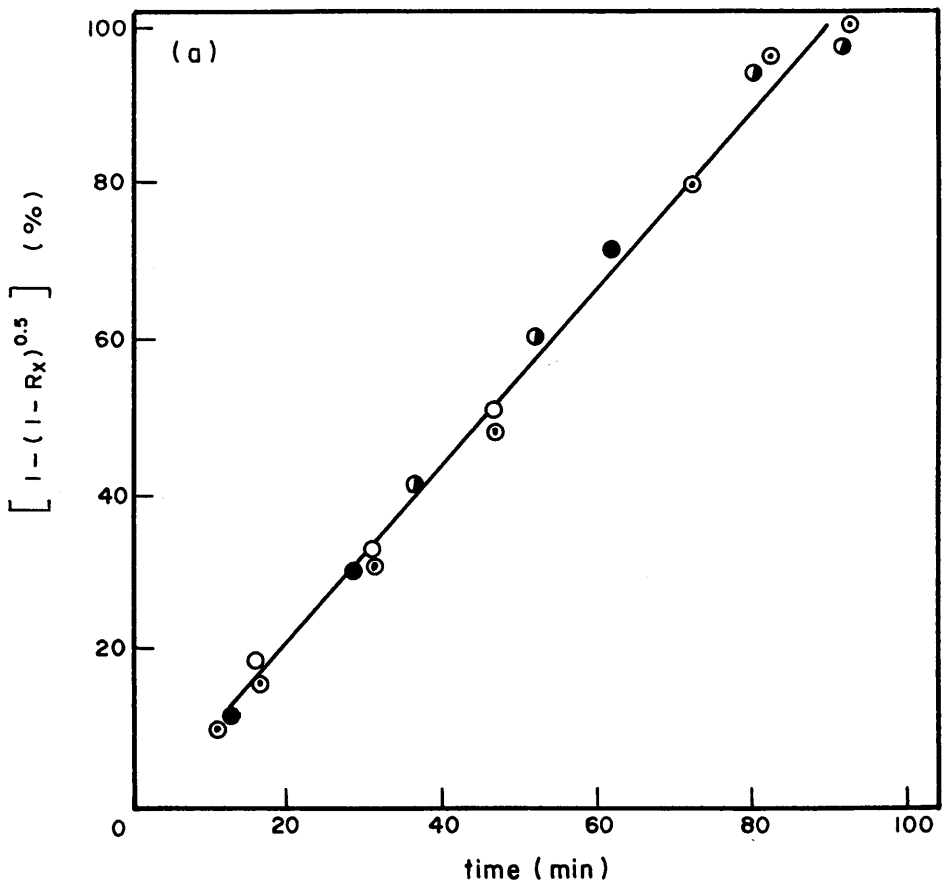
(a)
100
80
60
40
20
0
20
40
60
80
100
time (min)
[1-(1-Rx)^0.5] (%)

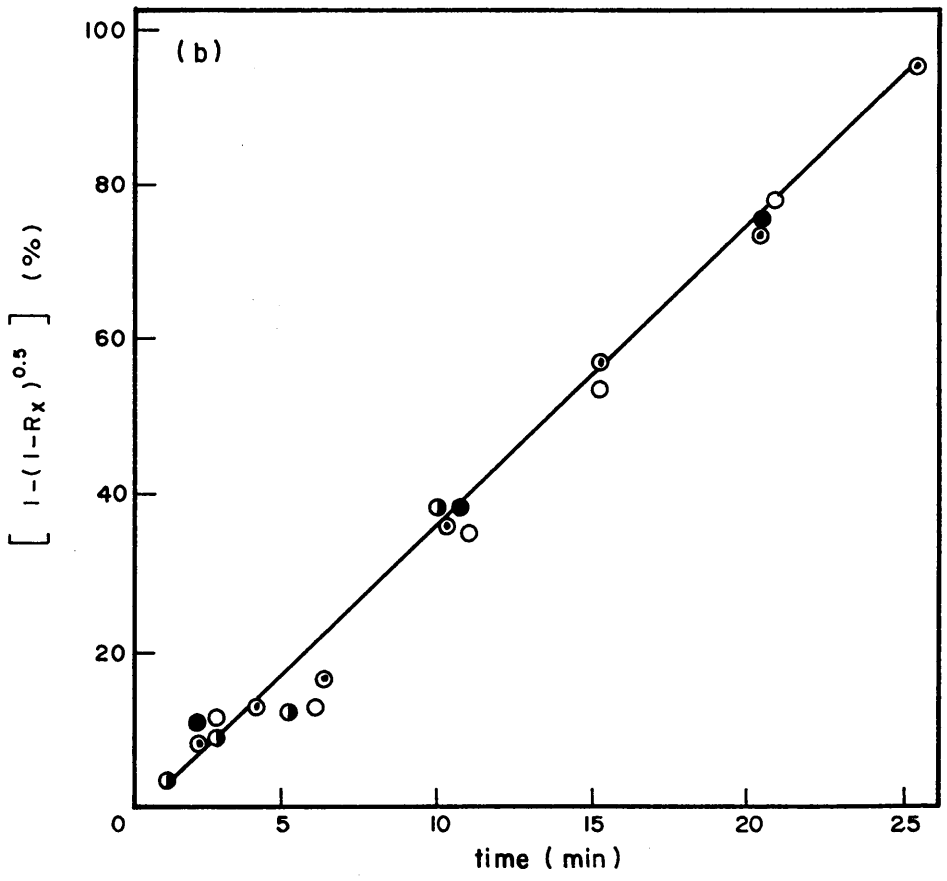
(b)
100
80
60
40
20
0
5
10
15
20
25
time (min)
[1-(1-Rx)^0.5] (%)

(a)
0
20
40
60
80
100
20
40
60
80
100
time (min)
$[2.0(xR-1)-1]^{-1}$ (%)

(b)
0
20
40
60
80
100
5
10
15
20
25
time (min)
$[2.0(xR-1)-1]^{-1}$ (%)

FIG. 4.1.7.c,d - reaction between liquid aluminium - manganese alloy and vitreous silica carried out under rotating conditions of the silica rod. Percentage of the left hand side of equation 4.1.1.1. versus time.

Maganese content = 5 at %

RATATIONS PER MINUTE	FIGURE	TEMPERATURE	REQUESSION LINE EQUATION (y = mx + c)	STANDARD DEVIATION (σ)
0 5.0	(c)	1170°C	0.88x - 3.26	0.77
	(d)	1265°C	2.69x + 2.17	3.09
◐ 15.0	(c)	1170°C	0.83x - 0.74	2.90
	(d)	1265°C	2.78x + 1.76	3.35
● 35.0	(c)	1170°C	0.83x - 0.74	2.17
	(d)	1265°C	2.85x - 0.93	3.00

reference plot for comparison:

⊙ static silica rod in Al-5.0 at % Mn

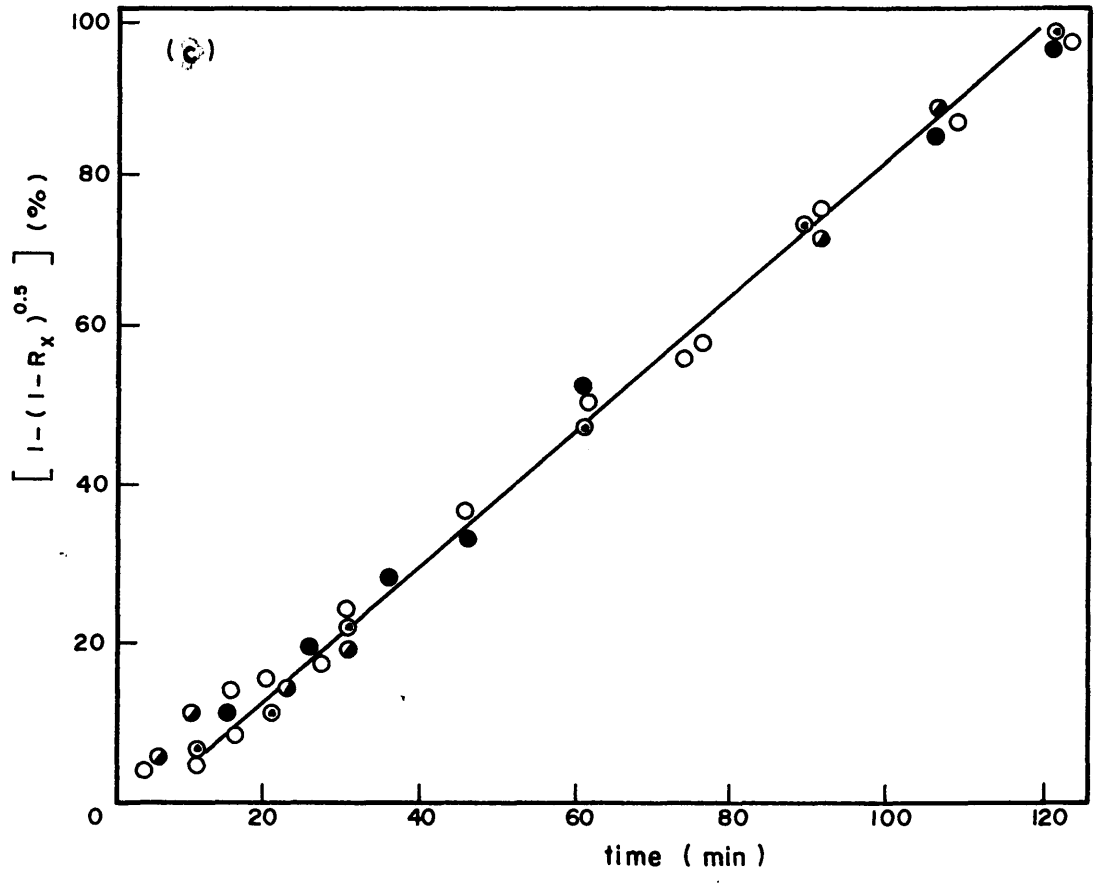
(c)
$[1-(1-R_x)^{0.5}]$ (%)
time (min)
0
20
40
60
80
100
120

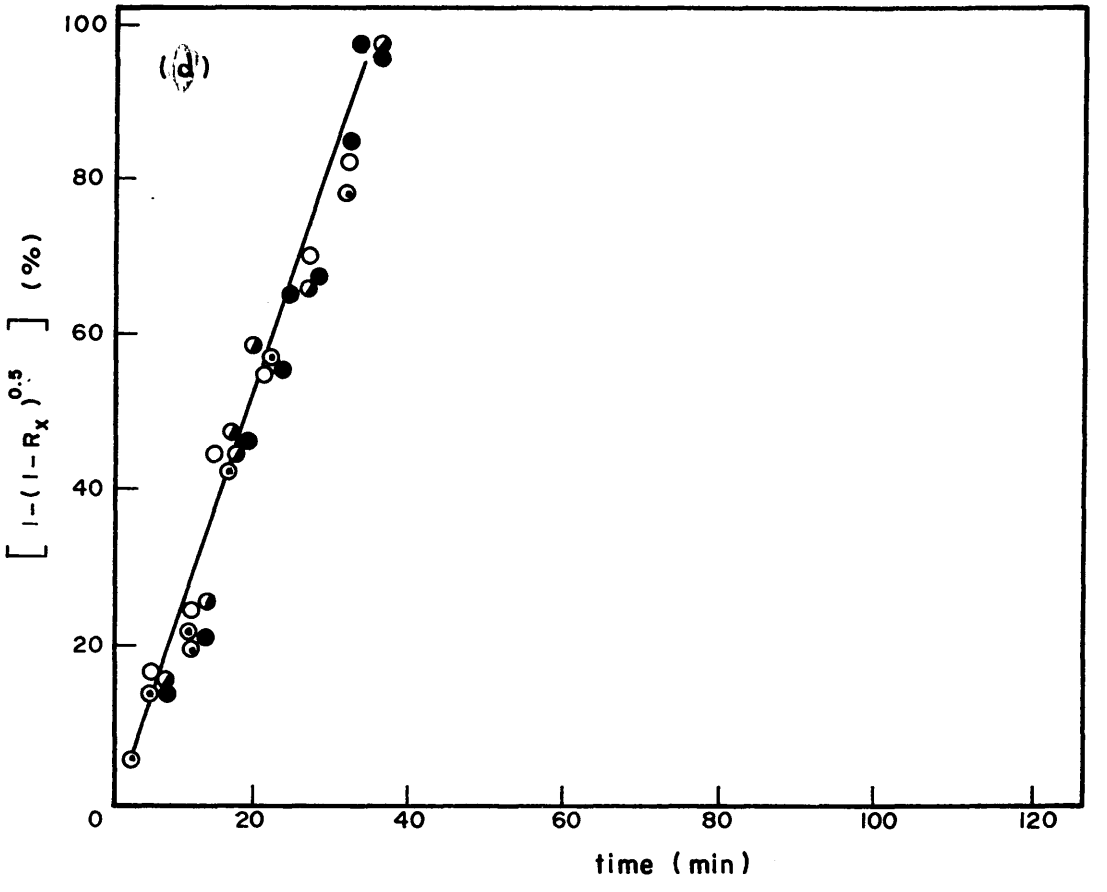
(d)
$[1-(1-R_x)^{0.5}]$ (%)
time (min)
0
20
40
60
80
100
120

(c)
0
20
40
60
80
100
120
time (min)
$[1-(1-R^X)^{0.5}]$ (%)

(d)
0
20
40
60
80
100
120
time (min)
$[1-(1-R^X)^{0.5}]$ (%)

FIG. 4.1.7.e,f - reaction between liquid aluminium-iron alloy and vitreous silica carried out under rotating conditions of the silica rod. Percentage of the product layer formed expressed as the left hand side of equation 4.1.1.1. versus time.

Iron content = 5 at %

RORATIONS PER MINUTE	FIGURE	TEMPERATURE	REGRESSION LINE EQUATION (y = mx + c)	STANDARD DEVIATION
0 5.0	(e)	1170°C	0.80x + 2.11	1.69
	(f)	1265°C	2.29x + 3.44	5.44
◐ 15.0	(e)	1170°C	0.81x + 0.04	2.44
	(f)	1265°C	2.55x - 0.38	3.57
● 35.0	(e)	1170°C	0.82x + 0.21	2.64
	(f)	1265°C	2.47x + 2.80	2.07

reference plot for comparison:

⊙ static silica rod in Al-5.0 at % Fe

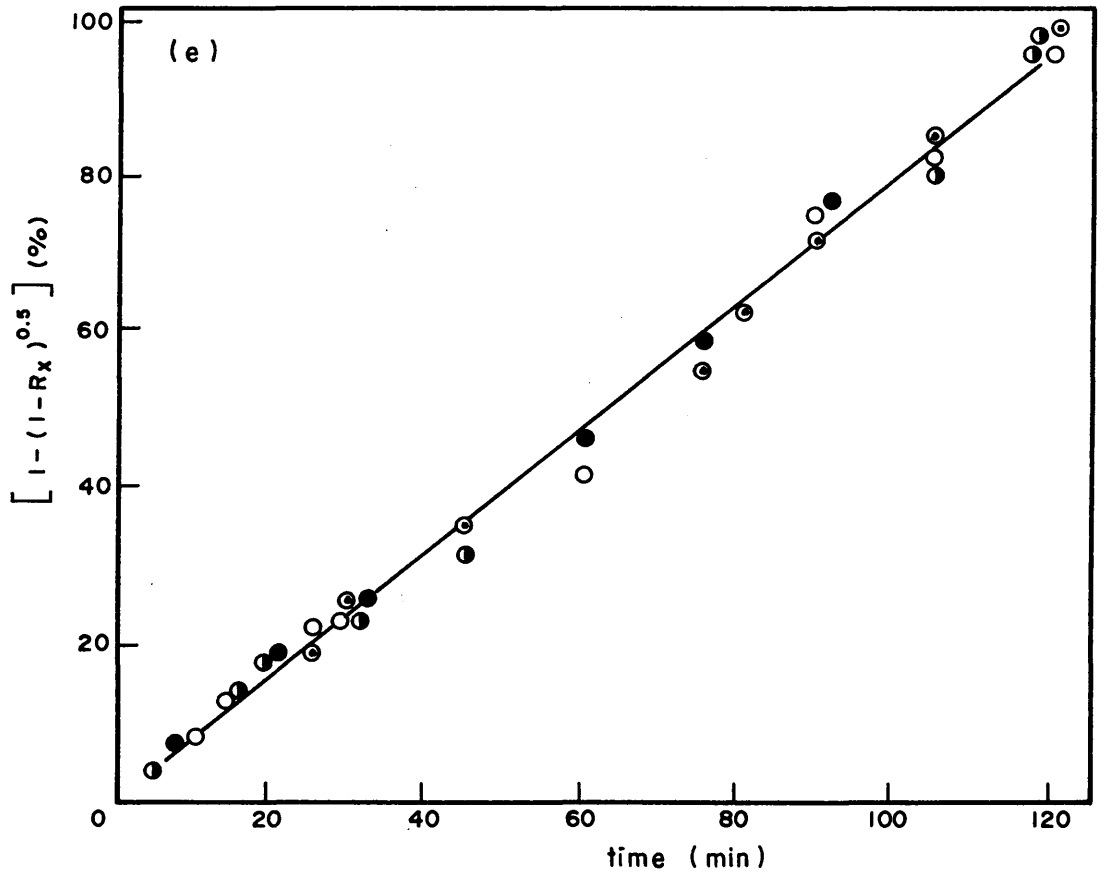
(e)
100
80
60
40
20
0
20
40
60
80
100
120
time (min)
[1-(1-Rx)^0.5] (%)

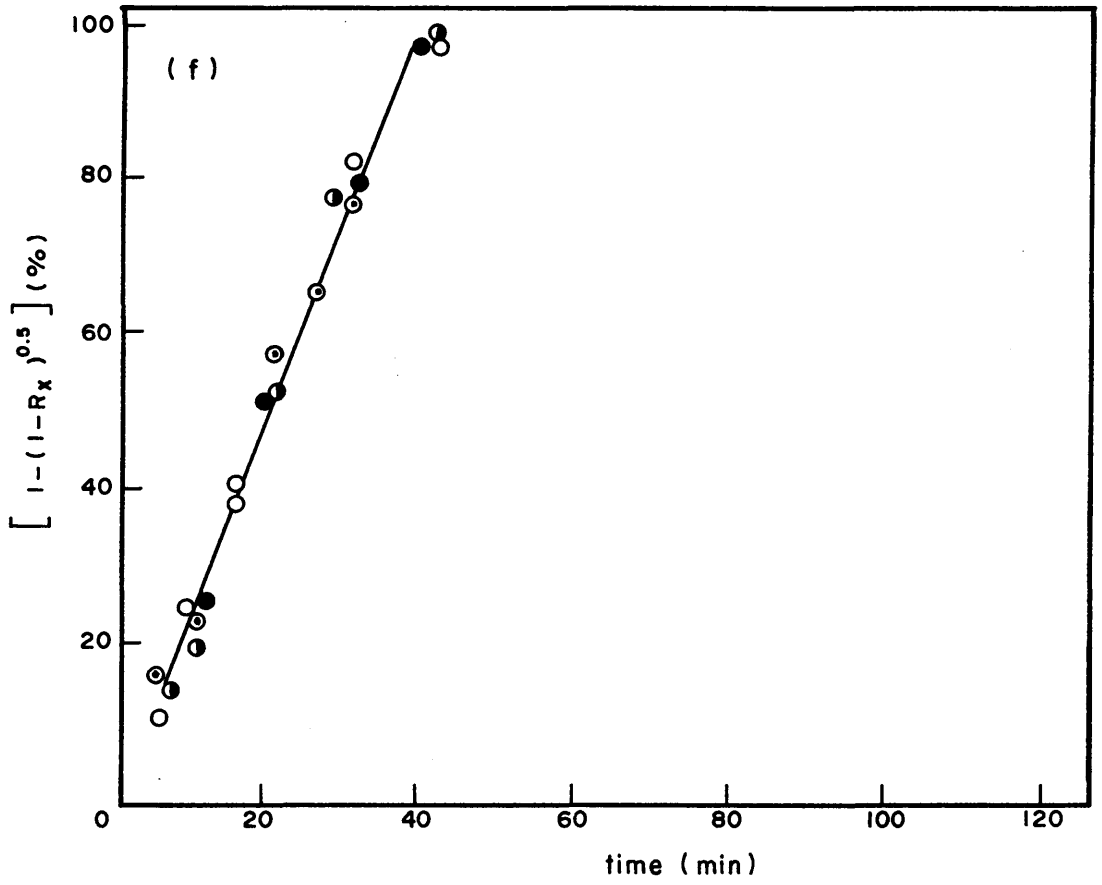
(f)
100
80
60
40
20
0
20
40
60
80
100
120
time (min)
[1-(1-Rx)^0.5] (%)

(a)
0
20
40
60
80
100
120
time (min)
$[1-(1-B^x)^{1/3}]$ (%)

(b)
0
20
40
60
80
100
120
time (min)
$[1-(1-B^x)^{1/3}]$ (%)

Fig. 4.3.1.1. Symmetric growth of product layer with increasing time of reaction at 860°C.

Specimen: 5.0 mm. in diameter.

Time: (a) - 2 minutes
(b) - 5 minutes
(c) - 20 minutes
(d) - 30 minutes

x 8 approximately

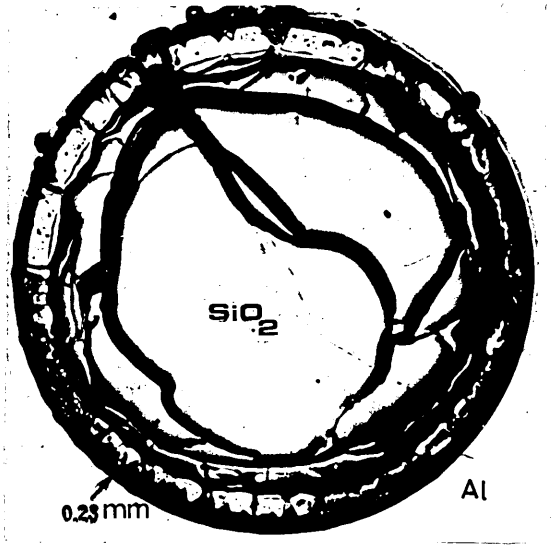

(a)/ 2 min

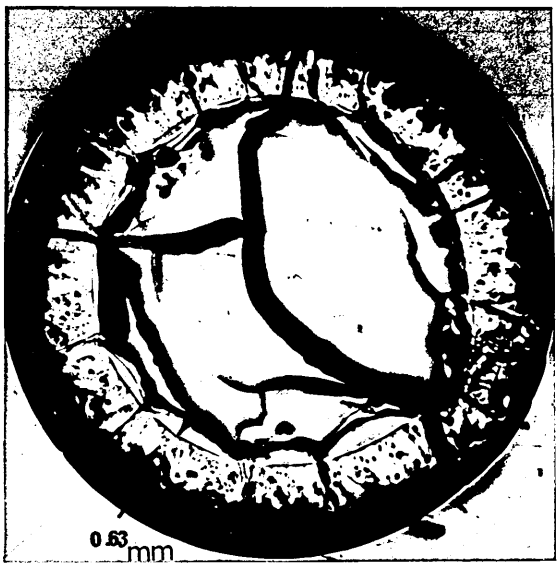

(b)/ 5 min

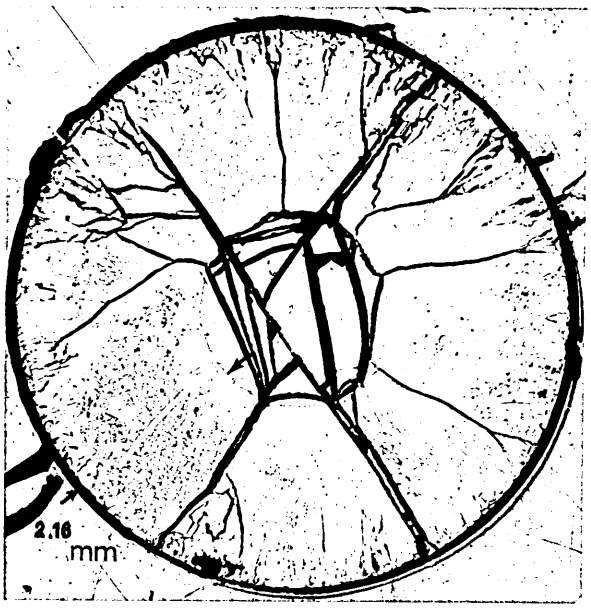

(c)/ 20 min

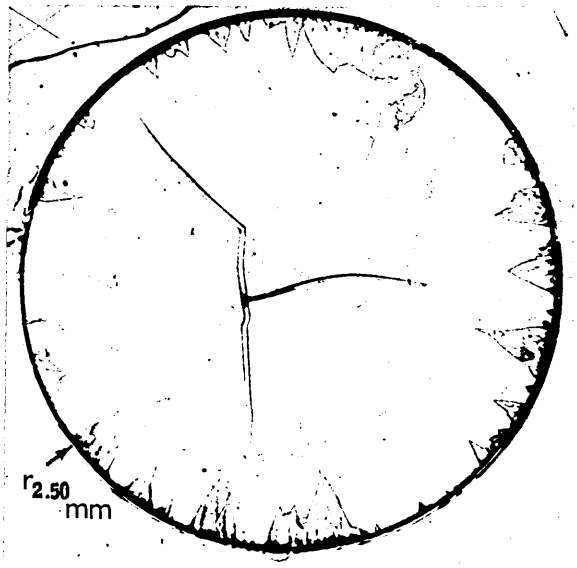

(d)/ 30min

Fig. 4.3.1.2. Spherical segments of product phases nucleated at first contact of silica with liquid aluminium

Specimen: 10 mm. in diameter.

temperature: 815°C; time: 2 minutes

Fig. 4.3.1.3. Example of delayed reaction from some portion of the silica surface, possibly as a result of adhesion of the melt surface film of aluminium oxide.

Fig. 4.3.1.4. Lateral growth of spherical segments.

Specimen: 10 mm. in diameter

temperature: 815°C; time: 5 minutes.

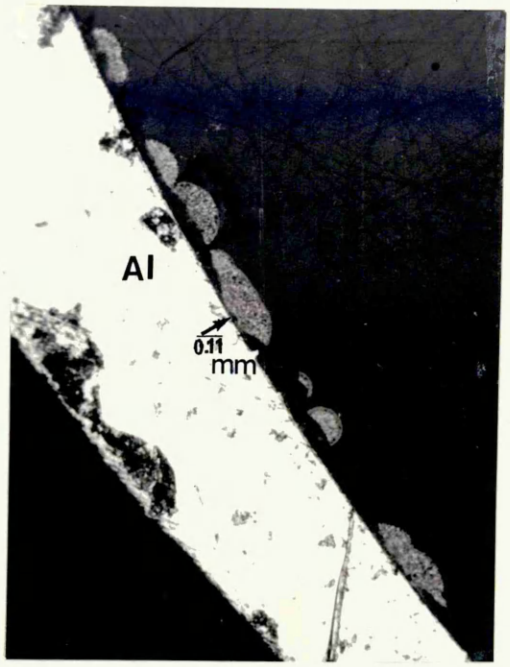

SiO_2

Al

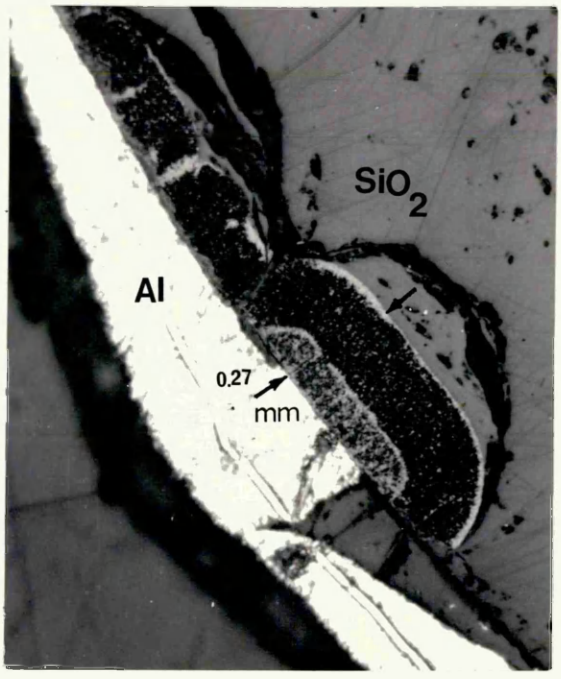

Fig. 4.3.1.5. Continuous layer of reaction products. Note Al-rich phase segregated on boundaries of individual large grains.

Specimen: 10 mm. in diameter.

temperature: 815°C; time: 15 minutes.

Fig. 4.3.1.6. Continuous layer of reaction products formed very rapidly.

Specimen: 3.0 mm. in diameter.

temperature: 860°C; time: 2 minutes.

Etched in etchant A - (Table 3.5) for ~1 minute.

Fig. 4.3.1.7. Large grains of recrystallized alumina with radially orientated Al-rich dendritic pools. Evidence of aluminium filled cracks without recrystallization of the alumina in near vicinity.

Specimen: 5.0 mm. in diameter.

temperature: 815°C; time: 30 minutes.

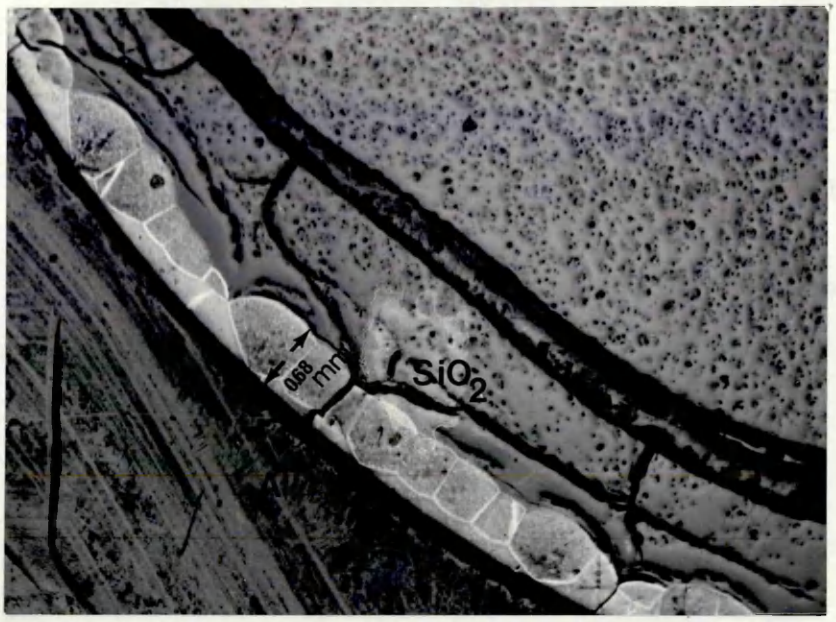
0.68 mm
SiO_2

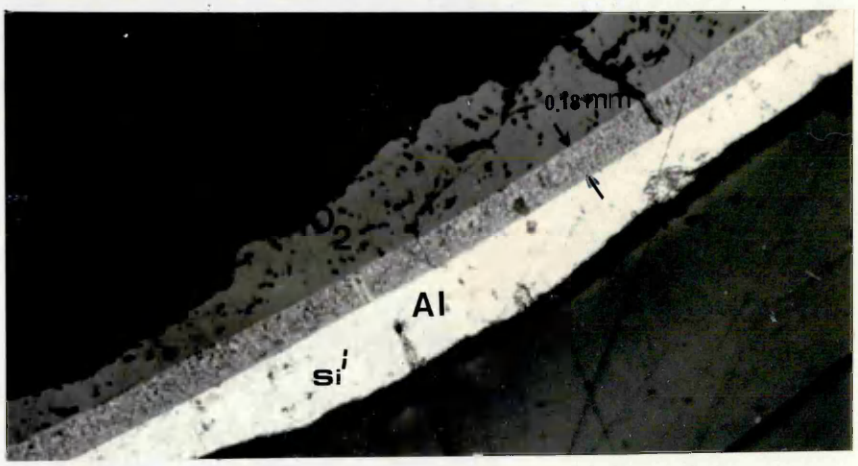
0.18 mm
Al
Si


1.55 mm

Fig. 4.3.1.8, a-c. Scanning electron micrograph of different fractured specimens showing columnar cells of alumina. Penetration of aluminium is in the arrowed direction. In some areas (b) the metal had peeled off, probably due to lack of bonding (wetting) at the oxide/metal interface.

Specimens: (a) 3.0 mm. in diameter.
temperature: 840°C;
time: 10 minutes MAG. 1250x.

(b) 5.0 mm. in diameter.
temperature: 840°C;
time: 10 minutes MAG. 1250x.

(c) 10 mm. in diameter.
temperature: 840°C
time: 10 minutes MAG.800x.

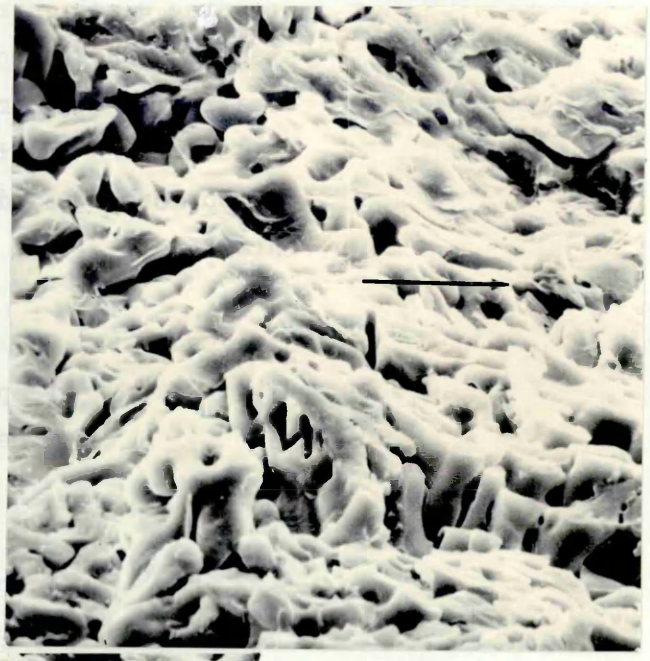

a.

b.

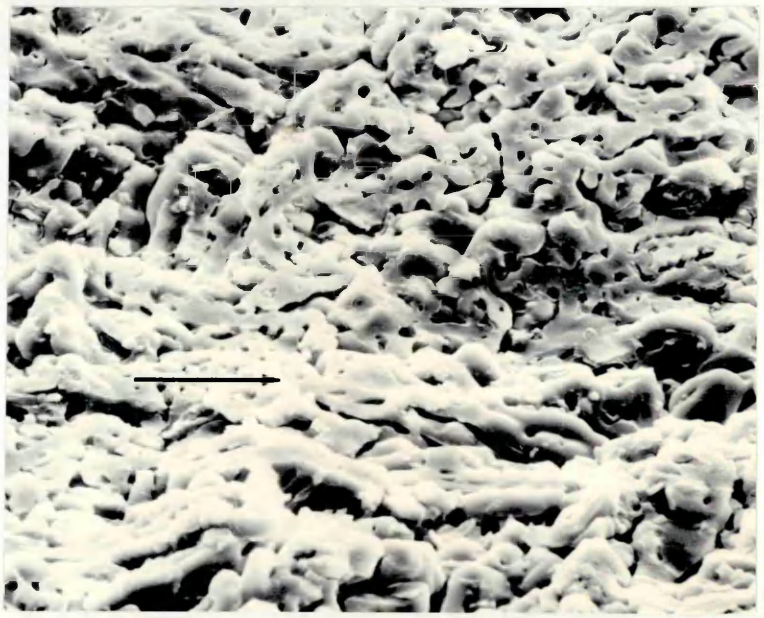

c.

Fig.4.3.1.9. Cracking during reaction. Large radial recrystallization with shrinkage and associated porosity.

Specimen: 3.0 mm. in diameter.

temperature: 8 15^{o}C;

time: 25 minutes MAG. 50x.

Fig.4.3.1.10 Non-symmetric interface of unreacted silica/product layer caused by cracks occurring during reaction (arrowed). Penetration of aluminium is prevented from access to complete the reaction symmetrically.

Specimen: 5.0 mm. in diameter.

temperature: 840^{o}C;

time: 25 minutes MAG. 80x

Etched for 2 minutes in etchant A - Table 3.5.

Fig.4.3.1.11. The porous interaction front formed at silica surface. Aluminium penetrates readily to the silica surface through this front.

Specimen: 10 mm. in diameter.

temperature: 840^{o}C;

time: 20 minutes MAG. 120x.

Etched for 3 minutes in etchant B - Table 3.5.


SiO2
1.08
mm

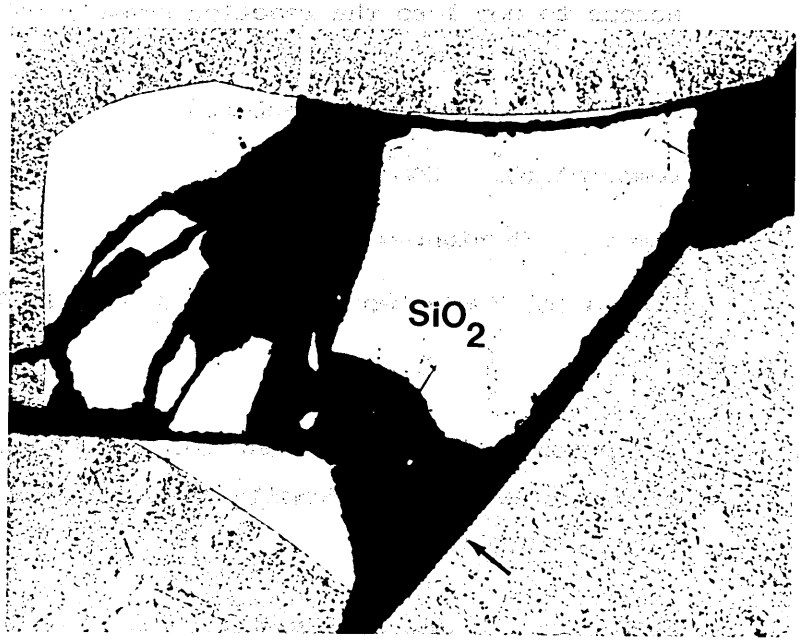
SiO2

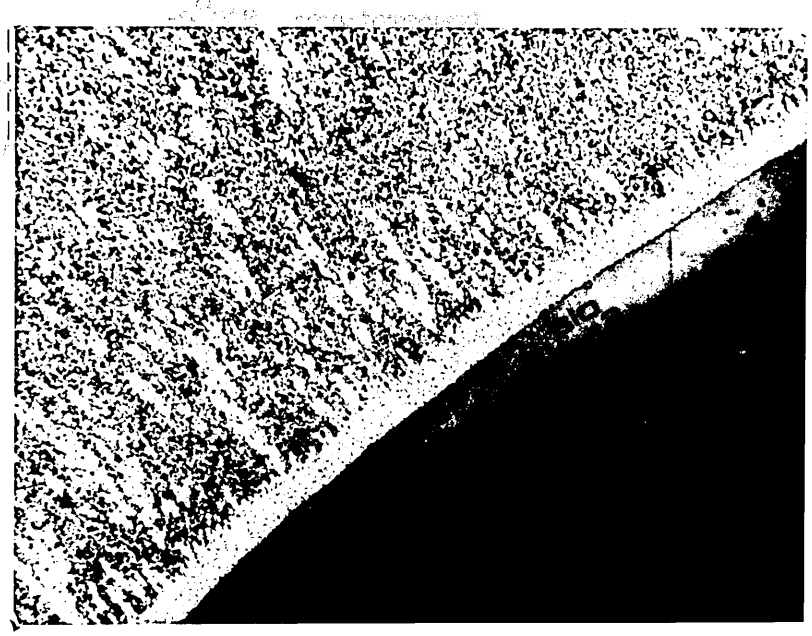
Al

Fig. 4.3.1.12. (a) Irregular radial growth of the product layer. Aggregate two phase structure penetrates inside the silica enveloping it.

(b) Broken plates of primary silicon precipitated in the bulk metal; the eutectic is relatively coarse.

(c) The lateral spread of protrusions with thickening of the product layer.

(a) Specimen: 10 mm. in diameter.
temperature: 860°C;
time: 5 minutes

(b) Specimen: 10 mm. in diameter.
temperature: 860°C;
time: 1 minute.

(c) Specimen: 10 mm. in diameter.
temperature: 860°C;
time: 10 minutes.

(a)

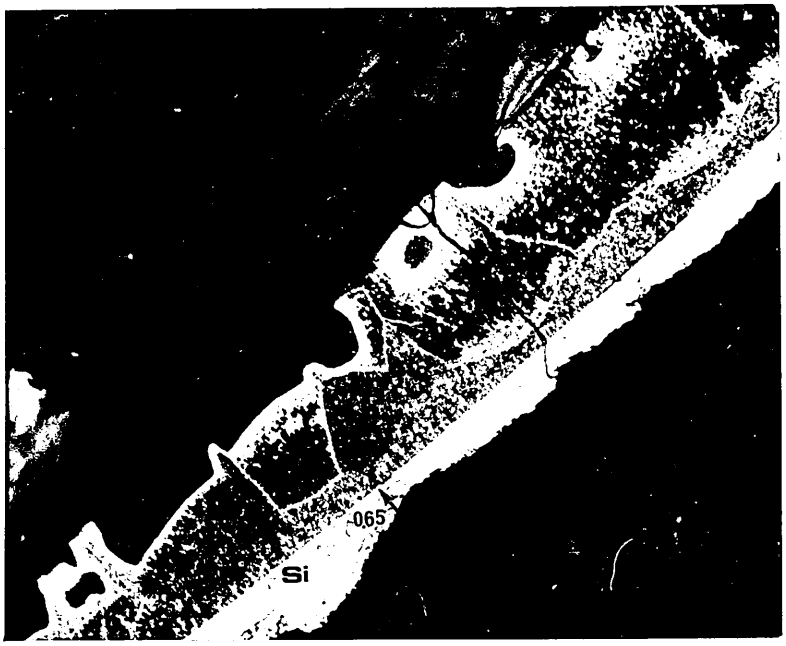

(b)

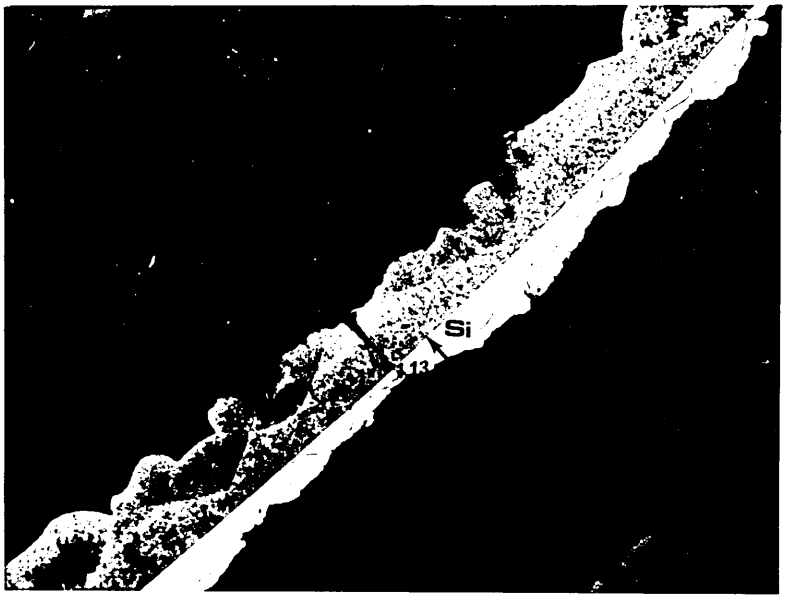

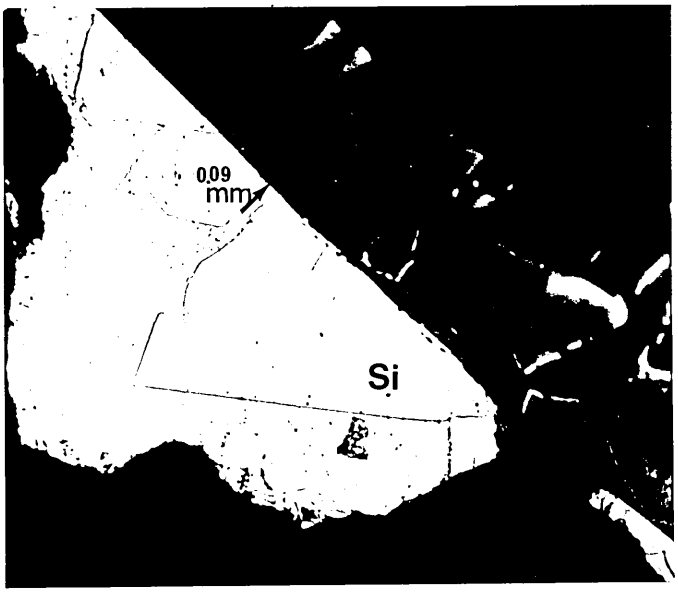

(c)

Fig. 4.3.1.13. The development of the coarse matrix during reaction. Aluminium (removed by etching) segregated at boundaries of the grain and associated with a dense structure similar to that of the interaction front.

Specimen: 5.0 mm. in diameter.

temperature: 815°C;

time: 10 minutes MAG. 120x.

Etched in etchant B for ~2 minutes - Table 3.5.

Fig. 4.3.1.14. Si-rich interface of interaction front/unreacted silica. Abundant silicon-rich metallic pools precipitated radially within the coarse matrix.

Specimen: 3.0 mm. in diameter.

temperature: 840°C;

time: 12 minutes MAG. 63x.

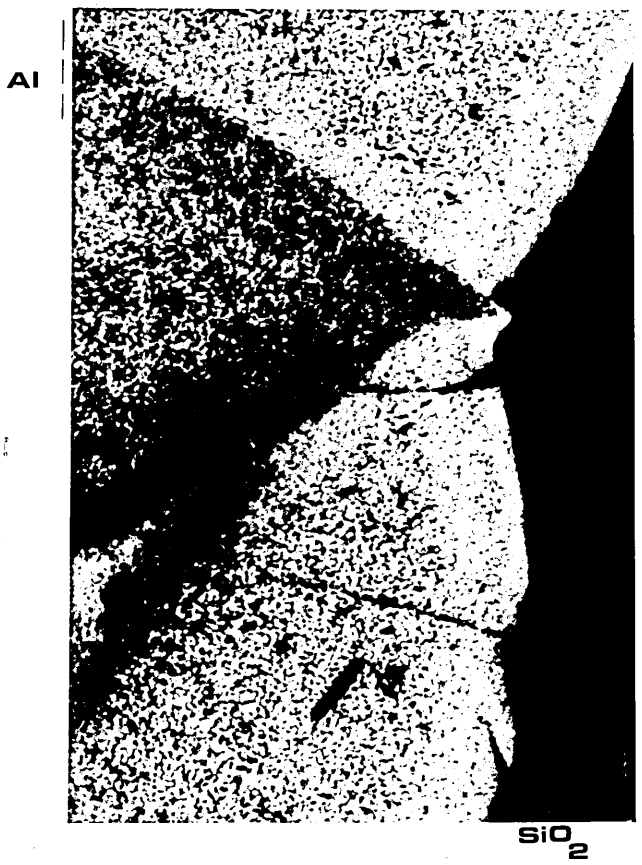
Al
SiO2

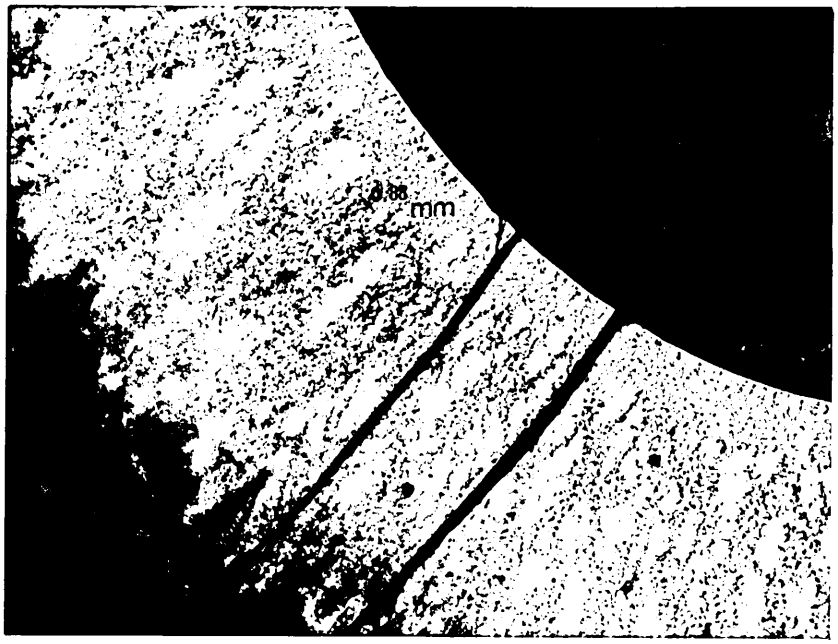
0.88
mm

Fig. 4.3.1.15. Elemental Al and Si x-ray map and corresponding line scanning for a specimen 3.0 mm. in diameter reacted at 760°C for 25 minutes. Note the Si depletion corresponding to the increasing Al-line. The lines on the maps denotethe approximate scanning path.

(a) General view Mag. 2500x

(b) Al x-ray map.

(c) Al-line scanning pattern.

(d) Si x-ray map.

(e) Si-line scanning pattern.

(f) Al + Si x-ray map.

(g) Full spectrum line scanning.

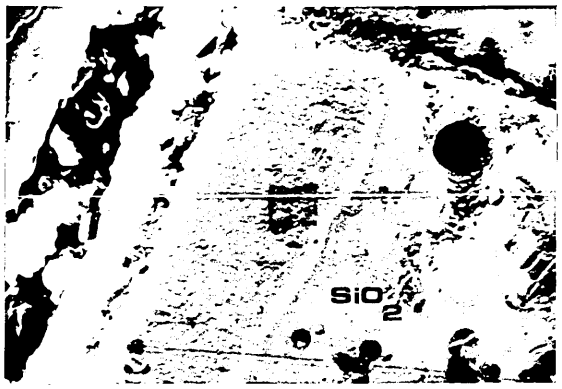

(a)

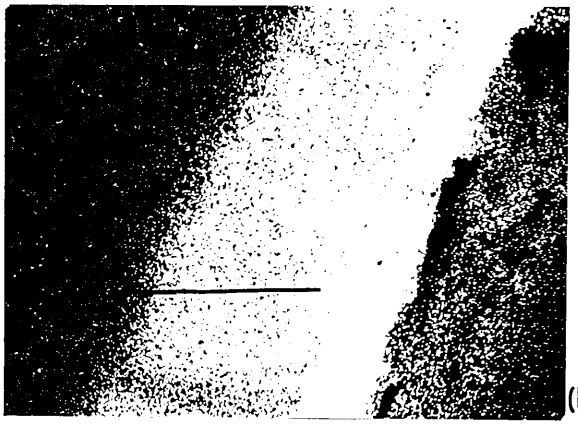

(b)

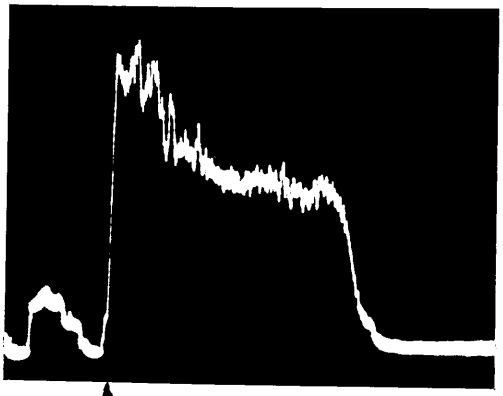

(c)

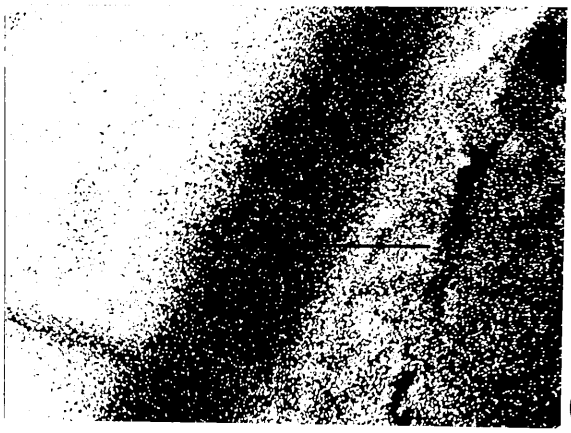

(d)

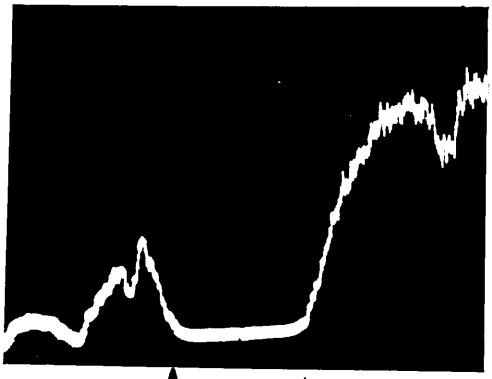

(e)

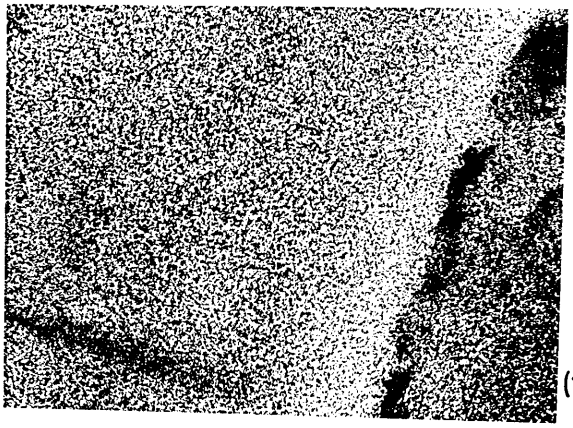

(f)

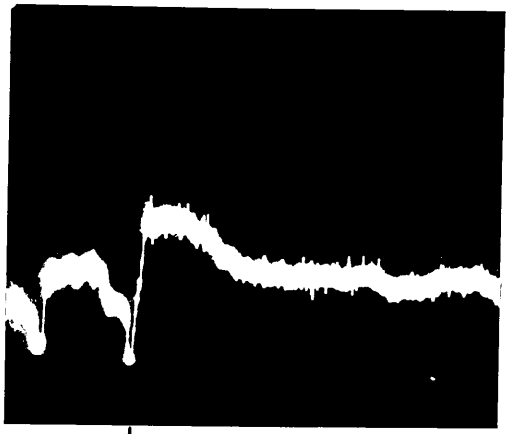

(g)

↑ : Denotes sample edge .

Fig.4.3.1.16. Deep etching (see Fig. 4.3.1.4.) indicating highly porous product layer with alumina phase, possibly theta alumina. Note the porous texture which will allow free flow of aluminium.

Mag. 320X

Etched for ~15 minutes (Table 3.5, etchant B)

Fig.4.3.1.17. Effect of etchant B on preparation of a specimen for microscopic observation. Note the decrease in resolution. (see Fig.4.3.1.11).

Mag. 120X

Etching time: ~5 minutes (Table 3.5)


Al

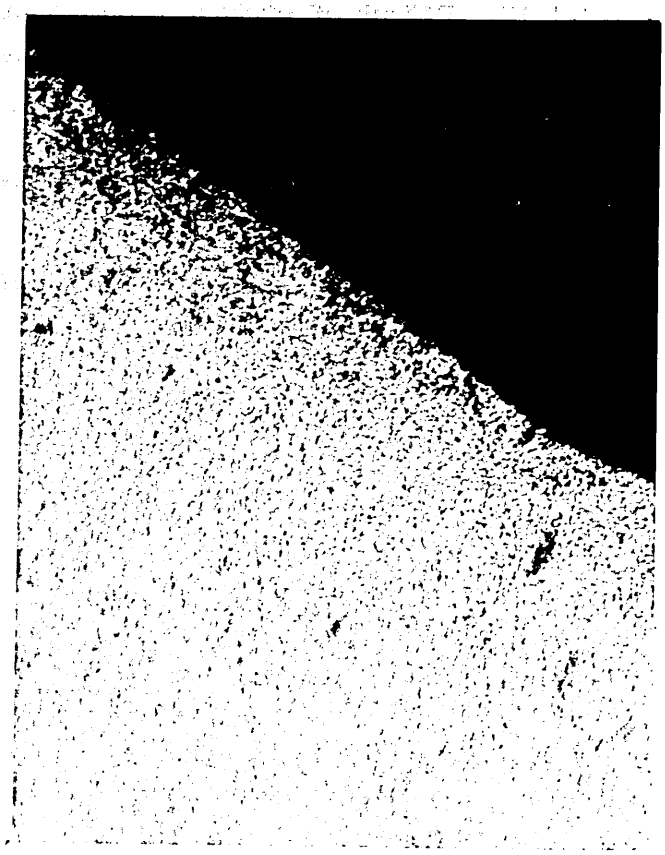

Fig. 4.3.1.18. Large grains growing in the coarse matrix. Metal segregation occurs at boundaries of the grains. Porous distribution in the grains and surrounding matrix contrast.

Mag. 100x

Specimen: 5.0 mm. in diameter.

temperature: 815°C; time: 40 minutes.

Etched in etchant A for ~3 minutes.

Fig. 4.3.1.19. This micrograph is a higher magnification of an area in Fig. 4.3.1.1,c. The dominant large grains are theta alumina. The neighbouring matrix is partially transformed into alpha-alumina. The metallic phase (white) is aluminium, precipitated at grain boundaries and in dendritic pools.

Mag. 80 x


SiO2


SiO2

Fig. 4.3.1.20, a. Specimen 5.0 mm. in diameter previously reacted at 840°C for 15 minutes and heat treated at 1220°C for 7 hours. Residual aluminium in the original product layer has reacted with remaining silica promoting total conversion. Note the "old" interaction front marking the outer limit of the "newly reacted system".

Mag. 63x

b. The interior of the "newly reacted system" with no means for diffusion, silicon largely precipitates together with some excess of aluminium still present with alumina sub-structure.

Mag. 320x

c. Portion of the "old" interaction front at higher magnification. Note the Al-rich edge of the main product layer. This implies that aluminium travelled beyond the "old" interaction front through the interface of the unreacted silica/interaction front. Due to depletion of aluminium, silicon precipitates in a continuous layer along the "old" interaction front.

Mag. 100x

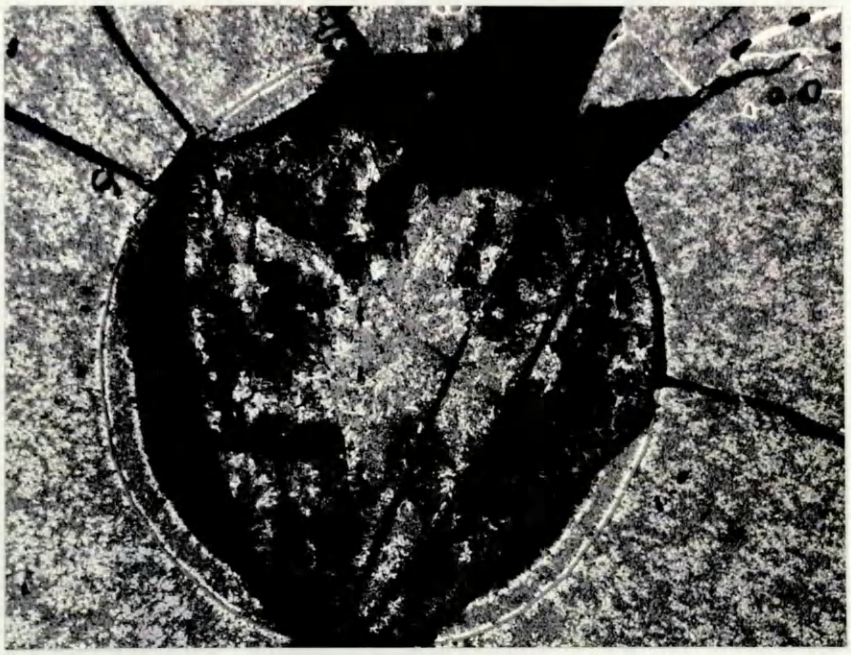

(a)

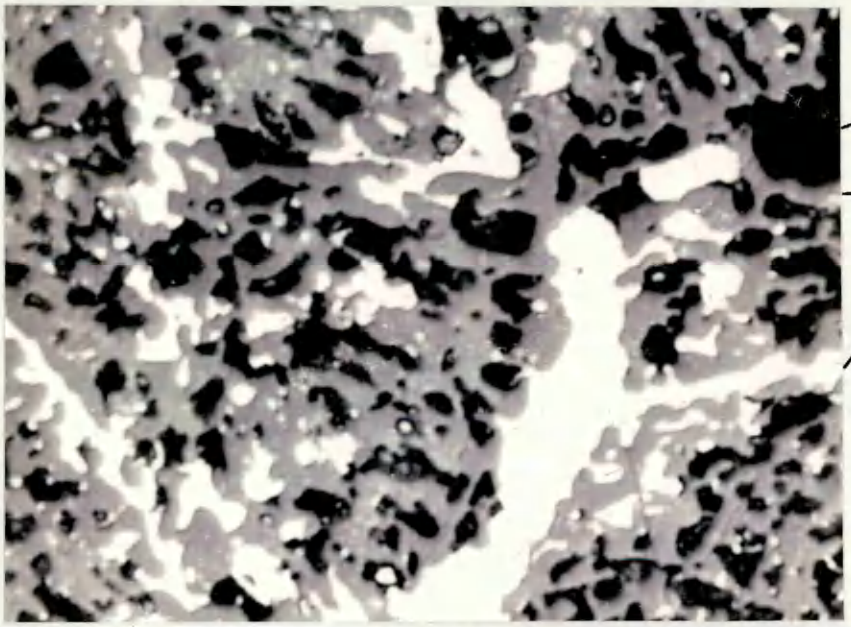

(b)

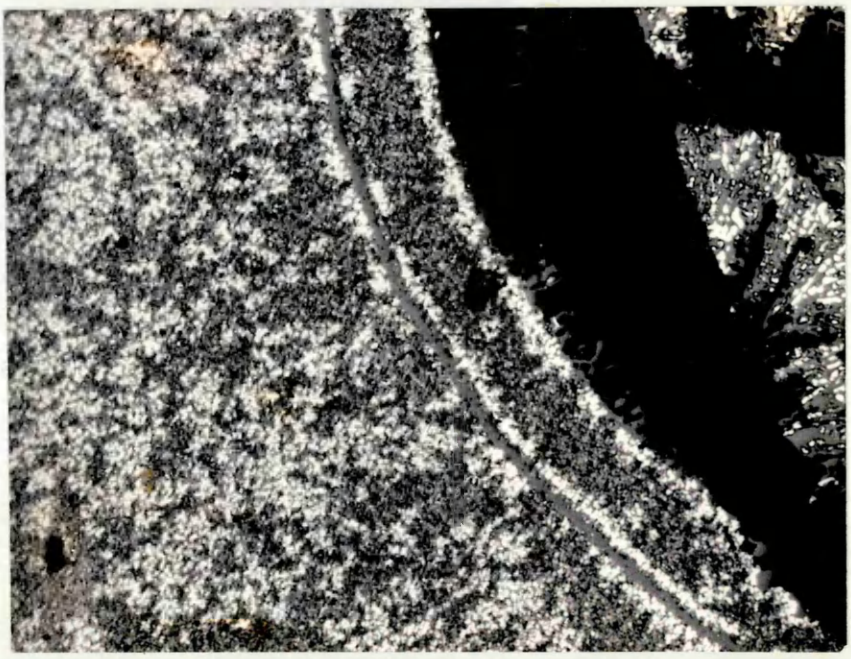

(c)

Fig. 4.3.1.21. Discontinuous precipitation and agglomeration of silicon particles along structure defects (cracking, grain boundaries).

Mag. 50x

Fig. 4.3.1.22. Branching of silicon precipitates in the interior of a large grain originally formed at 840°C. Note basis of the grain (periphery of the rod) with silicon which, in the absence of aluminium, forms a continuous layer of agglomerated particles with the alumina.

Mag. 70x

Fig. 4.3.1.23. Silicon precipitated in the original matrix and is interconnected with the interior of a large grain by branching. Note the silicon boundary, similar to the "old" interaction front.

Mag. 120x

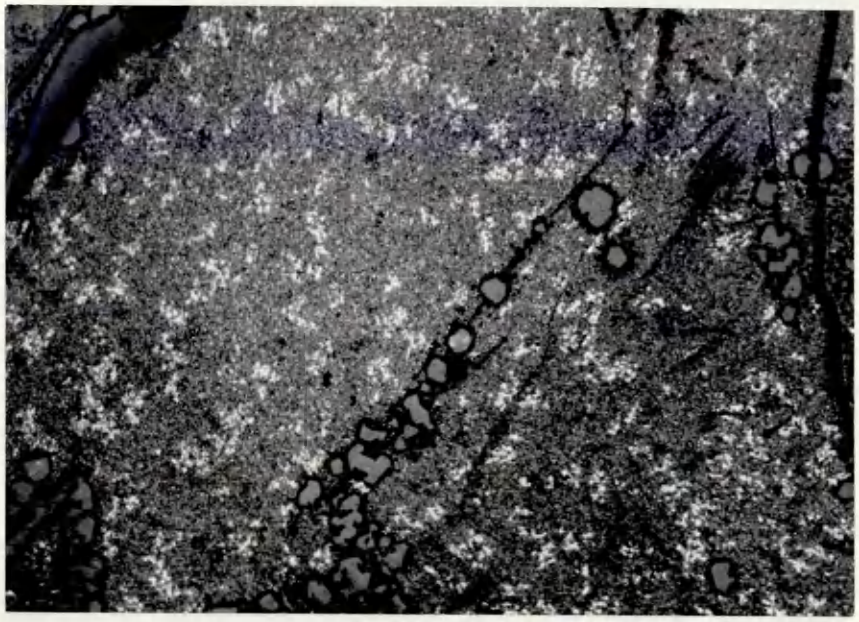

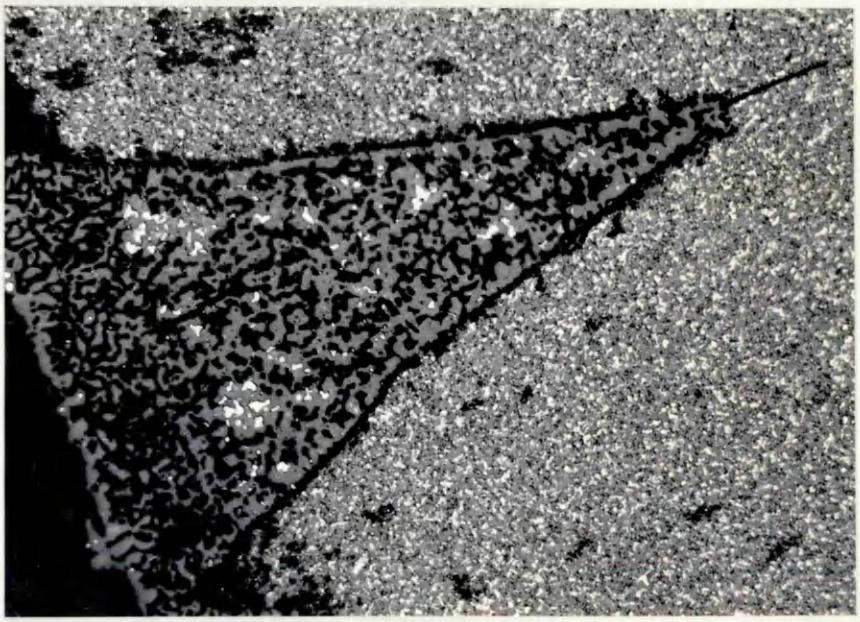

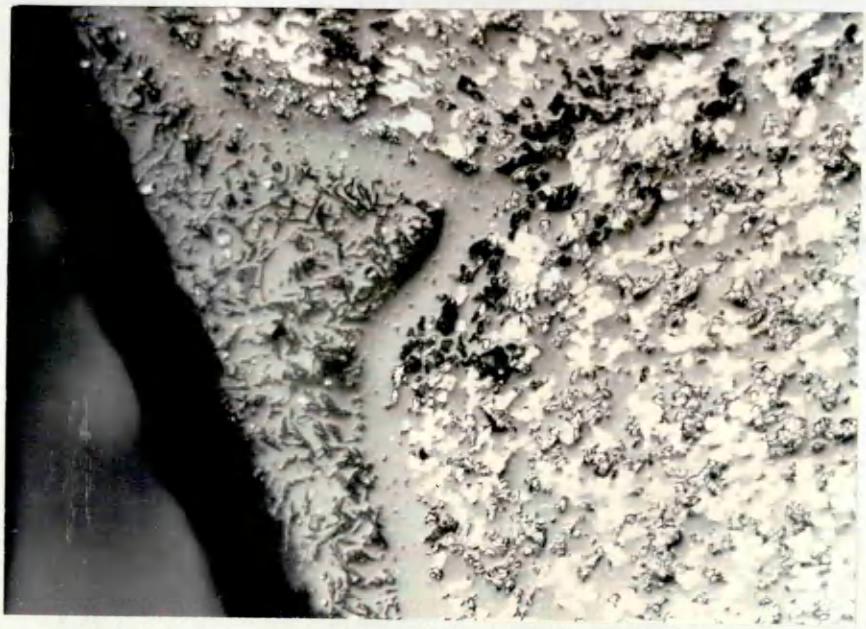

Fig.4.3.1.24 Electron scanning micrograph shows elongated cells of alumina in the coarse matrix. Spheroids are solidified pure aluminium squeezed out from the sintered matrix. Mag. 2500X.

Fig.4.3.1.25 Non-wetting behaviour of molten aluminium on alumina. Silicon does not appear to have any effect on the wetting as silicon has also been squeezed out from the product layer and partially spherodized on the surface of the rod. Mag. 63X.

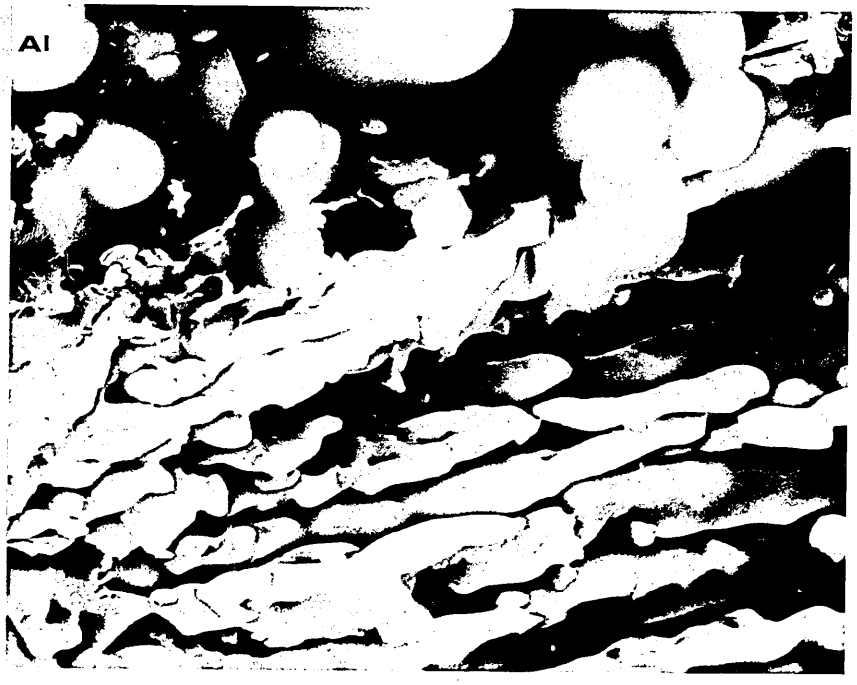
Al

Fig.4.3.1.26. Completely reacted specimen 5.0 mm in diam. reacted at 1170°C for 45 min. The product phases extend radially from the converted centre. The same path is used by the aluminium flow but in the opposite direction.

Mag. 50 X.

Fig.4.3.1.27 Spherical segments nucleated at first moments of the reaction.

Specimen: 3.0 mm in diam.

temperature: 1265°C; time: 1 min.

Fig.4.3.1.28 Lateral growth of the spherical segments into a continuous product layer.

Specimen: 10 mm in diam.

temperature: 1265°C; time: 2 min.


converted
silica

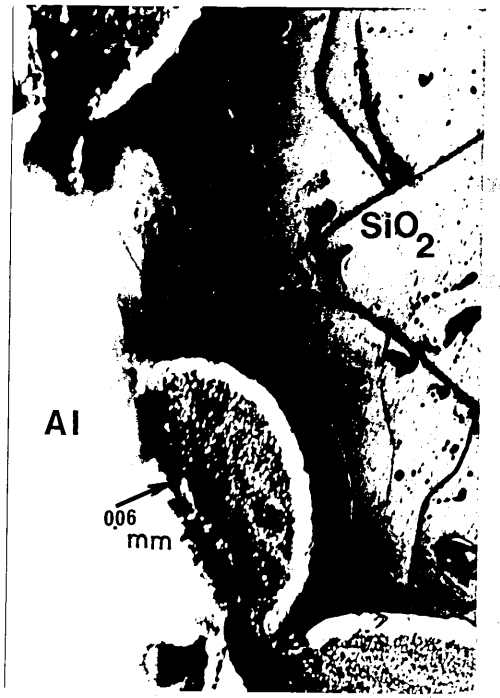
SiO2
Al
0,06
mm

Fig.4.3.1.29,a. Random growth of the interaction front at the beginning of the reaction with lateral spreading of the product layer.

Specimen: 5.0 mm in diam.

temperature: 1170°C; time: 5 min.

b. Continuous growth of the product layer. The interaction front has partly been left behind without recrystallization.

Specimen: 3.0 mm in diam.

temperature: 1220°C; time: 5 min.

c. With time of reaction the interaction front becomes more uniform in thickness. Note recrystallized region in the front. A similar effect is present in the regions left behind during reaction.

Specimen: 10 mm in diam.

temperautre: 1220°C; time: 15 min.

Etched in etchant B - Table 3.5 for ~15 min.

a.

b.

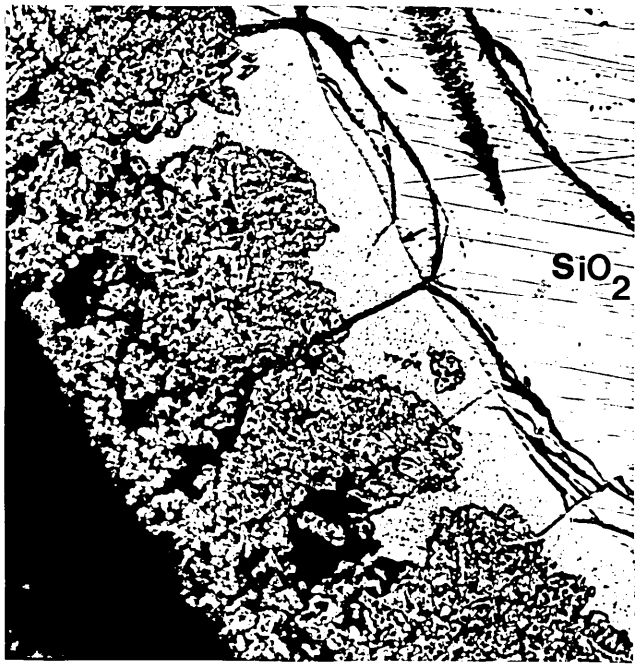

c.

Fig.4.3.1.30. Interaction front composed of two layers. Both layers are very fine in comparison to the porous recrystallized coarse matrix left behind with progress of reaction.

Mag. 120X.

Specimen: 3.0 mm in diam.

temperature: 1110°C; time: 40 min.

Figs.4.3.1.31,a. Recrystallization takes place within the interaction front during reaction. Alumina phases act as nucleant for silicon in a pool of aluminium rich metallic phase. Cracks which occurred during reaction are filled with metallic phases.

Mag. 240X.

Specimen: 10 mm in diam.

temperature: 1170°C; time: 30 min.

b. previous island structure at higher magnification:

X400

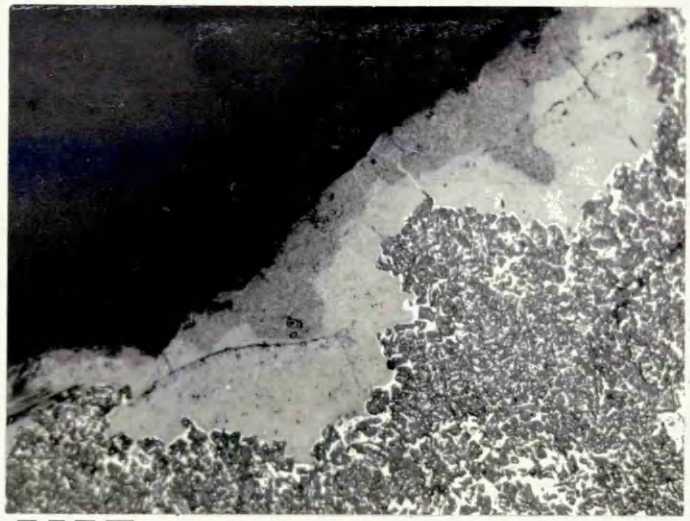

Al

a.

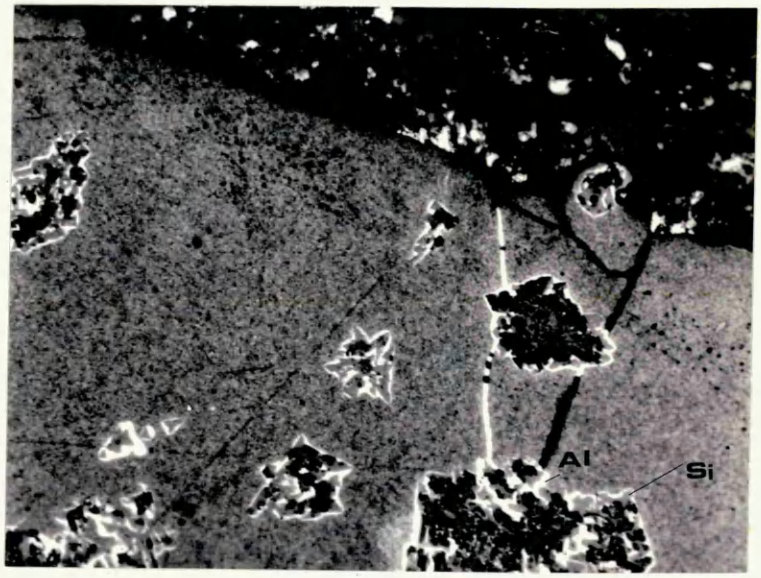

b.

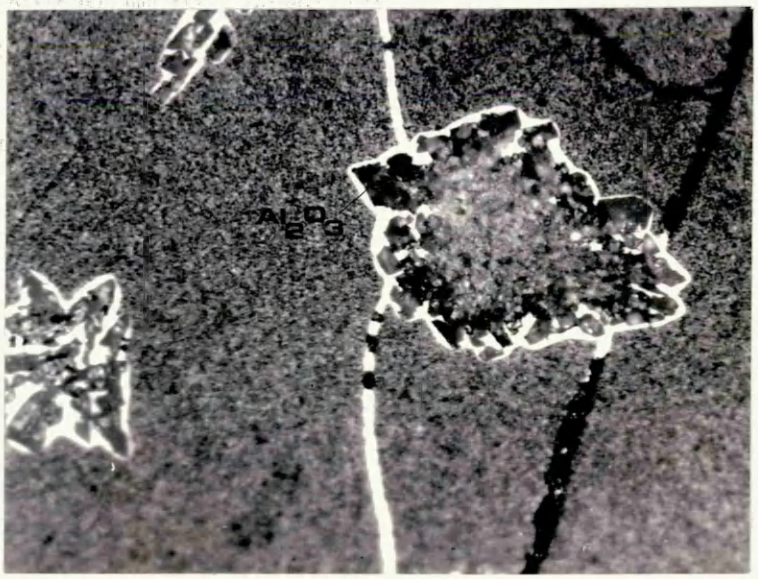

Fig.4.3.1.32. Elemental Al and Si X-ray maps and corresponding line scanning results for a specimen 5.0 mm in diam. reacted at 1220°C for 15 min. The lines on the maps denote the approximate scanning path.

a. General view. Mag. 160 X

b. Al X-ray map.

c. Al line-scanning pattern.

d. Si X-ray map.

e. Si line-scanning pattern.

f. Al + Si full spectrum.

g. Full spectrum line-scanning.

1,2. EDAX patterns at two different points near to the unreacted silica surface.

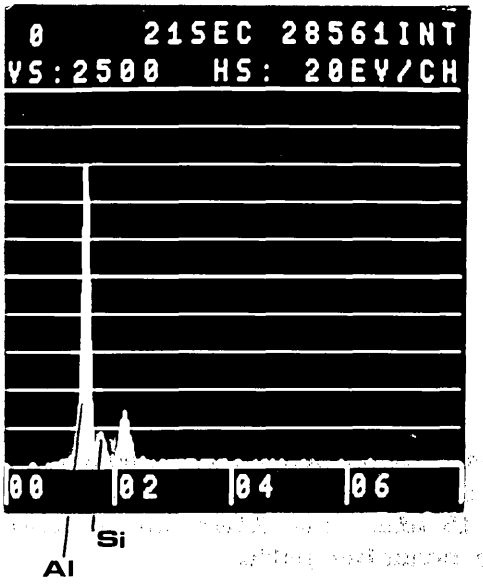
0 215EC 28561INT
VS:2500 HS: 20EV/CH
00
02
04
06
Al
Si

1.


Al
SiO2

a.

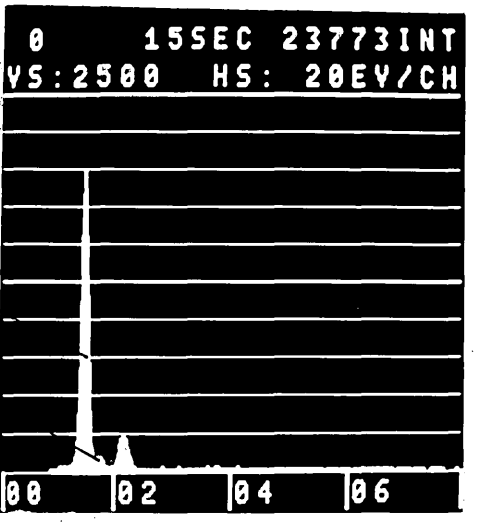
0 155EC 23773INT
VS:2500 HS: 20EV/CH
Al
Si
00
02
04
06

2.

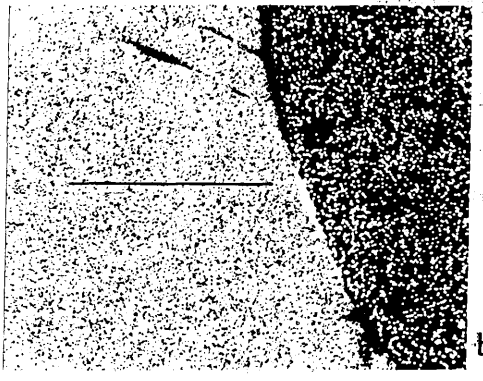

b.

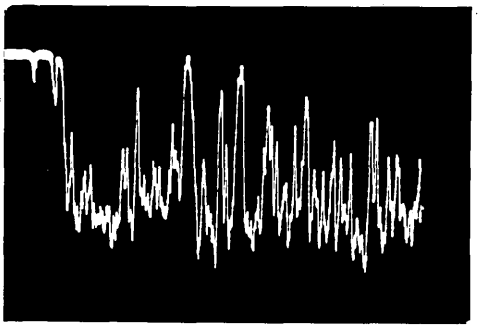

c.

d.

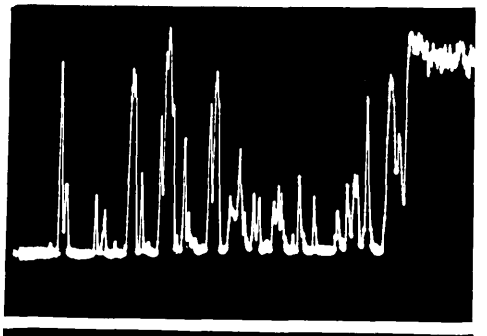

e.

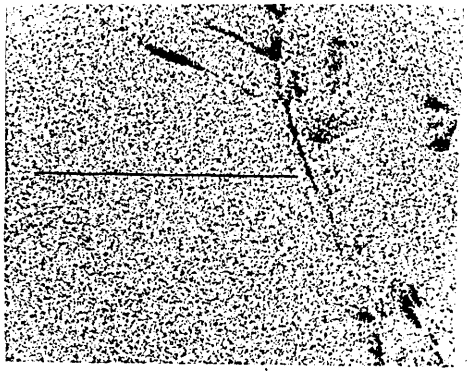

f.

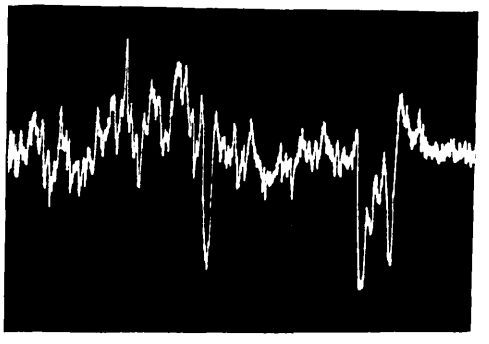

g.

Fig.4.3.1.33,a. Fine interaction front, double layer, apparently bonded to the unreacted silica. The layers are separated by a film of pure silicon (outlined).

Mag. 1250 X.

b. EDAX pattern shows silicon as the only phase present in the outlined region of the previous structure.

Specimen: 10 mm in diam.

temperature: 110°C; time: 120 min.

Fig.4.3.1.34 Growth of the product layer in a radial manner. The texture is orientated radially allowing the reacting and product species to counter-diffuse readily into and from the interaction front.

Mag. 80 X.

Specimen: 30 mm in diam.

temperature: 1170°C; time: 25 min.

Fig.4.3.1.35 Columnar growth of the coarse matrix from transformed interaction front. This frequently extends right up to the original surface of the silica rod.

Mag. 2500 X.

Specimen: 30 mm in diam.

temperature: 1170°C; time: 10 min.

a.

Al

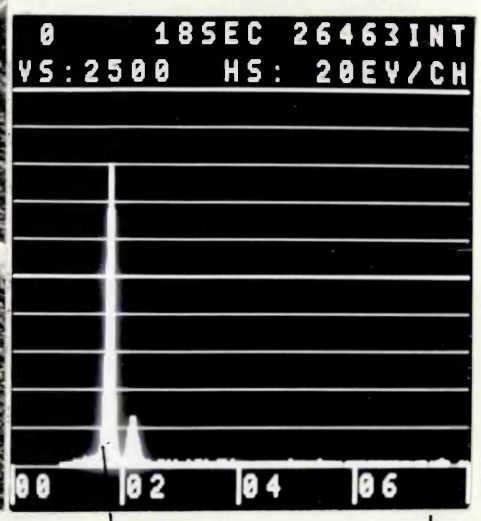

Si

b.

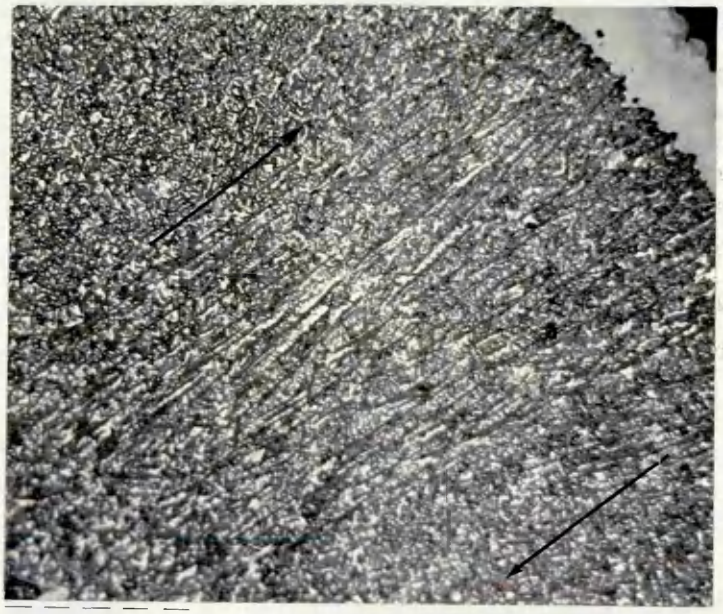

SiO_2

Al

SiO_2

Al

Fig.4.3.1.36. Columnar alumina texture in the product layer.
Mag. 5000 X.
Specimen: 5.0 mm in diam.
temperature: 1265°C; time: 10 min.

Fig.4.3.1.37. Radial counter flow in streams of silicon following the columnar texture of the coarse matrix.
Mag. 320 X.
Specimen: 10 mm in diam.
temperature: 1265°C; time: 15 min.

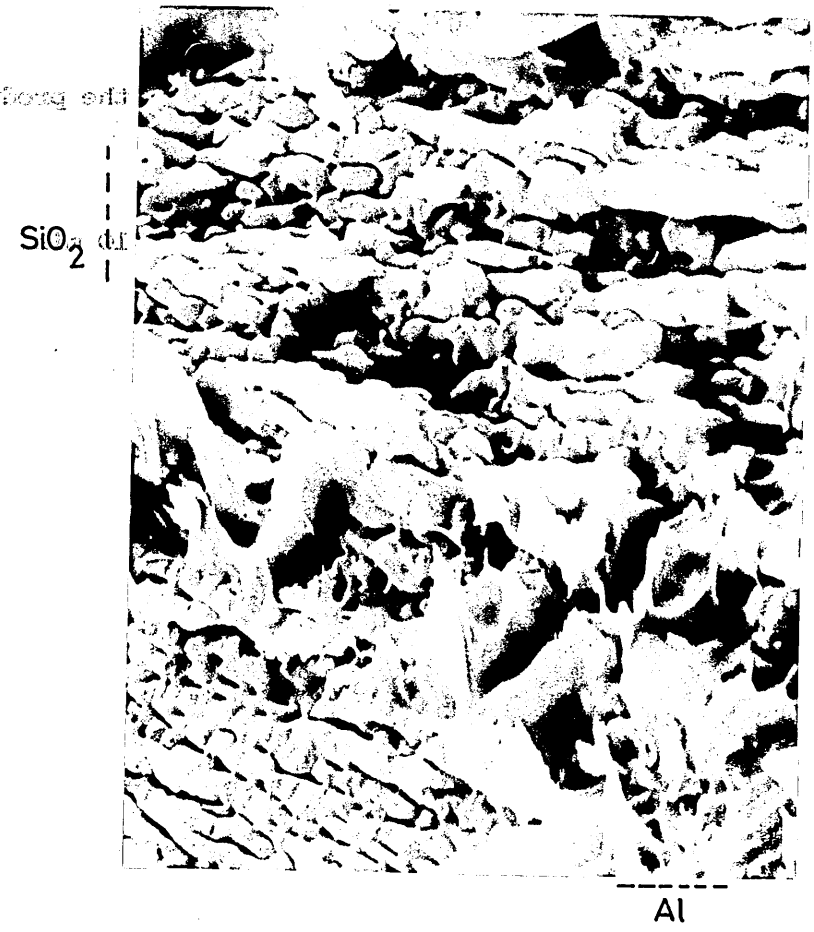
SiO_2
Al

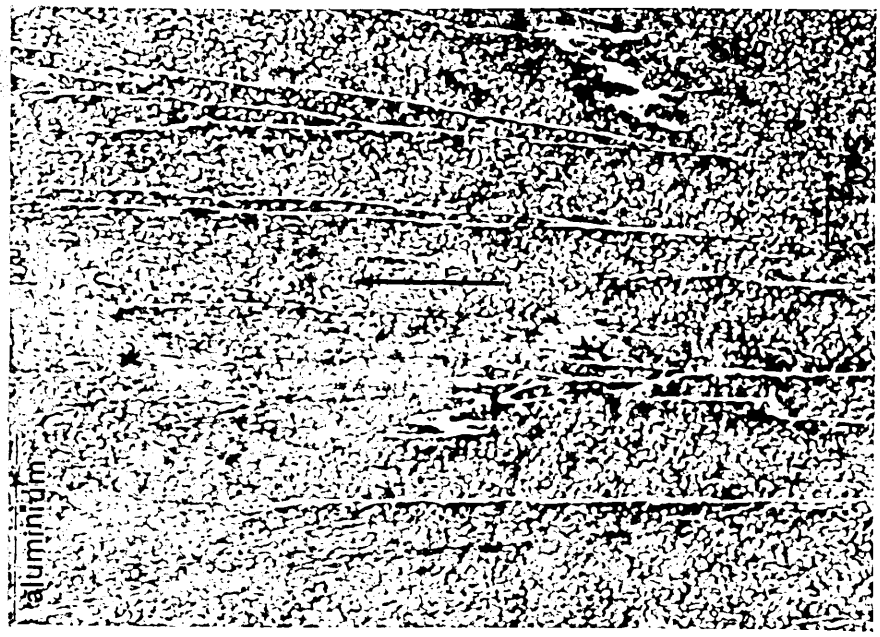
aluminium

Fig.4.3.1.38. Elemental Al and Si x-ray maps and corresponding line scanning for a specimen 3.0 mm in diam. reacted at 1110°C for 15 min. The lines on the maps denote the approximate scanning path.

(a) General view. Mag. 600 X

(b) Al x-ray map.

(c) Si x-ray map.

(d) Al line-scanning pattern.

(e) Si line-scanning pattern.

(f) Full spectrum line scanning.

(1), (2), (3) EDAX patterns at three different points near to the unreacted silica surface.

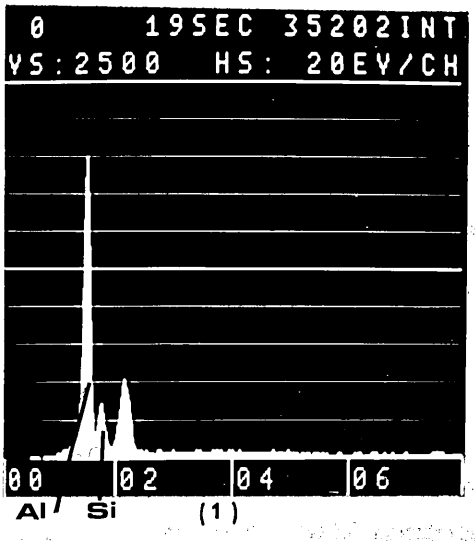
0 19SEC 35202INT
VS:2500 HS: 20EV/CH
00
02
04
06
Al
Si
(1)

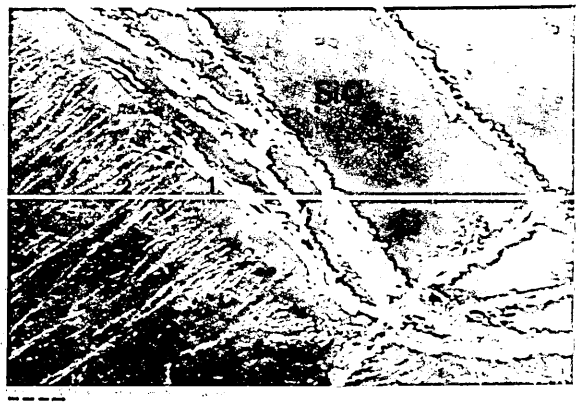
Si
1
(a)
Al

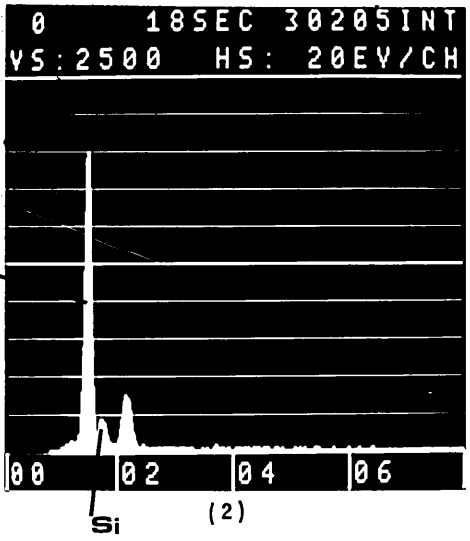
0 18SEC 30205INT
VS:2500 HS: 20EV/CH
Al
00
02
04
06
Si
(2)

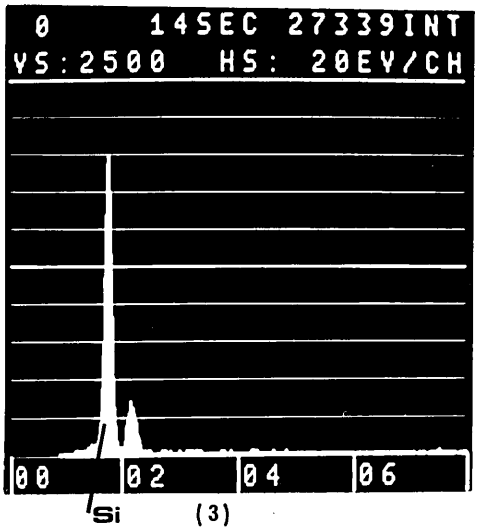
0 14SEC 27339INT
VS:2500 HS: 20EV/CH
00
02
04
06
Si
(3)


(b)

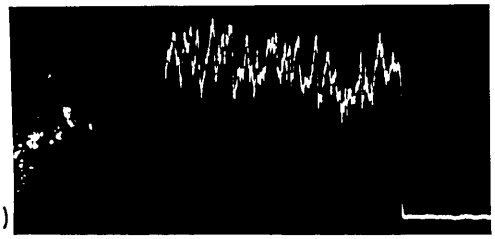
(d)

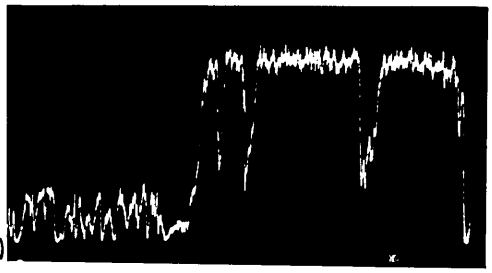
(e)

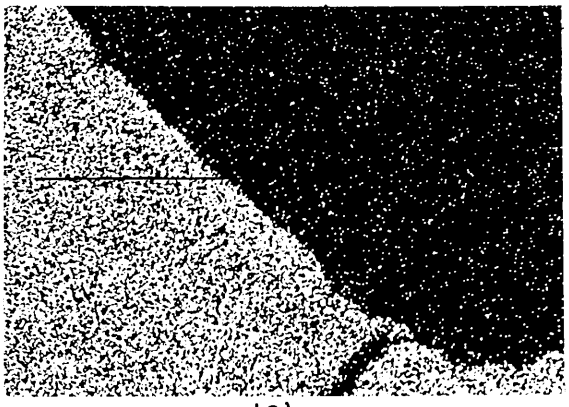
(c)

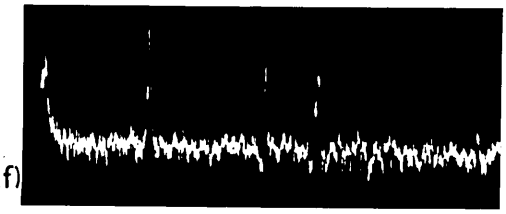
(f)

Fig.4.3.1.39. Cross-section of a specimen 5.0 mm in diam. reacted at 1170°C for 30 min.

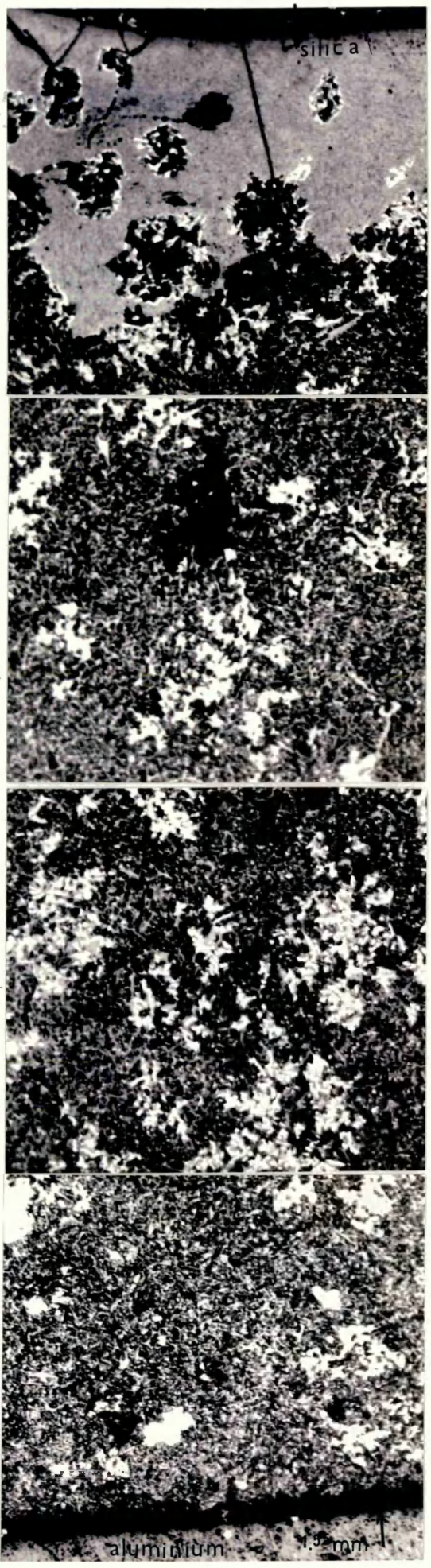
silica
— a —
— b —
— c —
— d —
aluminium
1.5 mm

Fig.4.3.1.40. Scanning electron micrograph of a delayed recrystallized region left behind the interaction front during progress of reaction - see fig.4.3.1.29,c. Columnar cells of alumina radiate from core with mounds of Al-Si alloy. Silicon has precipitated on periphery of the core.

Mag. 2500 X

Specimen: 10 mm in diam.

temperature: 1220^{o}C; time: 15 min.

Fig.4.3.1.41 Coarsened matrix interface with the fine interaction front. Note the irregular development of the alumina columns embedded in a metallic dendritic shape phase. Circular colonies of alumina have developed ultimately. See Fig.4.3.1.39 (height (a)).

Mag. 400 X

Specimen: 5.0 mm in diam.

temperature: 1170^{o}C; time: 30 min.

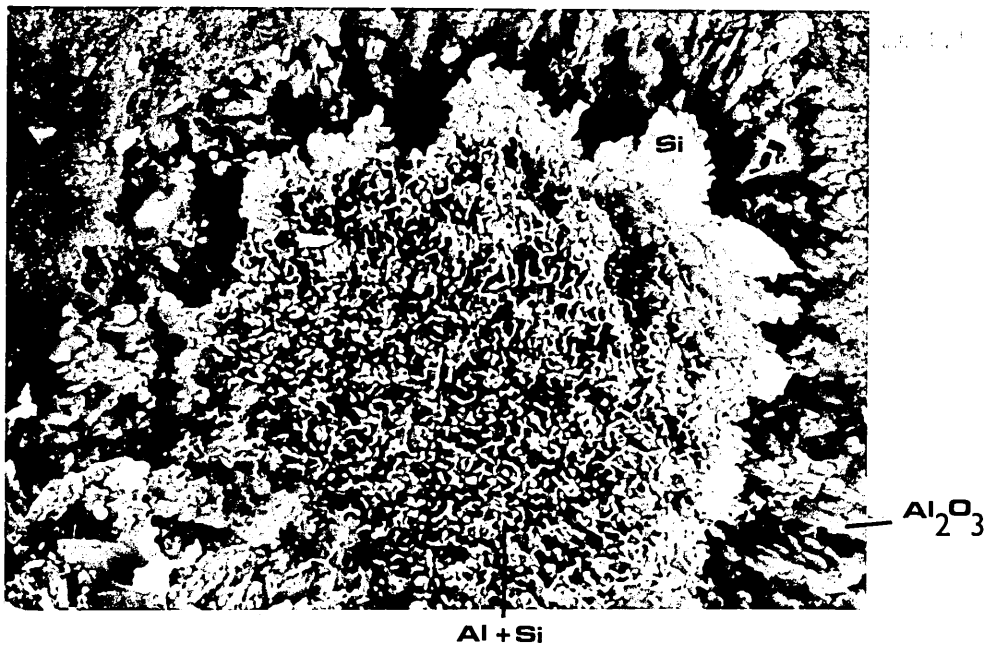
Si
Al_2O_3
Al + Si

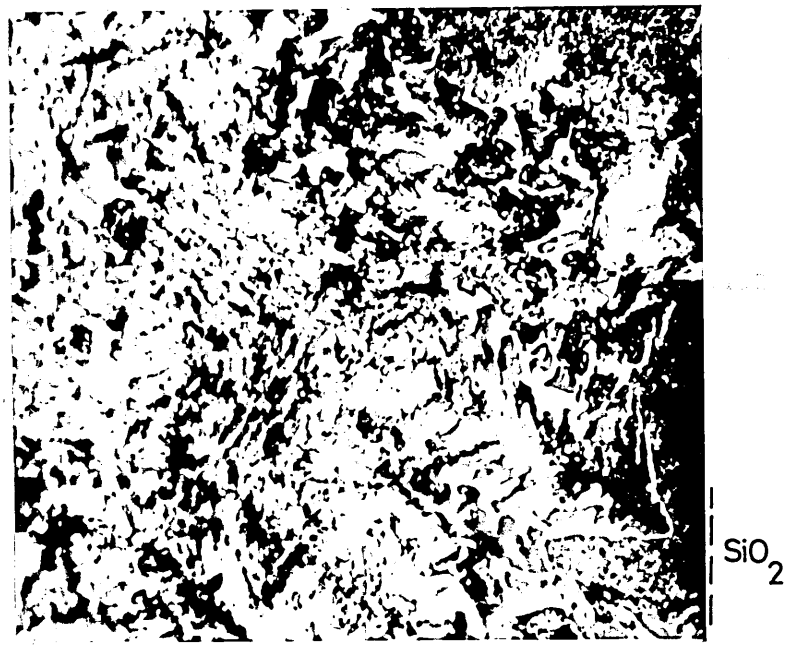
SiO_2

Fig.4.3.1.42,a Elongated alumina cells embedded in an Al + Si metallic phase. The cells are disposed in a tortuous manner and interconnected to a certain extent.

Mag. 120 X

b Electron-scanning micrograph showing agglomeration of alumina cells.

c Higher magnification of microstructure b.

Specimen: 10 mm in diam.

temperature: 1110°C; time: 20 min.

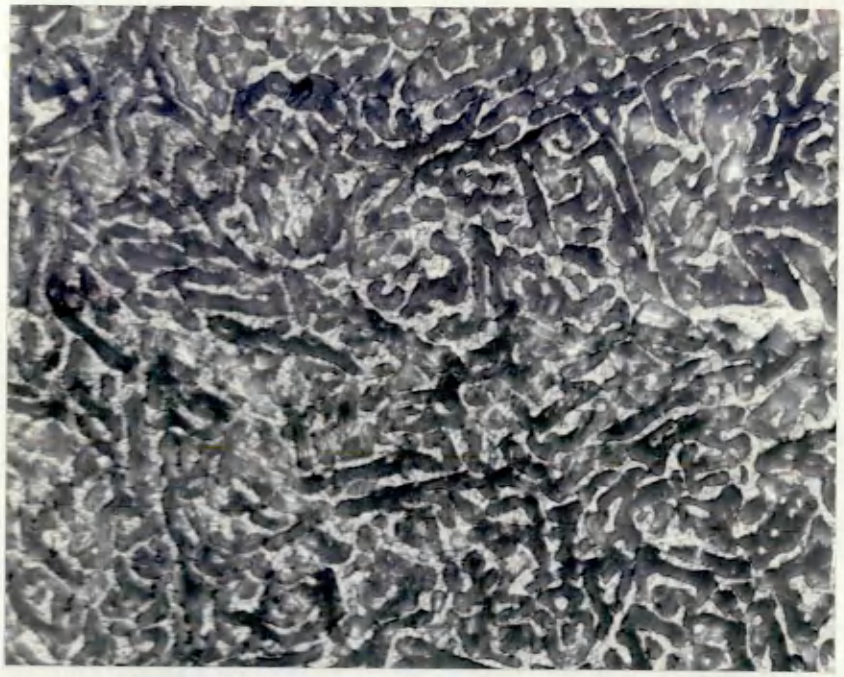

a.

b.

c.

Fig.4.3.1.43 a. Aluminium dendrite, close to the original periphery of the silica rod. mag. 2500X

b. EDAX pattern of marked region (x) shows aluminium as the element present.

c. Singular branches of an aluminium dendrite.

Mag. 5000 X

Specimen: 10 mm in diam.

temperature: 1220°C; time: 45 min.

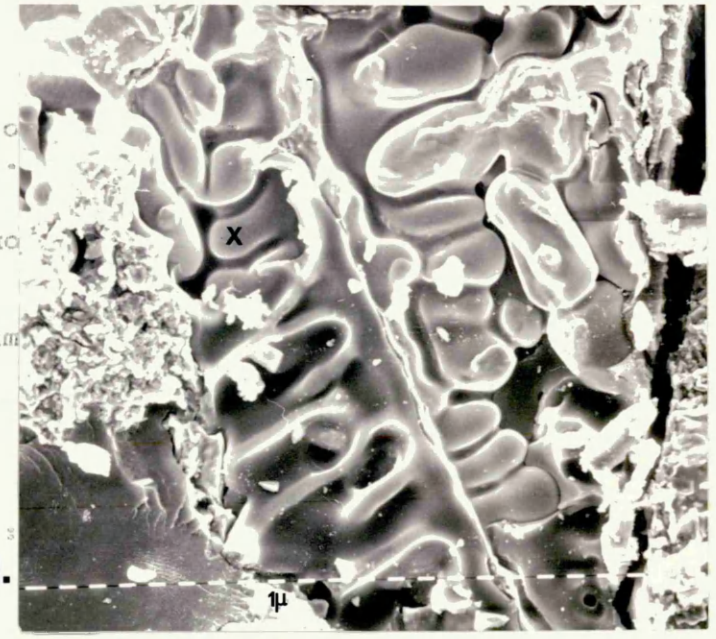

a.

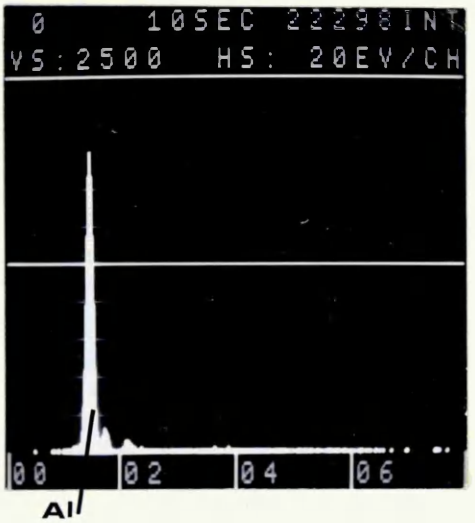

b.

c.

Fig.4.3.1.44. Circular colonies of alumina cells - see Fig.4.3.1.39 (height b).

Mag. 320 X

Fig.4.3.1.45. Al + Si distribution within alumina colonies.

Note Si as primarily precipitated from a Si-rich Al-Si alloy.

See Fig.4.3.7.29,c. Mag. 120 X

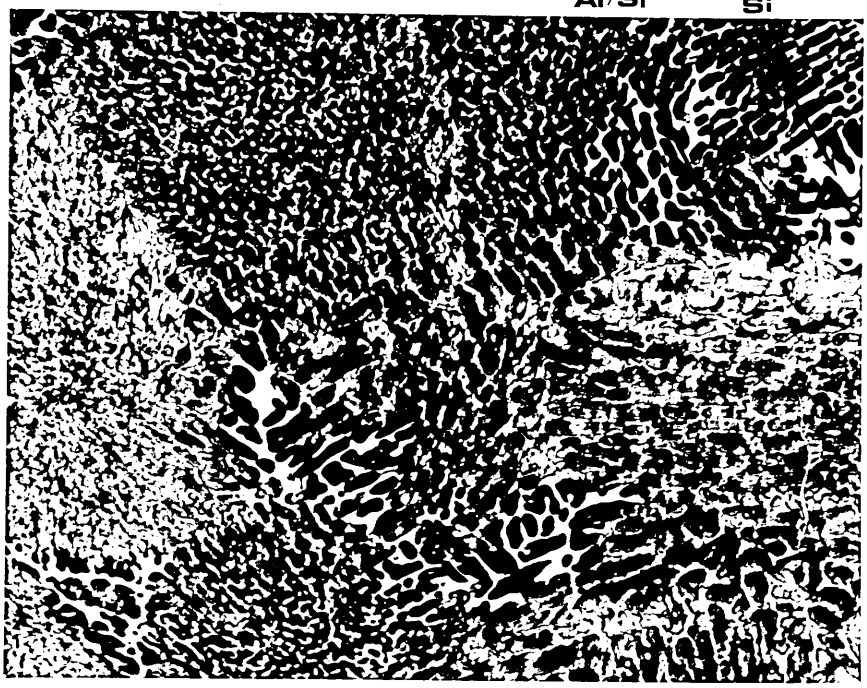
Al/Si
Si

Fig.4.3.1.46,a. Electron-scanning micrograph of elongated alumina cells grown in colonies of circular shape embedded in Al-Si metallic phase.

Mag. 2500 X. See Fig.4.3.1.45.

(o) EDAX pattern of marked region shows silicon as the element present.

(x) EDAX pattern of marked region shows Al-rich Al-Si metallic phase.

b. Better resolution of elongated cells of alumina. Related to the previous microstructure.

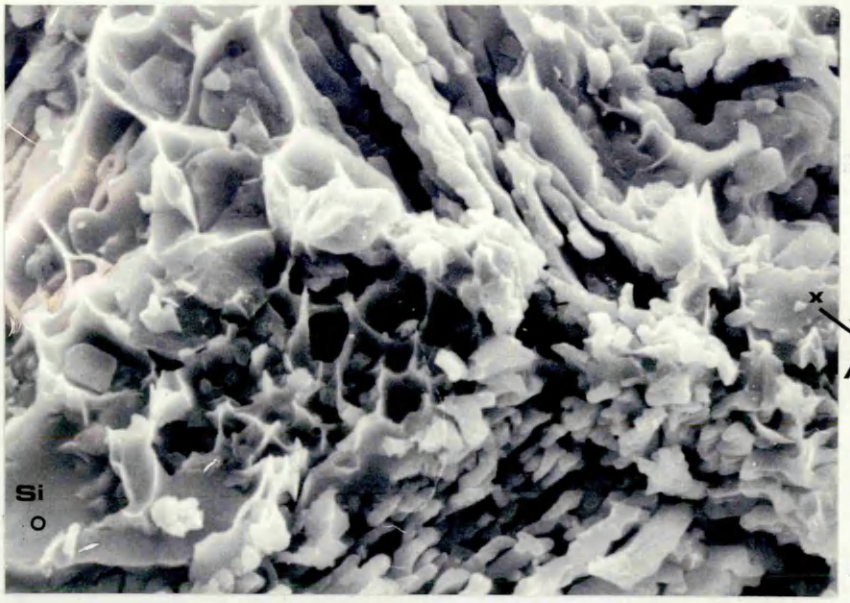
x
Al+Si
Si
o

a.

(x)

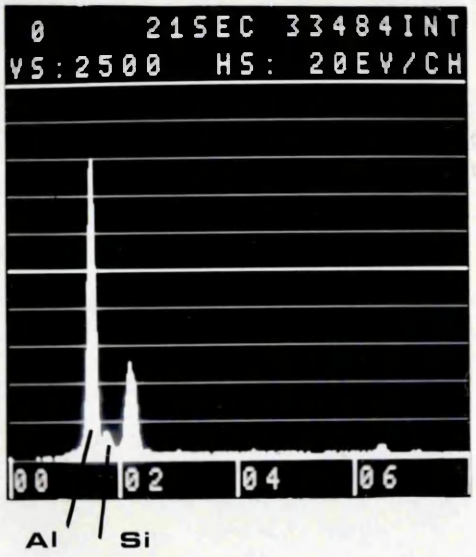
0 21SEC 33484INT
VS:2500 HS: 20EV/CH
00
02
04
06
Al
Si

(o)

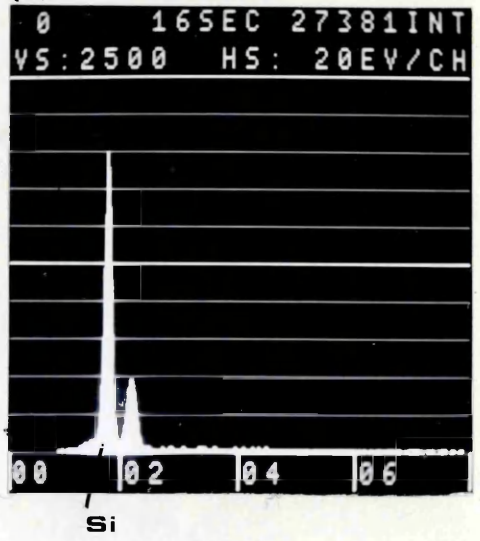
0 16SEC 27381INT
VS:2500 HS: 20EV/CH
00
02
04
06
Si

b.

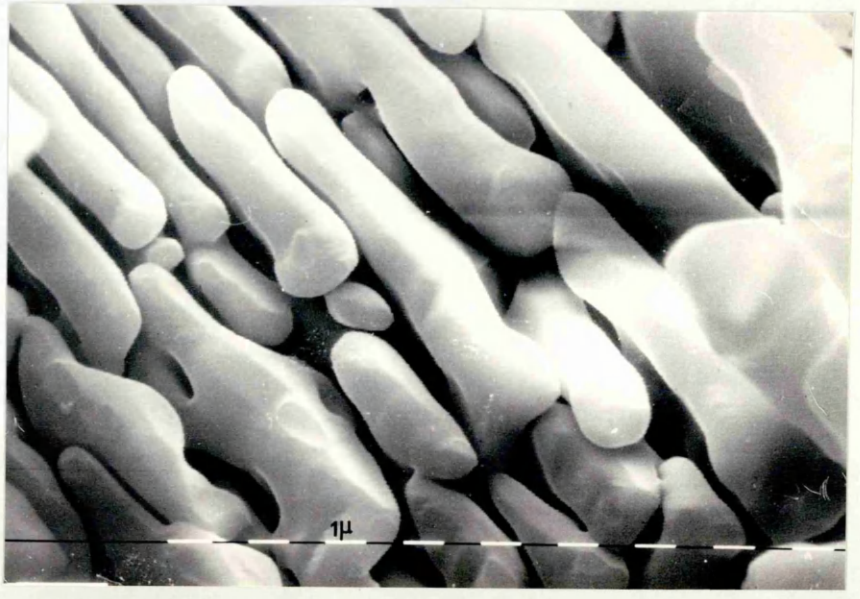
1μ

Fig.4.3.1.47. "Spider-web" Al-Si eutectic microstructure developed during cooling. Related to the decrease of silicon concentration in the Al-Si metallic phase across the coarse matrix towards periphery of the rod.

See Fig.4.3.1.39. Mag. 400 X.

Fig.4.3.1.48. Columns of alumina extending right up to the external surface of the product layer. The region is Al-rich.

Mag. 320 X.

Specimen: 10 mm in diam.

temperature: 1265^{o}C; time: 55 min.

Fig.4.3.1.49. Bulk metallic phase attached to the reacted silica rod. Aluminium dendritic regions with silicon in Al-Si eutectic. Mag. 63 X.

Specimen: 3.0 mm in diam.

temperature: 1110^{o}C; time 10 min.

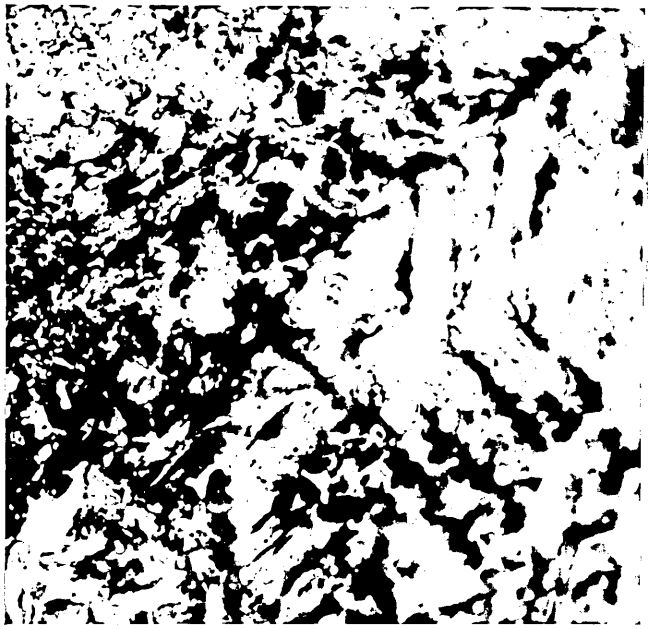


SiO2
Al

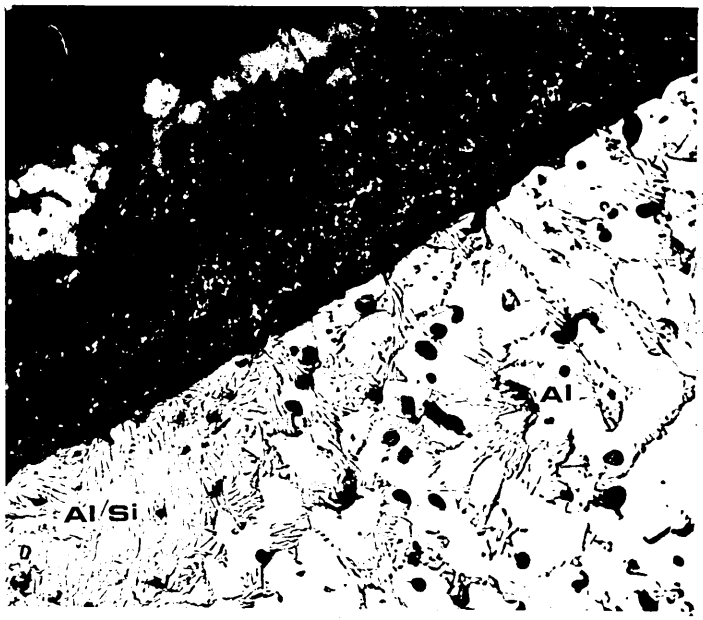
Al
Al/Si

Fig.4.3.1.50,(a) Interrupted continuity of the product layer of a specimen 5.0 mm in diam. reacted for 40 minutes at 920°C. Note unreacted silica outlined on periphery of the rod and left behind unconverted as reaction progressed.

Mag. 32 X.

(b) Interface of unreacted silica/product layer, at higher magnification (80 X). Impingement of spheroids protruding inside the silica. Contour of segments with non-recrystallized phase - similar to that commonly observed in the interaction front developed at lower temperature reaction.

(c) Detail of impinging columns.

Mag. 100 X.

a.

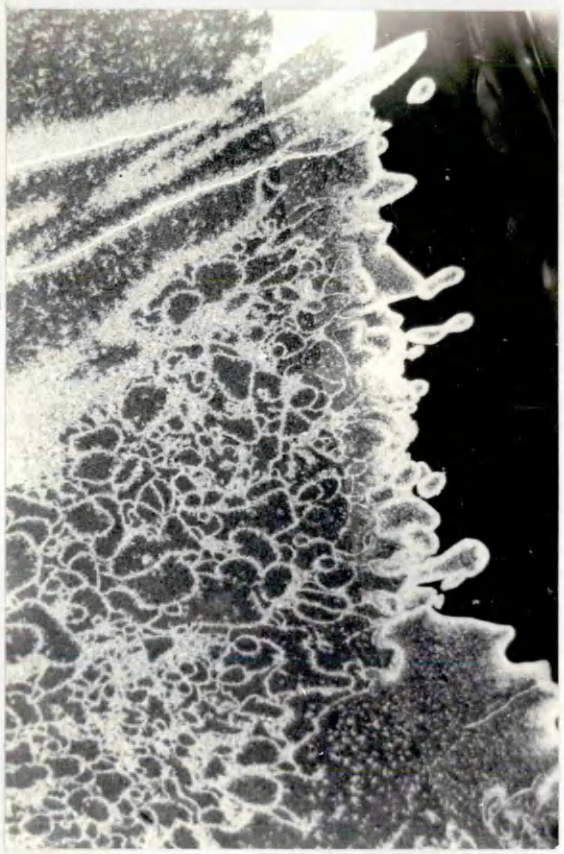

b.

c.

Fig.4.3.1.51. Interface of unreacted silica/product layer. Columnar lathes of the product layer are sidewise limited by precipitated silicon and protrudes inside the silica.

Specimen: 10 mm in diam.

temperature: 920°C;

time: 90 min.

Mag. 63 X.

Fig.4.3.1.52. Large grain growth with boundary precipitation of aluminium-silicon alloy. Elemental silicon precipitated at surface of unreacted silica.

Specimen: 5.0 mm in diam.

temperature: 980°C;

time: 90 min.

Fig.4.3.1.53. Morphological aspect of a silicon region close to the unreacted silica. "Broken plate-like" particles of precipitated silicon. Silicon is indicated by EDAX microanalysis (arrow in the outlined region). Mag. 800 X

Specimen: 10 mm in diam.

temperature: 980°C; time 20 min.

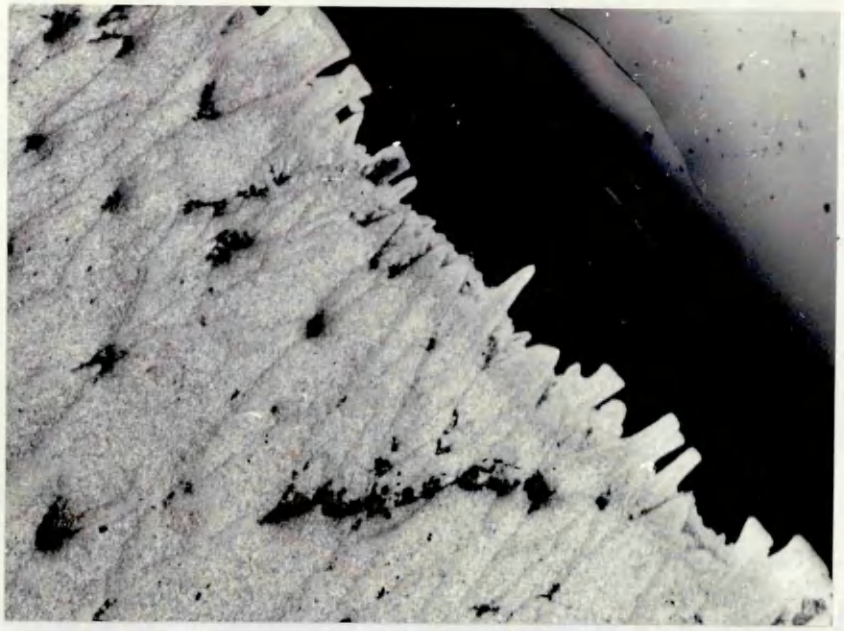

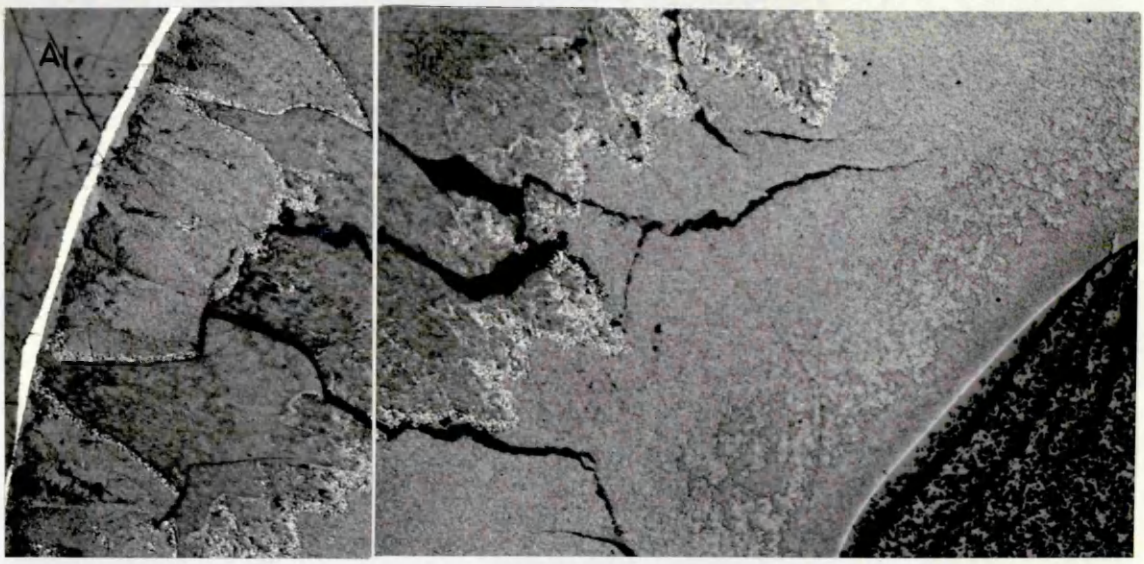
Al

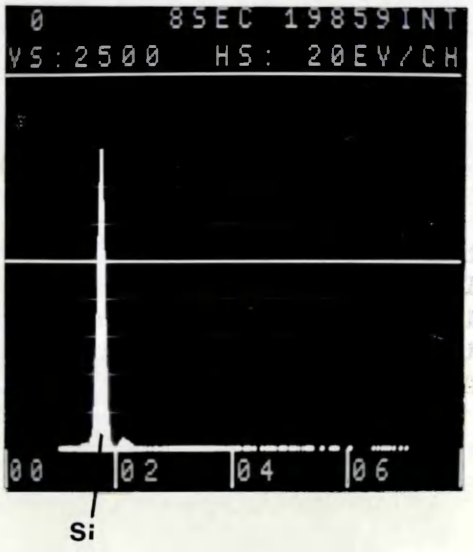
0 8SEC 19859INT
VS:2500 HS: 20EV/CH
00
02
04
06
Si


Si

Fig.4.3.1.54 (a) Precipitation of cuboid particles of intermediate phase on the surface of the fine interaction front. Specimen 5.0 mm in diam. reacted at 980°C for 120 min. Mag. 1250 X;

(b) view of cuboid particles at higher magnification 2500 X; energy-dispersive microanalysis of a cuboid (arrowed) indicates and (Al + Si) - rich constitution;

(c) cubes of intermediate phase on the surface of the interaction front of a specimen 10 mm. in diam. reacted at 980°C for 120 min; Mag. 5000 X; energy dispersive microanalysis of a cube (arrowed) shows Al + Si constitution.

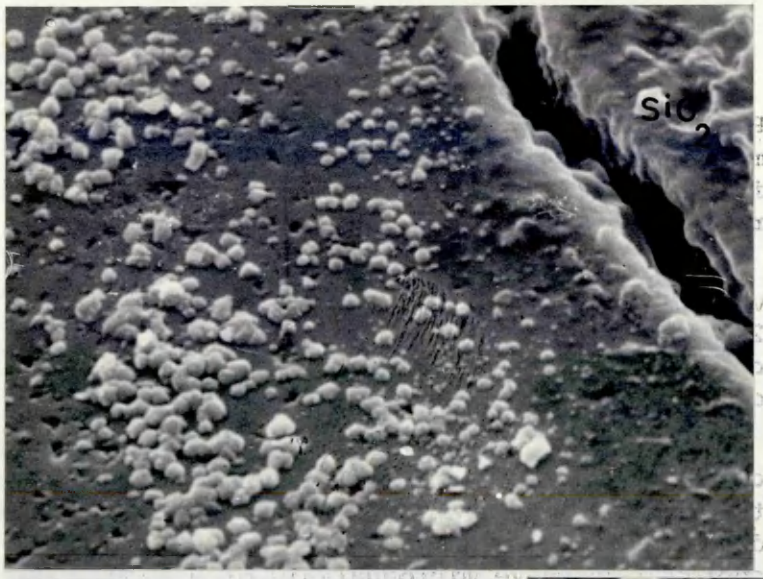
SiO_2

a.

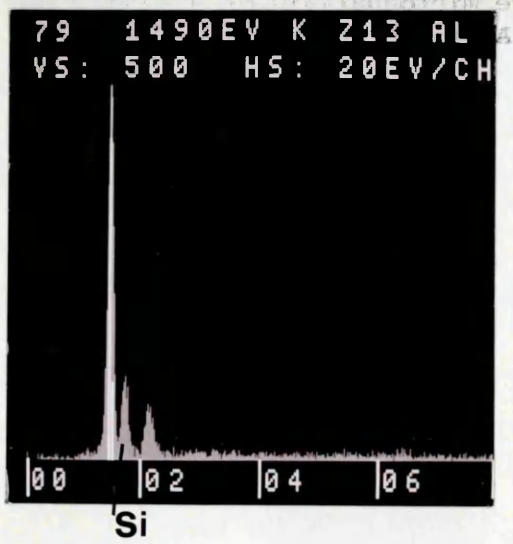
79 1490EV K Z13 AL
VS: 500 HS: 20EV/CH
00
02
04
06
Si

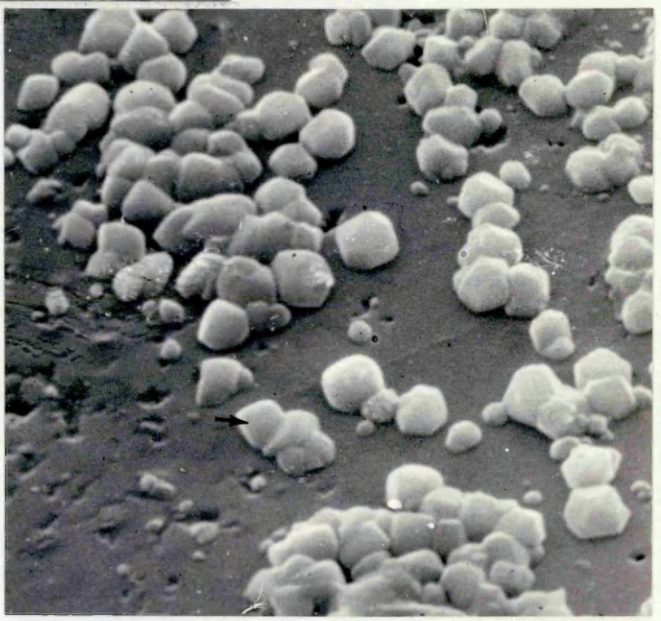

b.

c.

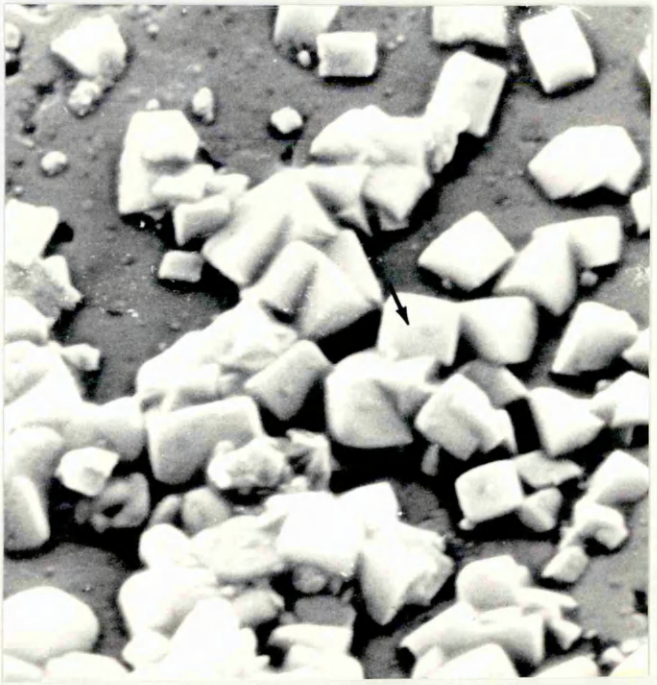

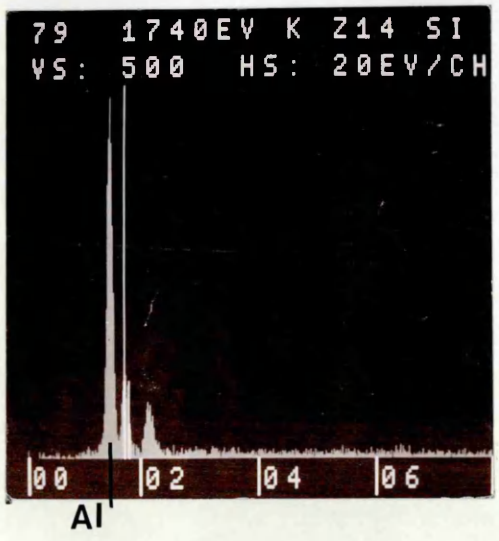
79 1740EV K Z14 SI
VS: 500 HS: 20EV/CH
00
02
04
06
Al

FIG. 4.3.2.1., a. Cross-section of a specimen reacted at 1220°C for 15 minutes. The silicon concentration in the starting aluminium was 10 atomic %.

b. Detail of the double layer fine interaction front with the coarse matrix left behind. Mag. approx. 80x

a.

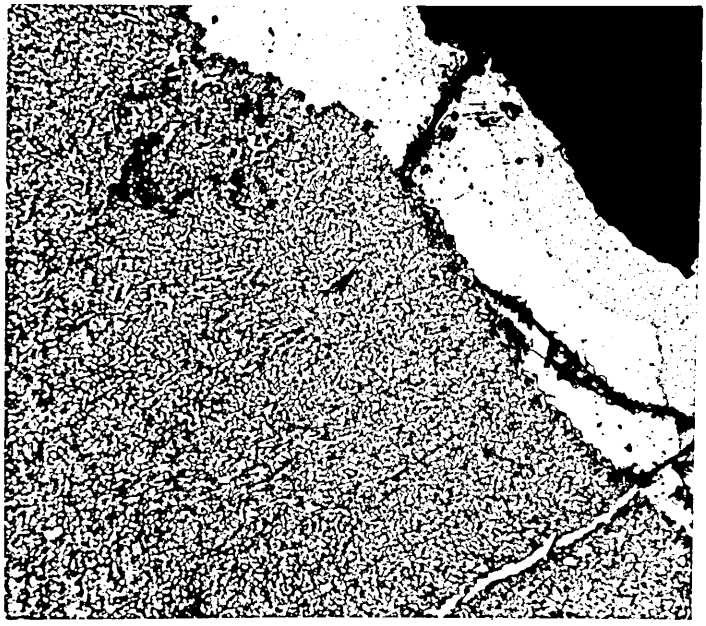

b.

FIG. 4.3.2.2. Symmetric progression of the reaction between liquid Al - 5.0 atomic %Fe alloy and vitreous silica at 1170°C. The time of the reaction was 105 minutes. The products radiate from a clearly identified interaction front in a columnar manner with the metal phase distributed in perpendicular streams. Mag. 32x

FIG. 4.3.2.3. Cross-section of a specimen reacted at 1265°C for 60 min. The aluminium contained 15 atomic %Mn. Mag. 63x

FIG. 4.3.2.4. Fine and irregular double layer in the interaction front. Columnar coarse matrix with parallel distribution of the metallic phase. Mag. 220x

Specimen: Al - 10 atomic %Fe
Temperature: 1110°C ; time: 240 min.

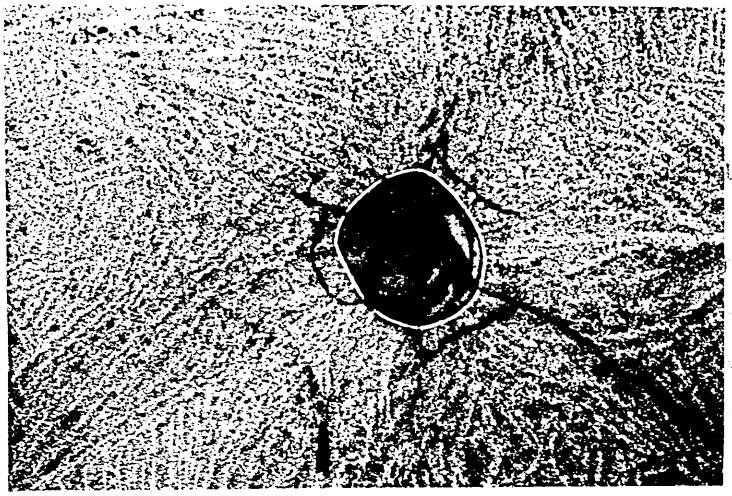

Al · 5at%

Al-10 at% Fe

FIG. 4.3.2.5.a. Selective coarsening occurs within the slowly moving interaction front. Some portions of the fine structure remains behind in the coarse matrix.

Specimen: 10 atomic %Mn
Temperature: 1220°C ; time: 120 min.
Etched for approx. 10 min. in 6% bromine alcohol Table 3.5.

b. Detail of selective coarsening within the interaction front. Radial crack occurs during reaction promoting the recrystallisation. Mag. 400x

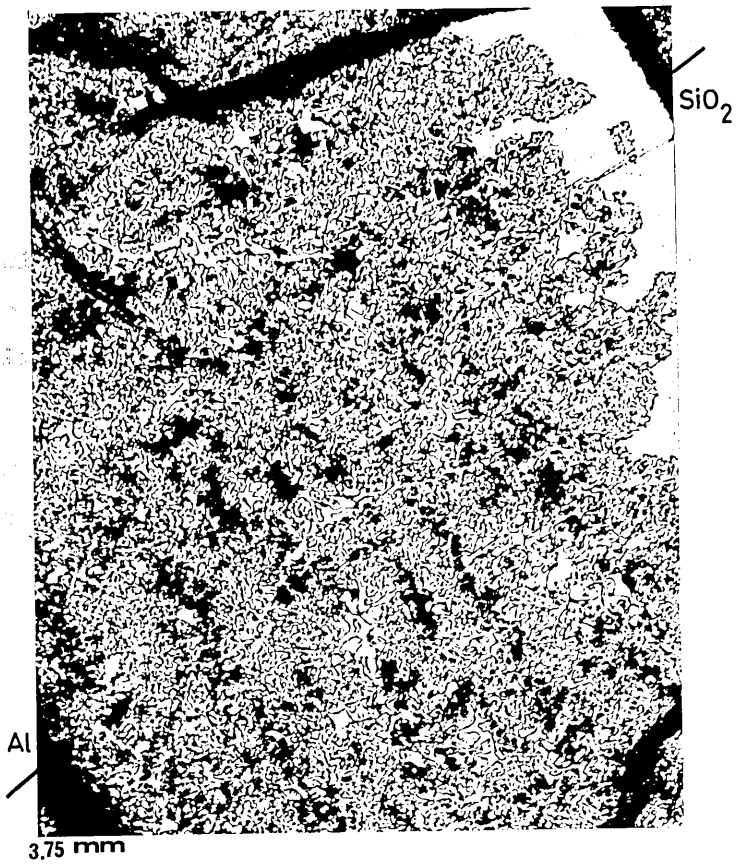
SiO_2
Al
3.75 mm

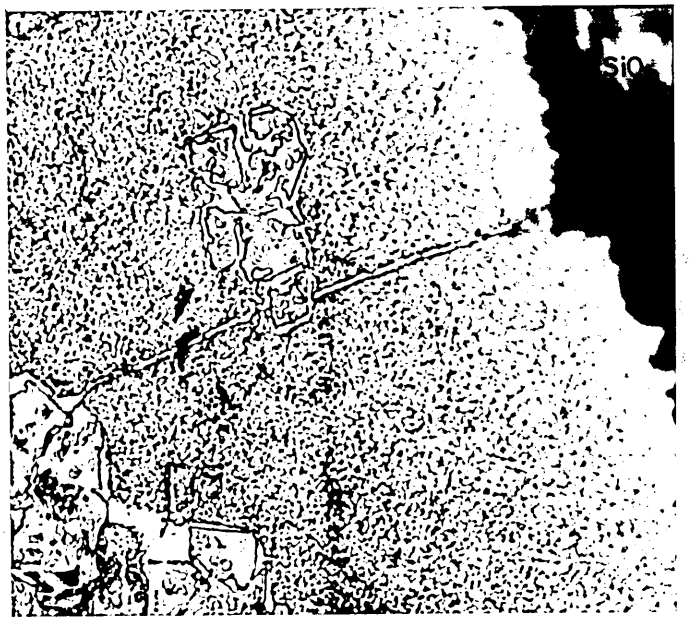
SiO

FIG. 4.3.2.6, a. Elemental line-scanning distribution of Al, Fe and Si across the interaction front of a specimen reacted for 20 minutes at 1220°C. Initial concentration of iron in the liquid Al - Fe alloy: 5.0 atomic %.

a. General view. Mag. 200x
b. Si scan line pattern
c. Al scan line pattern
d. Fe scan line pattern
e. Full spectrum scan line pattern

(1),(2),(3). EDAX patterns at 3 different marked positions across the interaction front.

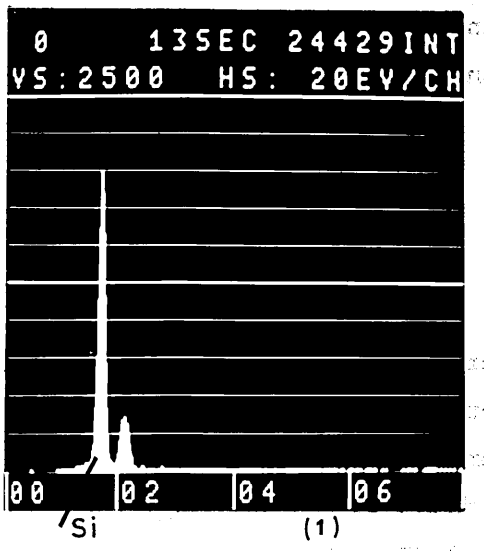
0 13SEC 24429INT
VS:2500 HS: 20EV/CH
00
02
04
06
Si
(1)

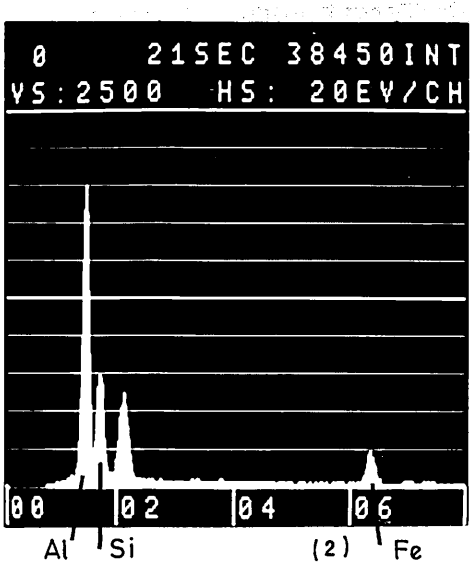
0 21SEC 38450INT
VS:2500 HS: 20EV/CH
00
02
04
06
Al
Si
(2)
Fe

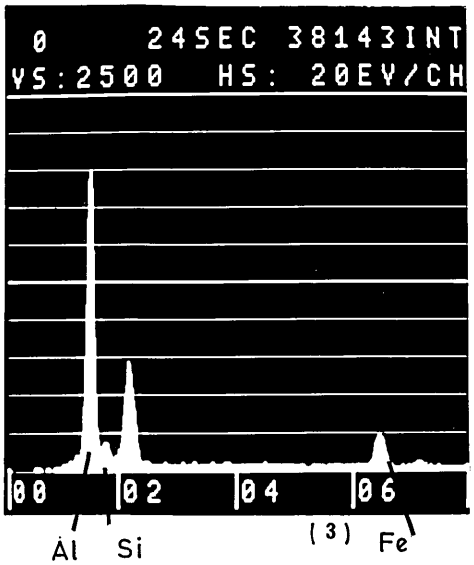
0 24SEC 38143INT
VS:2500 HS: 20EV/CH
00
02
04
06
Al
Si
(3)
Fe

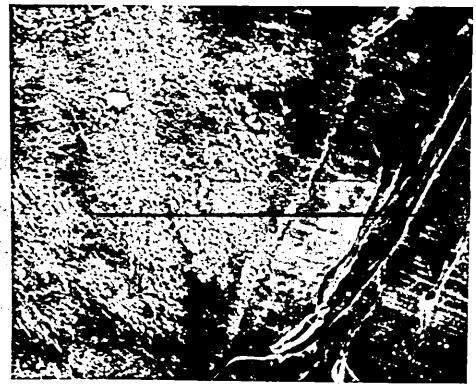
a

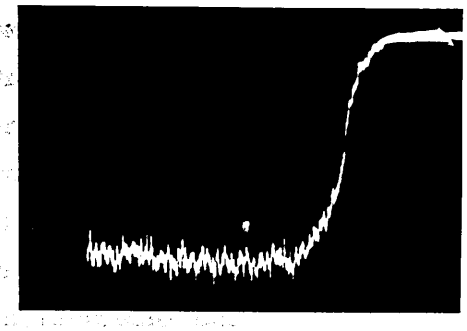
b

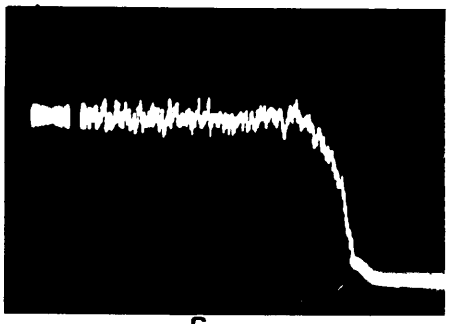
c

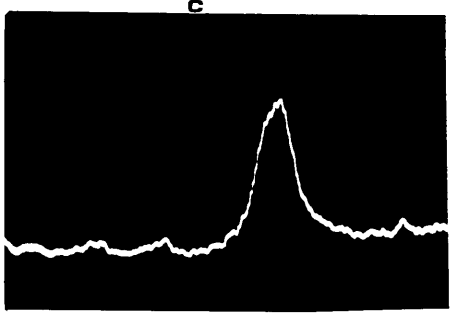
d

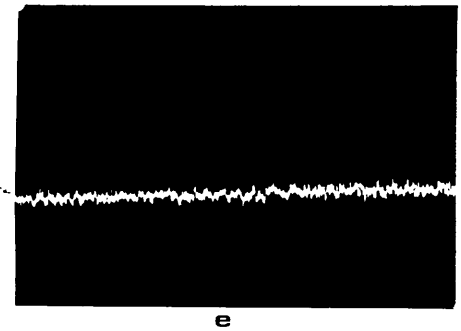
e

FIG. 4.3.2..6, b. Elemental Al,Fe and Si x-ray maps and corresponding line scanning across the interface of the interaction front with the recrystallised coarse matrix of a specimen reacted for 45 min. at 1220°C. Initial concentration of iron in the liquid aluminium - iron alloy: 10 atomic%. The lines on the maps denote the approximate scanning path.

a. General view Mag. 2500x
b. Al - line scanning pattern
c. Si - line scanning pattern
d. Fe - line scanning pattern
e. Full spectrum line scanning pattern
f. Si x-ray map
g. Fe x-ray map
h. Al + Fe + Si x-ray map

(1),(2). EDAX patterns at 2 different marked positions across the interaction front:

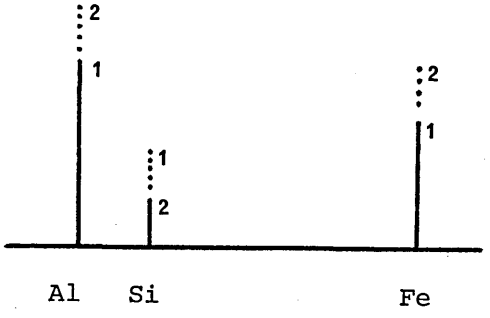

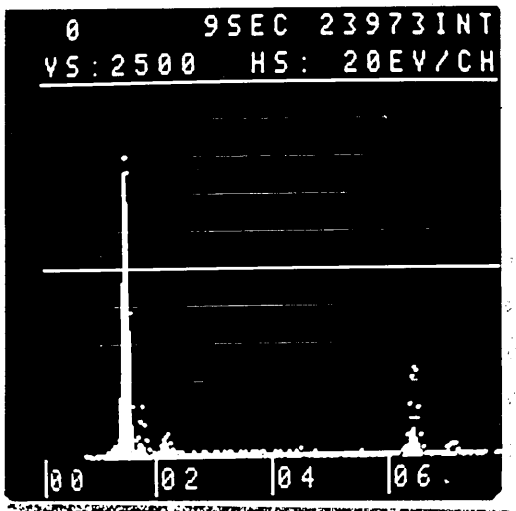

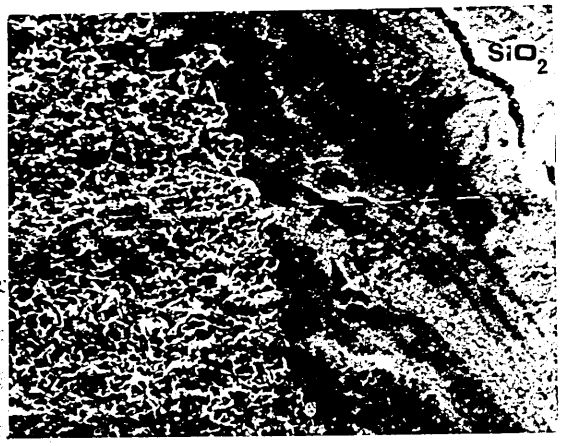

a

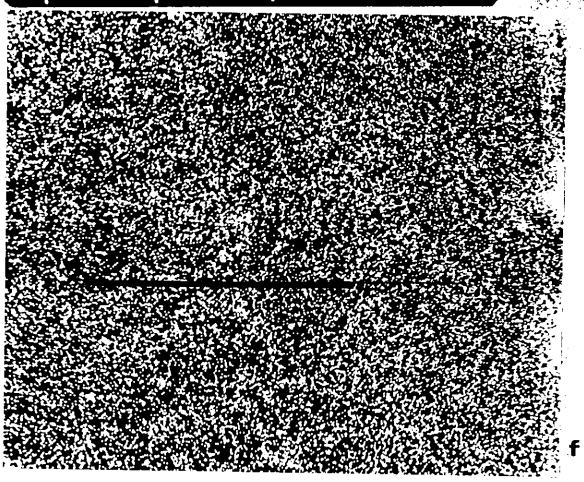

f

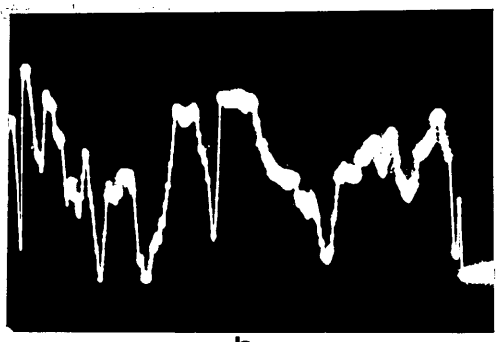

b

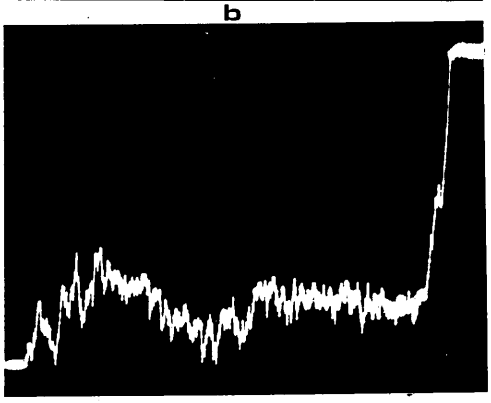

c

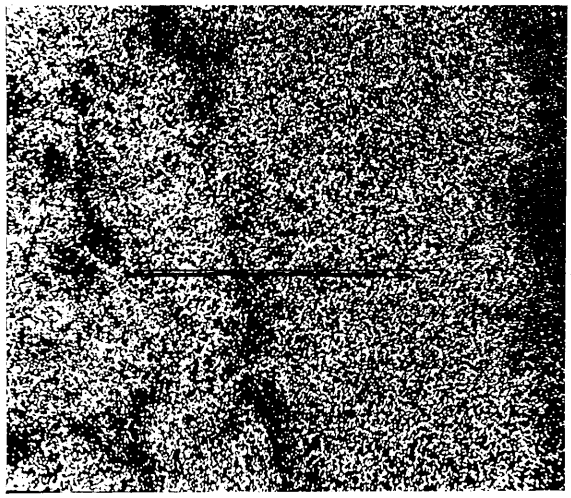

g

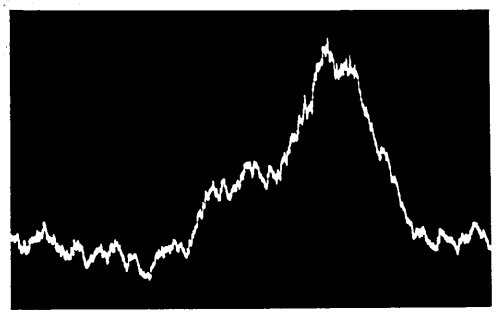

d

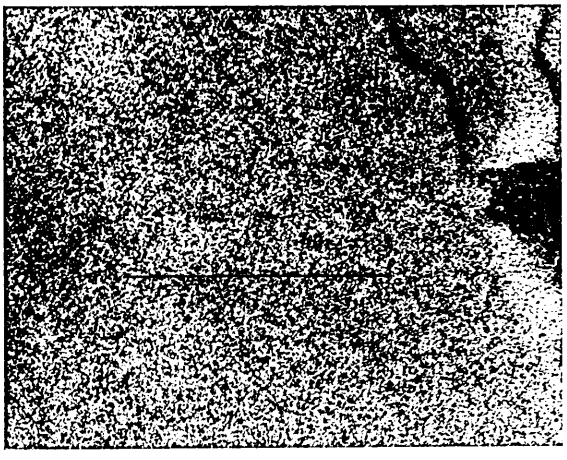

h

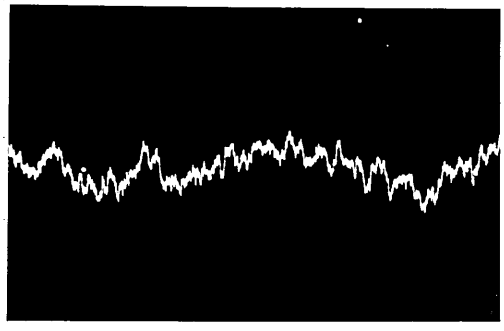

e

FIG. 4.3.2.6, c. Elemental line scanning distribution of Al,Fe and Si across the interface of the interaction front with recrystallised matrix of a specimen reacted at 1220°C for 90 min. Initial concentration of iron in the liquid Al-Fe alloy: 15 atomic%.

a. General view. Mag. 100x

b. Al line scanning pattern

c. Si line scanning pattern

d. Fe line scanning pattern

(1),(2),(3) . EDAX patterns at 3 different marked positions near the unreacted silica surface.

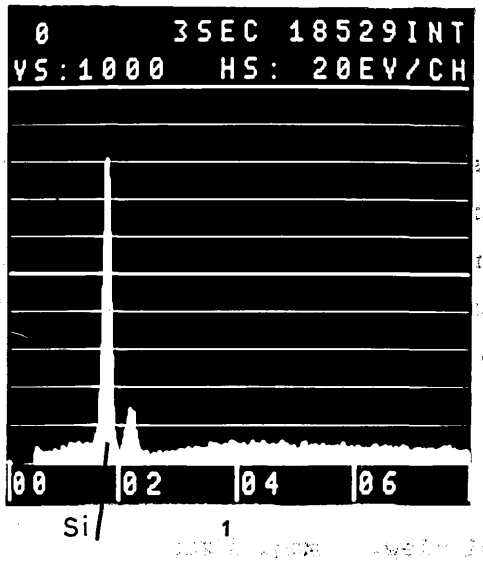
0 3SEC 18529INT
VS:1000 HS: 20EV/CH
00 02 04 06
Si
1

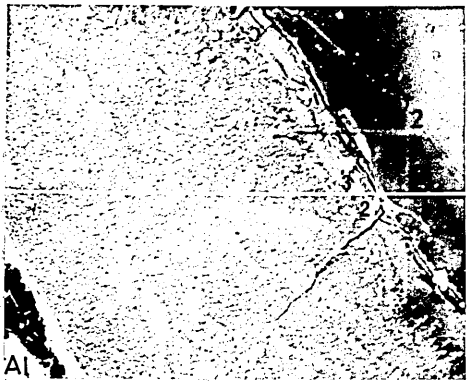
Al
2
3

a

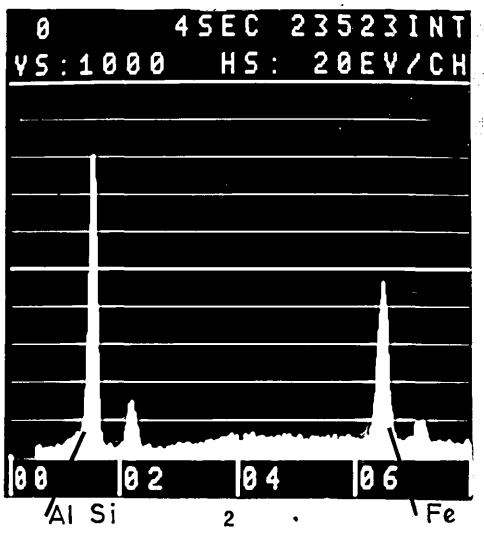
0 4SEC 23523INT
VS:1000 HS: 20EV/CH
00 02 04 06
Al Si
2
Fe

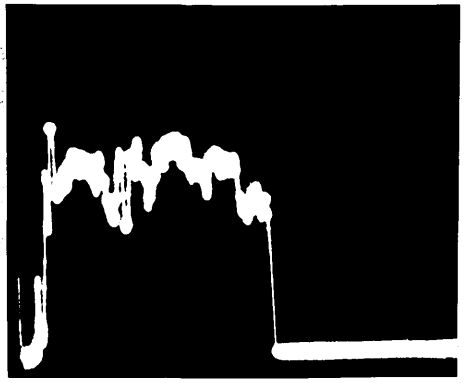

b

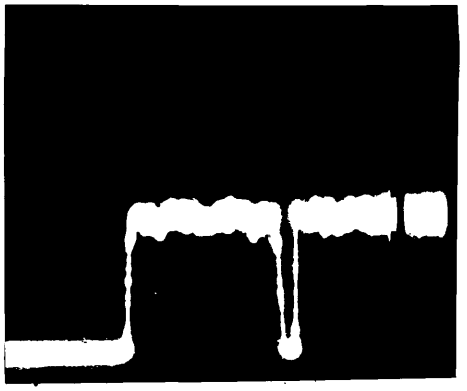

c

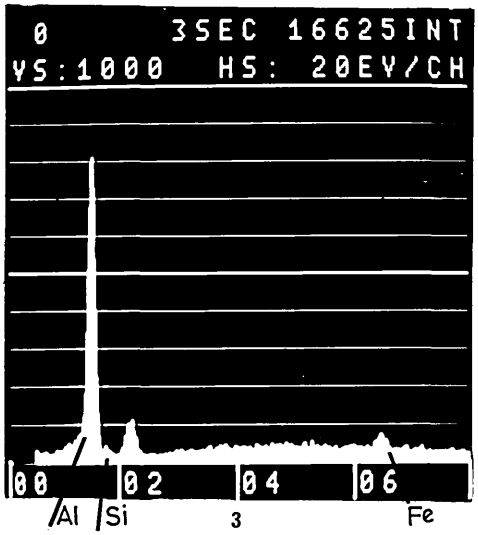
0 3SEC 16625INT
VS:1000 HS: 20EV/CH
00 02 04 06
Al Si
3
Fe

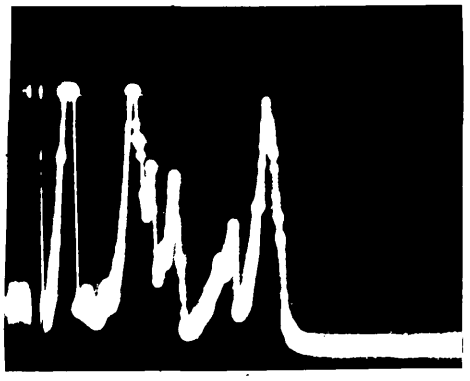

d

FIG. 4.3.2..6, d. Elemental Al, Mn and Si x - ray maps and corresponding line scanning patterns across the interaction front of a specimen reacted for 30 minutes at 1220°C. Initial concentration of manganese in the Al-Mn alloy: 5.0atomic%. The lines on the maps denote the approximate scanning path.

a. General view. Mag. 400x
b. Mn x -ray map
c. Al x -ray map
d. Si x -ray map
e. Si line scan pattern
f. Al line scan pattern
g. Mn line scan pattern

(1),(2). EDAX patterns at 2 different marked positions across the interface of the interaction front with the coarse matrix.

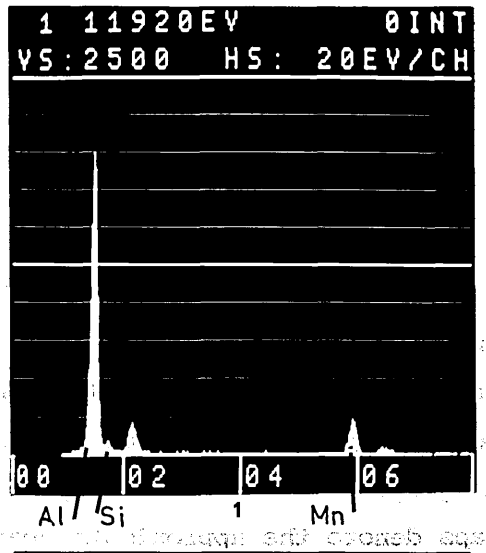
1 11920EV 0INT
VS:2500 HS: 20EV/CH
00
02
04
06
Al
Si
1
Mn


SiO2

a.

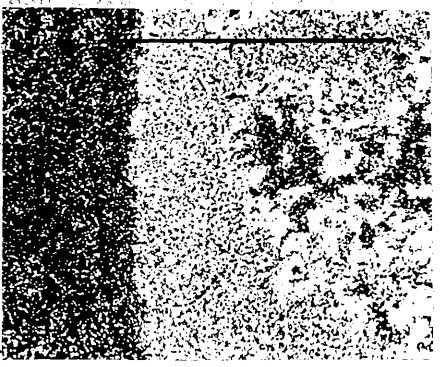

b.

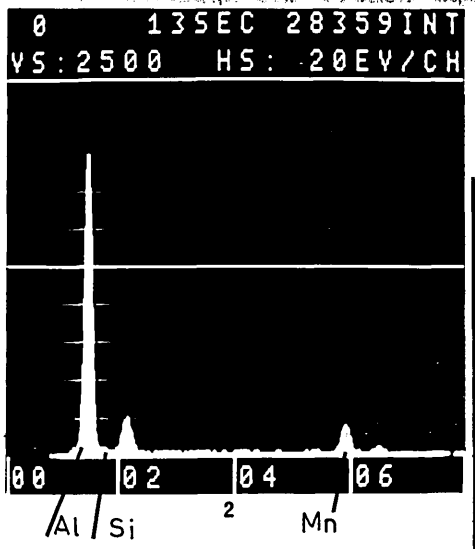
0 135EC 28359INT
VS:2500 HS: 20EV/CH
00
02
04
06
Al
Si
2
Mn

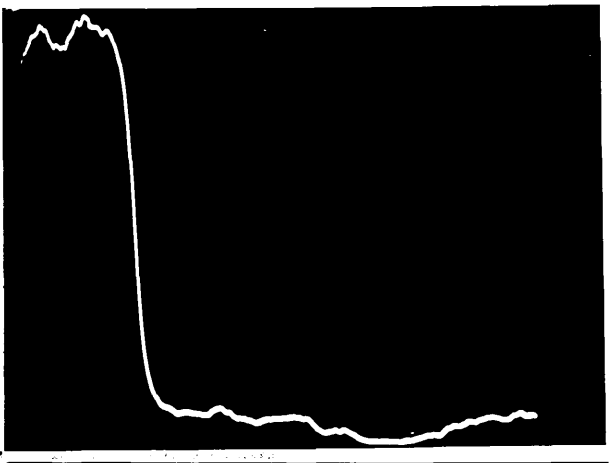

e.

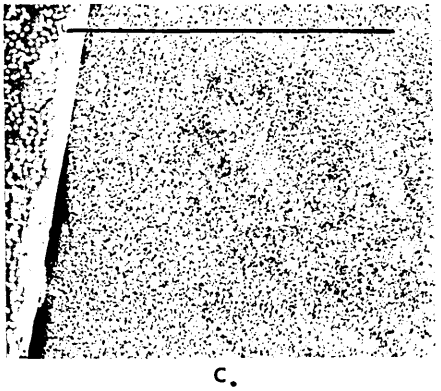

c.

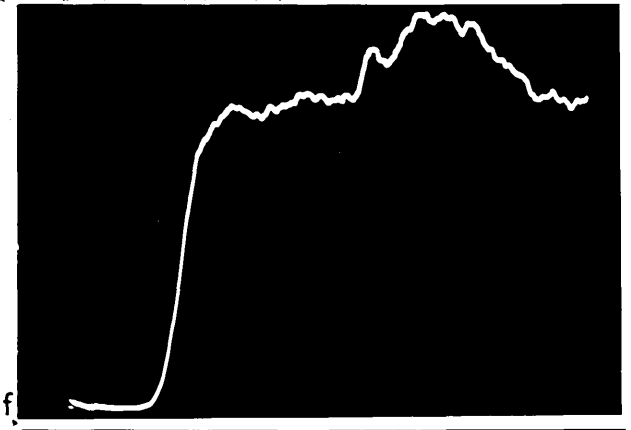

f.

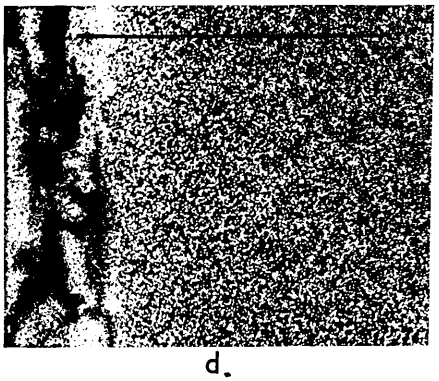

d.

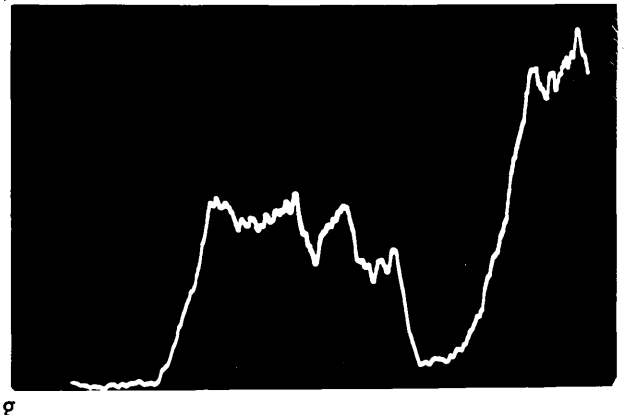

g.

FIG. 4.3.2.7, a. Ternary Al-Fe-Si eutectic valleys formed from the reaction between liquid Al-10 atomic%Fe and vitreous silica at 1170°C. Time of reaction: 60 min. Mag. 800x

b. Cells of alumina in a eutectic valley at higher magnification.
Specimen: 10 atomic%Fe
Temperature: 1220°C ; Time 75 min.

Mag. 1250x


Al-Fe-Si alloy
Al_2O_3

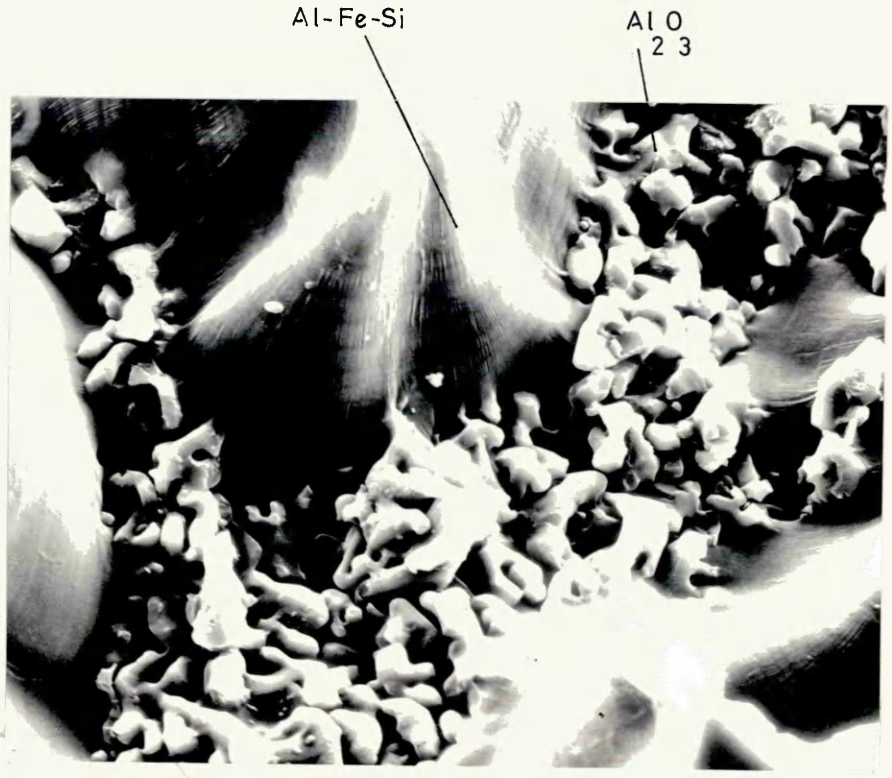
Al-Fe-Si
Al_2O_3

FIG. 4.3.2.7, c. Ternary Al-Mn-Si eutectic valleys formed from the reaction between liquid Al-5.0atomic%Mn and vitreous silica at 1265°C. Time of reaction: 30 min. Mag. 1250x

d. Detail at higher magnification of ternary Al-Mn-Si eutectic and alumina cells. Mag. 2500x.

e. Detail of alumina cells in the reaction system Al - 5.0atomic%Mn - SiO_2. Mag. 2500x.

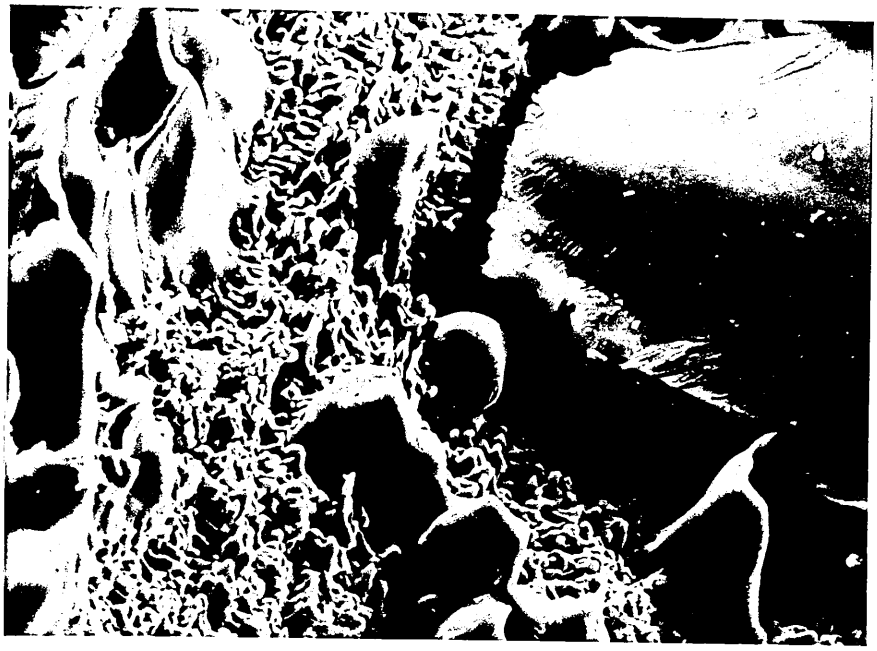

FIG. 5.1.1. Idealized scheme of a cross-section of a 75% converted silica rod lo mm in diameter by liquid pure aluminium at any reaction temperature.

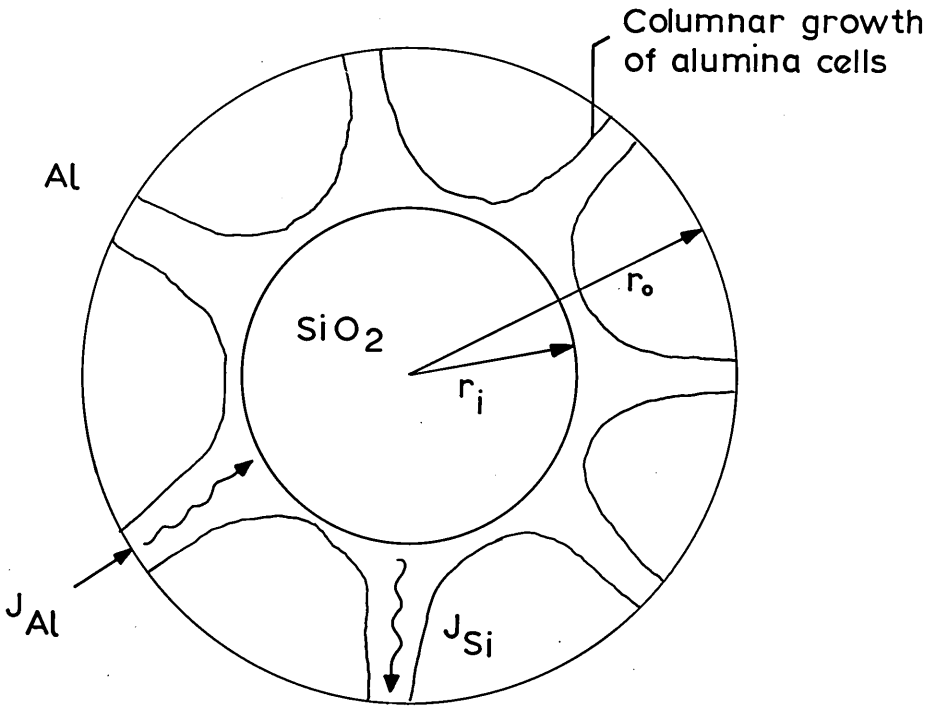

$$\left(r_i = \frac{1}{2} r_o\right)$$

$\equiv$ 75% conversion

FIG. 5.1.2. Calculated values of hypothetical reaction rate constants. See Appendix A-5.1. Comparison to calculated values of k for different sizes of rod versus temperature. See FIG. 4.1.2.4.

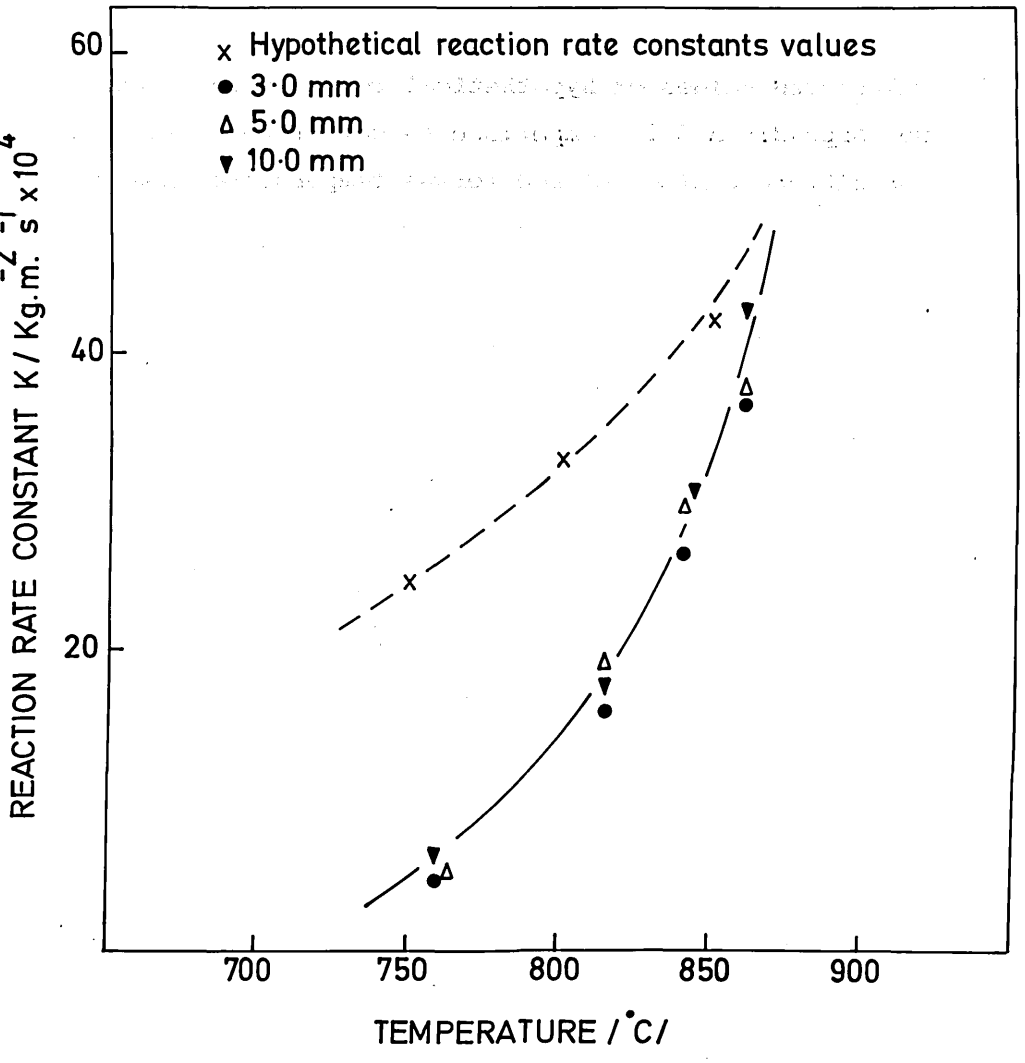
x Hypothetical reaction rate constants values
● 3·0 mm
Δ 5·0 mm
▼ 10·0 mm
60
40
20
700
750
800
850
900
REACTION RATE CONSTANT K / Kg.m.$^{-2}$ s^{-1} x 10^{4}
TEMPERATURE / °C /

FIG. 5.1.3. Thermodynamic relationship between the equilibrium constants and temperatures for processes possibly involved in the intermediate and higher temperature reactions.

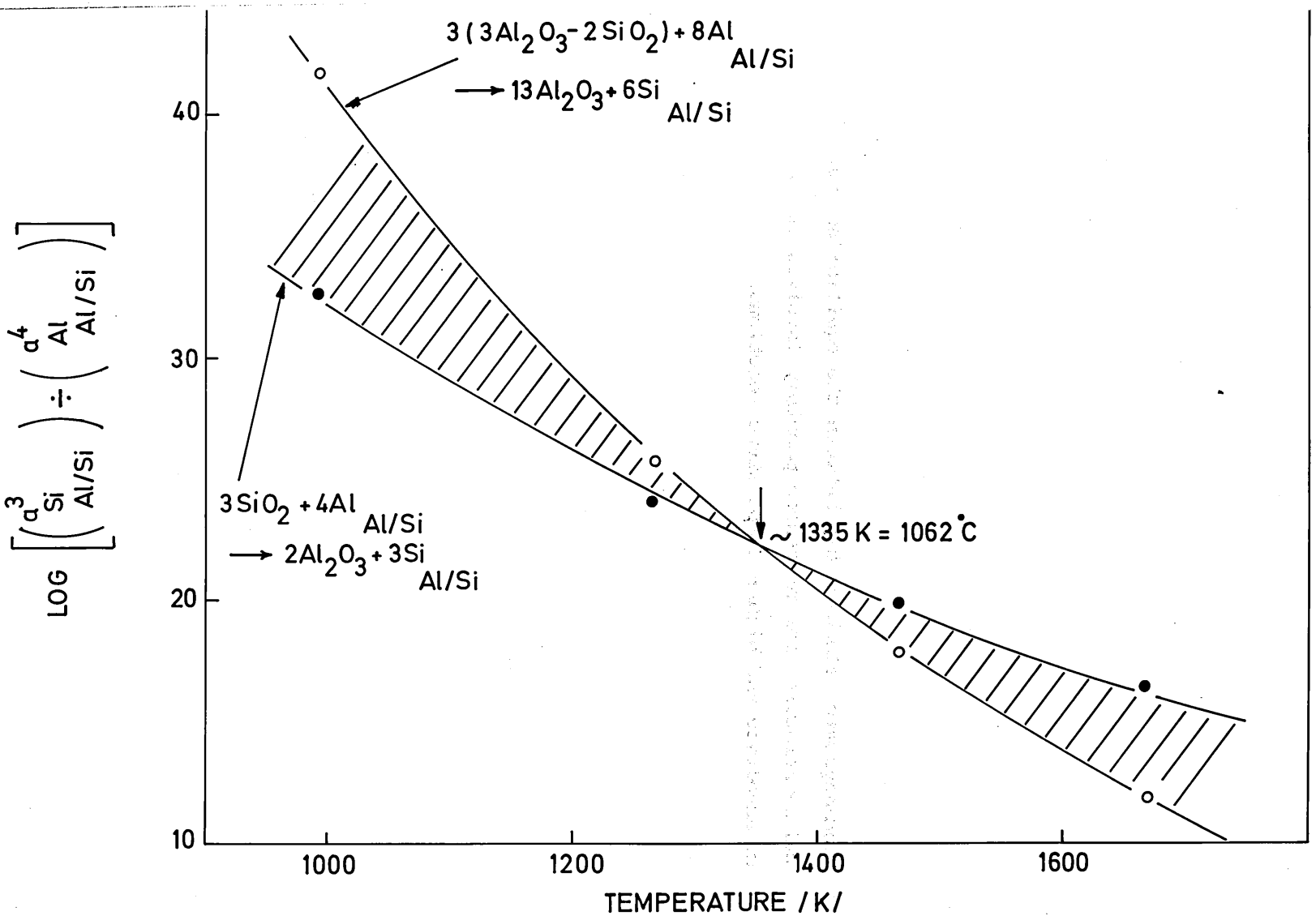
$3(3Al_2O_3 - 2SiO_2) + 8Al_{Al/Si}$
$\rightarrow 13Al_2O_3 + 6Si_{Al/Si}$
$3SiO_2 + 4Al_{Al/Si}$
$\rightarrow 2Al_2O_3 + 3Si_{Al/Si}$
~ 1335 K = 1062 °C
$LOG\left[\left(a^3_{Si}{}_{Al/Si}\right) \div \left(a^4_{Al}{}_{Al/Si}\right)\right]$
40
30
20
10
1000
1200
1400
1600
TEMPERATURE / K/

FIG. 5.1.4. Projected Liquidus relationships for the Al - Mn - SiO_2 reaction systems taken from the Al - Mn and Al - Mn - Si equilibrium phase diagrams , Figs. 2.7. and 2.9 ., respectively.

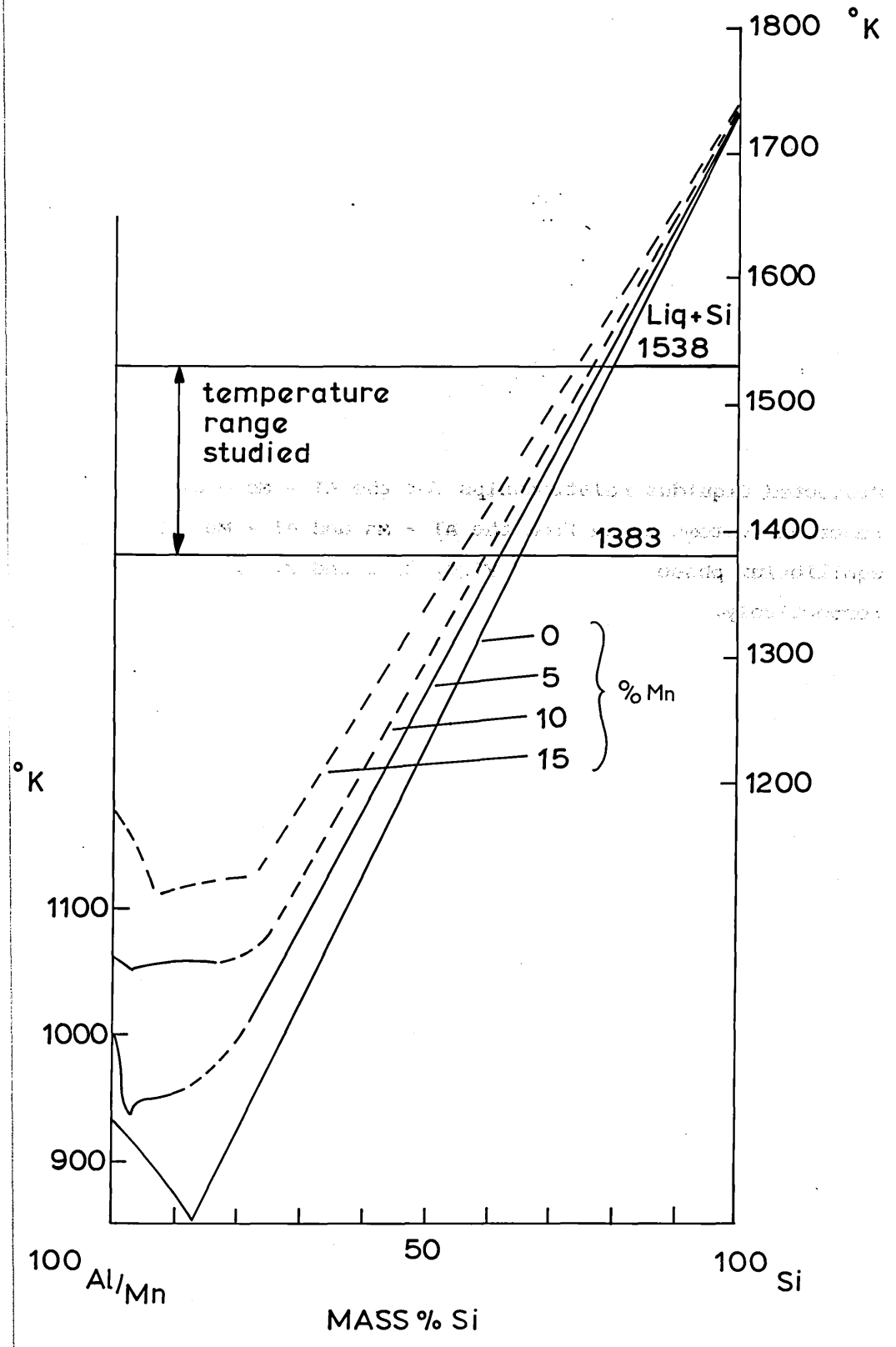
1800 °K
1700
1600
Liq+Si
1538
temperature
range
studied
1500
1400
1383
1300
1200
0
5
10
15
% Mn
°K
1100
1000
900
100 Al/Mn
50
100 Si
MASS % Si

FIG. 5.1.5. Projected Liquidus relationship for the Al - Fe - SiO_2 reaction systems taken from the Al - Fe and Al - Fe - Si equilibrium phase diagrams, Figs. 2.8 . and 2.10., respectively.

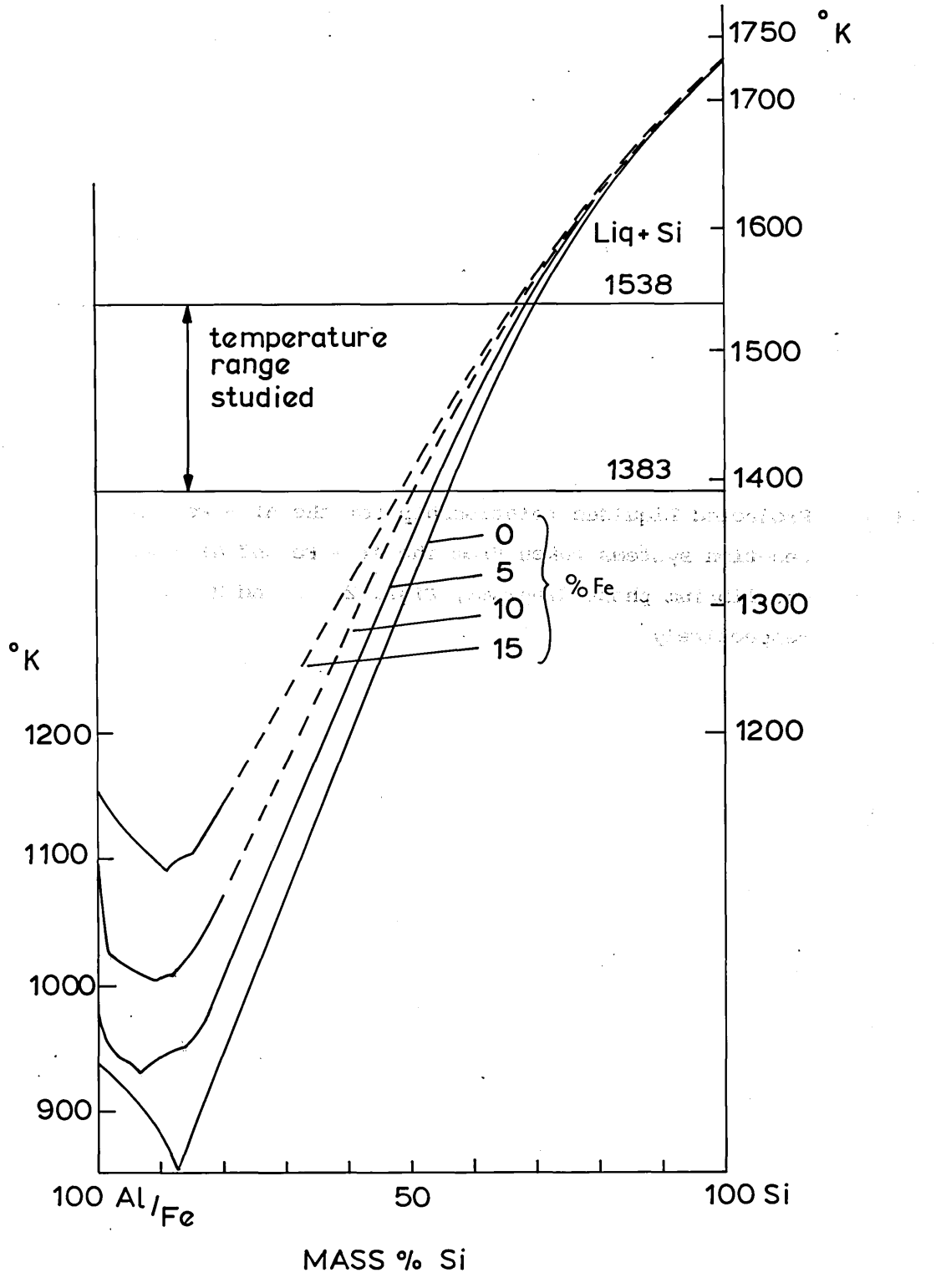
1750 °K
1700
1600
1500
1400
1300
1200
1100
1000
900
°K
Liq + Si
1538
1383
temperature
range
studied
0
5
10
15
% Fe
100 Al/Fe
50
100 Si
MASS % Si

Appendix A-2.1 — the derivation of the parabolic rate equation for the control of reaction rate by the diffusion of reactants through a solid product layer.

The rate of diffusion of an ionic species I across a plane at right angles to the diffusion direction is given by Fick's law:

$$J = -D \frac{\partial C}{\partial r} \qquad \text{A-2.1.1}$$

where J is the flux of I-ionic species through the plane, D is the diffusion coefficient and $\partial C/\partial r$ is the concentration gradient of I across the plane in the direction of diffusion.

A simple case is where a layer of new phase is formed and diffusion occurs through it, while the concentration of the diffusing species at the boundaries of the layer remains constant. Equation A-2.1.1 may then be integrated to obtain the flux of species I through the product layer:

$$J = D \frac{C_1 - C_2}{\Delta r} \qquad \text{A-2.1.2}$$

where C_1 and C_2 are the concentrations of I-species at interfaces 1 and 2, respectively, where $C_1 > C_2$, and Δr is the product layer thickness. It should be observed that equation A.2.1.2 is only an approximated form to express the flux of species I through a solid and interconnectedly porous product layer, since it supposes a constant gradient ΔC and that diffusion processes occur uni--dimensionally. In actual fact the form of equation A-2.1.2 depends upon the geometry of the system. This has been referred to in section 5.

If V is the volume of product per I-ion and C is the concentration of I-ions, then

$$V = {}^{1}/_{C} \qquad \text{A-2.1.3}$$

The rate of thickening of the product layer is given by:

$$\frac{d\Delta r}{dt} = J \cdot V = D \frac{(C_1 - C_2)}{\Delta r} \cdot V \qquad \text{A-2.1.4}$$

or

$$\frac{d\Delta r}{dt} = D \cdot \frac{(C_1 - C_2)}{C} \frac{1}{\Delta r} \qquad \text{A-2.1.5}$$

but

$$D \cdot \frac{(C_1 - C_2)}{C} = k_D = \text{constant} \qquad \text{A-2.1.6}$$

so that

$$\frac{d\Delta r}{dt} = k_D \cdot \frac{1}{\Delta r} \qquad \text{A-2.1.7}$$

Integrating it gives:

$$r^2 = 2\, k_D\, t \qquad \text{A-2.1.8}$$

the parabolic law of diffusion, which applies only to one--dimensional diffusion, when the geometry of the interface does not alter during the reaction. Stoichiometry and different densities of both products and reagents were not considered when deducing equation A-2.1.4.

Appendix A-2.2 — Jander's model for diffusion - controlled reactions

Jander applied the parabolic law to powdered compacts, and it is worth considering in detail the assumptions necessary in deriving his formula:

i. the reaction can be classified as an additive reaction with compound formation, i.e. solid solution does not occur;

ii. nucleation followed by surface diffusion occurs at temperature below that required for bulk diffusion, i.e. a coherent product layer is present before bulk diffusion commences;

iii. the solid state reaction is bulk diffusion controlled, i.e. the chemical reaction at the phase boundary is considerably faster than the transport process;

iv. bulk diffusion is uni-directional;

v. the reacting particles are all spheres of uniform radii;

vi. the ratio of the volume of the product layer to the volume of the reacted material is unity;

vii. the increase in thickness of the product layer follows the parabolic rate law;

viii. the diffusion coefficient of the transported species is time-independent;

ix. the activity of the reactants remains constant on both sides of the reaction interface;

x. the surface of the component in which the reaction takes place is completed coated with particles of the other

component as though the former particles were immersed in a melt of the latter.

Let V be the volume of unreacted material at time t. Then

$$V = \frac{4}{3}\pi(r_o - \Delta r)^3 \qquad \text{A-2.2.1}$$

or in terms of fractional conversion,

$$V = \frac{4}{3}\pi r_o^3 (1 - R_x) \qquad \text{A-2.2.2}$$

where R_x is the fractional conversion completed at time t and r_o is the initial radius of the unreacted particle.

Rearranging both equations, i.e.

$$1 - R = \frac{(r_o - \Delta r)^3}{r_o} \qquad \text{A-2.2.3}$$

and substituting Δr by its expression in equation A-2.1.8., then,

$$2k_D t/r_o^2 = \left[1 - (1 - R)^{1/3}\right]^2 \qquad \text{A-2.2.4}$$

Appendix A-2.3 — chemically-controlled reaction model

If the hypothesis is made that the reaction is controlled at the phase boundary product layer/unreacted material, a rate equation that fits the experimental data may be derived.

Let r_o be initial radius of a spherical particle with initial density ρ_o. Assume that the rate of formation of a uniform product layer is proportional to the receeding interface area S of the remaining unreacted material. If W is the mass of that part of the original material that has reacted, then:

$$\frac{dw}{dt} = k_c S \qquad \text{A-2.3.1}$$

where k_c is a proportionality constant having the dimensions $ML^{-2}t^{-1}$ and which is dependent upon the temperature, pressure and reactant concentration. From this, it follows that

$$r_o \rho_o \frac{\Delta r}{r_o} = k_c t \qquad \text{A-2.3.2}$$

where $\Delta r (= r_o - r)/r_o$ is the ratio of thickness of the product layer to the initial radius, and r is the radius of the unreacted material.

The fractional conversion R_x of the unreacted material is defined as the mass W of reacted material, divided by the total mass W_o of material originally present, before reaction started. Thus,

$$R_x = \frac{W}{W_o} = \frac{\frac{4}{3}\pi r_o^3 - \frac{4}{3}\pi\left[r_o - r_o\left(\frac{\Delta r}{r_o}\right)\right]^3}{\frac{4}{3}\pi r_o^3} \qquad \text{A-2.3.3}$$

rearranging,

$$1 - R_x = \left(1 - \frac{\Delta r}{r_o}\right)^3 \qquad \text{A-2.3.4}$$

or

$$\frac{\Delta r}{r_o} = 1 - (1 - R_x)^{1/3} \qquad \text{A-2.3.5}$$

Substituting in equation A-2.3.2, thus

$$1 - (1 - R_x)^{1/3} = k_c t / r_o \rho_o \qquad \text{A-2.3.6}$$

This equation states that, at the phase boundary, the amount of unreacted material reacting per unit area per unit time is constant or that the reaction interface advances linearly, i.e. at a constant rate.

The same equation can be derived for a disc reacting from the edge inward or for a cylinder:

$$r_o \rho_o \left[1 - (1 - R_x)^{1/2}\right] = k_c t \qquad \text{A-2.3.7}$$

APPENDIX A-3.1. OXIDIZING POTENTIAL CALCULATIONS FOR THE EXPERIMENTAL INERT GAS CONTROLLING ATMOSPHERE.

The oxidation of liquid aluminium may occur according to reaction

$$2\ A\ell_{(\ell)} + 3/2\ O_{2(g)} = A\ell_2O_{3(s)} \qquad \text{A-3.1.1.}$$

for which the standard free energy change is found to be

$\Delta G^o = 376000 - 61.56\ T$ (f.en.u)

At the extremes of both experimental intervals, ie. at 760°C (1033 K) and 1265°C (1538 K), ΔG^o - values are respectively

$\Delta G^o_1 = -312408.5$ (f.en.u) and $\Delta G^o_2 = -281628.5$ (f.en.u).

The equilibrium constant of reaction A-3.1.1. may be expressed as

$$k_{O_2} = \frac{1}{p_{O_2}^{3/2}} \qquad \text{A-3.1.2.}$$

Substituting this expression in the Free Energy equation it gives

$$\Delta G^o = RT\ \ell n \frac{1}{p_{O_2}^{3/2}} \qquad \text{A-3.1.3.}$$

and the equilibrium partial pressure of oxygen per fraction mol of gas and at temperatures may thus be calculated:

a) $T_1 = 1033$ K .... $-312408.5 = -1.987 \times 1033 \times \left| -\frac{3}{2}\ \ell n\ p_{O_2} \right|$

or $p_{O_2} = 8.56 \times 10^{-45}$ atm

b) $T_2 = 1538$ K .... $-281628.5 = -1.987 \times 1538 \times \left| -\frac{3}{2}\ \ell n\ p_{O_2} \right|$

or $p_{O_2} = 5.87 \times 10^{-26}$ atm

Assuming the maximum oxygen mass content in the commercial high purity argon as 0.005%, the oxygen molar fraction will be given by

$$N_{O_2} = \frac{n_{O_2}}{n_{O_2} + n_{Ar}} = \frac{\%mass O_2 / M_{O_2}}{\frac{100}{M_{Ar}} + \frac{\%mass O_2}{M_{O_2}}} \qquad \text{A-3.1.4.}$$

where N_{O_2} is the molar fraction

$n_{O_2,\ Ar}$ is the number of moles

$M_{O_2} = 32$; $M_{Ar} = 39.94$ are the atomic mass of oxygen and argon respectively

substituting and calculating it gives

$$N_{O_2} = 6.24 \times 10^{-5}$$

and thus

$$p_{O_2} = 6.24 \times 10^{-5} \times 1 \text{ atm} = 6.24 \times 10^{-5} \text{ atm}$$

Although the value of the oxygen partial pressure, due to its content in the inert gas, is markedly higher in comparison to the calculated values for pure oxygen and at temperatures and for reaction, there will still be a great oxidizing potential of the gas mixture and so aluminium oxide will be formed.

If the regression line equation is given by

$$y = mx + c \qquad \text{A-4.1.1}$$

It can thus be shown that the slope m and y-intercept c are determined a follows:

$$m = \frac{N \sum_{i=1}^{N} x_i y_i - \sum_{i=1}^{N} x_i \sum_{i=1}^{N} y_i}{\left[N \sum_{i=1}^{N} x^2 - \sum_{i=1}^{N} x_i \right]^2} \qquad \text{A-4.1.2}$$

Where

N = number of observations on the regression line

$\bar{x}$ = average x value $= \frac{\sum_{i=1}^{N} x_i}{N}$

$\bar{y}$ = average y value $= \frac{\sum_{i=1}^{N} y_i}{N}$

σ_x^2 = variance of the x values $= \frac{\sum_{i=1}^{N} x_i^2}{N} - \bar{x}^2$

$$c = \bar{y} - m\bar{x} \qquad \text{A-4.1.3}$$

The degree of association between the random variables $(x_i, y_i$ (x_n, y_n) is measured by the correlation coefficient r and is calculated using the expresion

$$r = \frac{\frac{\sum_{i=1}^{N} x_i y_i}{N} - \bar{x}.\bar{y}}{\sigma_x \sigma_y} \qquad \text{A-4.1.}$$

Where

$$\sigma_y = \text{variance of the y values} = \frac{\sum_{i=1}^{N} y_i^2}{N} - \bar{y}^2$$

By rewriting equation A-4.1.4. in terms of equation A-4.1.2. then

$$r = \frac{m \cdot \sigma_x}{\sigma_y} \qquad \text{A-4.1.}$$

or

$$m = \frac{r \cdot \sigma_y}{\sigma_y} \qquad \text{A-4.1.}$$

Using this expression, the linear regression curve, equation A-4.1.1. may be expressed as

$$y = \left[\frac{r \cdot \sigma_y}{\sigma_x}\right] . x + c \qquad \text{A-4.1.7}$$

Both equations A-4.1.5. and A-4.1.7 determine the best linear curve fit and assess the degree of association between the variables and the linear equations. As previously mentioned, the value of r measures the "degree of fit" of the given point to the least-squares straight line.

When $r = \pm 1$, the correlation is said to be exact.

When r = 0, however, the variables are said to be uncorrelated with a linear equation.

APPENDIX A-5.1

Notation		SI-units
A_{cyl}	surface of the reacting silica	M^2
C^*_{Si}	dimensionless concentration of silicon ($=C_{Si}/C_T$)	
C_{SiO_2}	molar concentration of reacting silica	$mol.cm^{-3}$
C_T	total concentration in the mixture where diffusion takes place, i.e. in the Al-Si alloy	$mol.cm^{-3}$
$D_{Si/Al}$	diffusion coefficient of silicon through liquid aluminium-silicon alloy	$m^3.sec^{-1}$
$D_{Si/Al_{eff}}$	effective diffusion coefficient of silicon through the porous product layer	$m^3.sec^{-1}$
J_{Al}	total flux of aluminium expressed per unit of the receding area of the silica	$kg.m^{-2}.sec^{-1}$
J_{Si}	total flux of silicon liberated by reaction between silica and aluminium	$kg.m^{-2}.sec^{-1}$
j_{Si}	molar flow of silicon per unit height (length) of the reacting cylinder	$moles.m^{-2}.sec^{-1}$
k	apparent reaction rate constant	$kg.m^{-2}.sec^{-1}$
ℓ	length	m
M_{SiO_2}	molecular mass of reacting silica	kg
r_i	radius of the reaction interface	m
r_o	original radius of the rod	m
R_x	fractional radius	dimensionless
r*	fractional radius	dimensionless
R	universal gas constant	$kJ.mol^{-1}K^{-1}$
Sh	Sherwoood number ($= \alpha.d/D$) $m.s^{-1}.m.m^{-2}.s$	dimensionless
t	time	sec
T	absolute temperature	K
x	distance between the receding silica surface and the external surface of the rod	m
W_{SiO_2}	mass of the reacting silica at any time of the reaction	kg

APPENDIX A-5.1 (Cont.)

Notation		SI units
$\alpha_{Si,Al}$	mass transfer coefficient of silicon through aluminium-silicon alloy	$m.s^{-1}$
γ	porosity	%
δ	thickness of the thin stagnant film of liquid surrounding the specimen	m
ρ_{SiO_2}	density of the reacting silica	$kg.m^{-3}$
τ	tortuosity factor	dimensionless

APPENDIX A-5.2 Calculation of hypothetical reaction rate constants

Hypothetical reaction rate constants have been calculated from equation (5.1.25):

$$k = \frac{(D_{Si/Al}).C_T\left[(Y_{Si})_i - (Y_{Si})_b\right] M_{SiO_2}}{\left(\frac{1.5}{Sh} + 0.20.\frac{\tau}{\gamma}\right).r_o} \qquad A - 5.1.$$

Section 5.1.2. shows that the following data are to be used:

$$= 1.1,\ \gamma = 0.15,\ \left(\frac{D_{Si/Al}}{cm^2 s^{-1}}\right) = 2 \times 10^{-3} \exp\left(-\frac{21.78\ kJ.mol^{-1}}{RT}\right)$$

$Sh \to \infty$; $r_o = 0.5cm$.

In addition, we will require values of C_T, M_{SiO_2}, $(Y_{Si})_i$ and $(Y_{Si})_b$.

C_T is the molar density of molten aluminium and is:

$$C_T = 2.4\ gm.cm^{-3}/27\ gm.mol^{-1}_{Al} = 8.9x10^{-2}\ mol_{Al}.cm^{-3}$$

M_{SiO_2} is the relative molecular mass of silica:

$$M_{SiO_2} = 60\ gm.mol^{-1}_{SiO_2}$$

The Y_{Si} values are to be calculated from equation (5.1.8.):

$$Y_{Si} = \frac{\ln\left[1-(1-\frac{4}{3})C^*_{Si}\right]}{1-\frac{4}{3}}$$

$(Y_{Si})_i$ is to be calculated from the value of $(C^*_{Si})_i$ which is the mole fraction of silicon in the liquid alloy at the liquidus taken from the phase diagram shown in Figure 2.1.

$(Y_{Si})_b$ is to be calculated for conditions in the bulk liquid where $(C^*_{Si})_b$ is zero.

The values of these variables actually used to calculate the values of k from which the dotted line in Fig. 4.1.2.4. has been drawn are shown in the table below:-

Temperature	$C^*_{Si\ i}$	$Y_{Si\ i}$	$D_{Si/Al}$ /cm^2.s^{-1}	k /kg.m^{-2}s^{-1}
750	0.23	0.22	$1.54x10^{-4}$	$24.7x10^{-4}$
800	0.27	0.26	$1.73x10^{-4}$	$32.8x10^{-4}$
850	0.32	0.30	$1.93x10^{-4}$	$42.2x10^{-4}$

APPENDIX A-5.3. Thermodynamic data and calculations for the possible existence of the intermediate crystalline cubic phase Si-Al (spinel) during reaction between silica and aluminium

The two processes assumed to be involved in the reaction system are as follows:

(1) $3(3Al_2O_3.2SiO_2) + 8\ Al = 13Al_2O_3 + 6\ Si$

$$\Delta G^o = 1417.3 + 0.62T \quad kJ.mol^{-1}$$

(2) $3SiO_2 + 4Al = 2Al_2O_3 + 3\ Si$

$$\Delta G^o = 767 + 1.44.10^{-3}T\ kJ.mol^{-1}$$

Since $(3Al_2O_3.2SiO_2)$, Al_2O_3 and SiO_2 are pure, their activities are unity and a common equilibrium constant for both processes may be simplified to the expression:

$$k_{eq.} = \frac{a_{Si}^3}{a_{Al}^4}$$

The change in free energy corresponding to the reduction of the spinel phase and silica by liquid aluminium is related to the equilibrium constant by $\Delta G_T^o = RT\ \ell n\ k_{eq}$. Substituting ΔG_T^o by its respective expressions above and where T varies for 1000 to 1673K, the values of k_{eq} for both processes and from which Fig.5.1.3. has been drawn are shown in the Table below:

(1)

Temperature K	1000	1273	1473	1673
$\Delta G^o/kJ.mol^{-1}/$	797.3	628.0	504.0	210.0
$\ell n\ k_{eg}$	$5.23x10^{41}$	$5.37x10^{25}$	$8.64x10^{17}$	$7.60x10^{11}$
a_{Si}^3/a_{Al}^4	41.7	25.7	17.9	11.9

(2)

Temperature K	1000	1273	1473	1673
$\Delta G^o/kJ.mol^{-1}/$	623.0	583.7	554.9	526.7
$\ell n\ k_{eg}$	$3.97x10^{32}$	$8.22x10^{23}$	$5.67x10^{19}$	$2.80x10^{06}$
a_{Si}^3/a_{Al}^4	32.6	23.9	19.8	16.5